Role of TRPM4 and Piezo1 ion channels in cardiac mechanotransduction underlying pressure overload-induced left ventricular hypertrophy

Author:
Guo, Yang

Publication Date:
2022

DOI:
https://doi.org/10.26190/unsworks/1986

Role of TRPM4 and Piezo1 ion channels in cardiac mechanotransduction underlying pressure overload-induced left ventricular hypertrophy

Yang Guo

A thesis in fulfilment of the requirements for the degree of Doctor of Philosophy

Victor Chang Cardiac Research Institute

St Vincent's Clinical School

Faculty of Medicine

University of New South Wales

December 2021

Thesis Title

Role of TRPM4 and Piezo1 ion channels in cardiac mechanotransduction underlying pressure overload-induced left ventricular hypertrophy

Thesis Abstract

Pathological left ventricular hypertrophy (LVH) induced by mechanical pressure overload is the most powerful independent predictor of cardiac mortality in clinic. Current treatment methods focus on removing the pressure overload stimulus for LVH, which does not reverse adverse cardiac remodelling completely. Importantly, the molecular signalling pathways involved in pressure overload induced-LVH are potential targets for therapeutic intervention. Although numerous molecular signalling steps in the induction of LVH have been identified to date, the initial step when mechanical stretch associated with cardiac pressure overload is converted into a chemical signal that initiates hypertrophic signalling remains unresolved.

As the primary molecular transducers of mechanical stimuli that function in the cardiovascular system, several ion channels, including mechanosensitive ones, have been considered as potential contributors to cardiac hypertrophy signalling pathways. The focus of this project is to investigate the role of two types of ion channels, including TRPM4 and Piezo1, in cardiac mechanotransduction underlying pressure overload-induced LVH.

By employing wild-type and conditional cardiac gene knockout mouse LVH model based on aortic transverse constriction, this project demonstrates that TRPM4 channel is an important component of the Ca^{2+}-dependent mechanosensory signalling pathway that contributes to LVH in response to pressure overload; selective deletion of TRPM4 channels in mouse cardiomyocytes results in an approximately 50% reduction in pressure overload-induced LVH. Also, this project provides methodological foundation of new *in vitro* approaches to investigate Piezo1-mediated cardiac mechanotransduction. Chemical agonist-evoked Piezo1 activation and likely isotropic stretch-induced Piezo1 activation were shown in both HL-1 atrial myocyte-like cell line and isolated mouse ventricular cardiomyocytes, visualised by Ca^{2+} imaging. In addition, the data from this project provide *in vitro* evidence of the functional interaction between Piezo1 and TRPM4 channels, reflected in altered action potential frequency in HL-1 cells. These findings contribute to better understanding of the mechano-electrochemical transduction which initiates the signalling pathway in pressure overload-induced LVH and thus provide the basis for development of potential novel therapeutic targets for prevention of pathological LVH.

ORIGINALITY STATEMENT

☑ I hereby declare that this submission is my own work and to the best of my knowledge it contains no materials previously published or written by another person, or substantial proportions of material which have been accepted for the award of any other degree or diploma at UNSW or any other educational institution, except where due acknowledgement is made in the thesis. Any contribution made to the research by others, with whom I have worked at UNSW or elsewhere, is explicitly acknowledged in the thesis. I also declare that the intellectual content of this thesis is the product of my own work, except to the extent that assistance from others in the project's design and conception or in style, presentation and linguistic expression is acknowledged.

COPYRIGHT STATEMENT

AUTHENTICITY STATEMENT

☑ I certify that the Library deposit digital copy is a direct equivalent of the final officially approved version of my thesis.

UNSW is supportive of candidates publishing their research results during their candidature as detailed in the UNSW Thesis Examination Procedure.

Publications can be used in the candidate's thesis in lieu of a Chapter provided:

- The candidate contributed **greater than 50%** of the content in the publication and are the "primary author", i.e. they were responsible primarily for the planning, execution and preparation of the work for publication.
- The candidate has obtained approval to include the publication in their thesis in lieu of a Chapter from their Supervisor and Postgraduate Coordinator.
- The publication is not subject to any obligations or contractual agreements with a third party that would constrain its inclusion in the thesis.

☑ The candidate has declared that **some of the work described in their thesis has been published and has been documented in the relevant Chapters with acknowledgement**.

A short statement on where this work appears in the thesis and how this work is acknowledged within chapter/s:

> In my thesis, Chapter 1 contains work published in two review articles (with original results) that I contributed to and were published in “Progress in Biophysics and Molecular Biology” and “Frontiers in Bioengineering and Biotechnology”. Chapter 1 also contains part of a research article published in “eLife”. The methods from the three published articles above are contained in parts in Chapter 2. Part of the results from the three published articles are contained in Chapter 3 and 4. Acknowledgement of the work of the other authors of these articles has been made at the beginning of each chapter as well as in the Acknowledgements section in my thesis.

Candidate's Declaration

I declare that I have complied with the Thesis Examination Procedure.

Acknowledgements

It has been a privilege to work in a great environment with an amazing team during my PhD project. I have learnt so much and was inspired largely from many people.

I would first like to express my sincere gratitude to my supervisors. Prof. Boris Martinac, thank you for providing me this opportunity of academic development and supporting me scientifically and financially together with Prof. Michael P. Feneley. As an internationally renowned biophysicist who has been mentioned by the Nobel Committee (Ernfors, El Manira, & Svenningsson, 2021), you are a role model for people who truly enjoy scientific research. I have been deeply influenced by your optimistic spirit, your tireless work attitude, and no doubt, your sense of humour.

Prof. Michael P. Feneley, it has been an honour to have you as my joint supervisor. As one of the initial founders of the Victor Chang Cardiac Research Institute (VCCRI), and one of the leading cardiologists, you have been providing me exceptionally valuable guidance not only for basic research but also from a clinical point of view, which is extremely important in translational research. I enjoyed your speech every time and have learnt a lot from you on meticulous logical thinking and research strategy.

Dr. Ze-Yan (Jane) Yu, you are a particularly important mentor to me, who made this project come true and implemented it thoroughly. Your expertise and your laughter are an indispensable part of the laboratory. Thank you for all the time and effort you devoted to my research plan, my experiments,

and manuscript writing. I enjoyed our time working together at the lab bench. Your contribution to the publications in this project is greatly appreciated.

Next, I would like to thank the colleagues who have (had) been working with me or helping me on my work. Many of them are the co-authors of my publications included in this thesis.

Dr. Jianxin Wu, thank you for your excellent surgical skills and performance, which helped us to conduct animal studies smoothly.

Mr. Scott Kesteven, thank you for conducting all the animal echo measurements and always helping me in arranging experimental equipment.

Dr. Charles D. Cox, thank you for your help all the time on my *in vitro* studies. Your extensive knowledge, creativity, and critical thinking impressed me a lot and had a very positive influence on me.

To all the other members and former members in the Feneley lab, Martinac and Cox lab, Mr. Hutao Gong, Dr. Louis Wang, Mr. Paul Rohde, Dr. Yury A. Nikolaev, Dr. Pietro Ridone, Dr. Yoshitaka Nakayama, Dr. Valentin Romanov, Dr. Delfine Cheng, Ms. Jinyuan (Vero) Li, Dr. Zijing Zhou, thank you all for your advice, support, and your friendship.

To Prof. Robert M. Graham and the current/former members in his lab, especially Dr. Siiri E. Iismaa, Ms. Sara R. Holman, Ms. Andrea Y. Chan, Dr. Amy M. Nicks, Dr. Xenia Kaidonis, thank you for kindly teaching me the skills for mouse cardiomyocytes isolation/purification, and helping me when I encountered problems in my study.

Prof. Richard P. Harvey, I am grateful to you and your team for donating HL-1 cells and providing cell culture protocols to us.

Dr. Adam P. Hill, thank you for your advice and assistance on membrane potential measurements and analysis. These helped me to improve the quality of my experiments largely.

To Prof. Jamie I. Vandenberg and his lab members, especially Dr. Matthew D. Perry, Dr. Chai-Ann Ng, and Dr. Jordan Thorpe, thank you a lot for helping me with your expertise on electrophysiology.

To Prof. Diane Fatkin and her team, especially Ms. Jasmina Cvetkovska and Dr. Celine Santiago; as well as to Prof. Peter S. Macdonald, Dr. Renjing Liu, Prof. Jason C. Kovacic, and Prof. Roland Stocker's lab members, thank you so much for your help and cooperation in the daily lab work.

Thanks to Dr. Jeffrey McArthur, Dr. Vanessa Lanoue, and Mr. Anton Shpak of the VCCRI Innovation Centre for training me in the use of imaging equipment as well as providing technical support.

Thanks to Mr. Richard Reyes and the VCCRI BioCORE team for taking very good care of our experimental animals.

Thanks to the VCCRI administration team and IT team for always supporting our work.

To our international collaborators, Prof. Dr. Dr. Oliver Friedrich and his team, especially Ms. Anna-Lena Merten, Ms. Ulrike Schöler, Dr. Dominik Schneidereit, and Dr. Sebastian Schürmann, it has been wonderful working with all of you. I enjoyed my time working in your lab at the Friedrich-

Alexander-University Erlangen-Nürnberg, Germany. Thank you all for your contribution to the publications.

To Prof. Rudi Vennekens and Ms. Silvia Pinto, thank you so much for providing us the experimental animals in the best environment for our TRPM4 study. I cherish my work experience in your lab at the Katholieke Universiteit Leuven, Belgium.

Special thanks to my previous supervisor Prof. Miho Saito at Waseda University, Japan, for supporting me from all aspects whether in good times or difficult times. You guided me to develop the basic qualities as a scientific researcher. I am very honoured to be your student.

In addition, I gratefully acknowledge funding from the National Health and Medical Research Council (NHMRC), the German Academic Research Council (DAAD) and Universities Australia (UA) scheme, and the Australian Government Research Training Program.

Last, but certainly not least, I would like to thank my whole family for their unconditional love, continual support, and enormous encouragement. Especially to my wife Eva, thank you for supporting me all these years and making me a better person!

Yang Guo

Publications arising from this thesis

Guo, Y.†, Yu, Z. Y.†, Wu, J., Gong, H., Kesteven, S., Iismaa, S. E., Chan, A. Y., Holman, S., Pinto, S., Pironet, A., Cox, C. D., Graham, R. M., Vennekens, R., Feneley, M. P.*, & Martinac, B.* (2021). The Ca^{2+}-activated cation channel TRPM4 is a positive regulator of pressure overload-induced cardiac hypertrophy. *eLife*, *10*, e66582.

Author contributions of Guo Y: data curation, formal analysis, validation, investigation, methodology, writing-original draft, writing-review and editing.

Guo, Y.†, Merten, A. L.†, Schöler, U., Yu, Z. Y., Cvetkovska, J., Fatkin, D., Feneley, M. P., Martinac, B.*, & Friedrich, O. (2021). *In vitro* cell stretching technology (*IsoStretcher*) as an approach to unravel Piezo1-mediated cardiac mechanotransduction. *Progress in Biophysics and Molecular Biology*, *159*, 22-33.

Author contributions of Guo Y: conceptualization, data curation, formal analysis, methodology, visualization, writing-original draft, writing-review and editing.

Friedrich, O., Merten, A. L., Schneidereit, D., **Guo, Y.**, Schürmann, S., & Martinac, B*. (2019). Stretch in Focus: 2D Inplane Cell Stretch Systems for Studies of Cardiac Mechano-Signaling. *Frontiers in Bioengineering and Biotechnology*, 7, 55.

Author contributions of Guo Y: conducted all *IsoStretcher* experiments and data analysis.

† These authors contributed equally.

* Corresponding author.

Permission for use in this thesis has been granted by the co-authors.

Conference presentations

Guo, Y., Merten, A. L., Yu, Z. Y., Cox, C. D., Feneley, M. P., Friedrich, O., & Martinac, B. (2019). Piezo1 channel activity examined by stretching HL-1 cells using *IsoStretcher* technology. *Proceedings of the 8th International Workshop Cardiac Mechano-Electric Coupling and Arrhythmias*, Poster 5. Universitäts-Herzzentrum Freiburg- Bad Krozingen, Germany.

Guo, Y., Merten, A. L., Schneidereit, D., Cox, C. D., Feneley, M. P., Friedrich, O., & Martinac, B. (2018). The response of mechanosensitive ion channels in cardiac cell stretching stimulation. *Asian Biophysics Association Symposium and Annual Meeting of the Australian Society for Biophysics Abstract Book*, 40. Royal Melbourne Institute of Technology, Australia.

Schöler, U., Merten, A. L., **Guo, Y.**, Martinac, B., Schürmann, S., & Friedrich, O. (2021). *In vitro* mechanical stimulation of an endothelial and a cardiac cell line using a cell stretching device (*IsoStretcher*) and visualization of the stretch induced response via calcium imaging. *The 100th Meeting of the German Physiological Society (Joint meeting with the Austrian Physiological Society and the Life Science Switzerland Physiology Section) Abstract Book*, 468. Goethe University Frankfurt, Germany.

Yu, Z. Y., **Guo, Y.**, Friedrich, O., Feneley, M. P., & Martinac, B. (2019). The role of Piezo1 in cardiac hypertrophy. *Proceedings of the 8th International Workshop Cardiac Mechano-Electric Coupling and Arrhythmias*, 13. Universitäts-Herzzentrum Freiburg-Bad Krozingen, Germany.

Table of Contents

List of figures

Chapter 1 Introduction

This chapter contains work published in:

Guo, Y.†, Yu, Z. Y.†, Wu, J., Gong, H., Kesteven, S., Iismaa, S. E., Chan, A. Y., Holman, S., Pinto, S., Pironet, A., Cox, C. D., Graham, R. M., Vennekens, R., Feneley, M. P.*, & Martinac, B.* (2021). The Ca^{2+}-activated cation channel TRPM4 is a positive regulator of pressure overload-induced cardiac hypertrophy. *eLife*, *10*, e66582.

Author contributions of Guo Y: data curation, formal analysis, validation, investigation, methodology, writing-original draft, writing-review and editing.

Guo, Y.†, Merten, A. L.†, Schöler, U., Yu, Z. Y., Cvetkovska, J., Fatkin, D., Feneley, M. P., Martinac, B.*, & Friedrich, O. (2021). *In vitro* cell stretching technology (*IsoStretcher*) as an approach to unravel Piezo1-mediated cardiac mechanotransduction. *Progress in Biophysics and Molecular Biology*, *159*, 22-33.

Author contributions of Guo Y: conceptualization, data curation, formal analysis, methodology, visualization, writing-original draft, writing-review and editing.

Friedrich, O., Merten, A. L., Schneidereit, D., **Guo, Y.**, Schürmann, S., & Martinac, B*. (2019). Stretch in Focus: 2D Inplane Cell Stretch Systems for Studies of Cardiac Mechano-Signaling. *Frontiers in Bioengineering and Biotechnology*, 7, 55.

Author contributions of Guo Y: conducted all *IsoStretcher* experiments and data analysis.

† These authors contributed equally.

* Corresponding author.

1.1 General introduction

Cardiovascular disease encompasses a range of disorders of the heart and blood vessels. Despite the advances in pharmacological and device therapies, cardiovascular disease remains the leading cause of mortality worldwide (Mudd & Kass, 2008; World Health Organization, 2020). In 2019, there were approximately 18.6 million deaths globally attributable to cardiovascular disease (Virani et al., 2021). In Australia, according to the 2017-2018 National Health Survey, cardiovascular disease is affecting approximately 1.2 million (5.6%) adults (≥18 years of age), who are currently the most extensive group of patients requiring treatment and care (Australian Institute of Health and Welfare, 2020). Caused by many possible factors such as ischemia, hypertension, and valvular abnormalities, left ventricular hypertrophy (LVH) is a major independent predictor of cardiovascular disease outcomes (Okwuosa et al., 2015). LVH is defined as thickening of the left ventricle wall due to the enlargement of the heart muscle (**Figure 1-1**). Initially, LVH can be classified into two types: physiological and pathological, which develop as adaptive responses to physiological and pathological stimuli, correspondingly. Although pathological LVH commonly occurs as a compensatory response to various cardiac stress, it may lead to a variety of heart diseases, such as coronary disease (Kannel, Gordon, Castelli, & Margolis, 1970), stroke, congestive heart failure, and even peripheral arterial disease (Levy, 1988). Therefore, LVH is considered a major risk factor for cardiovascular death (Levy, Garrison, Savage, Kannel, & Castelli, 1990; Mudd & Kass, 2008).

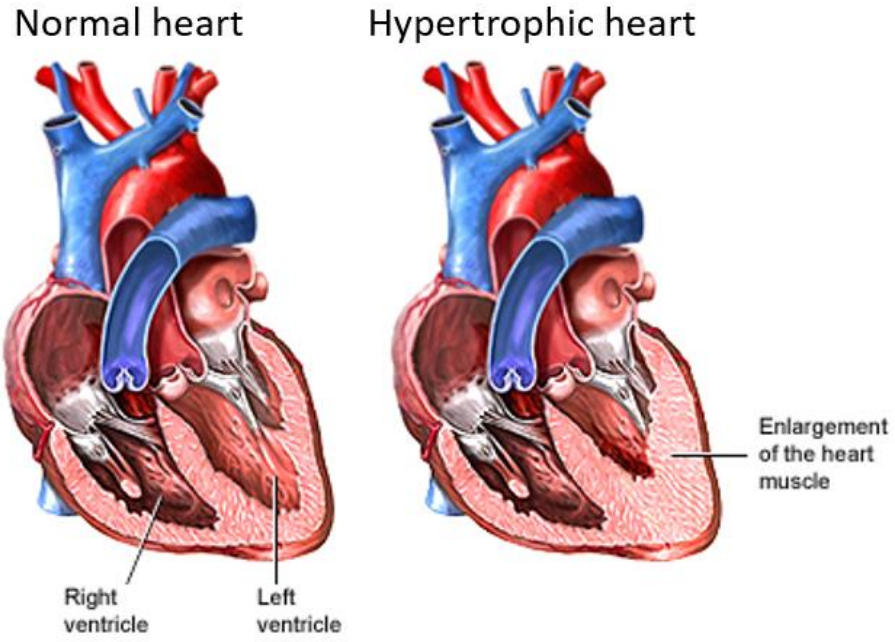

Figure 1-1 Normal heart and hypertrophic heart.

Image adapted from MedlinePlus (2019).

It is known that pathological LVH is regulated by distinct cellular signalling pathways (Tham, Bernardo, Ooi, Weeks, & McMullen, 2015). The mechanisms involved relate not only to the mechanical stress from elevated blood pressure or valvular insufficiency but also to the influences of neurohumoral stimulation, growth factors, and cytokines (Hill & Olson, 2008; Saucerman, Tan, Buchholz, McCulloch, & Omens, 2019a). Among many different triggers of LVH, pressure overload can be considered the most important reason for the clinical risk. So far, the only treatment for this condition is lowering elevated blood pressure or replacing a stenotic aortic valve. However, these treatments cannot completely reverse the pathological effects on the myocardium once LVH is established. Consequently, understanding the molecular mechanisms underlying

pathological LVH may lead to therapies directed at preventing, inhibiting, or reversing pathological LVH, and reducing its associated morbidity and mortality, thus being of significant research and clinical value.

The heart is an electro-mechanical pump. Working as primary molecular transducers of mechanical force of physiological processes (Martinac, 2004, 2012) , mechanosensitive (MS) ion channels may play important roles in the cardiovascular system (Reed, Kohl, & Peyronnet, 2014) by maintaining normal cardiac function or contributing to development of diseases. Thus, they potentially present new targets for therapeutic interventions (Izu et al., 2020; Peyronnet, Nerbonne, & Kohl, 2016; Quinn & Kohl, 2021). Some MS channel candidates, such as the transient receptor potential (TRP) channels and piezo type mechanosensitive ion channel component 1 (Piezo1), have emerged as potential contributors to cardiac hypertrophy. Particularly, in pressure overload-induced LVH, these MS channels may contribute to the initial step by which mechanical stretch associated with cardiac pressure overload is converted into a chemical signal that initiates hypertrophic signalling. However, although the structures of some of these candidates were recently solved using cryogenic electron microscopy (Cryo-EM) technology (Autzen et al., 2018; J. Guo et al., 2017; Saotome et al., 2018; Tang et al., 2018), the activity and involvement of these MS channels in heart and cardiovascular disease remain unclear.

Focusing on two types of ion channels, i.e. transient receptor potential melastatin 4 (TRPM4) and Piezo1, this project investigates the role of the TRPM4 channel in a hypertrophic signalling pathway responding to ventricular pressure overload, using *in vivo* models including wild-type (WT) and conditional gene knockout mice. This project also provides

methodological foundations of new approaches to investigate Piezo1-mediated cardiac mechanotransduction in HL-1 mouse atrial myocyte-like cells and isolated mouse ventricular cardiomyocytes, including using a novel *in vitro* cell stretching technology. Furthermore, this project provides *in vitro* evidence of the functional interaction between the Piezo1 and TRPM4 channels.

1.2 Anatomy and physiology of the healthy heart

1.2.1 Heart structure and blood circulation

The heart is a four-chambered hollow organ that contracts rhythmically to regulate the blood flow within the body. It is divided by a wall called the septum into the left and right side. Furthermore, the left and right sides of the heart are divided into two chambers on the top and bottom. The top chambers are the left atrium (LA) and right atrium (RA), while the bottom chambers are the left ventricle (LV) and right ventricle (RV) (**Figure 1-2**). By this heart structure, in the pulmonary circulation, deoxygenated blood can be carried from the RV to the lungs, and oxygenated blood can return to the LA, then to the LV. In the systemic circulation, oxygenated blood is delivered from the LV to the capillaries in the tissues of the whole body through arteries, while the deoxygenated blood can return to RA through veins (**Figure 1-2**).

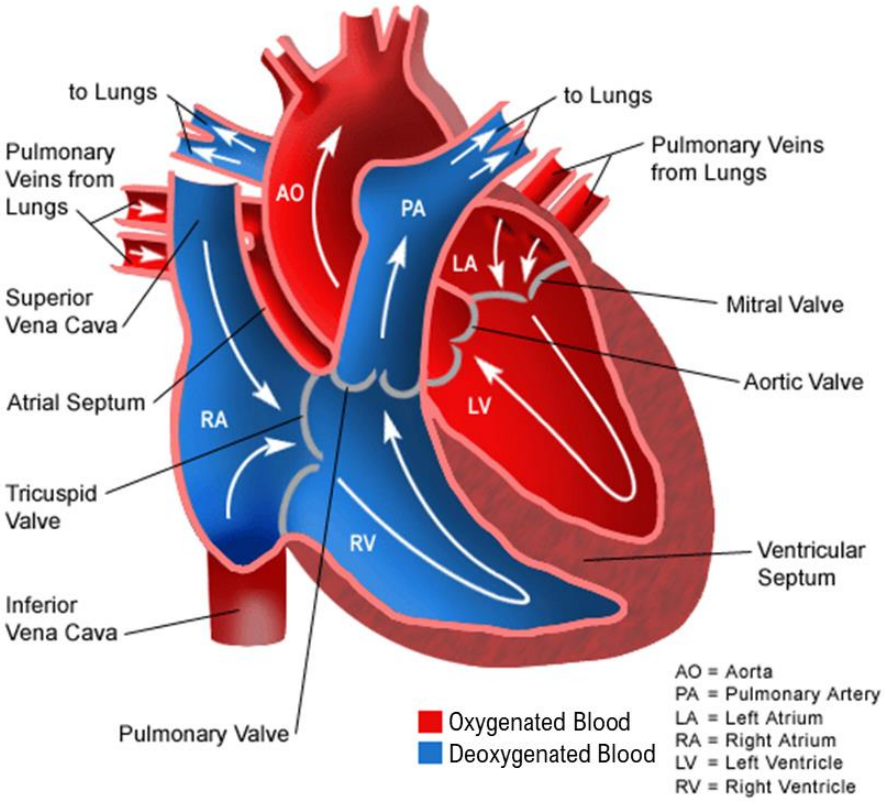

Figure 1-2 Heart structure and blood circulation.

The LV is conducting the main oxygenated blood output from heart to the body, through the largest artery called aorta. The superior vena cava is the large, valveless vein that delivers deoxygenated blood from the upper half of the body to the RA. Image reproduced from Stanford Children's Health (2021).

The heart wall is composed of three layers known as epicardium, myocardium, and endocardium, from outside to inside. These layers are surrounded by the pericardium, a membrane enclosing the heart, consisting of an outer fibrous layer and an inner double serous layer. Most of the heart is myocardium, a muscle layer that enables heart contractions. The myocardium is formed by individual cardiac muscle cells called cardiomyocytes. Although only approximately 30-50% of total number of

cells in human heart are cardiomyocytes (Banerjee, Fuseler, Price, Borg, & Baudino, 2007), they occupy 60-70% of the total heart mass due to their relatively larger size compared to other cells in the heart, e.g. fibroblasts, endothelial cells (ECs), smooth muscle cells, and circulating blood cells (Marian, 2008; Tirziu, Giordano, & Simons, 2010).

1.2.2 Cardiomyocyte structure

Cardiomyocytes are specialised muscle cells that form the cardiac muscle both in the atria and the ventricles. Most cardiomyocytes are binucleated with two separated nuclei located in the centre. Cardiomyocytes are enfolded by a plasma membrane known as the sarcolemma. The sarcolemma is composed of a lipid bilayer which allows sarcolemma's interaction with the intracellular and extracellular environment. The sarcolemma contains membrane proteins including receptors, pumps, and ion channels. These membrane proteins can respond to different stimulations and allow ions such as Ca^{2+}, Na^{+} and K^{+} through the sarcolemma, which is fundamental to the contractile process of cardiomyocytes (Walker & Spinale, 1999). Each cardiomyocyte contains longitudinally arranged myofibrils formed by long chains of sarcomeres, the fundamental structural and functional units of cardiac muscle (**Figure 1-3**). Also, each cardiomyocyte has numerous mitochondria which can supply energy through adenosine triphosphate (ATP) for cellular processes, such as contraction (Fatkin & Graham, 2002).

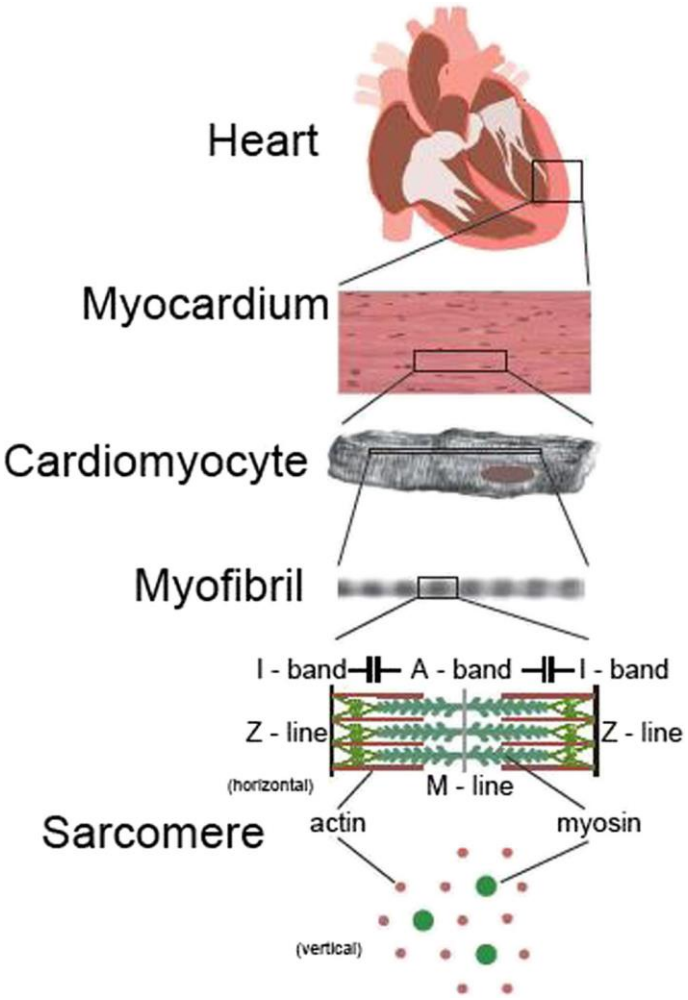

Figure 1-3 Hierarchical structure of heart.

Image adapted from Kagemoto, Li, Dos Remedios, and Ishiwata (2015).

Cardiomyocytes are physically and electrically connected to each other through intercalated disks composed of adherens junctions, desmosomes, and gap junctions (Fatkin & Graham, 2002) (**Figure 1-4**). The intercalated disks provide strong mechanical linkage and allow rapid conduction of action potential between cardiomyocytes (Walker & Spinale, 1999). This co-ordinated three-dimensional beating structure allows a concerted contractile activity of cardiomyocytes.

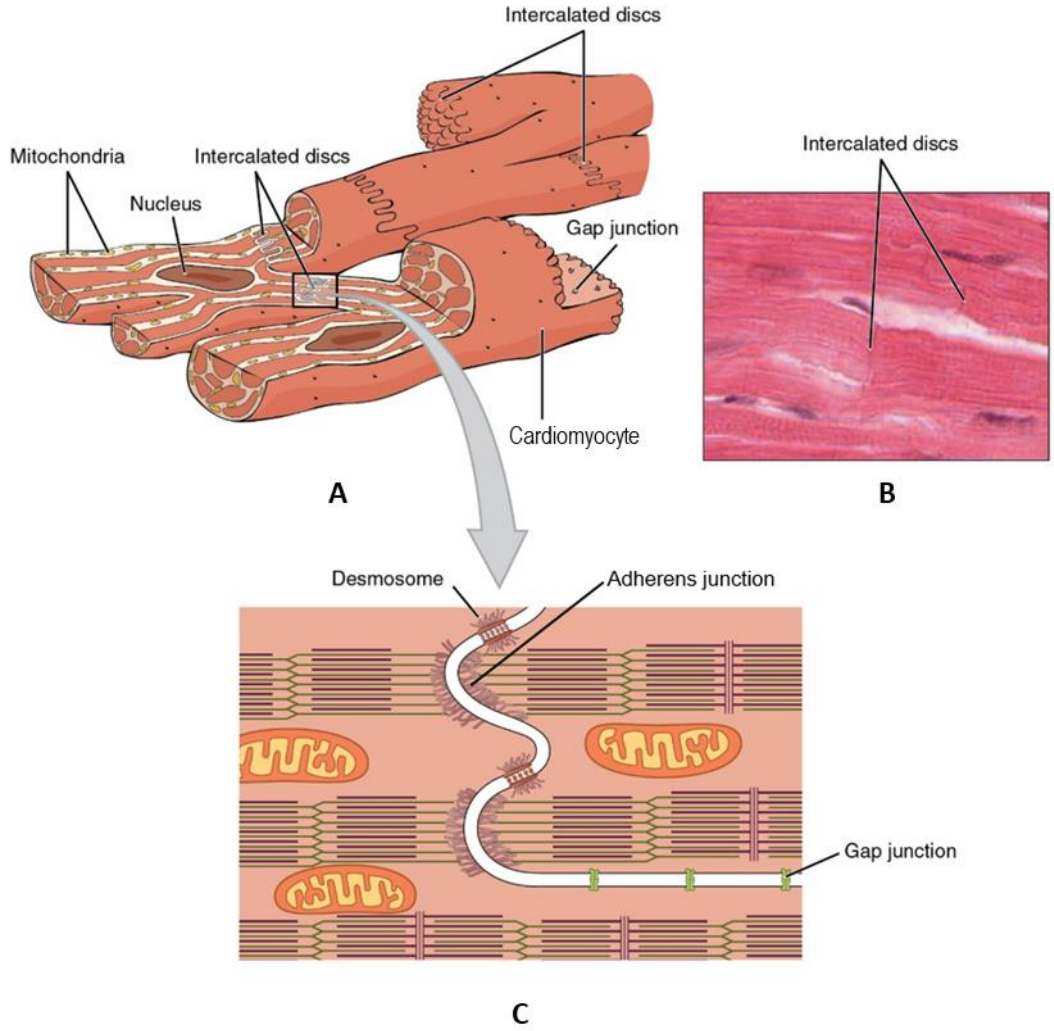

Figure 1-4 Cardiomyocytes connected by intercalated discs.

(A) Cardiomyocytes containing nucleus, mitochondria, and intercalated discs. (B) A photomicrograph of nucleus and intercalated discs in cardiomyocytes. (C) Cardiomyocytes connected by an intercalated disc comprised of adherens junctions, desmosomes, and gap junctions. Image reproduced from OpenStax College (2021).

1.2.3 Cardiac conduction system

The contractions of cardiac muscles, including the rate and rhythm, are controlled by electrical signals by the cardiac conduction system (**Figure 1-5**). At the beginning of each heartbeat, the electrical signal is normally

generated from the pacemaker cells located in the sinoatrial (SA) node in the RA. The signal excites RA, also travels through Bachmann's bundle to excite LA, causing the atria to pump blood into the ventricles. After that, via the internodal pathways, the signal reaches the atrioventricular (AV) node located between the atria and the ventricles. From the AV node, the signal then travels through the bundle of His and further down to the bundle branches, fibres specialised for rapid transmission of electrical signals, on either side of the interventricular septum. Both bundle branches terminate in the millions of small fibres projecting throughout the myocardium, which are called Purkinje fibres. The right and left bundle branches can depolarise the RV and LV, respectively. This depolarisation can cause the ventricles to contract and pump blood out. After that, the ventricles relax and the whole heartbeat process starts all over again in the SA node (Anderson, Yanni, Boyett, Chandler, & Dobrzynski, 2009; National Heart, Lung, and Blood Institute, 2021; Renwick, Kerr, McTaggart, & Yeung, 1993).

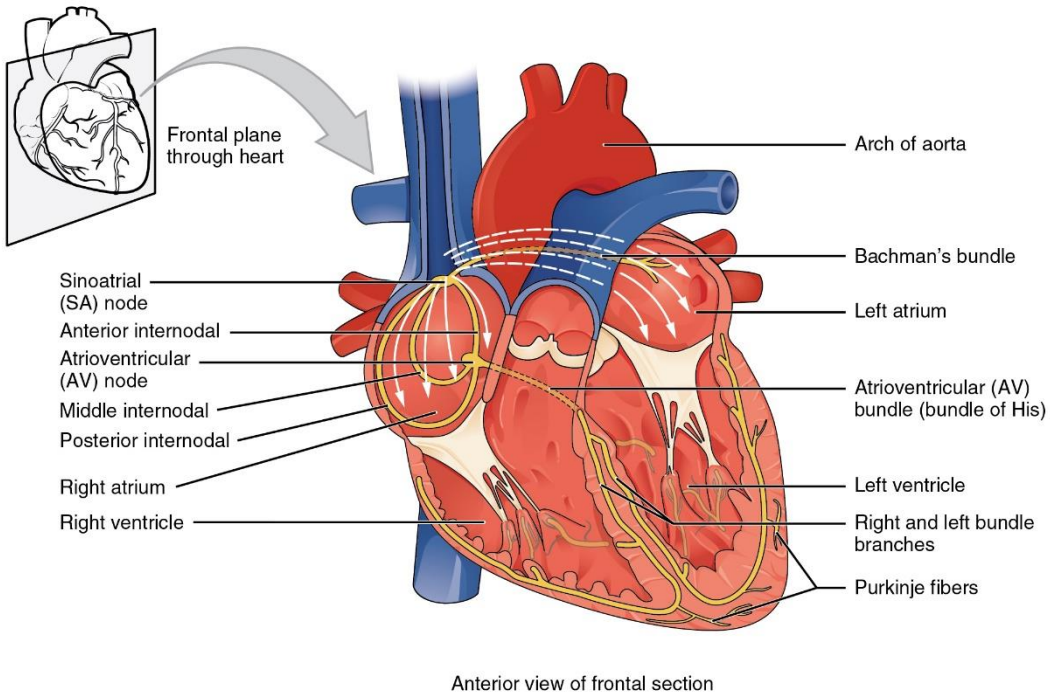

Figure 1-5 Cardiac conduction system.

The cardiac conducting components include the sinoatrial (SA) node, the Bachman's bundle, the internodal pathways, the atrioventricular (AV) node, the AV bundle, the right and left bundle branches, and the Purkinje fibres. Image adapted from OpenStax College (2021).

1.2.4 Cardiac electrophysiology

1.2.4.1 Cardiac ion channels

There are two major forces driving ions across cell membranes: chemical potential and electrical potential (Amin, Tan, & Wilde, 2010). Ion channels are proteins that respond to various stimuli to either allow or prevent the movement of specific ions across a cell membrane by changing their conformation. Each ion channel is coded by a unique set of DNA instructions which is expressed as a gene. The fundamental properties of ion channels

include ion permeation and gating (Hille, 1984), which allow the ion movement through the open channel, involving the mechanism of channel opening and closing (Grant, 2009). Based on size, valency, and hydration energy, etc., the selective permeability of ion channels to specific ions is a basis of classification of ion channels, e.g. Na^+, K^+, and Ca^{2+} channels.

Na^+ channels are the major type of voltage-gated ion channels. Via the activities of the voltage-gated Na^+ channels, the membrane potential is transduced into intracellular Na^+ transients which initiate many physiological events including affecting other downstream ion channels. For example, in non-pacemaker cardiac muscle cells, depolarisation of the cell membrane opens voltage-gated Na^+ channels to generate an early Na^+ current peak ($I_{Na,early}$) which causes the upstroke of the non-pacemaker action potential (Horvath et al., 2020; Mitsuiye & Noma, 2002; Scanley, Hanck, Chay, & Fozzard, 1990). After that, during the action potential plateau phase (shown later), Na^+ channels may recover from inactivation and reopen, generating a late Na^+ current ($I_{Na,late}$), which also contribute to the action potential morphology (Horvath et al., 2020). The cardiac Na^+ channels have consensus sites for phosphorylation by protein kinase A (PKA), protein kinase C (PKC), and Ca^{2+}/calmodulin (CaM) kinase (Grant, 2009). They are involved in the modulation of Na^+ and Ca^{2+} homeostasis of cardiomyocytes, playing important pathophysiological roles in the heart. Studies have shown that mutations in cardiac Na^+ channel gene is associated with cardiac arrhythmias (Clancy & Kass, 2005; Remme & Bezzina, 2010), causing Long QT syndrome, Brugada syndrome, primary cardiac conduction system disease, and even dilated cardiomyopathy (Clancy & Kass, 2005; Horvath et al., 2020). Clinically, classic small-molecule

Na^+ channel inhibitors include local anaesthetics, anticonvulsants, and antiarrhythmic agents such as lidocaine, carbamazepine, phenytoin, lamotrigine, and mexiletine (Horvath et al., 2020; Ragsdale, McPhee, Scheuer, & Catterall, 1996).

In the cardiovascular system, as an important (likely the most important) intracellular signalling ion, Ca^{2+} is involved in the modulation of action potential (details described in **1.2.4.2**), excitation-contraction coupling (details described in **1.2.4.3**), cell contraction, energy consumption and production (via the regulation of mitochondrial ATP production), cell death by apoptosis or necrosis, and transcriptional regulation (via, e.g. CaM-dependent activation) (Bers, 2002, 2008; Bers & Perez-Reyes, 1999; Clapham, 2007; Eisner, Caldwell, Kistamas, & Trafford, 2017; Grant, 2009). Ca^{2+} channels are the principal portal of the extracellular Ca^{2+} entry into the cells. In addition, the Intracellular Ca^{2+} storage system and Ca^{2+} transporters such as the Na^+/Ca^{2+} exchanger (NCX) are also contributing to intracellular Ca^{2+} modulation (Barcenas-Ruiz, Beuckelmann, & Wier, 1987; Bers, 2008; Grant, 2009; Sammels, Parys, Missiaen, De Smedt, & Bultynck, 2010). The majority of Ca^{2+} transport into the cardiac muscle cells is due to the activities of voltage-gated Ca^{2+} channels including the low threshold-type (L-type) and transient-type (T-type) Ca^{2+} channels (Bers & Perez-Reyes, 1999; Grant, 2009; Mesirca, Torrente, & Mangoni, 2015). In addition, some non-selective polyvalent ion channels which are permeable to Ca^{2+}, e.g. Piezo1 (details described later), are also involved in the intracellular Ca^{2+} influx. The activities of Ca^{2+} channels are associated with cardiac arrhythmias and hypertension, which can further lead to various heart diseases such as coronary artery disease, hypertrophic cardiomyopathy, even heart failure.

L-type Ca^{2+} channels are mainly expressed in the hearts and peripheral vasculature. They are generally targeted by Ca^{2+} channel antagonists for hypertension therapeutic purposes. Clinically relevant L-type Ca^{2+} channel blockers include 3 subclasses: the phenylalkylamines (e.g. verapamil), the benzothiazepines (e.g. diltiazem), and the dihydropyridines (e.g. nifedipine, amlodipine, isradipine) (Abernethy & Schwartz, 1999; Godfraind, 2017; Sica & Prisant, 2007). T-type Ca^{2+} channels are also expressed in various cell types in the heart, such as neurons, cardiomyocytes, vascular smooth muscle cells (SMCs) and endocrine cells. They have been shown to play an important role in the regulation of cardiovascular function, contributing to generation of pacemaker potential and regulation of arterial resistance. However, the clinical value of some T-type Ca^{2+} channels blockers including manidipine, nilvadipine, benidipine and efonidipine is still controversial, because they might also inhibit L-type Ca^{2+} channels (W. Ge & Ren, 2009; McGivern, 2006; Perez-Reyes, 2003). In addition, for *in vitro* studies on the cardiovascular system, some Ca^{2+} antagonist such as nifedipine, nisoldipine, isradipine were used as selective L-type Ca^{2+} channel blockers (Sica & Prisant, 2007).

Notedly, it has been indicated that Na^{+} and Ca^{2+} homeostasis is linked in cardiomyocytes. Firstly, the Na^{+} and Ca^{2+} are directly connected via the activities of the NCX, a secondarily active transporter protein that can exchange Ca^{2+} and Na^{+} at a ratio of 1:3 (Despa & Bers, 2013; Fujioka, Hiroe, & Matsuoka, 2000; Ginsburg, Weber, & Bers, 2013; Hilgemann, 1990; Janvier & Boyett, 1996). The function of NCX is via two different activities. Initially, it removes Ca^{2+} from the cardiomyocytes using the energy from the electrochemical gradient of Na^{+} influx, which is known as the forward mode

of NCX. Also, accumulation of intracellular Na^+ may force the NCX into the reverse mode, removing Na^+ and causing Ca^{2+} influx from the extracellular domain (Horvath et al., 2020; Philipson et al., 2002; Tykocki, Jackson, & Watts, 2012). Secondly, the activation of Na^+ channels can increase Na^+ influx and depolarise the cell membrane. Consequently, voltage-gated Ca^{2+} channels can be activated by the increased membrane potential and allow further Ca^{2+} entry into the cardiomyocyte (Banyasz, Horvath, Jian, Izu, & Chen-Izu, 2012; Horvath et al., 2020). Interestingly, studies have also shown that Na^+ channels may be regulated by Ca^{2+} (Wingo et al., 2004), although this effect may be mediated via Ca^{2+}-CaM complex (Kim et al., 2004; Tan et al., 2002).

There are three types of cardiac K^+ channels: voltage-gated channels, inward rectifier channels, and the background K^+ currents (Grant, 2009). Cardiac K^+ channels are playing an essential role in regulating the resting membrane potential, the heart rate, and the action potential form (Snyders, 1999; Tamargo, Caballero, Gomez, Valenzuela, & Delpon, 2004). The activities of these channels are contributing to the regional differences of the action potential configuration in the heart, such as in the atria, the ventricles, and across the myocardial wall (Clancy & Kass, 2005; Grant, 2009; Snyders, 1999; Tamargo et al., 2004). Particularly, voltage- and Ca^{2+}-dependent big K^+ (BK) channels (Takahashi & Naruse, 2012) conduct large amounts of K^+ ions across the cell membrane. Studies have indicated that BK channels are contributing to the regulation of heart rate and the cardioprotection during ischaemia (Imlach, Finch, Miller, Meredith, & Dalziel, 2010; Peyronnet et al., 2016; Xu et al., 2002). Also, genetic variants of BK channels may associate with systolic and general hypertension, and

increased risk of myocardial infarction (Peyronnet et al., 2016; Tomas et al., 2008). A selective BK channel opener NS 1619 (Olesen, Munch, Moldt, & Drejer, 1994) has been widely used in basic studies. Generally, inhibition of certain K^+ channel(s) can prolong the action potential duration and refractoriness without slowing impulse conduction (Snyders, 1999; Surawicz, 1992; Tamargo et al., 2004; Weisbrod, 2020). However, clinically used drugs that delay the repolarization may also cause long QT syndrome (Clancy, Kurokawa, Tateyama, Wehrens, & Kass, 2003; Roden, Balser, George, & Anderson, 2002).

1.2.4.2 Cardiac action potential

The cardiac action potential is a voltage change across the membrane of cardiac cells, caused by a sequence of ion influxes through the specialised ion channels (Nerbonne & Kass, 2005). Na^+, K^+, and Ca^{2+} channels are the major driving force of the cardiac action potentials. The NCX is also contributing to the cardiac action potentials by generating inward or outward currents (Armoundas, Hobai, Tomaselli, Winslow, & O'Rourke, 2003; Grant, 2009; Nerbonne & Kass, 2005).

The action potentials of cardiac conductive cells and contractile cells have different features. In contractile cells such as the ventricular myocytes, the action potential is composed of 5 phases shown below, beginning with phase 4 (**Figure 1-6**) (Grant, 2009; Nerbonne & Kass, 2005):

1) Phase 4 is the stable resting phase.

2) Phase 0 is the rapid depolarisation phase driven by influx of Na^+. The membrane potential shifts into positive voltage range.

3) Phase 1 is the early repolarization phase which sets the potential for the next phase.

4) Phase 2 is a plateau phase which is the longest part in the action potential. It represents the Ca^{2+} entry into the cell.

5) Phase 3 is a final repolarization phase that restores the membrane potential to its resting value.

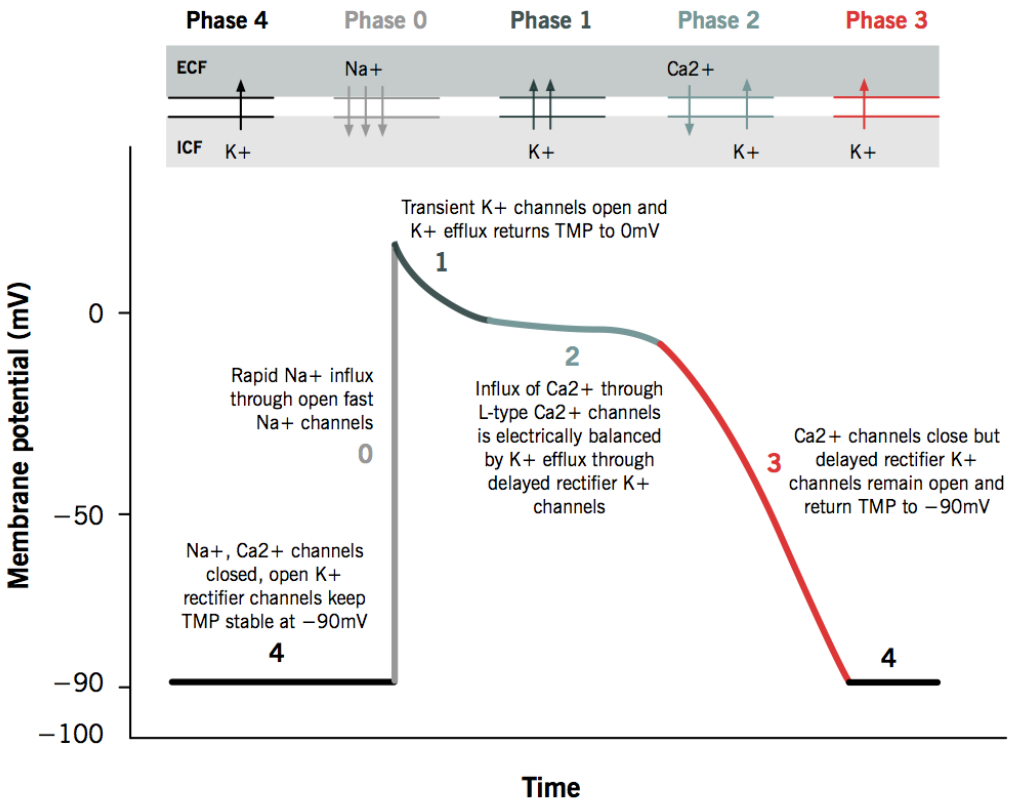

Figure 1-6 Schematic representation of ventricular action potential.

ECF: extracellular fluid; ICF: Intracellular fluid. The channel activities in different phases of the action potential are as marked. Image reproduced from McMaster Pathophysiology Review (2021).

The pacemaker cells, such as the SA node cells, can generate spontaneous depolarisation to trigger action potential, without external stimulations. There are no rapid depolarisation phase and plateau phase in the action potential of pacemaker cells (**Figure 1-7**) (Klabunde, 2011; McMaster Pathophysiology Review, 2021). The sequence of events for pacemaker action potential is shown below (Baruscotti, Bucchi, & Difrancesco, 2005; DiFrancesco & Borer, 2007; Grant, 2009; Klabunde, 2011; Nerbonne & Kass, 2005):

1) Phase 4: A slow influx of Na^+ creates a spontaneous slow depolarisation, which is called the "funny" current (I_f). While the membrane potential reaches to approximate -50 mV, the T-type Ca^{2+} channels open and continue slow depolarisation. When the membrane potential reaches to about -40 mV, the L-type Ca^{2+} channels open and depolarise cell membrane.

2) Phase 0: The L-type Ca^{2+} channels are primarily driving the further depolarisation. The upstroke slope is slower than that in contractile cells due to the lack of large Na^+ currents and rapid Ca^{2+} movement via channels.

3) Phase 3: The L-type Ca^{2+} channels become inactivated and close. Voltage-gated K^+ channels open and the outward K^+ currents cause repolarization.

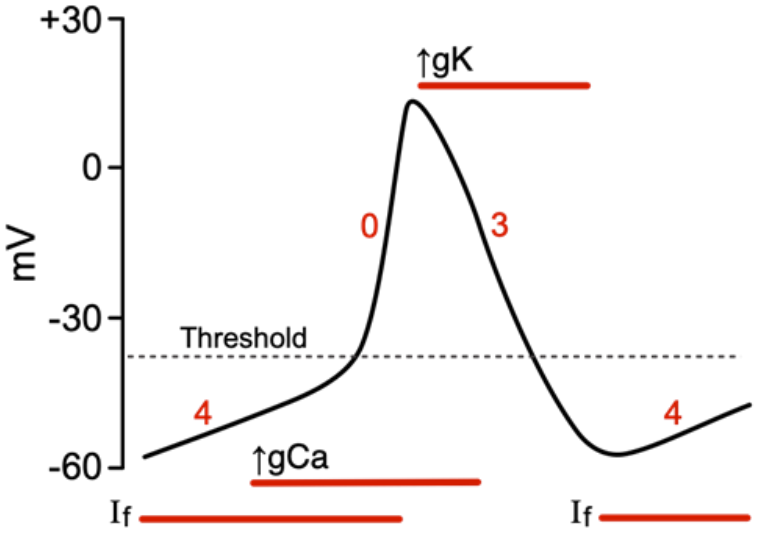

Figure 1-7 Schematic representation of SA node action potential.

A slow Na^+-driven prepotential is followed by a Ca^{2+}-driven depolarisation and a repolarization due to the outflux of K^+. I_f: the "funny" current, gCa: Ca^{2+} conductance, gK: K^+ conductance. Image adapted from Klabunde (2011).

In healthy heart, the electrophysiological behaviour is determined by ordered propagation of excitatory stimuli, which cause depolarisation and repolarization, thereby generating action potentials in individual myocytes (Roden et al., 2002). Also, all cardiac myocytes including pacemaker cells are electrically coupled through gap junctions, the transmembrane complexes of connexin proteins (Lambiase & Tinker, 2015; Moscato et al., 2018; Severs et al., 2001). An action potential in one individual cell will cause all neighbouring cells to depolarise, resulting in synchronous contractions. The cell with the highest inherent rate of pacemaker activity will have dominance to set the heart rate. Other pacemaker cells will be

depolarised and rendered inactive by this stimulus (Nerbonne & Kass, 2005). This mechanism allows the heart chambers to act as a unit.

1.2.4.3 Cardiac excitation-contraction coupling and mechano-electric coupling

Cardiac excitation-contraction coupling is the process whereby myocardial electrical excitation initiated from the SA node generates cellular action potentials, to give rise to mechanical activation, triggering the contractile activities of cardiac myocytes (Bers, 2002; Eisner et al., 2017) (**Figure 1-8** red box and arrows). This process is closely associated with intracellular Ca^{2+} handling, as intracellular Ca^{2+} concentration is playing a major role in the regulation of action potential and cardiac contractility. To maintain basic physiological function, a sufficiently high intracellular Ca^{2+} concentration is needed in systole and a low concentration is needed for diastole (Bers, 2002; Eisner et al., 2017). In ventricular myocytes, during the cardiac action potential, Ca^{2+} enters the myocyte mainly through depolarisation-activated Ca^{2+} channels located in the transverse tubule (T-tubule) system, as inward Ca^{2+} current (**Figure 1-9**). The Ca^{2+} entry can also trigger Ca^{2+} release from downstream systems such as the sarcoplasmic reticulum (SR), to further increase intracellular Ca^{2+} concentration through the activities of SR Ca^{2+} release channels (or ryanodine receptors; RyRs) and phospholamban (PLB) (Bers, 2002). This increase allows Ca^{2+} to bind to and activate the myofilament protein troponin C, which can switch on the contractile activity (Bers, 2002). While for relaxation following the contraction, the intracellular Ca^{2+} concentration decreases via the Ca^{2+} outflux through pathways including SR Ca^{2+}-ATPase, sarcolemmal Na^{+}/Ca^{2+} exchange, Ca^{2+}-ATPase and

mitochondrial Ca^{2+} uniport, resulting in the dissociation of Ca^{2+} and troponin (Bers, 2002) (**Figure 1-9**).

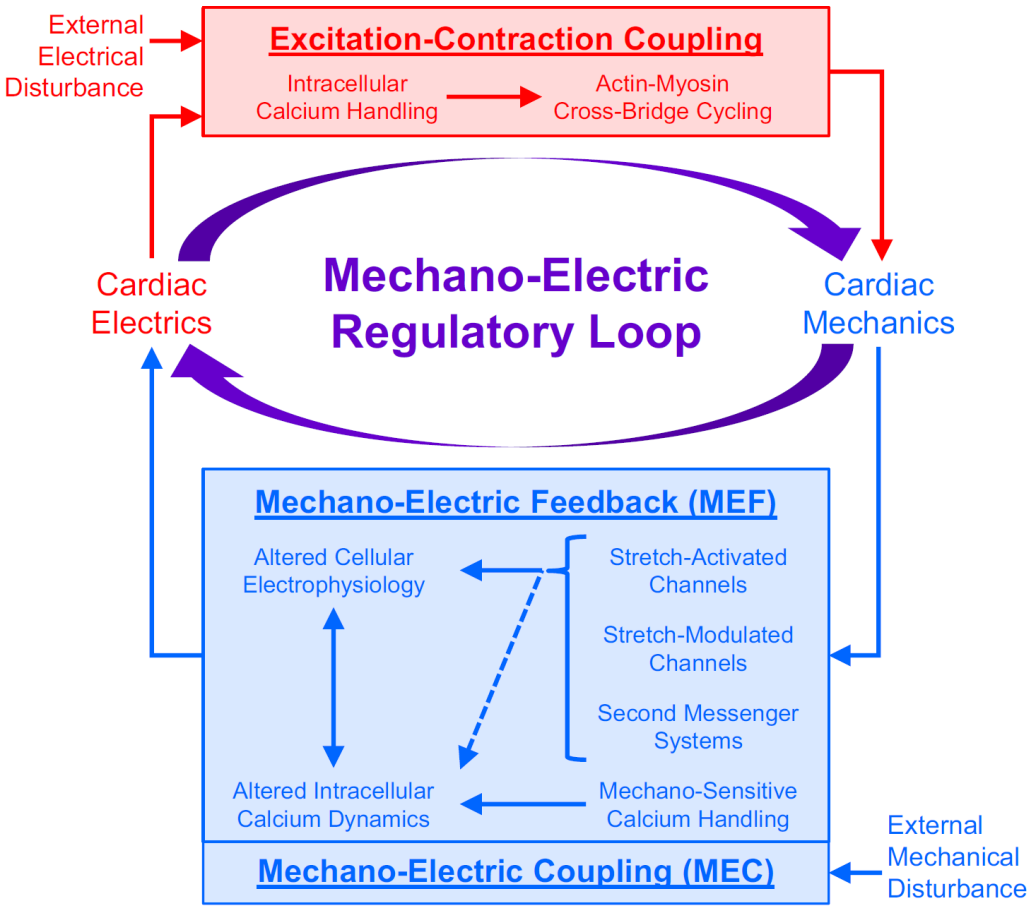

Figure 1-8 Cardiac mechano-electric coupling and excitation-contraction coupling.

Image adapted from Quinn and Kohl (2021).

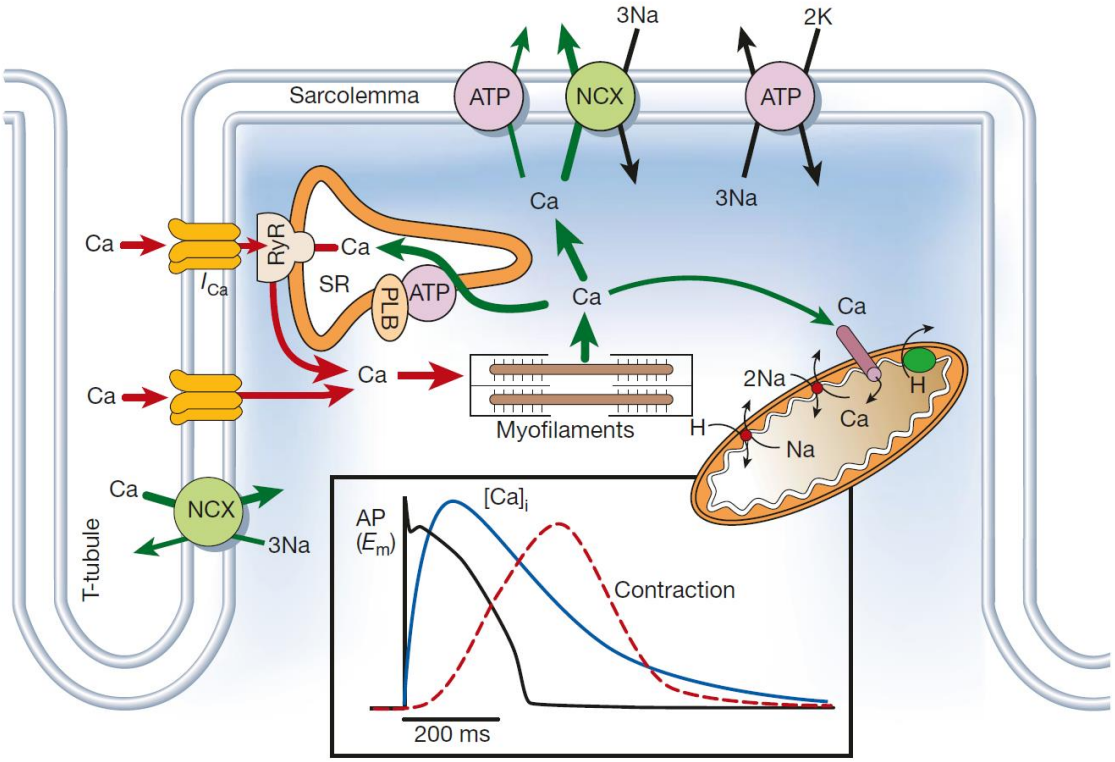

Figure 1-9 Schematic representation of Ca^{2+} transport in rabbit ventricular myocytes.

Inset in black box shows the time course of an action potential (AP, black trace), Ca^{2+} transient (blue trace) and contraction (red trace). I_{Ca}: inward Ca^{2+} current; $[Ca]_i$: intracellular Ca^{2+} concentration; NCX: Na^+/Ca^{2+} exchange; ATP: ATPase; PLB: phospholamban; SR: sarcoplasmic reticulum; RyR: ryanodine receptors. Image adapted from Bers (2002).

In the opposite direction, the cardiac electrical activities are affected by the mechanical status of the heart, including internal and external mechanical disturbances. In the mechano-electric coupling of cardiomyocytes (**Figure 1-8** blue box and arrows), the mechanical forces caused by myocardial deformation can affect the origin and spread of electrical excitation, involving intracellular Ca^{2+} dynamics via multiple interdependent mechano-

sensitive mechanisms (Quinn & Kohl, 2021). Notedly, apart from this acute mechano-electric feedback, medium-term gene expression changes, or longer term electrophysiological, mechanical, and structural remodelling caused by chronic mechanical alterations and heart disease may also affect the cardiac electrics (Michalak & Agellon, 2018; Quinn & Kohl, 2021).

1.3 Cardiac hypertrophy

1.3.1 Types of LVH

As its major function, the heart is responsible for maintaining the blood perfusion of peripheral organs in the body, under both normal and stress conditions. In adult heart, in order to adapt to circumstances with increased preload or afterload, instead of an increase in cardiomyocyte number, individual cardiomyocytes increase in size and the heart enlarges to develop cardiac hypertrophy (Porrello et al., 2011; Soonpaa & Field, 1998; Tam, Gu, Mahdavi, & Nadal-Ginard, 1995). In the heart, LV is the main output chamber of oxygenated blood to the body. In LVH, responding to an increased workload, following Laplace's law, left ventricular wall thickness is increased to reduce ventricular wall stress to maintain its function and cardiac efficiency.

Essentially, cardiac hypertrophy can be classified into two types: physiological hypertrophy and pathological hypertrophy (**Figure 1-10**). Both types of hypertrophy can be considered adaptive responses to cardiac stress. However, they vary widely in their molecular mechanisms, cardiac phenotype, and prognosis. Each type of hypertrophy is regulated by distinct cellular signalling pathways (Tham et al., 2015). In physiological

hypertrophy, the heart can continuously maintain its function. However, pathological hypertrophy may lead to further adverse cardiovascular events, such as arrhythmias, heart failure, even sudden death (Nakamura & Sadoshima, 2018). Confirmed by a series of studies, pathological LVH has been identified as the single strongest predictor of heart failure and the major risk factor for cardiovascular mortality (Levy et al., 1990; Mudd & Kass, 2008).

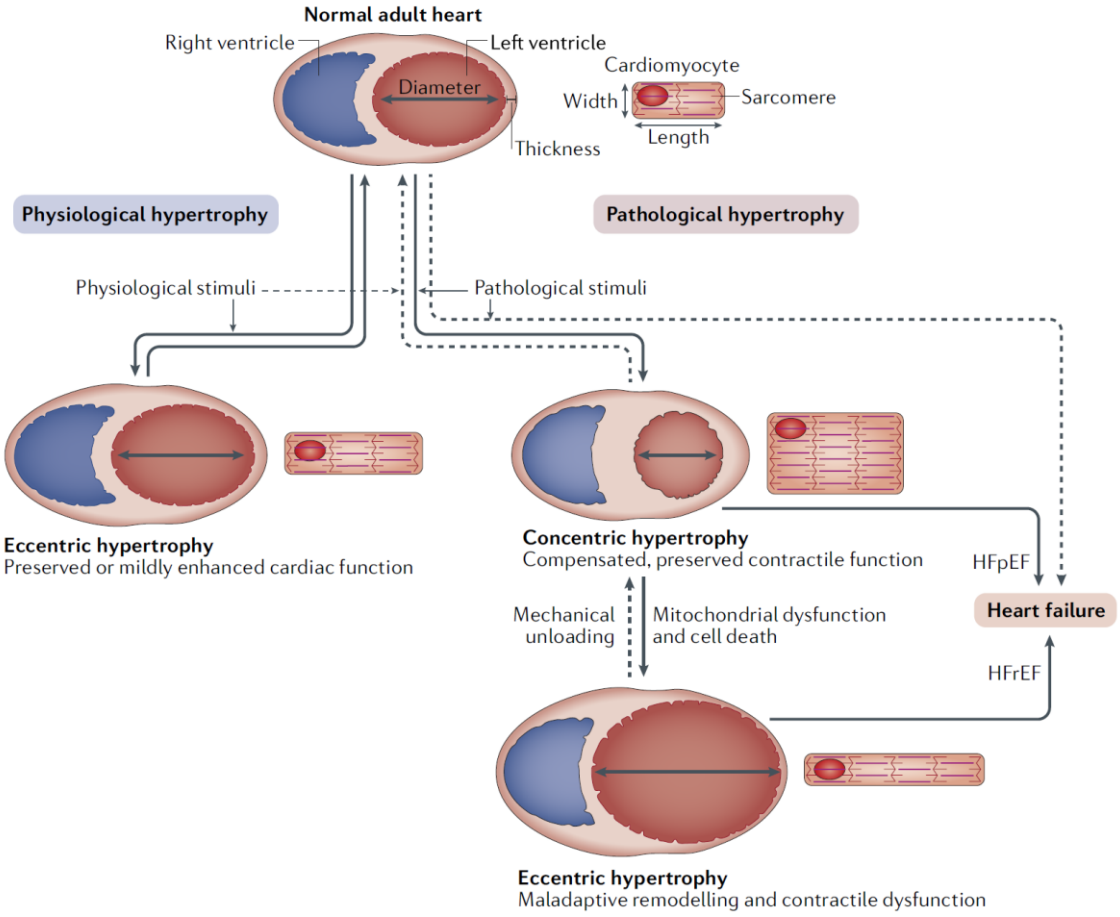

Figure 1-10 Overview of physiological and pathological hypertrophy.

Image adapted from Nakamura and Sadoshima (2018).

1.3.2 Triggers and characteristics of pathological LVH

Development of pathological hypertrophy is based on the upstream stimuli and signalling mechanisms (Maillet, van Berlo, & Molkentin, 2013; Tham et al., 2015; van Berlo, Maillet, & Molkentin, 2013). Pathological LVH could be induced by pressure overload (hypertension or aortic stenosis), volume overload (mitral and aortic regurgitation and chronic kidney disease), myocardial hypoxia (myocardial infarction, obesity, diabetes mellitus, ageing, chronic obstructive pulmonary), storage diseases (lipid, glycogen, or misfolded protein diseases), and inherited diseases (hypertrophic cardiomyopathy, etc.) (Nakamura & Sadoshima, 2018) (**Table 1-1**). Among these triggers, pressure overload-induced LVH could be considered the most important reason for the clinical risk.

Pathological LVH manifests as enlarged cardiomyocyte size (Porrello et al., 2011; Soonpaa & Field, 1998) and increase in heart mass, especially LV mass. The hypertrophy is associated with alterations within cardiomyocyte, such as impaired Ca^{2+} handling, metabolic reprogramming, mitochondrial dysfunction, altered sarcomere structure, and cell death including apoptosis and autophagy. Increased gene expression of natriuretic peptide A (ANP; *Nppa*), natriuretic peptide B (BNP; *Nppb*), myosin heavy chain cardiac muscle β-isoform (*MYH7/Myh7*), and skeletal muscle α- actin (α-SA; *Acta1*), etc., can be observed in pathological LVH as its indicators. In extracellular matrix, interstitial and perivascular fibrosis could be observed with increased levels of type I collagen and fibroblast activation. In addition, insufficient angiogenesis may occur in pathological LVH. As pathological LVH is a compensatory response with LV concentric growth, the contractility is usually preserved at normal level. However, during the

progresses of maladaptive remodelling, it may develop into decompensated eccentric hypertrophy, by which contractile dysfunction may occur and it will lead to heart failure (Nakamura & Sadoshima, 2018) (**Table 1-1**).

Table 1-1 Triggers and characteristics of hypertrophy.

Adapted from Nakamura and Sadoshima (2018).

Triggers and characteristics	Physiological hypertrophy	Pathological hypertrophy
Triggers	• Normal postnatal growth • Pregnancy • Exercise	• Pressure overload owing to hypertension or aortic stenosis • Volume overload induced by mitral and aortic regurgitation and chronic kidney disease • Myocardial hypoxia as a result of myocardial infarction, obesity, diabetes mellitus, ageing, chronic obstructive pulmonary disease, or anaemia • Storage diseases (lipid, glycogen, or misfolded protein diseases) • Inherited diseases such as hypertrophic cardiomyopathy
Reversibility	Yes	Might be possible with treatment
Adaptivity	Adaptive	Adaptive (initially) and maladaptive (advanced)
Cardiomyocyte size	Increased	Increased
Contractility	Preserved or increased	Preserved or decreased
Heart failure	No	Yes (heart failure with preserved ejection fraction, or with reduced ejection fraction at end stage)
Fibrosis	No	Yes (advanced)
Type I collagen levels	Unchanged	Increased
Myofibroblast activation	Unchanged	Yes (such as increased smooth muscle α-actin)
Cardiomyocyte death	No	Yes (advanced)
Capillary network	Increased and sufficient for nourishment	Insufficient for nourishment and oxygenation
Concentric or eccentric	Eccentric greater than concentric and/or mild growth	Concentric or eccentric (advanced) and/or severe wall thickness growth
Maladaptive remodelling	No	Yes
Fetal genes	Unchanged or decreased	Increased (for example, *ACTA1*, *MYH7*, *NPPA*, and *NPPB*)

1.3.3 Mechanism of pathological LVH

Pathological LVH could be induced by neuroendocrine hormones (e.g. angiotensin II; AngII) or mechanical forces (e.g. pressure overload), through

the activation of distinct cellular signalling pathways. These signalling can promote maladaptive cardiac remodelling and dysfunction, and eventually induce heart failure (**Figure 1-11**). Inhibition of the signalling pathways is thought to have potential therapeutic effect to LVH (Mudd & Kass, 2008; Tamargo & Lopez-Sendon, 2011).

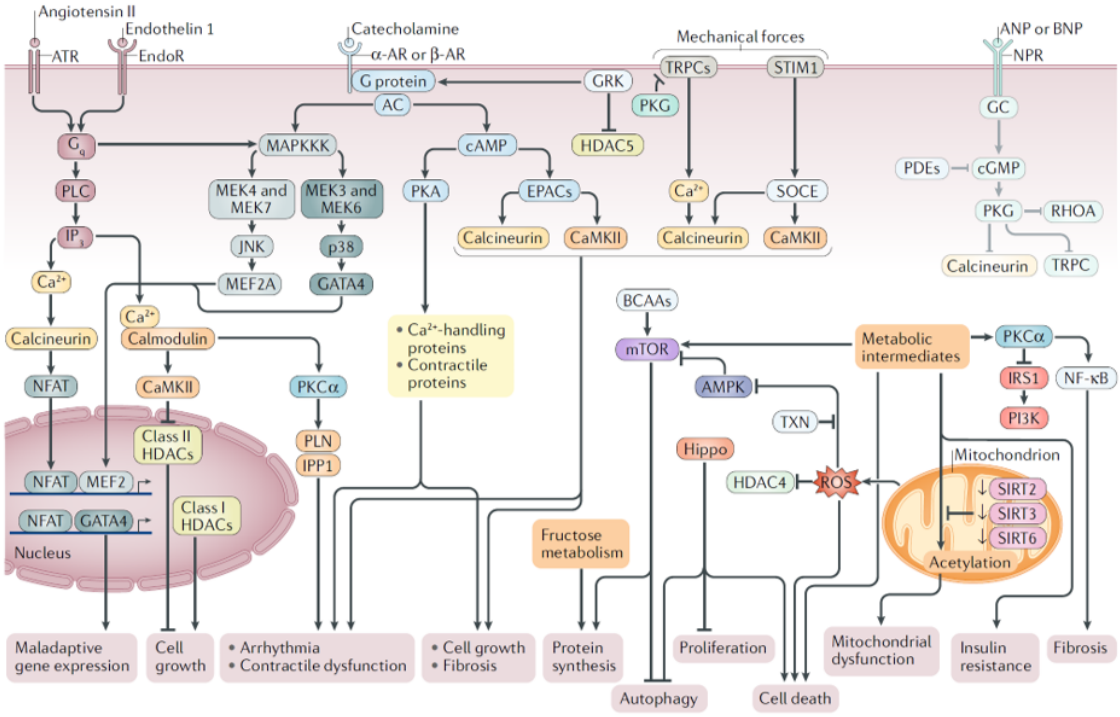

Figure 1-11 Pathological hypertrophy signalling pathways.

Image reproduced from Nakamura and Sadoshima (2018).

A large body of work implicates that the increase of intracellular Ca^{2+} and the activation of Ca^{2+}/CaM dependent pathways are necessary for the induction of pathological LVH (Bers, 2008; Kehat & Molkentin, 2010; Molkentin, 2000, 2013; Molkentin et al., 1998; Wilkins et al., 2004; Wilkins

& Molkentin, 2004; Zarain-Herzberg, Fragoso-Medina, & Estrada-Aviles, 2011). Gq-coupled receptors are thought to play an important role in the induction of pathological LVH that respond to both neurohumoral stimulation such as AngII, catecholamines and endothelin-1 (Adams et al., 1998; Paradis, Dali-Youcef, Paradis, Thibault, & Nemer, 2000), and mechanical forces such as the increase in LV afterload induced by experimental aortic constriction (Keys, Greene, Koch, & Eckhart, 2002). Also, mechanosensors such as the TRP channels (Eder & Molkentin, 2011) and the stromal interaction molecule 1 (STIM1) (Benard et al., 2016; Correll et al., 2015; Luo et al., 2012; Troupes et al., 2017) were reported to activate certain LVH signalling pathways owing to their responses to mechanical forces.

In pathological LVH, the activation of the Ca^{2+}/CaM-dependent phosphatase, calcineurin, can dephosphorylate the transcriptional regulator, nuclear factor of activated T cells (NFAT), promoting its translocation into the nucleus, resulting in activation of transcription factor GATA4 to initiate hypertrophic gene transcription (Kehat & Molkentin, 2010; Molkentin, 2000, 2013; Molkentin et al., 1998; Wilkins et al., 2004; Wilkins & Molkentin, 2004). On the other hand, activation of Ca^{2+}/CaM-dependent kinase II (CaMKII) can phosphorylate histone deacetylase 4 (HDAC4), promoting its nuclear export and relieving its inhibition of the critical nuclear transcriptional regulator, myocyte enhancer factor 2 (MEF2), to enhance hypertrophic gene transcription (Backs et al., 2009; Backs, Song, Bezprozvannaya, Chang, & Olson, 2006; Passier et al., 2000). Both the calcineurin-NFAT pathway and the CaMKII-HDAC-MEF2 pathway are thought to be sufficient and necessary for the induction of pathological LVH.

A study indicates that the acetylation of MEF2 is necessary in development and maintenance of pathological LVH. Therefore blocking MEF2 acetylation may allow recovery from mechanical pressure overload-induced LVH with no impairment in physiological adaptation (Wei et al., 2017).

Importantly, Yu, Gong, Wu, et al. (2021) identified that Gq-coupled receptors and the calcineurin-NFAT pathway are essential for neurohumoral stimulation (AngII)-induced LVH, but not responsible for pressure overload (transverse aortic constriction; TAC)-included LVH. They showed that only the CaMKII-HDAC-MEF2 LVH pathway is activated in response to mechanical pressure overload (TAC) (**Figure 1-12**) (Yu, Gong, Wu, et al., 2021). The activation of this pathway may involve the activities of certain MS channels (described later). Notedly, the activation of CaMKII was also proven to inhibit the calcineurin activity (De Koninck & Schulman, 1998; Kreusser et al., 2014; MacDonnell et al., 2009).

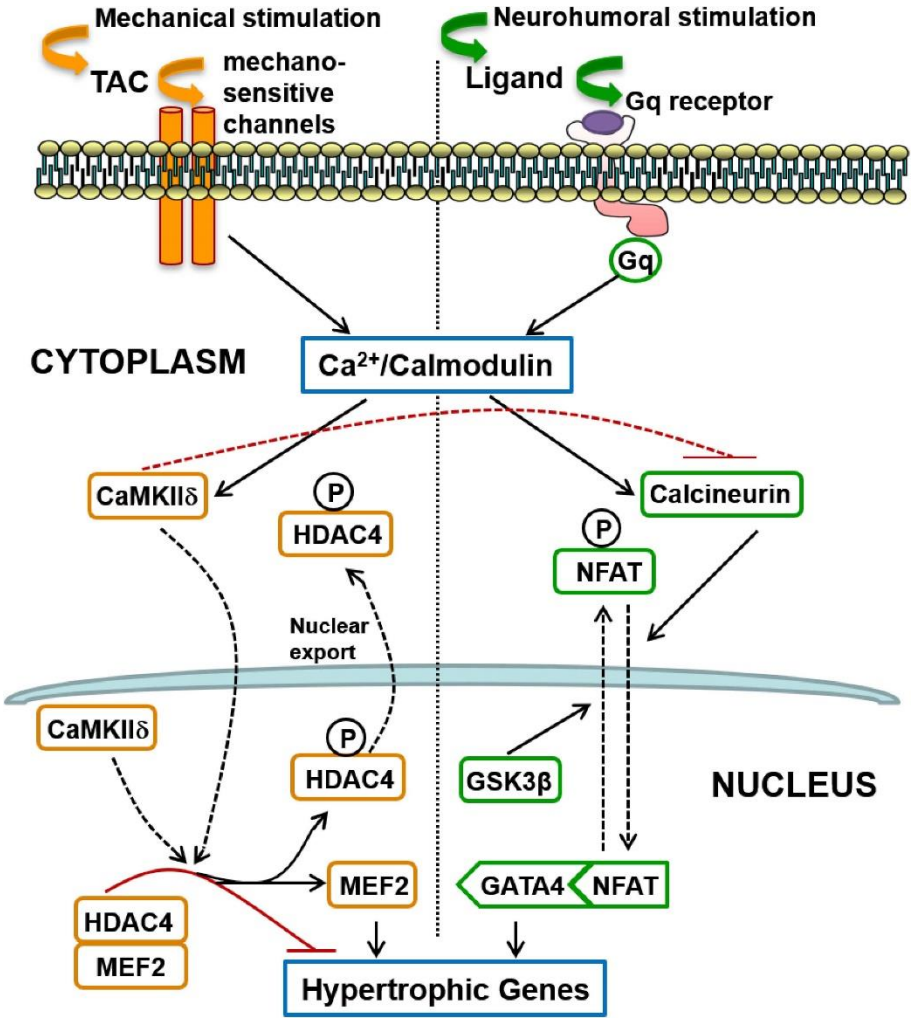

Figure 1-12 The two segregated signalling pathways of LVH.

Image adapted from Yu, Gong, Wu, et al. (2021).

1.4 Cardiac mechanotransduction

1.4.1 Mechanical forces in the heart

It is known that the heart begins functioning before its morphological characteristics is complete (Granados-Riveron & Brook, 2012; Takahashi, Kakimoto, Toda, & Naruse, 2013). During the development of cardiac cells and the functional activities of the heart, the heart is responding to various mechanical forces, such as stretch, compression, bending, and shear, in

different physiological/pathological processes (Izu et al., 2020; Peyronnet et al., 2016; Quinn & Kohl, 2021; Takahashi et al., 2013). For example, intracardiac fluid forces play an important role in the development of the embryonic heart. Pathological changes in blood flow can cause various cardiac morphological defects, such as ventricular septal and semilunar valve defects, etc. (Granados-Riveron & Brook, 2012; Hogers, 1999). There are two kinds of cyclic forces applied by pulsatile blood flow due to cardiac contraction: the force parallel to the blood flow, which induces shear stress over the endocardium; and the force perpendicular to the flow which can cause cyclic strain over the entire wall of the heart, affecting all cardiac cells (Andres-Delgado & Mercader, 2016; Granados-Riveron & Brook, 2012).

Generally, in physiological activities of the heart, stable hemodynamic forces are necessary for maintaining normal heart chamber dimensions and functional parameters. Along with the cardiac contraction, the cardiomyocytes in myocardium are subjected to various forces such as cyclic acute stretch. Stretch on atria and ventricle can cause two kinds of force increase. One is an acute increase following the Frank-Starling mechanism (Frank, 1895; Peyronnet et al., 2016; Starling & Visscher, 1927; Takahashi et al., 2013), which is based on the link between the initial length of myocardial fibres and the force generated by cardiac contraction. The other is a further slow increase (slow force response known as Anrep effect), by which the contractile proteins are stimulated by sustained Ca^{2+} transient after stretch for 5-10 minutes (Calaghan & White, 2004; Peyronnet et al., 2016; Takahashi et al., 2013; Ward & Allen, 2010). The acute stretch can cause diastolic depolarisation on both pacemaker cells (Cooper, Lei, Cheng, & Kohl, 2000) and conduction cells (Izu et al., 2020; Kaufmann & Theophile,

1967) to trigger excitation in resting atrial and ventricular myocardium (Izu et al., 2020). While in pathological processes in the heart, cyclic stretch can cause functional remodelling such as arrhythmias and/or structural remodelling such as hypertrophy (Izu et al., 2020; Quinn & Kohl, 2021).

1.4.2 The general role of MS channels in the cardiovascular system

MS channels are ion channels whose activity is basically dependent on mechanical forces on the plasma membrane. They are playing a central role in a process called mechanotransduction, the conversion of mechanical stimuli into electrical or chemical signals in biological cells (Chazi, Berrier, Ajouz, & Besnard, 1998; Izu et al., 2020; Martinac, Buechner, Delcour, Adler, & Kung, 1987; Quinn & Kohl, 2021). MS channels are functionally present in many organs and in different cell types. They are primary molecular transducers of mechanical force in a wide range of physiological and pathological processes, including conscious sensations such as touch, hearing, taste and balance, and unconscious sensation such as blood flow (Owen P Hamill & Maroto, 2007; Martinac, 2004; Ranade, Syeda, & Patapoutian, 2015). As MS channels may have different activation mechanisms, they could be classified into stretch-activated channels and volume-activated channels, etc. Interestingly, some of the MS channels have been shown not to be intrinsically mechanosensitive, such as mammalian TRP channels TRPM4 and TRPV4, as well as BK channels (Constantine et al., 2016; Gottlieb et al., 2008; Owen P Hamill & Maroto, 2007; Iribe, Jin, Kaihara, & Naruse, 2010; Nikolaev et al., 2019; O'Neil & Heller, 2005; Takahashi & Naruse, 2012). Although these channels cannot

be directly activated by mechanical stimuli, they might function as a "mechano-effector" (Owen P Hamill & Maroto, 2007) or a signal amplifier by associating with other MS channels or other mechanosensitive membrane proteins. Therefore, their activities are consequently modulated by mechanical stimulation. For example, TRPV4 has been proven to be coupled to an osmotic-sensitive Src protein tyrosine kinase (Cohen, 2005) or to the volume-sensitive phospholipase A2 (Vriens et al., 2004; Hiroyuki Watanabe et al., 2003). In order to investigate the responses of MS channels to mechanical stimuli, techniques such as Ca^{2+} imaging, patch clamp (O. P. Hamill, Marty, Neher, Sakmann, & Sigworth, 1981) , nanoindentation (Broitman, 2016), as well as cell stretch devices (O. Friedrich et al., 2017) were developed and widely used in MS channel studies.

As extensively characterised biological force-sensing systems, MS channels are acting as mechanical biosensors in the cardiovascular system, responding to mechanical forces such as stretch, compression, bending, and shear (Peyronnet et al., 2016). MS channels including the TRPs (TRPC1/3/6, TRPV4, TRPM4, etc.), Piezo1, $TREK_{-1}$, BK_{Ca}, and ATP-sensitive potassium (K_{ATP}), etc. are thought to contribute to maintaining normal cardiac function or to developing heart diseases (Peyronnet et al., 2016; Reed et al., 2014; Takahashi et al., 2013). For example, in the cardiac mechano-electric coupling process described in **1.2.4.3**, mechanical stimuli affect the electrophysiological properties through the MS channels, to modify the heart rate and rhythm, the action potential shape, and the electrical conduction (Quinn & Kohl, 2021). Therefore, modulation of MS

channels may potentially contribute to therapeutic interventions for heart diseases (Peyronnet et al., 2016; Takahashi et al., 2013).

1.4.3 Ion channel candidates in mechanotransduction underlying pressure overload-induced LVH

The increase of intracellular Ca^{2+} concentration contributes to the development of cardiomyopathy (Ward & Allen, 2010; Ward et al., 2008). It has been shown to be an important signal for LVH (Bers, 2008), and may further lead to heart failure (Gwathmey et al., 1987; Yao et al., 1998). It is known that cardiac pressure overload could activate certain cellular signalling pathways to induce pathological LVH. Acting as mechanical biosensors in cardiovascular system (Martinac, 2004), MS channels such as the TRPs and Piezo1 could be possible regulators of the LVH signalling pathway through their modulation on Ca^{2+} influx.

1.4.3.1 Transient receptor potential melastatin 4 (TRPM4)

As a member of the TRPM subfamily (**Figure 1-13**), TRPM4 is a Ca^{2+}-and voltage- dependent, non-selective monovalent cation channel (Pierre Launay et al., 2002; Nilius et al., 2003; Nilius, Prenen, Tang, et al., 2005). It is equally permeable to Na^{+} and K^{+}, but impermeable to Ca^{2+} and Mg^{2+} (Nilius, Prenen, Janssens, et al., 2005). Activation of TRPM4 can depolarise the plasma membrane through the Na^{+} entry to further modulate Ca^{2+} influx through other Ca^{2+}-permeable channels such as the voltage-gated Ca^{2+} channels and the non-voltage-dependent Ca^{2+} channels (Abriel, Syam,

Sottas, Amarouch, & Rougier, 2012; Hof et al., 2019; Pierre Launay et al., 2002) (**Figure 1-14**).

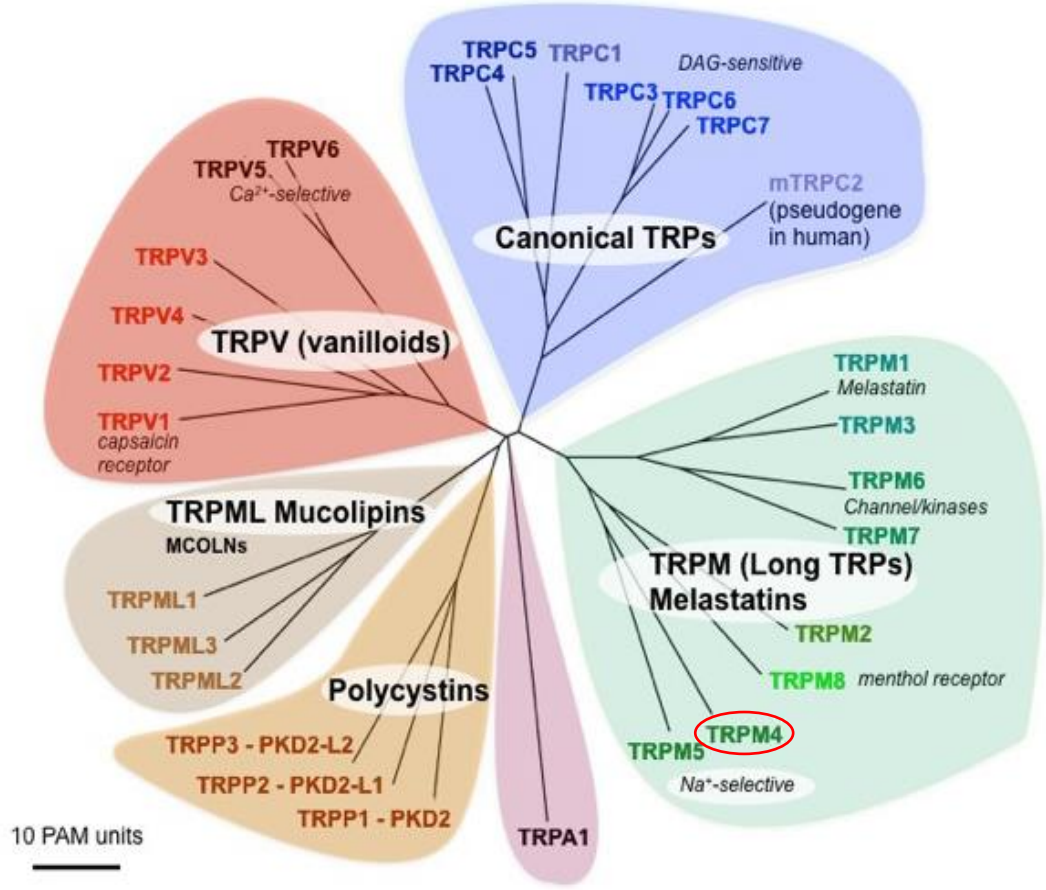

Figure 1-13 TRPM4 in the phylogenetic tree of the TRP channel family.

The evolutionary distances are shown by the branch lengths in point accepted mutation (PAM) units (the mean number of substitutions per 100 amino acids). Image reproduced from Clapham (2003).

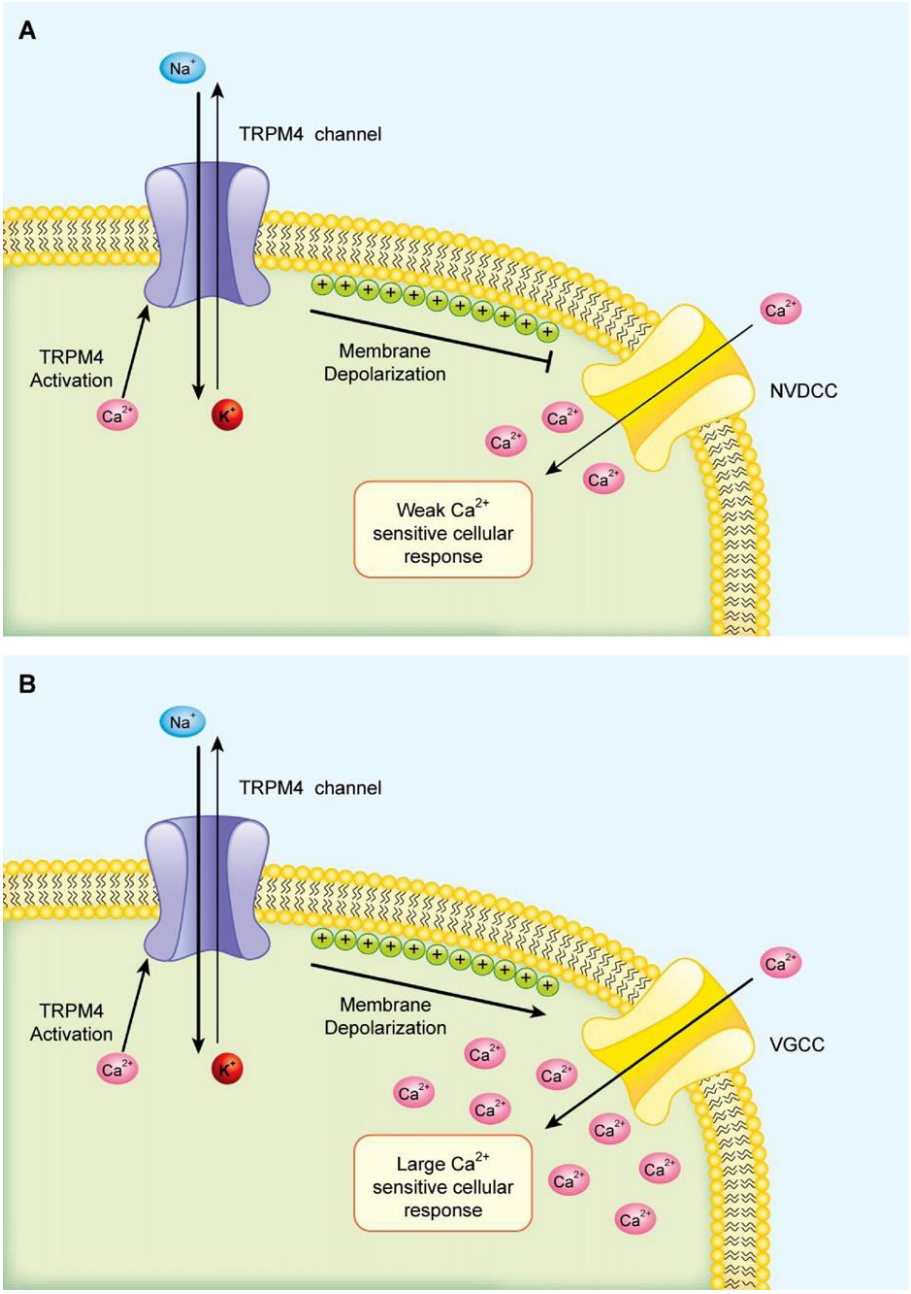

Figure 1-14 The effect of TRPM4 activation on Ca^{2+}-permeable channels.

(A) Membrane depolarisation by TRPM4 activation reduces the Ca^{2+} entry through the non-voltage-dependent Ca^{2+} channel (NVDCC), inducing a weak Ca^{2+}-sensitive cellular response. (B) Membrane depolarisation activates the voltage-gated Ca^{2+} channel (VGCC) and increases the Ca^{2+} entry, inducing a large Ca^{2+}-sensitive cellular response. Image adapted from Abriel et al. (2012).

TRPM4 structure

Both the mouse TRPM4 (J. Guo et al., 2017) and human TRPM4 (Winkler, Huang, Sun, Du, & Lu, 2017) structure have been solved using the Cryo-EM technology. TRPM4 contains multiple transmembrane and cytosolic domains which form a three-tiered structure (J. Guo et al., 2017; Winkler et al., 2017) (**Figure 1-15**). The N-terminal nucleotide binding domain and the C-terminal coiled coil participate in the tetrameric assembly of the TRPM4 channel. There are two ATP-binding cassette transporter-like motifs at the N-terminal nucleotide-binding domain, which can inhibit TRPM4 activity. In addition, a few other parts including several PKC phosphorylation sites, five CaM-binding sites, four Walker B motifs, a putative Phosphatidylinositol 4,5-bisphosphate (PIP2)-binding site, and a coiled-coil domain, are also involved in the modulation of the TRPM4 function (J. Guo et al., 2017; Vennekens & Nilius, 2007).

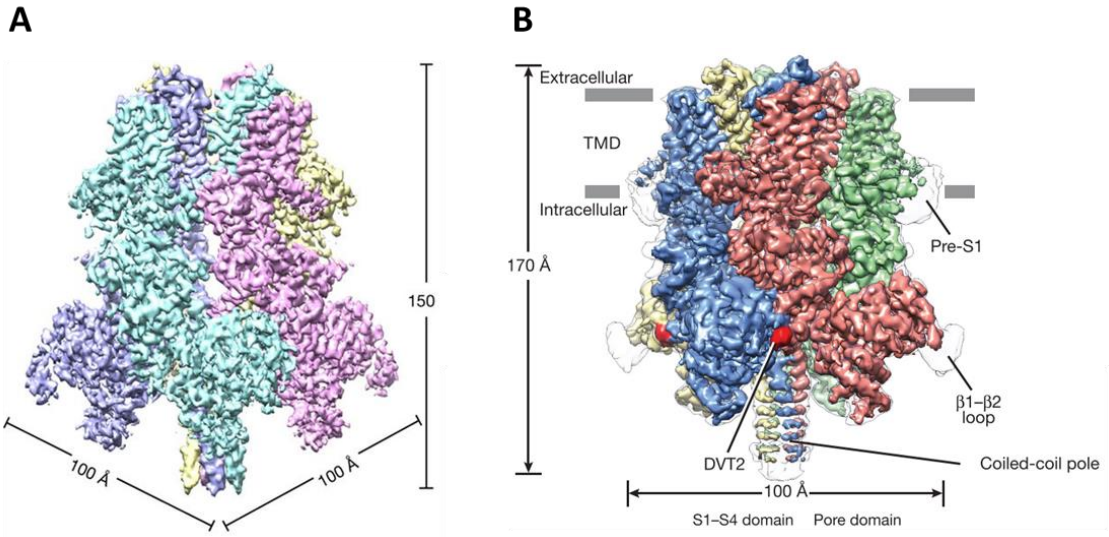

Figure 1-15 3D reconstruction of TRPM4 channel.

Each subunit in individual colour. (A) mouse TRPM4. Image adapted from J. Guo et al. (2017). (B) Human TRPM4. Image adapted from Winkler et al. (2017).

Activation and inhibition of TRPM4

TRPM4 can be activated by the increase of intracellular Ca^{2+}, membrane voltage, or temperature. The mechanism of its activity involves modulators such as PIP2, ATP, PKC-dependent phosphorylation, and CaM (Earley, Straub, & Brayden, 2007; Nilius et al., 2006; Nilius, Prenen, Tang, et al., 2005; Vennekens & Nilius, 2007). Some study suggests that TRPM4 may be mechanosensitive (Morita et al., 2007), although it has been demonstrated that mammalian TRP channels, including TRPM4, are not directly activated by membrane stretch. (Constantine et al., 2016; Gottlieb et al., 2008; Nikolaev et al., 2019).

In terms of pharmacology, a few compounds have been shown to activate or inhibit TRPM4. A molecule named decavanadate can inhibit voltage-dependent closure of TRPM4 by interfering with the ATP binding (Nilius, Prenen, Janssens, Voets, & Droogmans, 2004). This effect is specific for the TRPM4 channel. Another compound, BTP2, has been reported to increase the TRPM4 activity in heterologous expression systems, also to reduce the desensitization of the TRPM4 current after activation (Takezawa et al., 2006).

Two TRPM4 pharmacological inhibitors have been commonly used in electrophysiological studies: Flufenamic acid (Constantine et al., 2016; Guinamard, Demion, Magaud, Potreau, & Bois, 2006; Ullrich et al., 2005)(**Figure 1-16A**) and 9-phenanthrol (Grand et al., 2008; Hu et al., 2017;

Simard, Salle, Rouet, & Guinamard, 2012; Son et al., 2016)(**Figure 1-16B**). However, flufenamic acid has been proven to also inhibit Cl^- channels (Gwanyanya et al., 2010). Although 9-phenanthrol has no effect on TRPM5, transient receptor potential canonical 3/6 (TRPC3/6) and a number of K^+ channels (Abriel et al., 2012; Grand et al., 2008; Kruse & Pongs, 2014), it has been reported to affect certain voltage-gated K^+ and Ca^{2+} channels in primary cardiomyocytes (Kruse & Pongs, 2014).

For genetic inhibition, TRPM4 global knockout mice have been developed and evaluated by two groups (Barbet et al., 2008; Vennekens et al., 2007). It has been identified that TRPM4 is integrally involved in the immune system (Barbet et al., 2008; Guinamard, Demion, & Launay, 2010; Vennekens et al., 2007). However, there was a discrepancy in the results of studies on cardiac phenotypes by TRPM4 deficiency (Demion et al., 2014; Mathar et al., 2014). After that, Kecskes et al. (2015) generated a *Trpm4* cardiaomyocyte-specific knockout (*Trpm4* cKO) mouse model for AngII-mediated LVH study. Their baseline study showed that there is no difference in phenotype among WT, *Trpm4* cKO mice and its non-transgenic littermates. In addition, small interfering RNA (siRNA)- or small hairpin RNA (shRNA)-mediated gene knockdown have been used in TRPM4 studies on primary cells or immortalised cell lines, such as dental follicle stem cells (Nelson et al., 2013), T cells (P. Launay et al., 2004; Weber, Hildner, Murphy, & Allen, 2010), and HL-1 cells (Hu et al., 2017; Son et al., 2016), etc.

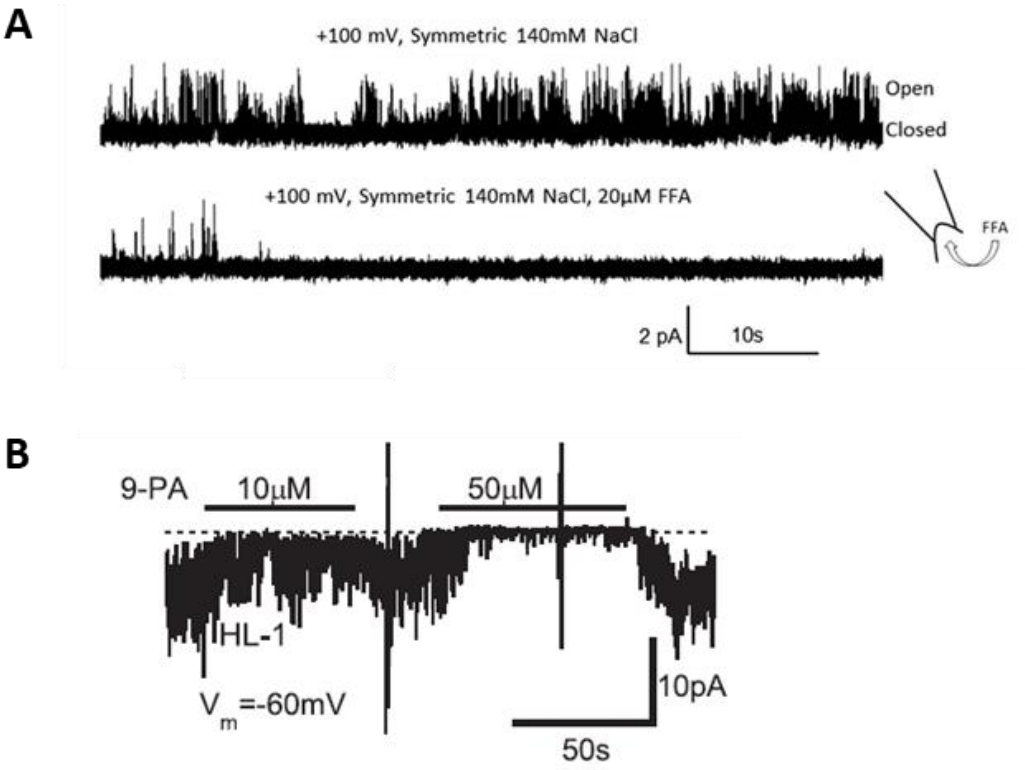

Figure 1-16 Pharmacological inhibition of TRPM4 current.

(A) Flufenamic acid (FFA, 20 μM) blocks TRPM4 current in liposome-reconstituted human TRPM4 single channel in patch clamp experiments. Image adapted from Constantine et al. (2016). (B) 9-phenanthrol (9-PA, 10 and 50 μM) inhibits TRPM4 current in HL-1 mouse atrial myocyte-like cells in patch clamp experiments. Image adapted from Hu et al. (2017).

The role of TRPM4 in the heart

TRPM4 is widely expressed in the heart, including in the atrial and ventricular myocytes, SA node cells, Purkinje fibres, fibroblasts, and ECs, involved in complicated physiological and pathological functions via the Ca^{2+}-dependent mechanisms (Guinamard et al., 2015; Hof et al., 2019; Kruse & Pongs, 2014; Mathar et al., 2014; C. Wang, Naruse, & Takahashi, 2018).

The TRPM4 channel is well known for its association with cardiac electrical activities, such as cardiomyocyte action potential formation and arrhythmia. Simard, Hof, Keddache, Launay, and Guinamard (2013) showed that TRPM4 is implicated in the waveform of the atrial action potential in isolated mouse atrium. Also, by inhibiting TRPM4 with 9-phenanthrol, a decrease in beating rate in varying degrees was observed in mouse and rat RA, and rabbit SA node (Hof, Simard, Rouet, Salle, & Guinamard, 2013) (**Figure 1-17**). Demion et al. (2014) indicated direct contribution of TRPM4 to action potential waveform in isolated mouse atrial myocytes. They showed that global knockout of the *Trpm4* gene can cause shortening in atrial myocyte action potential duration. These results suggest that TRPM4 is likely contributing to the action potential of pacemaker cells and participating in the modulation of the spontaneous beating rate (Guinamard et al., 2015) (**Figure 1-18**). Following that, Hof et al. (2016) observed that TRPM4-like single channel activity develops during the notch and early repolarization phases in isolated rabbit Purkinje cells. Another study reported that TRPM4 contributes to the mouse ventricular action potential (Mathar et al., 2014). A recent study suggested that the association of TRPM4 and the NCX may mediate transient Ca^{2+} amplitudes to further induce cellular arrhythmias (Hedon et al., 2021). The same study also indicated that TRPM4 is essential for survival after myocardial infarction (Hedon et al., 2021). Moreover, Simard et al. (2021) indicated that TRPM4 participates in mouse atrial electrical and structural remodelling, involved in aldosterone-induced atrial action potential shortening. In addition, *in vitro* studies using cultured HL-1 cells exhibited that TRPM4 is involved in the cellular signal transmission triggered by shear stress, as a downstream channel of type 2 inositol 1,4,5-trisphosphate receptors (IP3R2) (Son et al., 2016); the excessive activity of

TRPM4 can lead to arrhythmic changes in HL-1 cells (Hu et al., 2017). Interestingly, a follow-up study identified that the TRPM4 protein is closely localised with the CaMKII protein, a key component in Ca^{2+} related hypertrophic signalling pathways, in both HL-1 cells and TRPM4-expressing TSA201 cells, by confocal immunofluorescence microscopy, western blot, and proximity ligation assay (Hu et al., 2021). The same study also indicated functional interaction between TRPM4 and CaMKII, which might be involved in the arrhythmogenic mechanism in HL-1 cells.

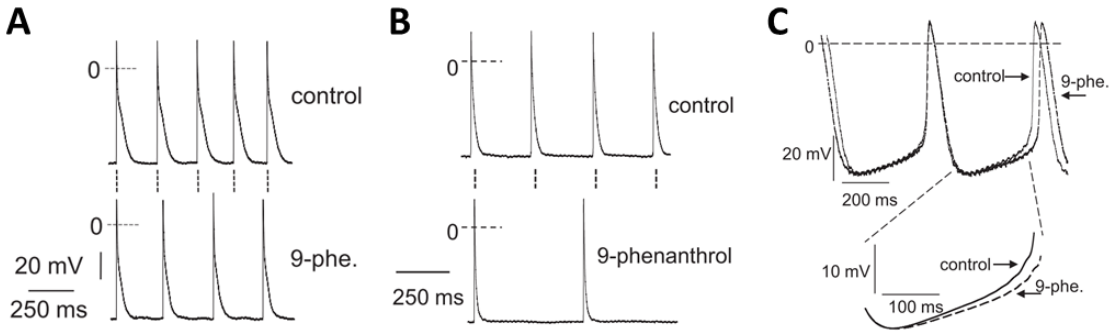

Figure 1-17 9-phenanthrol causes decreases in beating rate.

Schematized action potentials on (A) mouse RA, (B) rat RA and (C) rabbit SA node. 9-phenanthrol (9-phe.) concentration: 10 µM for all. Images adapted from Hof et al. (2013).

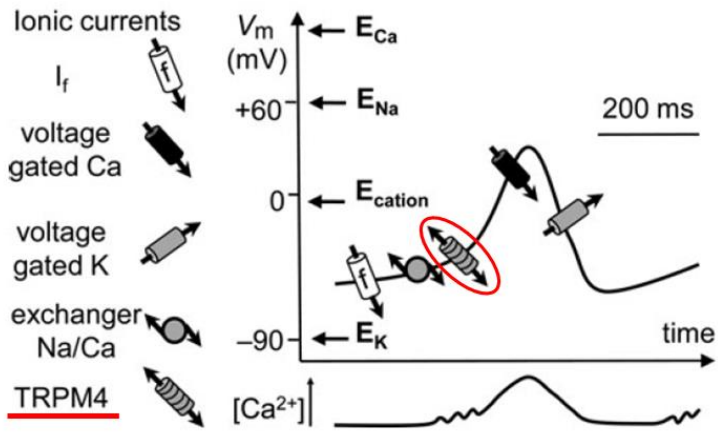

Figure 1-18 TRPM4 contributes to pacemaker cell action potential.

Schematized SA node cell action potential with theoretical reversal potentials (E_X) for ions. Main ionic currents involved in each phase of action potential are indicated. The Ca^{2+} level changes are shown under the action potential. Image reproduced from Guinamard et al. (2015).

Importantly, several studies indicated that TRPM4 is involved in mammalian ventricular remodelling in cardiac hypertrophy and heart failure. Mathar et al. (2014) reported that the TRPM4 channel protein is activated by Ca^{2+}-induced Ca^{2+} release in mouse ventricular cardiomyocytes. It is playing an essential role in the inotropic effect of β-adrenergic stimulation on the ventricular muscle as a negative regulator. Demion et al. (2014) reported that in TRPM4 global knockout mice, the increased hyperplasia in neonatal period can affect the LV mass in adulthood, leading to eccentric cardiac hypertrophy. A study using *Trpm4* cKO mice identified that TRPM4 is a negative regulator of AngII-induced cardiac hypertrophy (**Figure 1-19**) (Kecskes et al., 2015). This study suggests that TRPM4 activation can limit the driving force for Ca^{2+} influx via store-operated calcium entry (SOCE) (Clapham, 2007) through other ion channels such as TRPC1 and TRPC3, to

supress the activation of the calcineurin-NFAT hypertrophic signalling pathway (Kecskes et al., 2015). Moreover, Jacobs et al. (2015) demonstrated that deletion of the *Trpm4* gene in mice can enhance β-adrenergic cardiac reversal and improve survival after severe ischaemic heart failure. Frede et al. (2020) reported that TRPM4 expression was downregulated in response to monocrotaline treatment-induced right ventricular pressure load in rats. Also, the global deletion of TRPM4 results in increased right ventricular hypertrophy by pressure load (Frede et al., 2020).

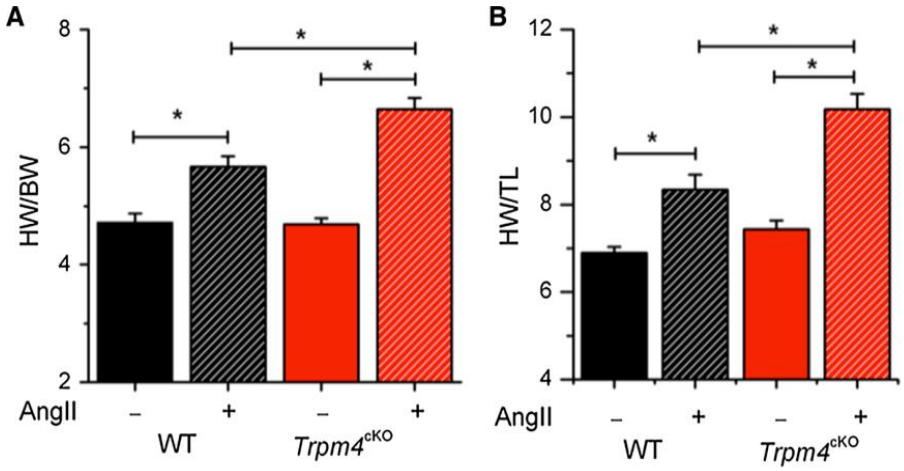

Figure 1-19 *Trpm4* cKO mice display increased heart mass with AngII treatment compared to WT mice.

(A) Heart weight/body weight (HW/BW) and (B) heart weight/ tibial length (HW/TL) ratios of WT and *Trpm4* cKO mice after sham or Ang II (3 mg/kg/day for 2 weeks) treatment. (mean ± SEM; WT sham: n = 7; WT treated n = 10; *Trpm4* cKO sham: n = 7; *Trpm4* cKO n = 10; *p < 0.05). Image adapted from Kecskes et al. (2015).

In summary, TRPM4 has been shown to contribute to various physiological and pathological functions in the heart due to its Ca^{2+} modulation. Because of its involvement in ventricular remodelling in cardiac hypertrophy and heart failure, it can be considered a channel candidate which potentially contributes to the mechanotransduction underlying pressure overload-induced LVH. However, because the lack of activation of TRPM4 by membrane stretch, its contribution to pressure overload-induced LVH might be closely associated with other upstream ion channels which function as the primary mechanotransducer.

1.4.3.2 Piezo type mechanosensitive ion channel component 1 (Piezo1)

Piezo1 structure

Piezo1 is a trimeric membrane channel protein. It has an ion pore in the central cap and three flexible blades around the pore, forming a propeller shape located in a curved transmembrane region (Saotome et al., 2018) (**Figure 1-20A, B**). The channel gating is controlled allosterically by the three blades of the propeller. The resolution of the Piezo1 structure provides a basis to further reveal the activation mechanism of this channel in response to mechanical force. Although the gating mechanism is not fully understood, some studies indicated that Piezo1 can distort the membrane to form local membrane curvature, which may be related to the channel opening (J. Ge et al., 2015; Y. R. Guo & MacKinnon, 2017).

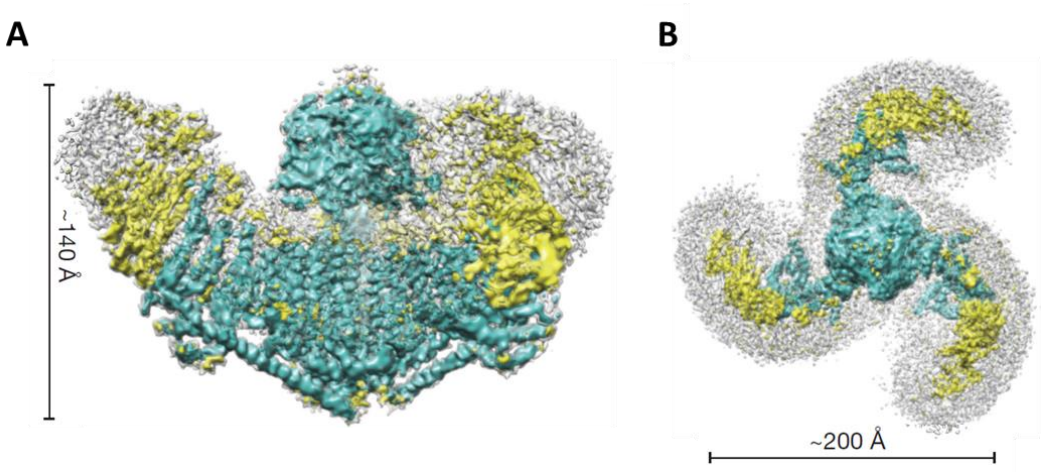

Figure 1-20 3D reconstruction of Piezo1.

(A) Top view and (B) side view of the of the 3D structure of Piezo1. Image reproduced from Saotome et al. (2018).

Activation and inhibition of Piezo1

Piezo1 is a Ca^{2+}-permeable non-selective cation channel. It can be activated by both mechanical and chemical stimulation. Previous studies show that mechanical indentation and cell membrane stretch can activate the Piezo1 channel in both cell and liposome membranes (Coste et al., 2010; Cox et al., 2016; Jaggers, Ridone, Martinac, & Baker, 2019; Lewis & Grandl, 2015; Syeda et al., 2016) (**Figure 1-21**). In addition to being mechanically activated, the Piezo1 channel can respond to certain chemical compounds and agents. A small molecule named Yoda1 (Syeda et al., 2015) has been discovered as a specific Piezo1 activator. Because Yoda1 can chemically activate the Piezo1 channel, also can increase the mechanosensitivity of Piezo1 (Botello-Smith et al., 2019; Syeda et al., 2015), it provides an experimentally practical agonist in Piezo1 regulation and function studies.

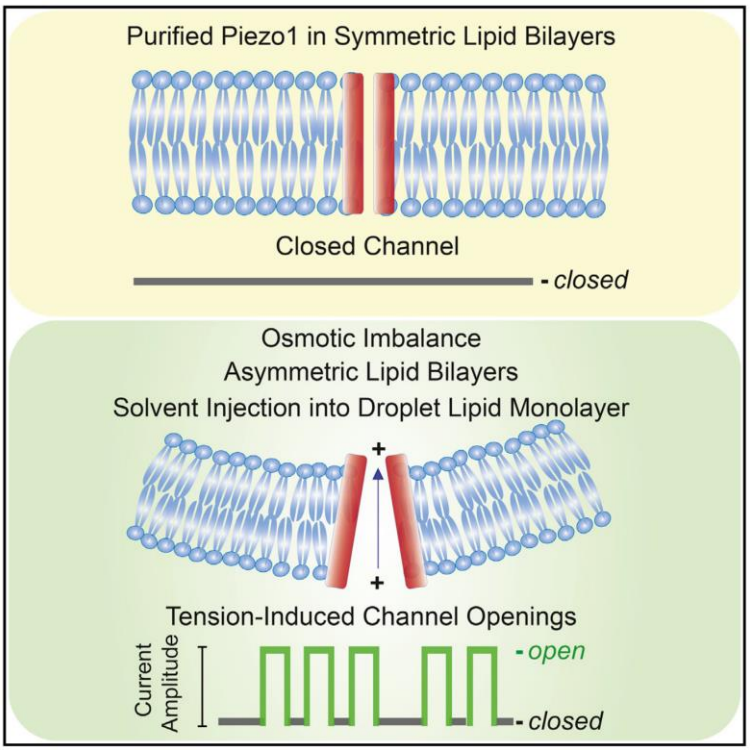

Figure 1-21 Activation of Piezo1 by mechanical indentation and stretching of cell membranes.

Image adapted from Syeda et al. (2016).

For chemical inhibition, The GsMTx4 peptide (Suchyna, Tape, et al., 2004) extracted from the venom of Grammostola spatulate spider, has been known to block multiple MS channels including Piezo1 (Bae, Sachs, & Gottlieb, 2011; Gnanasambandam et al., 2017) (**Figure 1-22A, B**). Although it has been widely used in mechanobiological studies, GsMTx4 was thought to suppress mechanical activation rather than chemical activation because it acts by modulating local membrane tension near the MS channels and behaves as a gating modifier (Douguet, Patel, Xu, Vanhoutte, & Honore, 2019; Gnanasambandam et al., 2017). This suggests that GsMTx4 may not

completely block the Piezo1 activation induced by Yoda1 (**Figure 1-22B**). Furthermore, other MS channel inhibitors such as lanthanides Gd^{3+} and La^{3+} (Suchyna, Besch, & Sachs, 2004), as well as some aminoglycoside antibiotics, e.g. streptomycin (O. P. Hamill & McBride, 1996), can also inhibit Piezo1. However, none of the above-mentioned compounds has been proven to be specific for the Piezo1 channel. In addition, a small-molecule compound named Dooku1 has been reported to selectively antagonize Yoda1-evoked activation of Piezo1 (E. L. Evans et al., 2018)(**Figure 1-23A, B**). A recent study also identified that a triterpenoid saponin highly contained in the Chinese herbal medicine Bolbostemma paniculatum (Maxim) Franquet (Cucurbitaceae), named tubeimoside I (TBMS1) is an effective inhibitor of the Yoda1 response for the Piezo1 channel with relative selectivity, as it has no effect on the TRPC5, TRPM2, and transient receptor potential vanilloid 4 (TRPV4) channels (S. Liu et al., 2020).

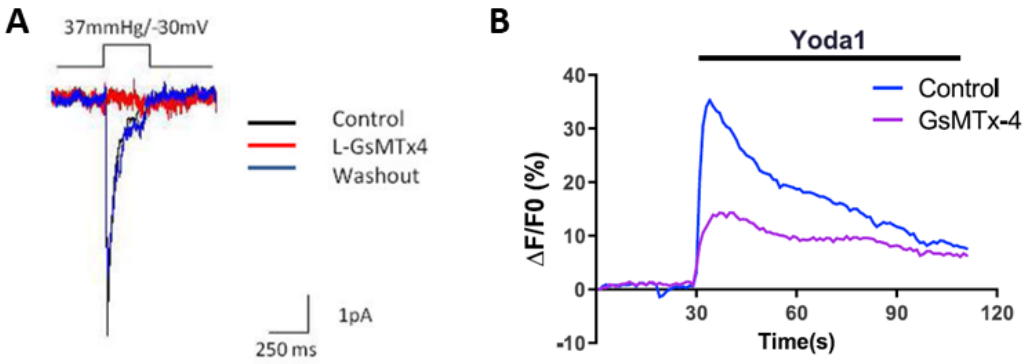

Figure 1-22 GsMTx4 inhibits Piezo1 activation.

(A) GsMTx4 (2.5 μM) blocks Piezo1 whole cell currents expressed in human embryonic kidney (HEK) 293 cells by patch clamping. Image adapted from Bae et al. (2011). (B) GsMTx4 (40 μM) partially inhibits Yoda1 (10 μM)-evoked Piezo1 activation in primary

mouse primary neurons, indicated by Ca^{2+} measurements. Image adapted from Qiu et al. (2019).

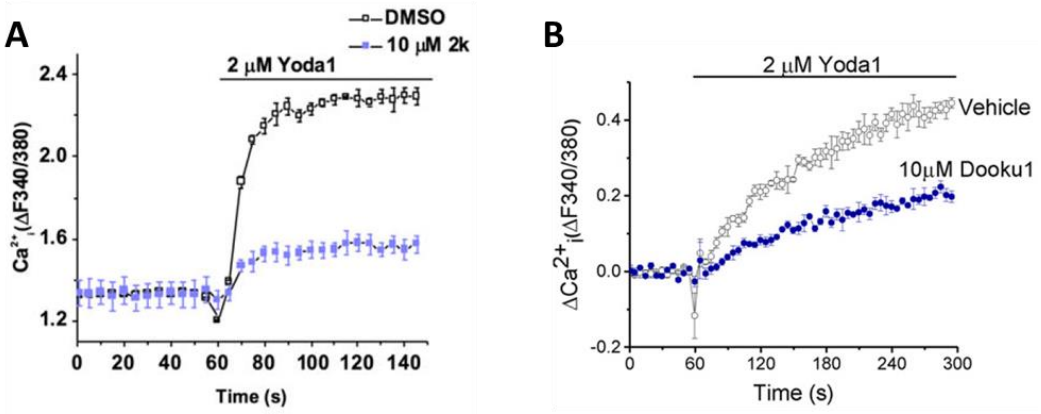

Figure 1-23 Dooku1 inhibits Yoda1-evoked Piezo1 activation.

Ca^{2+} measurements indicate that Dooku1(10 μM) inhibits Yoda1 (2 μM)-evoked Piezo1 activation in (A) Piezo1 T-Rex cells and (B) mouse cardiac fibroblasts. Dooku1 is designated "2k" in (A). Images adapted from E. L. Evans et al. (2018) (A) and Blythe et al. (2019) (B).

For genetic inhibition, *Piezo1* gene knockout mice have been used for various research purposes. J. Li et al. (2014) generated *Piezo1* endothelial-specific knockout mice to investigate the shear-stress-evoked ionic current and Ca^{2+} influx in ECs. Recently, Jiang et al. (2021) investigated the role of Piezo1 in cardiac mechano-chemo transduction by using *Piezo1* cardiac-specific knockout mice. Furthermore, *Piezo1* cardiac-specific knockout mice with tamoxifen-inducible Cre-recombinase have been developed by two groups for LVH studies (Yu, Gong, Kesteven, et al., 2021; Zhang et al., 2021). In addition, *in vitro* studies have been widely using siRNAs against Piezo1

on cardiac fibroblasts (Blythe et al., 2019) or epithelial cells (Nava et al., 2020), etc, but not yet on HL-1 cells.

Piezo1 as a stretch sensor

So far, many *in vitro* studies examined Piezo1's response to mechanical stretch. These studies have helped to reveal the role of Piezo1 channels as stretch sensors, which can induce further downstream cellular activities in contractile organs and tissues, including the heart. Techniques such as the patch clamp (O. P. Hamill et al., 1981), nanoindentation (Broitman, 2016), and cell stretching technologies (O. Friedrich et al., 2017) were developed and widely used along with Ca^{2+} imaging to examine activities of various MS channels.

As an effective experimental method to activate mechanically gated ion channels, stretching cell membranes by the patch clamp has been generally employed in Piezo1 studies. Firstly, Piezo1 was identified as a mechanically activated (MA) cation channel in 2010 by confirming stretch-activated currents in Neuro2A (N2A) mouse neuroblastoma cells and HEK293T cells in patch clamp experiments (Coste et al., 2010). The following studies demonstrated efficient application of patch clamp technology for stimulation to Piezo1 channels by mechanical stretch in biological research. Peyronnet et al. (2013) showed significantly decreased stretch-activated currents upon inhibition of Piezo1 activity in renal tubular epithelial cells. This study verified that renal mechanical force sensing depended on Piezo1 (Peyronnet et al., 2013). From the comparison of mechanically activated inward currents by patch clamp in several mutations of human Piezo1 in

HEK293T cells, another study suggested that Piezo1's "gain-of-function" mutants differed in cation permeability in red blood cell (RBC) (patho)physiology (Albuisson et al., 2013). Yet another study using patch clamp stimulation recording also showed that Piezo1 and its mutants exhibited variant channel inactivation, different responses to osmotic stress and membrane protein trafficking in hereditary xerocytosis (Glogowska et al., 2017). Similarly, the patch clamp technique was used to examine "gain-of-function" Piezo1 mutants expressed in RBCs and T Cells and revealed the relationship between RBC dehydration and prevention of plasmodium infection (Ma et al., 2018). Piezo1 activation by membrane stretching using the patch clamp in human neural stem cells was also shown to affect cell differentiation by influencing neuronal or astrocytic lineage through its Ca^{2+} influx regulation (Pathak et al., 2014). Furthermore, the patch clamp-induced mechanical response of Piezo1 could be affected by the lipid content and dietary fatty acids metabolism changes in mouse N2A cells (Romero et al., 2019). Along with the addition of Yoda1, patch clamp was used to demonstrate the presence of Piezo1 in pulmonary ECs, and to reveal the contribution of Piezo1 to intrapulmonary vascular relaxation by controlling Ca^{2+} influx and production of nitric oxide (Lhomme et al., 2019).

Meanwhile, mechanical stretch induced by stretch devices appeared as another approach to examine Piezo1 mechanosensitivity. Compared to patch clamp acting on certain locations within cells, stretch devices can apply direct mechanical stretch to all membrane sections. Some of these devices are also able to apply cyclic stretch to cells for observation of long-term stretch effects. According to a study by Miyamoto et al. (2014), changes in Ca^{2+} influx and ATP release level both responded to cyclic

mechanical stretch stimulation in mouse primary cultured urothelial cells. Confirmed by siRNA-mediated Piezo1 knockdown and addition of chemical inhibitor GsMTx4, these responses were proven to be linked to Piezo1 function (Miyamoto et al., 2014). Also, verified by clustered regularly interspaced short palindromic repeats (CRISPR)-based Piezo1 knockdown and Piezo1 inhibition by Gd^{3+}, mechanical stretch applied to Madin-Darby canine kidney (MDCK) epithelial cells activated Piezo1 channels and triggered further downstream response to promote cell division (Gudipaty et al., 2017). Furthermore, compared to WT control group, cultured nucleus pulposus cells transfected with *Piezo1* gene lentivirus interference shRNA-Piezo1 vector showed less increase in intracellular Ca^{2+} levels and lesser mitochondrial membrane potential changes in response to 24-hour cyclic stretch (Q. Yang, Zhou, Wang, Fu, & Li, 2019). A recent study showed that the epithelial cell nuclear deformation induced by cell stretching can trigger Piezo1-mediated mechano-signalling which could drive calcium-dependent nuclear softening to prevent DNA damage (Nava et al., 2020). This study also suggested that this Piezo1-driven signalling might be mediated by a CaMKII isoform (Nava et al., 2020). In cardiac cells, cultured AC16 human ventricular myocytes were observed to respond to varying cyclic stretch levels in cell population and Piezo1 localization (Wong et al., 2018). However, a study also reported that the Piezo1 expression level in the neonatal rat ventricular myocytes (NRVM) did not increase significantly after cyclic stretching (Liang et al., 2017).

The role of Piezo1 in the cardiovascular system

Piezo1 is a critical component of cardiac mechanotransduction involving ionic current and Ca^{2+} influx (Albarran-Juarez et al., 2018; Coste et al., 2010; Coste et al., 2012; Douguet et al., 2019; J. Li et al., 2014; Morley et al., 2018; Rode et al., 2017). It has been shown to be involved in cardiovascular development and functions through its regulation of Ca^{2+} homeostasis. Acting as a membrane mechanosensor, Piezo1 can be activated by vascular shear stress resulting from the blood flow and/or mechanical force of the heart contraction. This means that Piezo1 can respond to both long-term and acute stimuli in the cardiovascular system.

Piezo1 is highly expressed in ECs, RBCs, and SMCs. Several studies have suggested that Piezo1 is required for embryonic mouse vascular development (J. Li et al., 2014; Ranade et al., 2014). A study has shown that along with the TRP channels, Piezo1 is playing a central role in the modulation of zebrafish outflow tract valve development, involving both ECs and SMCs (Duchemin, Vignes, & Vermot, 2019). Also, blood pressure-related studies showed that Piezo1 has regulatory effects on relaxation of blood vessels in mice (E. L. Evans et al., 2018) and rats (John et al., 2018). Although some parts of the shear stress activation mechanism remain unclear, the Piezo1 channel is considered necessary for the release of vasodilatory factor nitric oxide, required for the regulation of vascular tone, as well as for blood pressure control in mouse (Lhomme et al., 2019; Rode et al., 2017; S. Wang et al., 2016; Zeng et al., 2018). It has also been indicated that Piezo1 functions as a baroreceptor of blood pressure sensing along with Piezo2 (Zeng et al., 2018). Because of its role as a baroreceptor, inhibition of Piezo1 could be effective for reducing capillary stress failure

responding to acute increased vascular pressure (E. E. Friedrich et al., 2019). Furthermore, from the perspective of vascular remodelling and recovery, Piezo1 in mouse vascular SMCs was also considered necessary in hypertension-dependent adult arterial structural remodelling (Retailleau et al., 2015). Activation of mouse endothelial Piezo1 may promote sprouting angiogenesis resulting in blood flow recovery after hindlimb ischemia and wound closure (Kang et al., 2019). In addition, some studies showed that Piezo1 was also playing an essential role in erythrocyte volume regulation. Its effect resulted from Piezo1-driven Ca^{2+} influx and subsequent dehydration of RBCs, involving Kca3.1 Gardos channel activation (Cahalan et al., 2015; Faucherre, Kissa, Nargeot, Mangoni, & Jopling, 2014).

In contrast to Piezo1 in ECs, there are only limited reports on the presence and activities of Piezo1 in cardiac myocytes and fibroblasts. In 2017, a study reported upregulation of Piezo1 mRNA and protein expression in rat ventricular tissue from a myocardial infarction-induced heart failure model (Liang et al., 2017). In the same study, increase in Piezo1 mRNA and protein expression levels was observed in isolated neonatal rat cardiomyocytes under AngII treatment compared to interleukin-6 or hydrogen peroxide treatment or application of 10% cyclic cell stretching. These Piezo1 responses were considered to relate to the AngII receptor type 1 (AT1) receptor- and extracellular signal-regulated kinase (ERK)1/2 signalling pathways (Liang et al., 2017). However, experimental reproducibility with the anti-Piezo1 antibody (Proteintech, USA) used may be a problem. Another study showed that in cultured ventricular myocytes from AC16 human cardiomyocyte cell line, cell realignment and Piezo1 redistribution both responded to 5% and 25% uniaxial 24-hour cyclic stretch stimulation.

Combining stretch stimulation with or without a Piezo1 channel inhibitor, the findings from this study suggest that Piezo1 may be involved in mechanical force sensing and activation of low-density lipoprotein (LDL) receptor-related protein 6 (LRP6)/b-catenin signalling as well as the c-Jun N-terminal kinase (JNK) signalling pathways as a mechanical stretch sensor (Wong et al., 2018). Importantly, a few very recent studies indicated that Piezo1 is directly involved in the mechanotransduction in mouse cardiomyocytes. Jiang et al. (2021) demonstrated that Piezo1 channels transduce mechanical stretch into Ca^{2+} and reactive oxygen species (ROS) signalling in mouse ventricular cardiomyocytes. These results were verified by using both Piezo1 cardiac-specific knockout and overexpression animals. Two other studies both using conditional cardiac-specific Piezo1 knockout mice exhibited that Piezo1 is upregulated in pressure overload-induced LVH (Yu, Gong, Kesteven, et al., 2021; Zhang et al., 2021). Zhang et al. (2021) showed that Piezo1 is mainly located near the intercalated disc and the T-tubule; Piezo1 activation can initialise Ca^{2+} related signalling pathways. Yu, Gong, Kesteven, et al. (2021) specifically identified that Piezo1 is responsible for the activation of CaMKII-HDAC4-MEF2 pathway in pressure overload (TAC)-induced LVH, potentially associated with some other downstream ion channels and transporters such as TRPM4, NCX1, $Ca_{V3.2}$. This study suggests that Piezo1 is the primary mechanotransducer which initiates the hypertrophic response to pressure overload (Yu, Gong, Kesteven, et al., 2021).

Notedly, compared to other contractile tissue or organs, such as vessels and lungs, a lower level of Piezo1 expression in mouse ventricular cardiomyocytes is identified (Yu, Gong, Kesteven, et al., 2021) (**Figure 1-24A,**

B). Also, the *Piezo1* mRNA expression is at a much lower level in ventricular cardiomyocytes compared to other cardiac cells (Blythe et al., 2019) (**Figure 1-24C**). In the study from Jiang et al. (2021), a rather high dose of Yoda1 (30 µM) was applied to activate Piezo1 in mouse ventricular cardiomyocytes (**Figure 1-24D**). In addition, no reliable antibody for mouse Piezo1 protein is commercially available. Thus, mouse lines expressing a fusion protein of Piezo1 and the fluorophore tdTomato were employed as alternatives for western blot experiments (**Figure 1-24B**) (Jiang et al., 2021; Yu, Gong, Kesteven, et al., 2021).

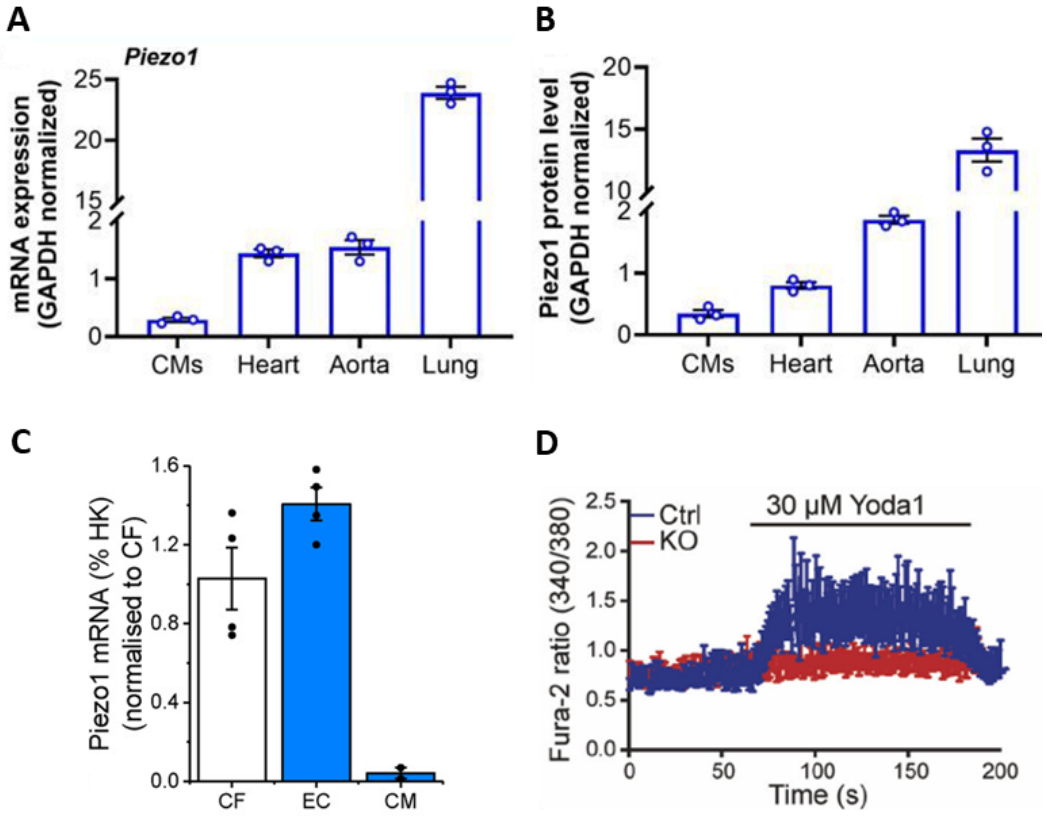

Figure 1-24 Piezo1 expression and activation in cardiomyocytes.

(A) *Piezo1* mRNA and (B) Piezo1 protein (fluorophore fused) expression in mouse cardiomyocytes (CMs), heart, aorta, and lung. Images adapted from Yu, Gong, Kesteven, et al. (2021) (C) *Piezo1* mRNA expression in mouse cardiac fibroblasts (CF), endothelial cells (EC) and cardiomyocytes (CM). Image adapted from Blythe et al. (2019). (D)

Increased Ca^{2+} level (in blue) indicating Yoda1-evoked Piezo1 activation in mouse cardiomyocytes. Image adapted from Jiang et al. (2021).

Apart from cardiomyocytes, a study using cultured mouse and human cardiac fibroblasts confirmed that mechanical stimulation by pressure clamp activated Piezo1 channels in cardiac fibroblasts (Blythe et al., 2019). This Piezo1 response may lead to interleukin-6 expression and secretion which is involved in hypertrophic remodelling after cardiac injury (Blythe et al., 2019).

1.4.3.3 Other candidates

As nonselective cation channels expressed in heart, the TRPCs are involved in pathological hypertrophy through signalling effectors such as calcineurin and NFAT (Eder & Molkentin, 2011). Among these, especially TRPC6 is highly expressed in human heart homogenates (Riccio et al., 2002) and are present in mouse T-tubules in ventricular cardiomyocyte (Dyachenko, Husse, Rueckschloss, & Isenberg, 2009). TRPC3 has also been identified in mouse and rat ventricular cardiomyocytes (O. Friedrich, Wagner, Battle, Schurmann, & Martinac, 2012). Reported by multiple studies, TRPC3 and TRPC6 are playing important roles in the development of pathological LVH, through calcineurin-dependent signalling pathway (Bush et al., 2006; Kuwahara et al., 2006; Onohara et al., 2006; Seo et al., 2014; Wu, Eder, Chang, & Molkentin, 2010). Also, TRPC3 and TRPC6 have been shown to contribute to pathological functional and structural remodelling after myocardial infarction along with TRPC4 (Makarewich et al., 2014). In

addition, acting as atrial mechanosensors, endocardial TRPC6 may modulate myocardial Ca^{2+} homeostasis under basal conditions and protect against stretch-induced atrial arrhythmias (Nikolova-Krstevski et al., 2017). Notedly, TRPC3/6 channels are not stretch sensitive (Nikolaev et al., 2019). They are activated by local membrane curvature caused by diacylglycerol (DAG), which together with inositol 1,4,5-trisphosphate (IP3) is generated by phospholipase C (PLC) activity by the G-protein-coupled receptors (GPCR) (Biaggioni & Robertson, 2009; Hofmann et al., 1999; Numata, Kiyonaka, Kato, Takahashi, & Mori, 2011).

1.5 *In vitro* cell stretching stimulation

1.5.1 Cell stretching technologies

There is complex mechanical stress in tissues and organs such as the heart, vessel, lung alveoli, and bladder. Working as molecular transducers to mechanical stimuli, MS channels can convert mechanical forces that impact on biological cells into electro-chemical intracellular signals (Cox, Bavi, & Martinac, 2019; O. Friedrich et al., 2017; Martinac, 2004). To investigate the role of MS channels in cellular signalling pathways, various devices have been developed to apply mechanical stretch to cells (O. Friedrich et al., 2017). Along with fluorescence microscopy, using these devices allows to observe Ca^{2+} transients during acute mechanical stretch at the single cell level. The investigation of cellular mechanotransduction processes combined with live cell imaging is available (O. Friedrich et al., 2017).

Uniaxial membrane stretch systems

Uniaxial stretch systems were firstly developed and have been continuously improved to meet the needs of different research purposes. Some devices have been commercialized by Biotech companies, e.g. *Strex Inc.* (www.strexcell.com).

Matsumoto, Delafontaine, Schnetzer, Tong, and Nerem (1996) developed a cyclic stretch cell culture system by which a cyclic stretch between 0-10% at 1 Hz was applied to a monocyte-like cell line (U937, ATCC) seeded on a silicone elastomer membrane. In a system designed by Yost et al. (2000), the stretch unit was designed as a dual stretch-actuator for two culture dishes simultaneously. Silicone rubber membranes of 250 mm thickness clamped into poly-ether-etherketone (PEEK) rods by polytetrafluorethylene (PTFE) snap-on clamps were displaced by a stepper motor. By using this device, neonatal rat cardiac fibroblasts seeded on collagen-coated membranes were subjected to a 0-12% stretch at 0-10 cycle/minute.

A device built by (Gerstmair, Fois, Innerbichler, Dietl, & Felder, 2009) provides a way to apply both uniaxial stretch and compression to cells on an elastic membrane. The membrane is attached to two sliding blocks which transfer compression or stretch by moving towards or away from each other. To guarantee uniform movement of the two blocks during stretch, they are attached to the same linear motor. Compression is implemented through the force of a spring connecting the two blocks to each other. Importantly, the system was designed to mount onto an inverted microscope to allow live cell imaging during the experiments. As the sample will move during stretch or compression, and the field of view will therefore change, the entire system sits on a carrier plate which is

connected to a second linear motor. This second motor shifts the carrier plate to compensate for lateral movement of the sample during the experiment. In this way, the sample is automatically being kept within the field of view. Experiments on adherent alveolar type II cells showed that the compensation motor indeed kept the cells within the field of view although the focus needs to be adjusted manually after the movements. Moreover, staining with Fura-2, a ratiometric Ca^{2+} sensitive dye, revealed a response of the cells to the strain, although the magnitude of the reaction was rather variable in the individual cells (Gerstmair et al., 2009).

Another approach by (Hecht et al., 2012) consists of the combination of a stretching device with an atomic force microscope (AFM), while still keeping the sample accessible for a fluorescence/ brightfield microscope (FM/BM). A polydimethylsiloxane (PDMS) membrane is mounted between two brackets that can be moved away from each other by a stepper motor. A window was implemented below the membrane, therefore the sample is accessible by FM at the same time with an inverted microscope. Cells of a squamous cell carcinoma were used to demonstrate the stretching and examination of the cells via AFM and FM, as well as BM. The amount of stretch was calculated from the deformation of the cells (parallel to the stretch axis) after the experiment. In the FM images, the cells show a less detailed structure after stretching (16%, 30%, 50%). The results of the AFM measurements back these findings up, by showing a decrease in the elastic modulus of the cytoskeleton network after 20% stretch (Hecht et al., 2012). However, the cells always had to be re-centred precisely after applying strain, as the AFM measurements were only conducted in a limited area.

For larger non-adherent cells, a system that can manually hold the ends of individual cardiomyocytes and stretch them uniaxially, was developed and used to investigate the X-ROS signalling in heart (Prosser, Ward, & Lederer, 2011). However, it is limited because of the potential risk of causing cell damage, and the usage for only short-term observations.

Multiaxial membrane stretch systems

As the heart is a contractile hollow organ, the hemodynamic volume/pressure load in the heart is associated with multiaxial wall tension, stretching individual cardiomyocytes in multiple directions. Therefore, multiaxial isotropic stretch is thought to be essential for stretch stimulation of cardiac cells especially cardiomyocytes (**Figure 1-25A, B**) (O. Friedrich et al., 2017).

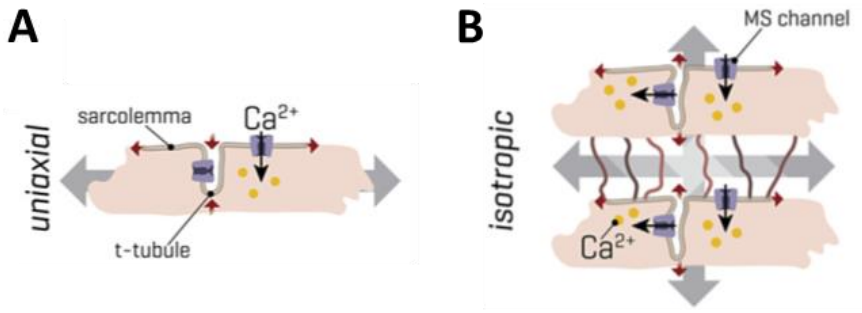

Figure 1-25 Comparison between models of uniaxial and isotropic stretch in mouse ventricular cardiomyocytes.

(A) Uniaxial cell stretching devices can stretch the sarcolemma and slacken the tubules. (B) Multiaxial isotropic stretch represents a more physiological stretch regime where

organ wall tension is transduced onto both membrane systems. Image modified from O. Friedrich et al. (2017).

To accurately implement multiaxial stretch, an early design by Cheng et al. (1997) used a motor-driven indentation of Teflon-made plates underneath a culture dish, the bottom of which was sealed with a silastic membrane, and displaced sinusoidally by a speed controlled motor-driven cam. Adhered human vascular SMCs were stimulated with a homogeneous and uniform equi-biaxial stretch in this study (Cheng et al., 1997). In a related study, Yamamoto, Dang, Kelly, and Lee (1998) applied stretch to neonatal rat cardiomyocyte using this system. Furthermore, a subsequent system developed by Rana et al. (2008) with increased equi-biaxial stretch output was used to investigate the stretch response of proteins including calcineurin, calcineurin-interacting protein 1 and voltage-gated Kv4.2 in neonatal rat atrial cardiomyocytes. However, the data acquired was considered from post-stretch protein biochemistry because real-time image recording was not available with these systems. Huang, Mathieu, and Helmke (2010) designed a vertically actuated system pushing an indenter ring against a horizontal PDMS membrane. The modular indenter design allowed switching between equiaxial and uniaxial strain profiles (Huang et al., 2010), as verified by fluorescent bead displacements. Also, it is indicated that continuous observation of cells cultured on the elastic membrane is possible with this system. Rapalo et al. (2015) developed an in-plane isotropic cell stretch device with six evenly spaced clamps attached to a flexible large culture dish-cast membrane. By using this system, isotropic membrane strain was applied to human bronchial epithelial cells adhered on collagen-I coated PDMS dishes. However, it was lacking the

measurements of the actual increased cell membrane area due to the isotropic stretch. Therefore, the actual transmission efficiency of PDMS membrane stretch to the cell membrane was unknown. Furthermore, a bi-axial stretching device was microfabricated using PDMS by Tremblay, Chagnon-Lessard, Mirzaei, Pelling, and Godin (2014). Four low pressure channels create the bi-axial strain. As they are independent from each other, it is also possible to apply uni-axial stretch in either direction. For imaging, the device can be set up on an inverted microscope. Applying the stretch in both directions was found to lead to a non-uniform strain profile across the membrane surface, with noticeable deformation gradients. Human foreskin fibroblasts were used for experiments. The cells were stretched through 20% in horizontal and vertical direction and their morphology was observed to change immediately with stretch. Further experiments were conducted where uni-axial stretch was imposed onto randomly orientated cells, which resulted in the alignment of the cells perpendicular to the direction of the strain (after 8 hours). Once the direction was changed, the same cells proceeded to re-align accordingly (after 16 hours). While stretching the membrane along only one axis, the low pressure channels on the other axis can be used to prevent compression of the membrane in direction perpendicular to the uni-axial stretch (Tremblay et al., 2014). No problems were reported in terms of focus shift during the stretching. Supposedly there was no excessive movement of the focus plane, as the membrane is stabilised by the fluid pressure on both sides.

The *IsoStrecher* (O. Friedrich et al., 2017; Schürmann et al., 2016) is a novel stretching device which applies isotropic mechanical strain onto cells cultured in a PDMS chamber. The device is shown in **Figure 1-26A** with an

enlarged image of the unstretched chamber (**Figure 1-26B**) and the stretched chamber (**Figure 1-26C**). Every component of the *IsoStretcher* can be seen in the exploded view (**Figure 1-26D**). There are six sliders which sit in individual, linear ducts and apply stretch to the chamber while they are actuated radially. They have two pins each, one in front and one in the back. The chamber is mounted on the front pins, whereas the back pins are inserted into the oblique grooves of the translation disc. The translation disc is connected to the stepper motor via a belt wheel and the corresponding V-belt. Rotating the translation disc leads to radial movement of the pins and thereby, stretching/relaxing of the PDMS chamber occurs. The device can be set up on the stage of any inverted microscope (**Figure 1-26E**), allowing live imaging of the experiments. Furthermore, experiments on non-adherent cells can also be run by embedding them into a hydrogel (e.g. PVA-PEG gel) and curing the gel on the PDMS chamber (O. Friedrich et al., 2017). Thus, the embedded cells can be stretched with the chamber.

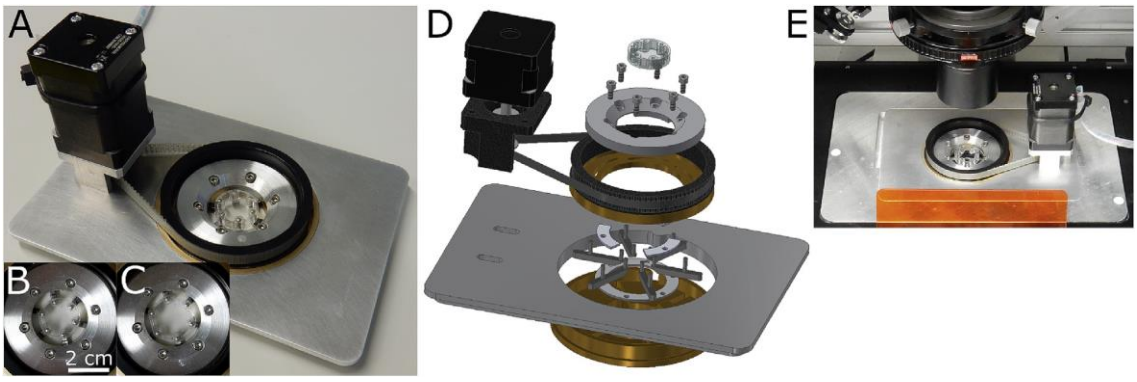

Figure 1-26 The *IsoStretcher* device.

(A) Image of the *IsoStretcher*, (B) Close-up of the unstretched chamber, (C) Close-up of the stretched chamber, (D) exploded drawing of the *IsoStretcher*. The stepper motor moves a belt wheel which is attached to a translation disc with oblique grooves. The

chamber is mounted on six sliders which sit in linear ducts and have two pins each; one in the front to hold the chamber and one in the back, inserted in one of the translation disc's grooves. According to the movement of the translation disc, the sliders are pulled outward or pushed inward and thereby, stretch or relax the chamber. (E) The *IsoStretcher* can be placed on top of a microscope stage, for live imaging during experiments.

1.5.2 HL-1 mouse atrial myocyte-like cell line

HL-1 cells represent an adherent mouse atrial myocyte-like cell line, which can be serially passaged and yet maintain a cardiac-specific phenotype (Claycomb et al., 1998; White, Constantin, & Claycomb, 2004). HL-1 cells can exhibit spontaneous action potentials (**Figure 1-27A**) and synchronous beating in confluent cultures (**Figure 1-27B**).

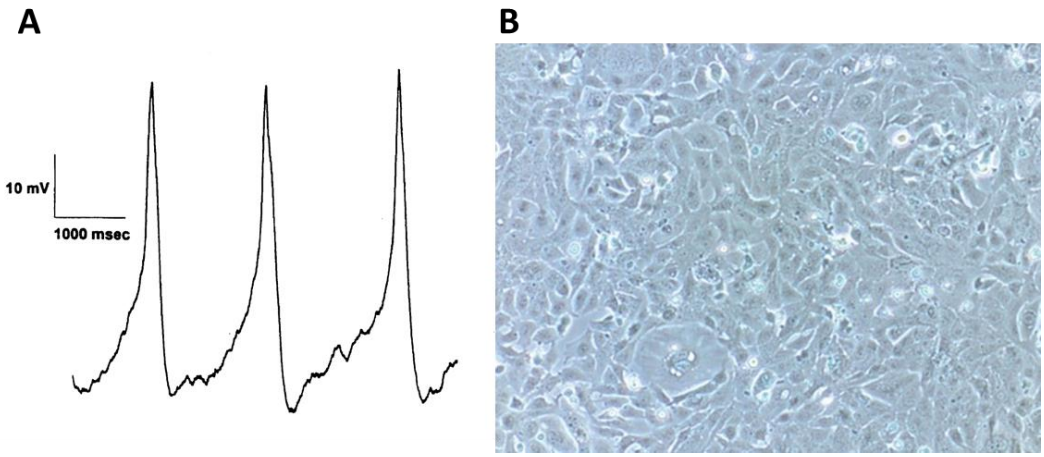

Figure 1-27 HL-1 cell action potential.

(A) Spontaneous action potential from a HL-1 cell. Image adapted from Claycomb (2001). (B) HL-1 cells in in confluent culture. Image adapted from Merck (2021).

The HL-1 cell line and its stable clones have been characterized by using various methods including immunohistochemistry, electrophysiology, and pharmacology (Claycomb et al., 1998; Dias et al., 2014; Sartiani, Bochet, Cerbai, Mugelli, & Fischmeister, 2002; White et al., 2004; Z. Yang & Murray, 2011). HL-1 cells have been shown to share some similarities with primary adult mouse atrial or ventricular myocytes, in expression of mature sarcomeric proteins, atrial granules, and some typical cardiomyocyte membrane receptors and signalling molecules (Claycomb et al., 1998; White et al., 2004). **Figure 1-28** shows the α-myosin heavy chain, atrial natriuretic factor, cardiac α-actin, and connexin 43 gene expression in HL-1 cells along with other cell line or tissues including AT-1 cells (Delcarpio, Lanson, Field, & Claycomb, 1991), adult mouse atrial muscle, ventricular muscle, skeletal muscle, and embryonic rat ventricular muscle (Claycomb et al., 1998). It has been determined that approximately 30% of the HL-1 cells have hyperpolarization-activated I_f, which is a characteristic of the pacemaker cells of the SA node or atrium (Sartiani et al., 2002; Z. Yang & Murray, 2011). This presence of I_f is not affected by the passage number or cell confluency (Sartiani et al., 2002). These I_f current might contribute to the spontaneous contractions in HL-1 cells. Furthermore, Z. Yang and Murray (2011) investigated the ionic basis of automaticity in HL-1 cells by using pharmacological inhibitors. They exhibited that the PKA activation can cause a large (115%) increase in the beating rate of HL-1 cells, which might involve mechanisms such as the enhancement of I_f and SR Ca^{2+} release. While inhibition of SR Ca^{2+} release channels or ATPase can cause slowing in the beating rate. In addition, I_f inhibitor, Na^+ channel inhibitor and T-type and L-type Ca^{2+} channel inhibitors can cause different degrees (< 20% - > 40%) of slowing in HL-1 cell beating rate (Z. Yang & Murray, 2011). Inhibition

of K^+ channels can cause prolongation of action potential duration (Z. Yang & Murray, 2011). While Lugenbiel et al. (2018) reported that inhibition of class I/II HDACs can induce K^+ channel remodelling and action potential prolongation in HL-1 cells. These results indicate the contributions of the internal and membrane-based components, especially various ion channels, in the generation of the spontaneous HL-1 cell action potential.

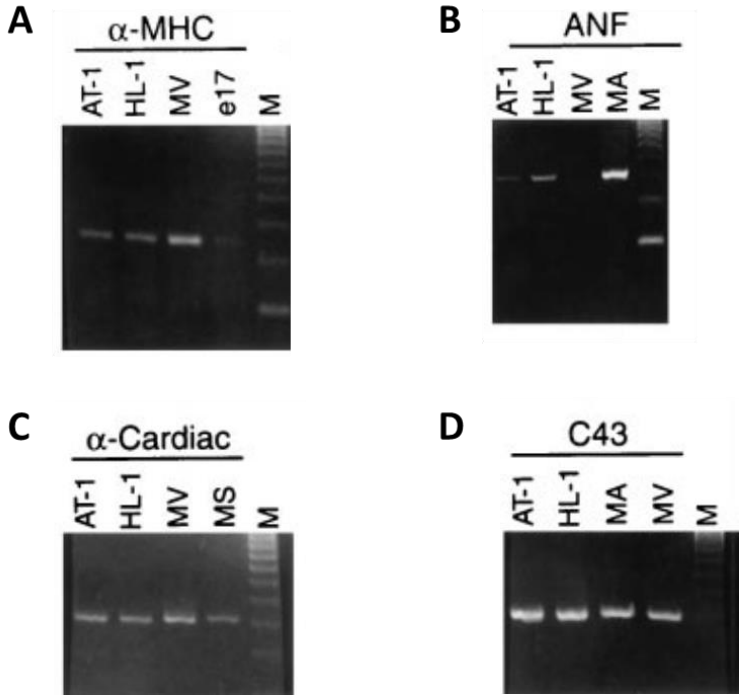

Figure 1-28 RT-PCR-based analysis of gene expression in HL-1 Cells.

Gene expression of (A) α-myosin heavy chain (α-MHC), (B) atrial natriuretic factor (ANF), (C) cardiac α-actin (α-Cardiac), and (D) connexin 43 (C43) in HL-1 cells, compared to AT-1 cells, adult mouse ventricular muscle tissue (MV), atrial muscle tissue (MA), skeletal muscle tissue (MS), and embryonic rat (17 days) ventricular muscle tissue (e17). DNA molecular weight markers: ΦX174 RF DNA-HaeIII (New England Biolabs, UK) (M). Image modified from Claycomb et al. (1998).

In cardiac biological studies, the HL-1 cell line has been widely used to create *in vitro* models of arrhythmia, hypoxia, hyperglycaemia, as well as hypertrophy, etc., for various investigations such as cellular signalling and electrophysiology (van Gorp, Trines, Pijnappels, & de Vries, 2020; White et al., 2004). HL-1 cells have been adopted as a comparison to other cardiac cells such as mouse atrial or ventricular myocytes, human induced pluripotent stem cells (hiPSCs), H9C2 rat cardiomyoblast cells, and NRVM, etc. (Minato et al., 2020; Nalliah et al., 2020; Wells et al., 2019). For example, Del-Canto et al. (2020) investigated the antianginal drug ranolazine's effect on HL-1 cells under uniaxial stretch. The results indicated that ranolazine can weaken the electrophysiological property change induced by the Na^+ influx and Ca^{2+} increase via mechanical stretch, to help preventing the induction of arrhythmia. Minato et al. (2020) reported that a Ca^{2+} channel blocker cilnidipine can shorten HL-1 cell APD and enhances nitric oxide production during hypoxia/reoxygenation injury to increase the survival ratio of HL-1 cells. A study reported that under rotation-simulated microgravity and hypergravity, increased spontaneous Ca^{2+} oscillations and cytosolic Ca^{2+} concentration in HL-1 cells led to activation of CaMKII-HDAC4 signalling and upregulation of ANP and BNP genes, indicating cardiac remodelling (C. Liu et al., 2020). Another study suggested that the T-type Ca^{2+} channel CACNA1H is a potential mediator for cellular hypertrophy, because pharmacological inhibition of T-type calcium channels can reduce the diameter, volume and BNP expression levels of HL-1 cells (Stroedecke et al., 2021). Particularly, as described previously, Son et al. (2016) exhibits the cellular signal transmission triggered by shear stress via IP3R2 to TRPM4 in HL-1 cells. Also, HL-1 cells were used to investigate the relationship between TRPM4 activities and atrial arrhythmias in a series of experiments

(Hu et al., 2017; Hu et al., 2021). Notedly, some optical mapping technology has appeared to measure Ca^{2+} transients and action potentials at the same time in HL-1 cells (Yan et al., 2015).

1.6 Hypothesis

Ion channel candidates such as TRPM4 and Piezo1 are potential contributors to the initial step of the pressure overload-induced LVH signalling pathway, by which the mechanical stretch associated with cardiac pressure overload is converted into a biochemical signal initiating hypertrophic signalling. As Piezo1 is a potential primary menchanotransducer, its activation might activate TRPM4 as a downstream channel to further modulate Ca^{2+} influx. Because the activation of pressure overload-induced LVH signalling pathway might be achieved by the interaction of multiple channels including Piezo1 and TRPM4, cardiac hypertrophy could be reduced or reversed by modulating the activities of certain ion channels.

1.7 Aims

The aim of this project is to investigate the role and the functional interaction of the TRPM4 and Piezo1 ion channels in cardiac mechanotransduction underlying pressure overload-induced LVH, via both *in vivo* and *in vitro* studies.

In vivo

To identify the role of the TRPM4 channel in pressure overload-induced LVH by physiological and molecular biological studies, using TAC-induced mouse LVH models including WT and *Trpm4* cKO mice.

In vitro

1. To develop *in vitro* cell stretching models as approaches to examine Piezo1-mediated cardiac mechanotransduction, using a novel isotropic cell stretching technology (the *IsoStretchor* system).
2. To develop methodology for the investigation of the functional presence of the Piezo1 channel in isolated mouse cardiomyocytes.
3. To investigate the functional interaction between the Piezo1 and TRPM4 channels in HL-1 cells via both action potential recording and Ca^{2+} imaging.

Chapter 2 Materials and methods

This chapter contains work published in:

Guo, Y.†, Yu, Z. Y.†, Wu, J., Gong, H., Kesteven, S., Iismaa, S. E., Chan, A. Y., Holman, S., Pinto, S., Pironet, A., Cox, C. D., Graham, R. M., Vennekens, R., Feneley, M. P.*, & Martinac, B.* (2021). The Ca^{2+}-activated cation channel TRPM4 is a positive regulator of pressure overload-induced cardiac hypertrophy. *eLife*, *10*, e66582.

Author contributions of Guo Y: data curation, formal analysis, validation, investigation, methodology, writing-original draft, writing-review and editing.

Guo, Y.†, Merten, A. L.†, Schöler, U., Yu, Z. Y., Cvetkovska, J., Fatkin, D., Feneley, M. P., Martinac, B.*, & Friedrich, O. (2021). *In vitro* cell stretching technology (*IsoStretcher*) as an approach to unravel Piezo1-mediated cardiac mechanotransduction. *Progress in Biophysics and Molecular Biology*, *159*, 22-33.

Author contributions of Guo Y: conceptualization, data curation, formal analysis, methodology, visualization, writing-original draft, writing-review and editing.

Friedrich, O., Merten, A. L., Schneidereit, D., **Guo, Y.**, Schürmann, S., & Martinac, B*. (2019). Stretch in Focus: 2D Inplane Cell Stretch Systems for Studies of Cardiac Mechano-Signaling. *Frontiers in Bioengineering and Biotechnology*, 7, 55.

Author contributions of Guo Y: conducted all *IsoStretcher* experiments and data analysis.

† These authors contributed equally.

* Corresponding author.

2.1 Animals and cells

2.1.1 Mice

In the first part of the TRPM4 study in **Chapter 3** and in the studies in **Chapter 4**, the experiments were performed on 11 to 13-week-old male C57BL/6J WT mice at the Victor Chang Cardiac Research Institute, Australia. In the second part of the TRPM4 study in **Chapter 3**, experiments were conducted using C57BL/6N WT and age-and sex-matched cardiac-specific *Trpm4* cKO mice at the Katholieke Universiteit Leuven, Belgium. *Trpm4*^{flox} mice were crossbred with *Myl7*-Cre mice to generate the *Trpm4* cKO mice (Kecskes et al., 2015) (**Figure 2-1**). All animals were entered into the study in a randomised order. All experimental procedures were approved by the Animal Ethics Committee of Garvan/St Vincent's (Australia) or Katholieke Universiteit Leuven (Belgium), respectively, in accordance with the guidelines of both the Australian code for the care and use of animals for scientific purposes (8th edition, National Health and Medical Research Council, AU, 2013) and the Guide for the Care and Use of Laboratory Animals (8th edition, National Research Council, USA, 2011).

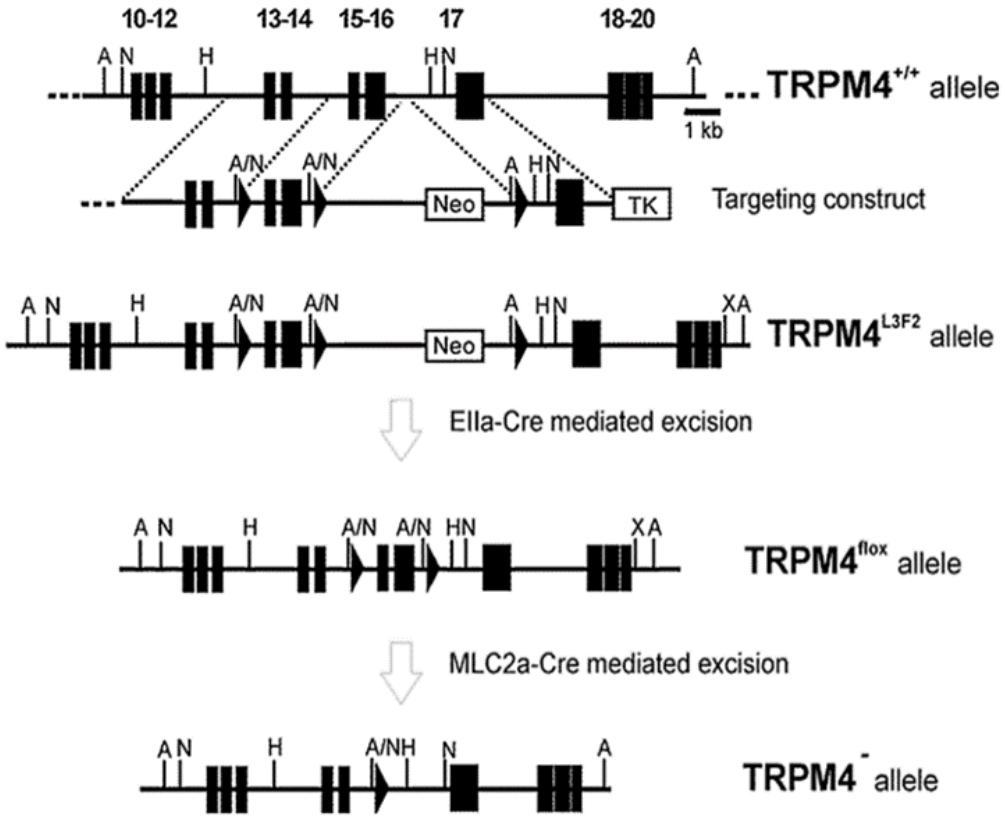

Figure 2-1 Generation of cardiac-specific *Trpm4* knockout (*Trpm4 cKO*) mice.

Trpm4^{flox} mice were crossbred with *Myl7* (protein: MLC2a)-Cre mice to generate the *Trpm4* cKO mice. Image adapted from Kecskes et al. (2015).

2.1.2 HL-1 cell culture

The HL-1 cells were donated by the Harvey Laboratory of the Victor Chang Cardiac Research Institute, Australia. The HL-1 cells were maintained at 37 °C with 5% CO_2 in a special culture medium mixture containing 87% Claycomb Medium (Sigma-Aldrich, USA), 10% Fetal Bovine Serum (FBS, Sigma-Aldrich, USA), 1% Penicillin-Streptomycin (10,000 units penicillin and 10 mg streptomycin/mL) (Sigma-Aldrich, USA), 1% Norepinephrine (Stock: 10 mM, Sigma-Aldrich, USA), and 1% L-Glutamine (Stock: 200 mM, Sigma-

Aldrich, USA), using an optimised protocol from the Claycomb Laboratory (Claycomb et al., 1998). Trypsin-EDTA (Sigma-Aldrich, USA) was used to split or collect the cells after they reached more than 90% confluency.

2.1.3 Adult mouse cardiac fibroblast isolation and primary culture

Three 12-week-old male C57BL/6J mice with an average body weight of 29.53 g (SD = 0.81) were euthanized according to guidelines of the Animal Research Act 1985 No 123 (New South Wales, Australia). Mouse cardiac fibroblasts were isolated and primary cultured using a protocol optimised from the protocols of the University of Virginia (2013) and Zeigler, Richardson, Holmes, and Saucerman (2016).

Mouse ventricles were rinsed with Krebs Henseleit Buffer (KHB, Sigma-Aldrich, USA), minced into ~1 mm pieces, then digested using Liberase enzyme (Roche, Switzerland). Successive digestions were centrifuged for 10 minutes at 400 x g then the cells were seeded into 100 mm cell culture dishes in Dulbecco's Modified Eagle's Medium (DMEM, Sigma-Aldrich, USA) supplemented with 10% FBS (Sigma-Aldrich, USA) and 1% Penicillin-Streptomycin (10,000 units penicillin and 10 mg streptomycin/mL) (Sigma-Aldrich, USA). After primary culture for 7 days at 37 °C with 5% CO_2, the fibroblasts were rinsed by phosphate-buffered saline (PBS) and collected for further experiments (**Figure 2-2**).

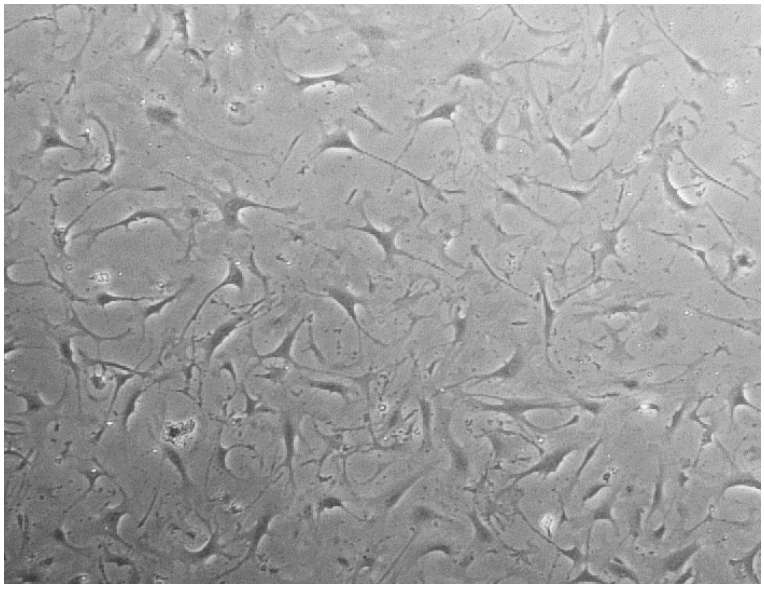

Figure 2-2 Mouse cardiac fibroblasts in primary culture.

2.2 Induction of pathological LVH

WT and *Trpm4* cKO mice were subjected to TAC surgery to induce pressure overload. Mice were anesthetized with 5% isoflurane and ventilated at 120 breaths/minute with a rodent ventilator (Harvard Apparatus, USA). The transverse aortic arch was accessed via an incision in the second intercostal space, and constricted with a ligature tied around a 25-gauge needle, which was then removed. The TAC surgical procedure was modified from a published paper (Rockman, Wachhorst, Mao, & Ross, 1994). Sham mice underwent the same procedure but the ligature was not tied. Simultaneous direct pressure recordings (described in **2.4**) from both the right carotid artery and the aorta distal to the ligature (n = 20 mice) indicated a TAC pressure gradient of 60 ± 8 mmHg with this technique. Animals were sacrificed after 2 days or 14 days. All sham and TAC surgeries were performed by Dr. Jianxin Wu from the Victor Chang Cardiac Research Institute, Australia, assisted by myself.

2.3 Invasive hemodynamic measurements

After 14 days of sham or TAC, mice were anesthetized by inhalation of isoflurane (1.5%) and a 1.4 F micro-tip pressure catheter (Millar Instruments Inc, USA) was inserted into the left ventricle via the right carotid artery. The heart rate, systolic aortic pressure, LV systolic pressure, +dP/dt, and -dP/dt were recorded by LabChart Reader 6 (ADInstruments, Australia). The hemodynamic measurements were conducted by Dr. Jianxin Wu from the Victor Chang Cardiac Research Institute, Australia, assisted by myself. After animals were sacrificed, the heart weight (HW) and left ventricle weight (LVW) normalized to body weight (BW) and to tibia length (TL) were measured as indicators of LVH.

2.4 Mouse LV cardiomyocytes isolation and purification

Adult WT mice were heparinized and euthanized according to the Animal Research Act 1985 No 123 (New South Wales, Australia). Mouse hearts were dissected and perfused through the aorta and the coronary arteries by 10 mL pH 7.2 perfusion buffer containing 135 mM NaCl, 4 mM KCl, 1 mM $MgCl_2$, 0.33 mM NaH_2PO_2, 10 mM HEPES, 10 mM Glucose, 10 mM 2,3-butanedione monoxime (BDM), and 5 mM Taurine, with a Langendorff apparatus at 37 °C for 5 minutes. Next, 30 mL digestion buffer composed of the above solution and Collagenase B, D (dose by BW: 0.4 mg/g, Roche, Switzerland) and Protease Enzyme Type XIV (dose by BW: 0.07 mg/g, Sigma-Aldrich, USA) was used to perfuse the hearts for 15 minutes (**Figure 2-3A**). After the perfusion, the heart was removed from the setup and placed into

a pH 7.4 transfer buffer (Buffer A) containing 135 mM NaCl, 4 mM KCl, 1 mM $MgCl_2$, 0.33 mM NaH_2PO_2, 10 mM HEPES, 5.5 mM Glucose, 10 mM BDM, and 5 mg/mL bovine serum albumin (BSA). Both atria and the right ventricle were discarded, and the LV muscle was torn into small pieces and gently dispensed into the transfer buffer repeatly with a pipette to isolate cardiomyocytes. The suspension was then filtered through a 200 micro Filcon cup filter (BD Pharmingen, USA), and centrifuged at 20 g for 2 minutes.

For Ca^{2+} imaging experiments, another pH 7.4 transfer buffer (Buffer B) which contained 135 mM NaCl, 5.4 mM KCl, 0.5 mM $MgCl_2$, 1.8 mM $CaCl_2$, 10 mM HEPES, 5.5 mM Glucose, 10 mM BDM and 5 mg/ml BSA was used to adjust the Ca^{2+} concentration. Buffer A and B were mixed with different ratios to create solutions with a Ca^{2+} concentration of 0.06, 0.24, 0.6, and 1.2 mM. Isolated mouse LV cardiomyocytes were transferred sequentially into the solutions to gradually adapt to a final Ca^{2+} concentration of 0.6 mM or 1.2 mM. After this step, more than 70% of the cardiomyocyte still maintained rod shape (**Figure 2-3B**).

For mRNA or protein extraction purposes, after the isolation, the cardiomyocytes were purified by a method that provides 95% purity using Purified Rat Anti-Mouse CD31 antibody (BD Pharmingen, USA) and Dynabeads Sheep Anti-Rat IgG (Invitrogen, USA), following a protocol developed by Nicks et al. (2021). It was confirmed everytime that rod-shaped cardiomyocytes accounted for more than 85% of the total purified cardiomyocytes. The purified cardiomyocytes were used immediately for further experiments or frozen in liquid nitrogen and stored at -80 °C for future use.

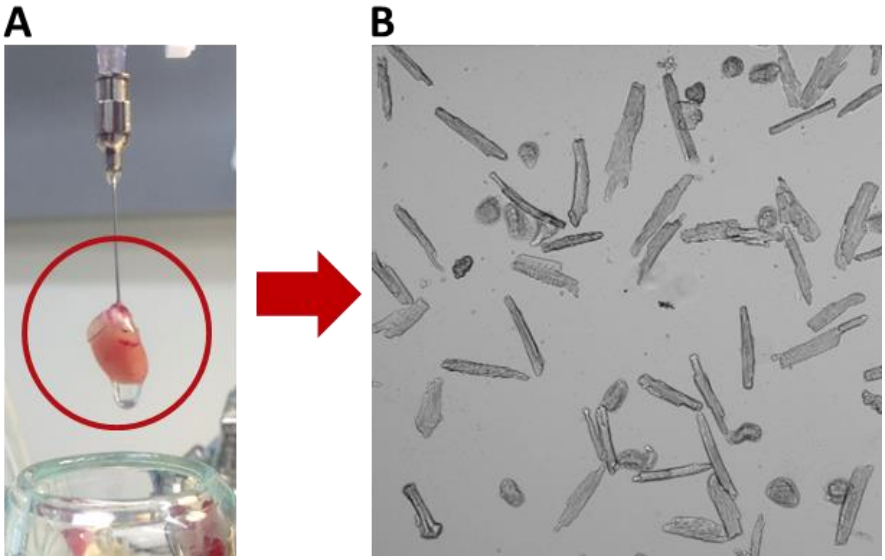

Figure 2-3 Isolation of mouse LV cardiomyocytes.

(A) Mouse heart on Langendorff apparatus during digestion. (B) Isolated mouse LV cardiomyocytes in a pH 7.4, 1.2 mM Ca^{2+} buffer.

2.5 Isotropic cell stretching

The *IsoStretcher* system (O. Friedrich et al., 2017; Schürmann et al., 2016) (details described in **1.5.1**) was used to apply isotropic stretch to HL-1 cells and isolated mouse LV cardiomyocytes, in collaboration with the Institute of Medical Biotechnology, Friedrich-Alexander-University Erlangen-Nürnberg, Germany. The PDMS chambers casted (**Appendix-figure 1**) for this project were modified from the original version (Schürmann et al., 2016) to a refined version which can contain volumes up to 1 mL, also has better transparency for microscopy. The PDMS chamber can be mounted on the six sliders of the *IsoStrether* through the six surrounding holes, and be stretched radially (**Figure 2-4A, B, C**).The entire membrane surface area of the PDMS chamber is 188.909 mm^2 (**Figure 2-4C**, blue + green area); the central area of the PDMS chamber is 158.37 mm^2 (**Figure 2-4C**, green area).

Also, 3D-printed supporting racks were mounted on the PDMS chambers to facilitate its installation on the *IsoStretcher* (**Figure 2-4D**). For HL-1 cell stretching, the PDMS chambers were pre-coated by adding 300 µL fibronectin-gelatin (250 µL fibronectin in 50 mL 0.02% gelatin in H_2O)/chamber and being stored at 4^oC, overnight. HL-1 cells were seeded in the PDMS chambers with a density of 120,000 cells/chamber for 4 hours prior to the experiments to allow them to attach to the surface of the PDMS chambers (**Figure 2-4D**).

Since mouse ventricular cardiomyocytes show low surface adherent properties, a special preparation method for isolated cardiomyocytes was developed based on the protocols by O. Friedrich et al. (2017). Isolated mouse LV cardiomyocytes were embedded in a polyethylene glycol-polyvinyl alcohol (PVA-PEG) hydrogel using *3-D Life* PVA-PEG Hydrogel SG Kit (Cellendes, Germany) and *3-D Life* RGD Peptide (Cellendes, Germany). Therefore the isotropic membrane stretch applied by the *IsoStretcher* can be transduced to the cells anchored within the hydrogel attached to the PDMS chamber (O. Friedrich et al., 2017). To form a hydrogel of 15 µL volume containing 4.5 µM cross-linked thiol groups and 0.5 µM RGD peptides, 1.25 µL CB, 2.5 µL SG-PVA, 0.375 µL RGD were mixed in 5 µL H_2O, and incubated for 30 minutes at 37 °C with 5% CO_2 to allow for annealing of the peptides to the PVA thiol groups. Then 2.5 µL of cell suspension containing approximate 250 mouse LV cardiomyocytes, and 3.375 µL PEG-Link were added into the mixture. The gel mixture was immediately transferred into the PDMS chamber, forming a droplet in the centre of surface area. A standard 0.15 mm thick glass coverslip with a diameter of 10 mm was gently placed on top of the droplet to control the gel thickness

and liquid evaporation during gel curing (**Figure 2-4E**). The gel mixture was kept at 37 °C with 5% CO_2 for 20 minutes, then the coverslip was removed gently by forceps. The stabilised gel disc containing LV cardiomyocyte was approximate 250 µm thick (**Figure 2-4E**), measured with a ZEISS LSM700 inverted confocal microscope (ZEISS, Germany). The cured gel was then covered with 300 µL Hank's Balanced Salt Solution (HBSS, Gibco, USA) supplemented with 1.2 mM $CaCl_2$ until followed experiments.

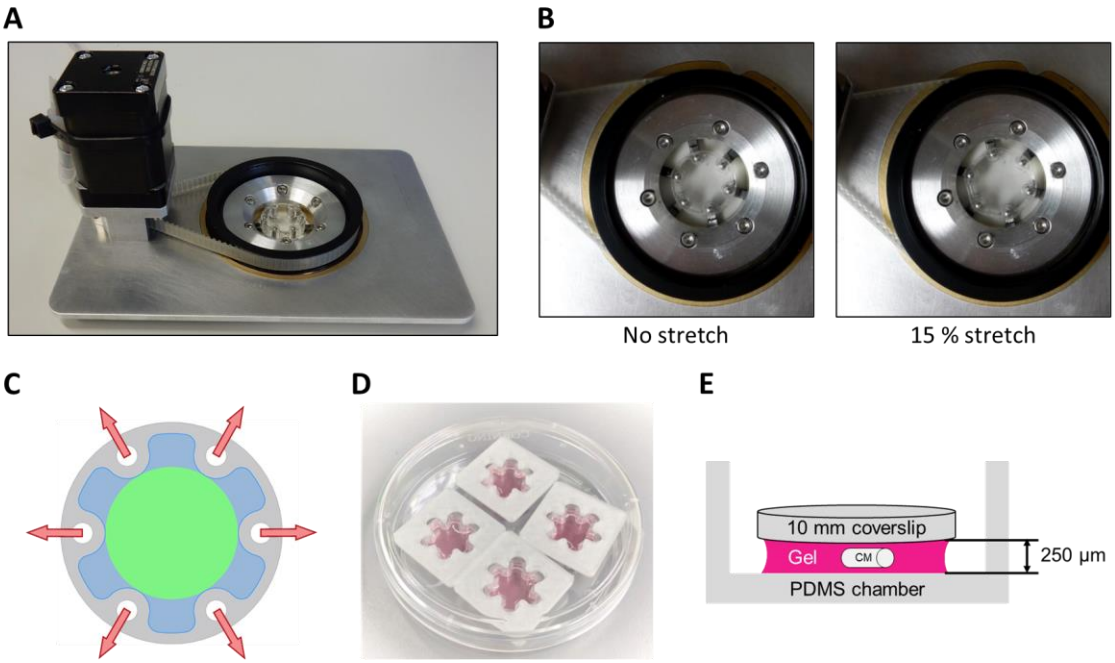

Figure 2-4 The *IsoStrether* system.

(A) The *IsoStrether* with a PDMS chamber mounted on the sliders. (B) PDMS chamber under no stretch (left) and 15% stretch (right). (C) A diagram of the PDMS chamber (top view). Arrows indicate the direction of stretch. Blue + green: entire membrane surface for cell seeding; green: central area of the membrane surface. (D) HL-1 cells in PDMS chamber with Claycomb medium. Supporting racks (white) were mounted on the PDMS chambers to facilitate its installation on the *IsoStretcher*. (E) Schematic image of embedding mouse LV cardiomyocytes (CM) into the hydrogel in PDMS chamber.

After initialised the *IsoStretcher*, the chambers were mounted on in a relaxed position (0% stretch). The HL-1 cells were imaged through the bottom of the PDMS chambers using an inverted microscope. During the experiments, the chambers were subjected to 15% isotropic stretch and then released to 0% at a speed of 20%/s based on previous study (O. Friedrich et al., 2017). The stretch magnitude and speed are adjustable via the built-in software (**Figure 2-5**). The applied percentage of stretch is positively related to the cell area change according to Schürmann et al. (2016) (**Figure 2-6**).

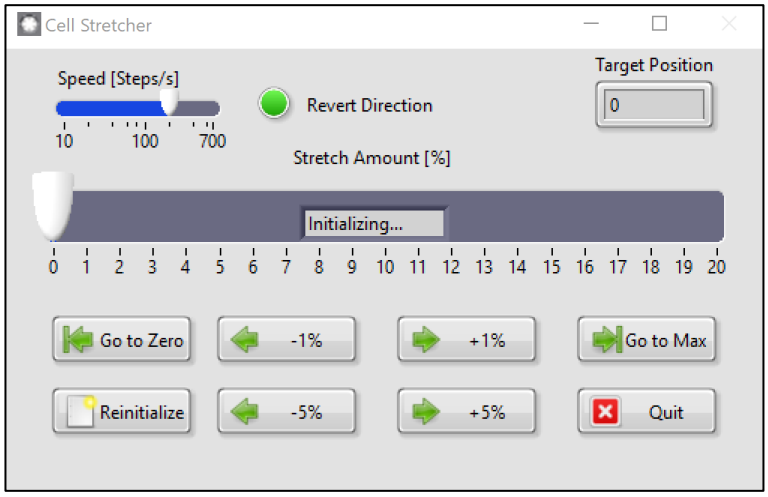

Figure 2-5 Operation interface of the *IsoStretcher* build-in software.

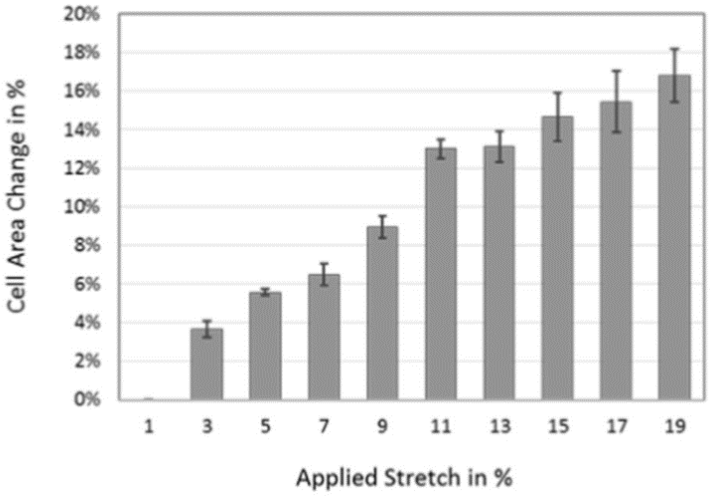

Figure 2-6 Relative area change of HEK cells at different stretch levels.

Image adapted from Schürmann et al. (2016).

2.6 siRNA transfection

HL-1 cells from a full confluence-culture were dissociated by Trypsin-EDTA (Sigma-Aldrich, USA), then seeded in cell culture plates with Claycomb Medium mixture (described previously in **2.1.2**). After 5 hours the medium mixture was replaced by a serum- and antibiotic-free culture medium mixture for overnight incubation (16 hours). After that, the serum- and antibiotic-free culture medium was replaced by normal Claycomb Medium mixture, at which time the cells reached an approximate 50% confluency. siRNA against *Trpm4* (Invitrogen, USA, MSS229248) or *Piezo1* (Invitrogen, USA, s107969 and s107970; 1:1 mixture) was transfected for corresponding gene knockdown. In addition, two non-targeting siRNAs, Stealth RNAi siRNA Negative Control (Invitrogen, USA) and Silencer Negative Control No. 1 siRNA (Invitrogen, USA) were transfected as negative control for *Trpm4* and *Piezo1* knockdown, respectively. *Trpm4*, *Piezo1*, or non-targeting siRNA (70 nM for all) was transfected together with Lipofectamine RNAiMAX

Transfection Reagent (Invitrogen, USA) diluted in Opti-MEM transfection medium (Invitrogen, USA), for 24 hours at 37 °C with 5% CO_2, following the manufacturer's instructions. The cells were used for further experiments after additional 48 hours of culture. siRNA transfection was confirmed every time in a seperate control well in the same cell culture plate, using BLOCK-iT Alexa Fluor Red Fluorescent Control (Invitrogen, USA) which is an indicator of lipid-mediated transfection efficiency (**Appendix-figure 2**).

2.7 Reverse transcription quantitative real-time polymerase chain reaction (RT-qPCR)

Gene expression was determined by reverse transcription quantitative real-time polymerase chain reaction (RT-qPCR). Total RNA was extracted and purified from mouse LV tissue, LV cardiomyocytes, cardiac fibroblasts, and HL-1 cells with the RNeasy Fibrous Tissue Mini Kit (QIAGEN), following the manufacturer's protocol. RNA (500 ng) was reverse transcribed into cDNA using the SuperScript III First-Strand Synthesis SuperMix kit (Invitrogen, USA). cDNA was subjected to PCR amplification to detect ANP (*Nppa*), BNP (*Nppa*), α-SA (*Acta1*), collagen III (*Col3a1*), *Trpm4*, and *Piezo1* gene expression, performed with the CFX384 Touch Real-Time PCR Detection System (Bio-Rad, USA), PCR master mix LightCycler 480 SYBR Green I Master (Invitrogen, USA). Samples were run in technical triplicate and the mRNA expression levels were normalized to those of GAPDH to calculate relative gene expression using delta-delta Ct method. The mouse RT-PCR primers (Sigma-Aldrich, USA) used are shown in (**Table 2-1**).

Table 2-1 RT-qPCR primers.

Gene	RT-qPCR primer 5'-3'
ANP (*Nppa*)	Forward: TGATAGATGAAGGCAGGAAGCCGC
	Reverse: AGGATTGGAGCCCAGAGTGGACTAGG
BNP (*Nppb*)	Forward: TCTCCAGAGCAATTCAAGAT
	Reverse: AACAACTTCAGTGCGTTACA
α-SA (*Acta1*)	Forward: GTGAGATTGTGCGCGACATC
	Reverse: GGCAACGGAAACGCTCATT
Collagen III (*Col3A1*)	Forward: GACAGATTCTGGTGCAGAGA
	Reverse: CATCAACGACATCTTCAGGAAT
Trpm4	Forward: GAGAAGCCCACAGATGCCTATG
	Reverse: AGCACCGACACCACCAAGTTTG
Piezo1	Forward: CTATGAGCCACTGTTCACCAT
	Reverse: CTGCATGGCTAGTGGATAGG
GAPDH	Forward: TATGTCGTGGAGTCTACTGG
	Reverse: AGTGATGGCATGGACTGTGG

2.8 Western blot analysis

For total protein extraction, mouse LV tissue, isolated cardiomyocytes, and HL-1 cells were lysed in a pH 7.4 lysis buffer containing 150 mM NaCl, 50 mM Tris-HCL, 1% Triton X-100, 1 mM sodium orthovanadate, 1 mM beta-glycerophosphate, 5 mM dithiothreitol, and MiniComplete protease inhibitors (Roche, Switzerland); for cytoplasmic and nuclear protein extraction, LV tissue was lysed using NE-PER Nuclear and Cytoplasmic Extraction Reagents (Thermo Fisher Scientific, USA) and Halt Protease and Phosphatase Inhibitor Cocktail (Thermo Fisher Scientific, USA), both with a homogenizer (PRO Scientific, USA). In addition, total protein extracted from

HEK293 cells and human RBCs (J. V. Li et al., 2021) were donated from the Cox Laboratory of the Victor Chang Cardiac Research Institute, Australia. For western blot, protein (40 μg for each sample) was loaded on NuPAGE 3-8% Tris-Acetate Gels (Invitrogen, USA) for Piezo1, and 4-20% Mini-PROTEAN TGX Gels (Bio-Rad, USA) for all the other proteins, and separated by electrophoresis. Samples were transferred to PVDF membranes (Bio-Rad, USA), blocked with 5% bovine serum albumin (BSA) then labelled overnight with primary antibodies (**Table 2-2**): anti-TRPM4, anti-Piezo1, anti-CaMKIIδ, anti-p-CaMKII, anti-HDAC4, anti-p-HDAC4, anti-MEF2A, anti-NFATc4, anti-GSK3β, anti-p-GSK3β, and anti-GATA4. Anti-GAPDH and anti-Histone H2B were used as standards for loading. Horseradish peroxidase-conjugated (HRP) goat anti-rabbit or rabbit anti-mouse secondary antibodies (**Table 2-2**) were used at room temperature for one hour. Immunological detection was accomplished using Amersham ECL Western blotting detection reagents (GE Healthcare, USA). Protein levels were quantified by densitometry using ImageJ (National Institutes of Health, USA; http://rsbweb.nih.gov/ij/) software. The total and cytoplasmic protein levels were normalized to relative changes in GAPDH; The nuclear protein level was normalized to relative changes in Histone H2B. The results were expressed as fold changes relative to control animals in each experiment.

Table 2-2 Antibodies for western blot.

Antibody	Source or reference	Identifiers	Dilution for Western blot
anti-TRPM4 (rabbit polyclonal)	Alomone Labs	Cat# ACC-044, RRID: AB_2040250	1:200
anti-Piezo1 (rabbit polyclonal)	Proteintech	Cat# 15939-1-AP RRID: AB_2231460	1:500
anti-CaMKII delta (rabbit monoclonal)	Abcam	Cat# ab181052, RRID: AB_2891241	1:1000
anti-p-CaMKII (Thr287) (rabbit polyclonal)	Thermo Fisher Scientific	Cat# PA5-37833, RRID: AB_2554441	1:5000
anti-HDAC4 (rabbit monoclonal)	Cell Signaling Technology	Cat# 7628 RRID: AB_10860255	1:1500
anti-p-HDAC4 (Ser246) (rabbit monoclonal)	Cell Signaling Technology	Cat# 3443 RRID: AB_2118723	1:1500
anti-MEF2A (rabbit polyclonal)	Cell Signaling Technology	Cat# 9736 RRID: AB_10691852	1:3000
anti-NFATc4 (rabbit polyclonal)	Abcam	Cat# ab99431, RRID: AB_10675673	1:1500
anti-GSK3β (rabbit monoclonal)	Cell Signaling Technology	Cat# 9315, RRID: AB_490890	1:500
anti-p-GSK3β (Ser9) (rabbit polyclonal)	Cell Signaling Technology	Cat# 9336, RRID: AB_331405	1:1500
anti-GATA4 (mouse monoclonal)	Santa Cruz Biotechnology	Cat# sc-25310, RRID: AB_627667	1:1000
anti-GAPDH (rabbit monoclonal)	Cell Signaling Technology	Cat# 2118, RRID: AB_561053	1:10000
anti-Histone H2B (rabbit polyclonal)	Abcam	Cat# ab1790, RRID: AB_302612	1:5000
goat anti-rabbit IgG (goat polyclonal)	Abcam	Cat# ab6721, RRID: AB_955447	1:10000
rabbit anti-mouse IgG (rabbit polyclonal)	Abcam	Cat# ab6728, RRID: AB_955440	1:5000

2.9 Histology

Masson's trichrome stain was used to quantify fibrosis in the LV (collagen fibres stain blue). The hearts were excised from isoflurane-euthanized mice, washed with PBS. Then the hearts were longitudinally cut at the frontal plane, embedded into optimal cutting temperature (OCT) compound (Sakura Finetek), gradually frozen in liquid nitrogen via isopentane to avoid tissue damage. Serial sections with a thickness of 6 µm were sliced with a cryostat (Leica). The slides were then stained with a Masson's trichrome staining kit (Sigma-Aldrich, USA) following the manufacturer's instructions. Images of the LV were obtained with 4 to 6 fields per section (McMullen et al., 2004) using a brightfield microscope (Leica). Blue-stained fibrosis areas within sections were determined using colour-based thresholding (Abràmoff, Magalhães, & Ram, 2004) and measured with ImageJ (National Institutes of Health, USA). The percentage of total fibrosis area was calculated by taking the sum of the blue-stained areas divided by the total LV area.

2.10 Ca^{2+} transient measurements

2.10.1 Ca^{2+} imaging using epifluorescence microscope

HL-1 cells were rinsed with physiological salt solution (PSS) supplemented with 1 mM $CaCl_2$; mouse LV cardiomyocytes in 96 well cell culture microplate (Greiner Bio-One, Germany) or the hydrogel containing cardiomyocytes were rinsed with HBSS supplemented with 1.2 mM $CaCl_2$. Then the cells were incubated with 2 µM Fluo-4 AM (Invitrogen, USA), a fluorescent Ca^{2+} indicator, in the same PSS/HBSS mixture at 37 °C with 5%

CO_2 for 30 minutes. After that, the cells were rinsed twice with PSS/HBSS mixture and then kept in PSS/HBSS mixture during the experiment.

Ca^{2+} imaging and data recording was carried out on a Nikon Eclipse Ti2-E Inverted Optical Mapping epifluorescence microscope (Nikon Instruments, USA), using 20 x objective lens, with 2 x 2 binning, and 5, 100, or 200 ms frame interval. **Figure 2-7** is an example of acquired HL-1 cell intracellular Ca^{2+} image.

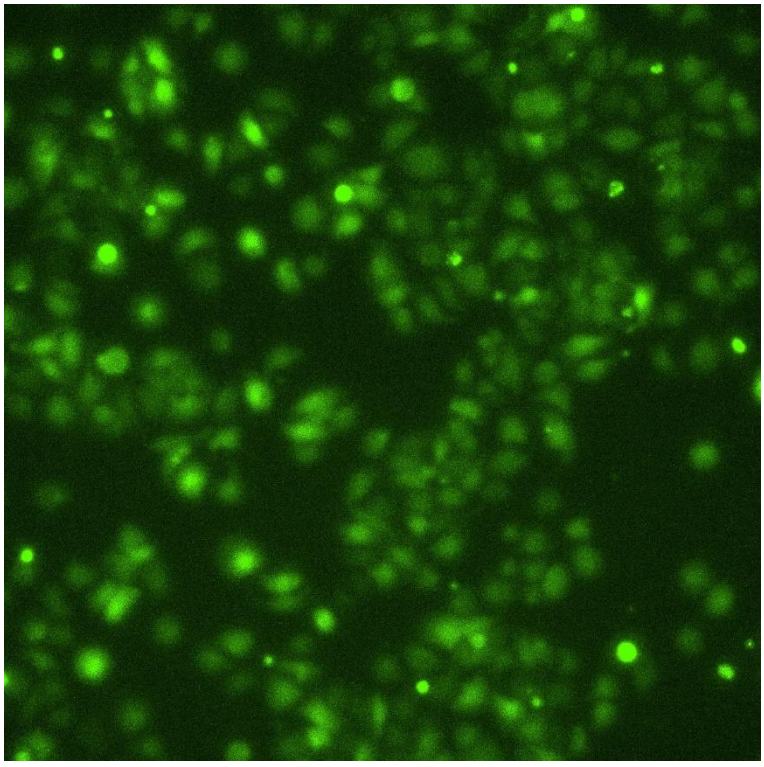

Figure 2-7 Acquired HL-1 cell intracellular Ca^{2+} image.

Image area = 333 µm x 333 µm.

2.10.2 Ca^{2+} transient measurements using kinetic imaging cytometry (KIC)

Mouse LV cardiomyocytes were isolated and maintained in Buffer A and B mixture with a Ca^{2+} concentration of 0.6 mM (described in **2.5**). The cells were seeded into a 96-well cell culture microplate (Greiner Bio-One, Germany) and incubated with 2 µM Fluo-4 AM (Invitrogen, USA) at 37 °C with 5% CO_2 for 45 minutes. After that, the cells were rinsed with and kept in the same Buffer A and B mixture (0.6 mM Ca^{2+}).

Kinetic imaging cytometry (KIC, IC-200, Vala Sciences) was used to perform time series Ca^{2+} transient recording with application of electrical pacing (1Hz). Fluorescent Ca^{2+} images were acquired using CyteSeer Scanner v2.2.32.0 software (Vala Sciences) at a sampling frequency of 100Hz. Obtained data was initially analysed using the CyteSeer v2.8.0.91 software (Vala Sciences).

2.11 Action potential measurements

2.11.1 HL-1 cell membrane potential acquisition

HL-1 cells were rinsed with DMEM supplemented with 10% FBS (both from Sigma-Aldrich, USA) and incubated with a fluorescent voltage sensitive dye FluoVolt (Invitrogen, USA) which was 1:500 diluted in Claycomb Medium mixture (described in **2.1.2**), at 37 °C with 5% CO_2 for 45 minutes. After that, the cells were rinsed twice with the same DMEM mixture and then kept in Claycomb Medium mixture during the experiment.

HL-1 cell membrane potential data acquisition was carried out on a Nikon Eclipse Ti2-E Inverted Optical Mapping epifluorescence microscope (Nikon Instruments, USA), using 20 x objective lens, with 75% power and 2 x 2 binning. The recording interval was 5 or 10 ms for different experiments. **Figure 2-8** is an example of acquired HL-1 cell membrane potential image.

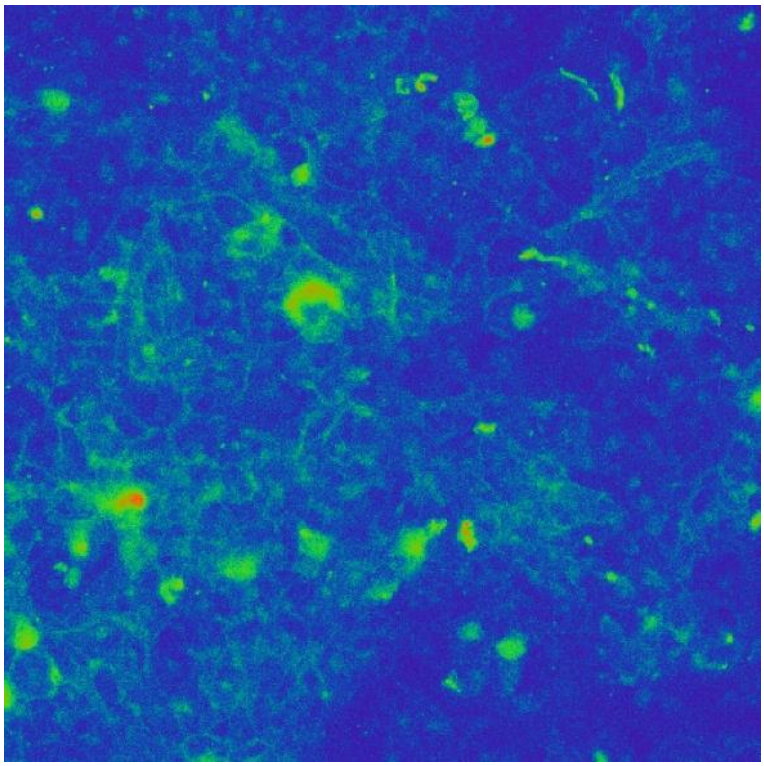

Figure 2-8 Acquired HL-1 cell membrane potential image.

Image area = 333 µm x 333 µm.

2.11.2 HL-1 cell action potential data analysis

The recorded membrane potential data was initially analysed using the build-in NIS-Elements Microscope Imaging Software, version 5.11.03 (Nikon Instruments, USA) to extract the intensity profile during time measurement.

After that, a MATLAB (Mathworks)-based data analysis software (authors: Anton Shpak and Satya Arjunan from the Innovation Centre, Victor Chang Cardiac Research Institute, Australia.) was used to express the HL-1 cell action potentials and to calculate a variety of parameters, including the frequency, duration, amplitude, and maximum upstroke velocity, etc. of the action potential (**Figure 2-9A**). This software also calibrates the baseline change of the action potentials due to the sample bleaching under the microscope (**Figure 2-9B**). In final data analysis the action potential duration at 90% repolarization (APD90) was analysed as an alternative to the actual action potential duration to avoid potential recognition errors caused by noise.

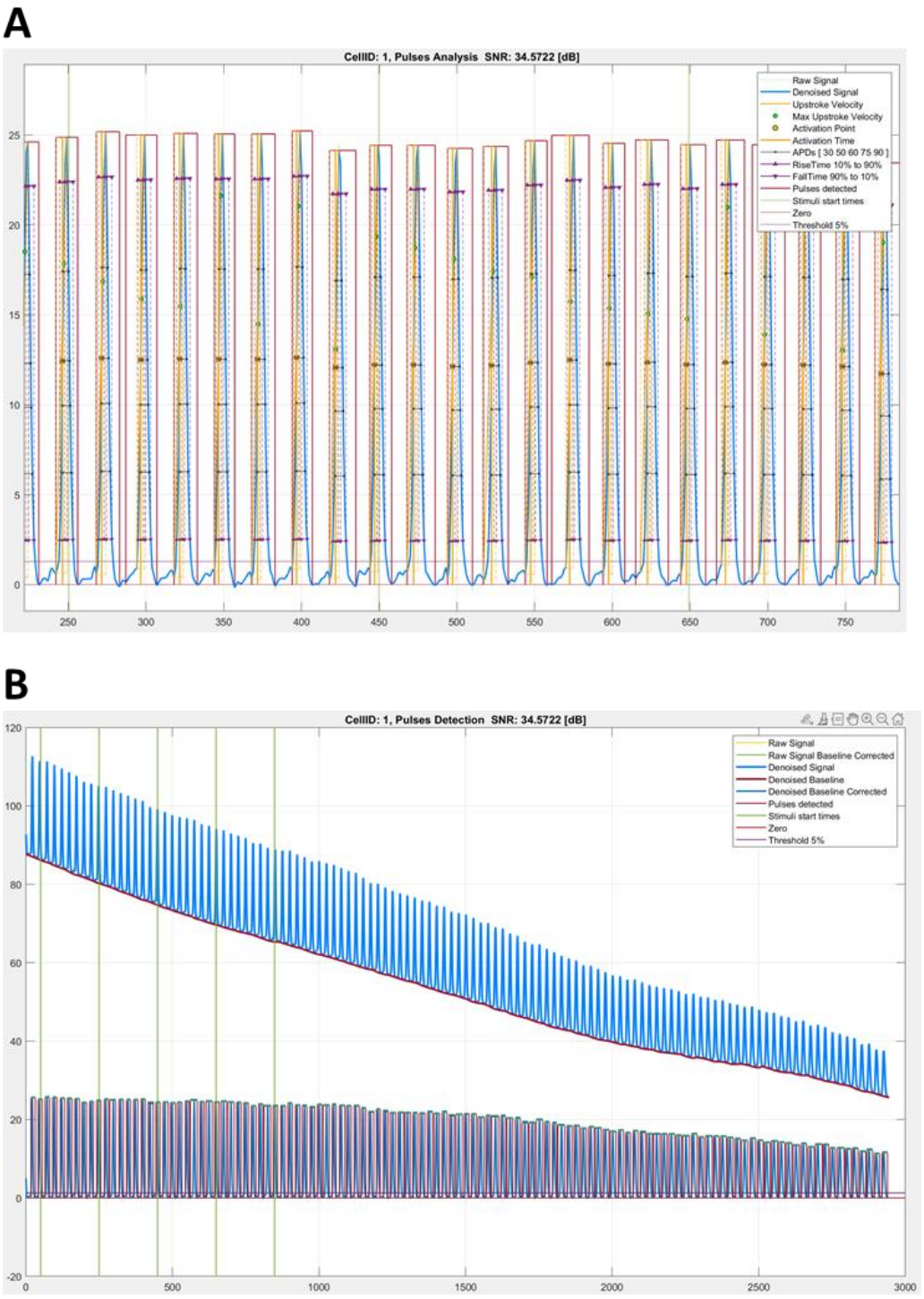

Figure 2-9 Example of HL-1 cell action potential data analysis.

(A) HL-1 cell action potentials in data analysis. (B) Baseline calibration. Top panel: before calibration; bottom panel: after calibration.

2.12 Chemicals for pharmacological studies

The chemicals used for pharmacological studies are shown in **Table 2-3**.

Table 2-3 Chemicals for pharmacological studies.

Chemical	Source	Identifiers	Stock solution concentration
Nifedipine	Sigma-Aldrich	Cat# N7634	20 mM in DMSO
Lidocaine	Sigma-Aldrich	Cat# L7757	20 mM in H_2O
9-phenathrol	Sigma-Aldrich	Cat# 211281	20 mM in DMSO
Flufenamic acid	Sigma-Aldrich	Cat# F9005	20 mM in DMSO
GsMTx4	Tocris Bioscience	Cat# 4912	5 mM in H_2O
Yoda1	Tocris Bioscience	Cat# 5586	20 mM in DMSO
NS 1619	Sigma-Aldrich	Cat# N170	50 mM in DMSO

2.13 Statistics

All experiments and analyses were conducted blinded. Averaged data are presented as means ± standard error of the mean (SEM). The statistical analysis was performed using GraphPad Prism software, version 7.04 (GraphPad). For comparisons between two sets of data, unpaired t-test was used to determine the statistical significance. For comparisons among multiple sets of data with one factor or two factors, one-way or two-way

ANOVA was used accordingly, followed by Tukey's post-hoc test. $p < 0.05$ was considered statistically significant.

Chapter 3 The role of TRPM4 channels in pressure overload-induced LVH

This chapter contains work published in:

Guo, Y.†, Yu, Z. Y.†, Wu, J., Gong, H., Kesteven, S., Iismaa, S. E., Chan, A. Y., Holman, S., Pinto, S., Pironet, A., Cox, C. D., Graham, R. M., Vennekens, R., Feneley, M. P.*, & Martinac, B.* (2021). The Ca^{2+}-activated cation channel TRPM4 is a positive regulator of pressure overload-induced cardiac hypertrophy. *eLife*, *10*, e66582.

Author contributions of Guo Y: data curation, formal analysis, validation, investigation, methodology, writing-original draft, writing-review and editing.

† These authors contributed equally.

* Corresponding author.

3.1 Introduction

As described previously, pathological LVH can occur in response to mechanical pressure overload and remains the single most important clinical predictor of cardiac mortality (Levy et al., 1990; Mudd & Kass, 2008). Understanding the molecular mechanisms underlying pressure overload-induced pathological LVH may expand the current limited options of treatment, by preventing, inhibiting, or reversing its development, thus of significant value both in research and in clinic.

Previous study (Yu, Gong, Wu, et al., 2021) has demonstrated that the Ca^{2+}/CaM dependent CaMKII-HDAC-MEF2 pathway is activated by the increased intracellular Ca^{2+} levels in response to TAC, which is the most common experimental approach for the induction of LV pressure overload. On the other hand, Gq-coupled receptors and the calcineurin-NFAT pathway are not responsible for TAC-induced LVH (Yu, Gong, Wu, et al., 2021).

However, the mechanism by which the CaMKII-HDAC-MEF2 pathway is activated by TAC remains unclear. Prime candidates for mediating this mechanism are MS channels. In cardiac mechanotransduction, where mechanical stimuli are converted into electrical or biochemical signals (Cox et al., 2019; Martinac & Cox, 2017; Peyronnet et al., 2016), Ca^{2+}-dependent ion channels, such as the TRP channels, act as important modulators of intracellular Ca^{2+} homeostasis (C. Wang et al., 2018) and are thought to be unique biosensors that activate specific pathological LVH signalling pathways (Eder & Molkentin, 2011; Wu et al., 2010).

As a Ca^{2+}- and voltage-activated non-selective monovalent cation channel, TRPM4 may contribute to an increase in intracellular Ca^{2+} concentration by causing membrane depolarisation (Pierre Launay et al., 2002), although it has been known not to be directly activated by membrane stretch (Constantine et al., 2016; Gottlieb et al., 2008; Nikolaev et al., 2019). Consequently, if TRPM4 plays a role in TAC-induced LVH, it may act as an amplifier of the primary Ca^{2+} or voltage signal from a yet to be determined MS ion channel, or channels. TRPM4 has been functionally characterized in atrial and ventricular cardiomyocytes, in both human and rodent (Guinamard et al., 2004; Guinamard et al., 2006; H. Watanabe, Murakami, Ohba, Takahashi, & Ito, 2008). Other studies indicate that TRPM4 contributes to both cardiac function and disease development, including cardiac hypertrophy and heart failure (Frede et al., 2020; Gueffier et al., 2017; Hedon et al., 2021; Jacobs et al., 2015; Mathar et al., 2014). Previous studies using *Trpm4* cKO mice have shown that TRPM4 is a negative regulator of AngII-induced cardiac hypertrophy in mice, which involves the calcineurin-NFAT pathway (Kecskes et al., 2015), and that TRPM4 is essential for survival after myocardial infarction (Hedon et al., 2021; Jacobs et al., 2015). However, whether TRPM4 plays a role in mechanical pressure overload-induced LVH has yet to be determined.

In this study, the role of TRPM4 in pressure overload LVH induced by TAC was investigated in homozygous *Trpm4* cKO mice (Kecskes et al., 2015) and compared to WT control mice. The results demonstrate that loss of cardiomyocyte TRPM4 significantly attenuates the development of LVH observed in response to TAC in WT mice. Moreover, this effect is associated with reduced activation of the CaMKII-HDAC4-MEF2 pathway.

3.2 Results

3.2.1 Development of LV hypertrophy in response to pressure overload at 14 days after TAC in WT mice

As identified by previous study (Yu, Gong, Wu, et al., 2021), TAC-induced cardiac hypertrophy is a response to LV pressure overload. As expected, LV systolic pressure increased by ~65 mmHg ($p < 0.001$) 14 days after TAC, whereas heart rate, dP/dt_{max} and dP/dt_{min} remained unaltered (**Table 3-1**). Consistent with 14 days of TAC resulting in a compensated LVH model, body weight (BW) and lung weight (LW) (**Table 3-1**) remained unchanged in TAC mice compared to sham-operated mice. These results indicate that this TAC model at 14 days remains an excellent model of compensated LVH rather than heart failure.

Table 3-1 Hemodynamic and anatomical parameters 2 days or 14 days after induction of pressure overload in WT mice.

Hemodynamic parameters were measured in WT mice 14 days after being subjected to TAC versus sham-operated controls (n = 7-11/group). Post-mortem analysis of mice 2 days or 14 days after sham or TAC*;* LVH developed 14 days after TAC, indicated by the ratios of HW/BW, LVW/BW and LVW/TL in WT mice subjected to TAC versus sham-operated controls. Cardiac fibrosis was evaluated by Masson's trichrome staining of LV tissue from WT mice subjected to 2 days or 14 days of TAC versus sham-operated controls; cardiac fibrosis areas were graded (n = 5-6/group). Relative Collagen III (*Col3α1*) mRNA expression was normalized by GAPDH and calculated as fold change relative to sham in 2 days and 14 days groups, respectively (n = 4/group). LVSP: Left ventricular systolic pressure; HR: heart rate; dP/dt: first derivative of pressure with respect to time; BW: body weight; HW: heart weight; LVW: left ventricular weight; LW: lung weight; TL: tibia length; HW/BW: heart weight to body weight ratio; LVW/BW: LV weight to body

weight ratio; LVW/TL: LV weight to tibia length ratio; LW/BW: lung weight to body weight ratio. Results are presented as means ± SEM. $^{**}p < 0.01$, $^{***}p < 0.001$, compared between sham- and TAC-operated groups.

	2 days		14 days	
	Sham	**TAC**	**Sham**	**TAC**
Hemodynamic parameter				
n			7	7
HR (bpm)			506 ± 4	506 ± 3
Aortic systolic pressure (mmHg)			103 ± 1	164 ± 2 ***
Aortic diastolic pressure (mmHg)			76 ± 1	74 ± 1
LV systolic Pressure (mmHg)			105 ± 3	164 ± 8 ***
dP/dt_{max} (mmHg/s)			9438 ± 367	9838 ± 259
dP/dt_{min} (mmHg/s)			-9666 ± 377	-10108 ± 364
Anatomical parameter				
n	8	8	11	11
BW (g)	28.5 ± 0.3	27.7 ± 0.5	28.6 ± 0.3	27.2 ± 0.5
HW (mg)	136.7 ± 2.2	132.8 ± 1.3	133.1 ± 1.9	176.1 ± 3.6 ***
LVW (mg)	98.0 ± 2.0	97.7 ± 1.4	96.4 ± 1.8	136.1 ± 1.4 ***
LW (mg)	141.9 ± 0.9	143.6 ± 1.5	146.9 ± 1.8	147.0 ± 1.9
TL (mm)	17.4 ± 0.1	17.5 ± 0.2	17.5 ± 0.2	17.2 ± 0.1
HW/BW (mg/g)	4.8 ± 0.1	4.8 ± 0.1	4.6 ± 0.1	6.6 ± 0.1 ***
LVW/BW (mg/g)	3.4 ± 0.1	3.5 ± 0.1	3.4 ± 0.1	5.1 ± 0.1 ***
LVW/TL (mg/mm)	5.6 ± 0.1	5.6 ± 0.1	5.3 ± 0.1	7.9 ± 0.1 ***
LW/BW (mg/g)	5.0 ± 0.1	5.2 ± 0.1	5.2 ± 0.1	5.4 ± 0.1
Assessment of cardiac fibrosis				
n	5	5	6	6
Fibrosis areas (%)	4.0 ± 0.2	3.6 ± 0.2	4.4 ± 0.1	12.4 ± 0.5 ***
n	4	4	4	4
Collagen III mRNA expression (fold change)	1.0 ± 0.1	5.7 ± 0.8 **	1.0 ± 0.1	5.1 ± 0.7 **

Representative photos illustrate the size differences of WT mouse hearts after 2 days and 14 days of sham or TAC (**Figure 3-1A**). LVH was not detected 2 days after TAC (**Table 3-1**, **Figure 3-1A**), whereas significant LVH in WT mice 14 days after TAC was observed, as evidenced by increases in heart weight (HW, $p < 0.001$), left ventricular weight (LVW, $p < 0.001$) and the ratios of heart weight/body weight (HW/BW, $p < 0.001$), left ventricle

weight/body weight (LVW/BW, $p < 0.001$) and left ventricle weight/tibial length (LVW/TL, $p < 0.001$), without changes in BW or TL, when compared with the sham-operated animals **(Table 3-1).** Consistent with the development of pathological hypertrophy, TAC was associated with an increase in cardiac fibrosis ($p < 0.001$, **Table 3-1, Figure 3-1B**) and enhanced collagen III (*Col3a1*) expression ($p < 0.001$, **Table 3-1**).

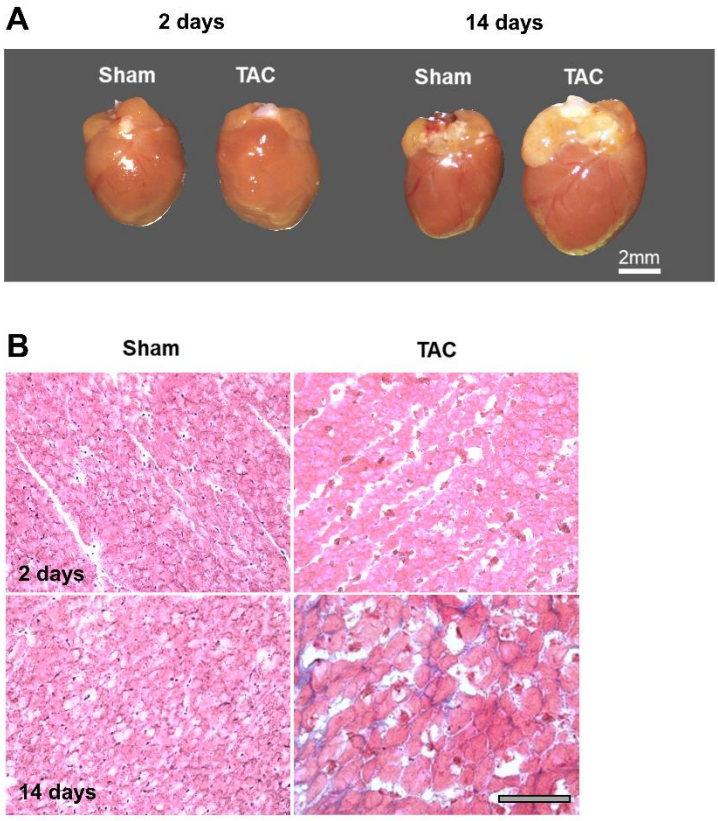

Figure 3-1 Enlarged heart and cardiac fibrosis were detected 14 days after TAC.

(A) Representative photos of hearts from WT mice 2 days or 14 days after sham or TAC. (B) Representative photos of cardiac fibrosis, evaluated by Masson's trichrome staining of LV tissue from WT mice subjected to TAC versus sham-operated controls. Scale bar = 100 μm.

3.2.2 Early gene markers of induction of pathological hypertrophy in WT mice

Although there was no significant LVH 2 days after TAC (**Table 3-1**, **Figure 3-1A**), induction of hypertrophy-associated genes [atrial natriuretic peptide (ANP, *Nppa*; 9.9 fold, $p < 0.01$), brain natriuretic peptide (BNP, *Nppb*; 8.1 fold, $p < 0.01$) and α-skeletal actin (α-SA, *Acta1*; 4.5 fold, $p < 0.01$)] was already evident at this time (**Table 3-2**), and expression of these genes remained high at 14 days (ANP, *Nppa*; $p < 0.001$, BNP, *Nppb*; $p < 0.001$, and α-SA, *Acta1*; $p < 0.001$, **Table 3-2**).

Table 3-2 Early markers of LVH induction in response to left ventricular pressure overload in WT mice.

Relative mRNA expression of ANP (*Nppa*), BNP (*Nppb*) and α-SA (*Acta1*) after 2 days or 14 days of TAC compared to sham (n = 4-5/group). The relative mRNA expression was normalized by GAPDH and calculated as fold change relative to sham in the 2 days and 14 days groups, respectively. Results are presented as means ± SEM. $^{**}p < 0.01$, $^{***}p < 0.001$, compared between sham- and TAC-operated groups.

	2 days		14 days	
	Sham	**TAC**	**Sham**	**TAC**
LVH markers (fold change)				
n	4	4	5	5
ANP	1.0 ± 0.1	9.9 ± 1.1 **	1.0 ± 0.1	9.6 ± 0.7 ***
BNP	1.0 ± 0.1	8.1 ± 0.8 **	1.0 ± 0.2	7.5 ± 0.4 ***
α-SA	1.0 ± 0.1	4.5 ± 0.5 **	1.0 ± 0.1	4.2 ± 0.4 ***

3.2.3 TRPM4 expression was downregulated in response to TAC-induced LV pressure overload in WT mice

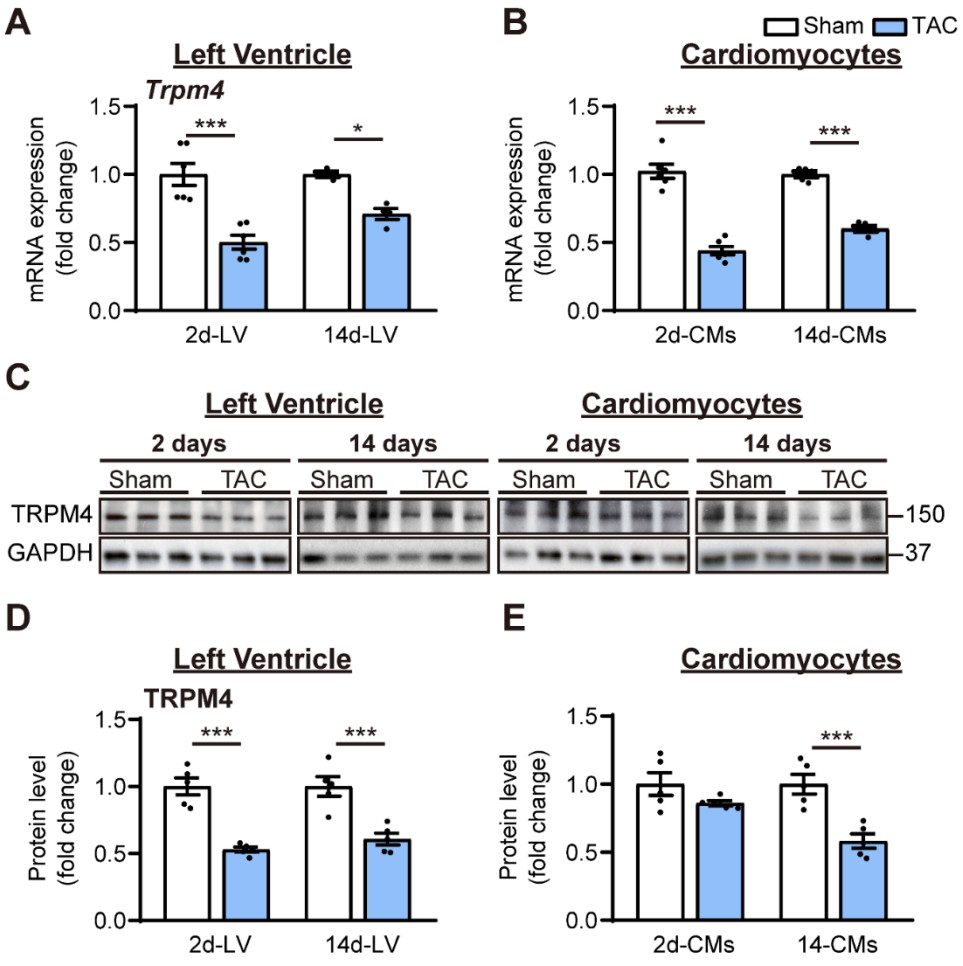

Figure 3-2 TRPM4 expression was downregulated in response to left ventricular (LV) pressure overload.

(A) Relative mRNA expression of *Trpm4* in LV tissue and (B) in LV cardiomyocytes (CMs) after 2 days and 14 days of sham and TAC. (C) Representative western blots of TRPM4 protein expression in LV tissue (left panel) and in LV cardiomyocytes (right panel). (D) Western blots from LV tissue and (E) LV cardiomyocytes after 2 days and 14 days of TAC were quantified for TRPM4 protein expression. Relative TRPM4 mRNA and protein expression in the LV tissue and cardiomyocytes were normalized by GAPDH and

calculated as fold change relative to sham in 2 days and 14 days groups, respectively. Results are presented as means ± SEM. *p < 0.05, ***p < 0.001 vs. sham-operated groups.

To examine whether the TRPM4 ion channel is involved in TAC-induced LVH, RT-PCR was conducted on LV tissues or isolated LV cardiomyocytes from TAC- or sham-operated hearts. *Trpm4* mRNA expression in LV tissue (**Figure 3-2A**) and isolated cardiomyocytes (**Figure 3-2B**) fell by 50% (p < 0.001) and 57% (p < 0.001), respectively, in response to 2 days of TAC, and expression continued to be reduced by 30% (p < 0.05, **Figure 3-2A**) and 40% (p < 0.001, **Figure 3-2B**), respectively, at 14 days. Consistent with the mRNA changes, TRPM4 protein expression in LV tissue and isolated cardiomyocytes also fell significantly, particularly in cardiomyocytes, after 14 days of TAC (p < 0.001) (**Figure 3-2C-E**).

3.2.4 TRPM4 deficiency decreases the hypertrophic response to TAC-induced LV pressure overload

To further investigate the role of TRPM4 channels in pressure overload-induced LVH, TAC or sham surgery was performed in mice with cardiomyocyte-specific, conditional deletion of *Trpm4* (*Trpm4* cKO) using Cre expression driven by the *Myl7* promoter (Kecskes et al., 2015). Results obtained in these *Trpm4* cKO mice were compared with those in WT ($Trpm4^{+/+}$) mice. Hemodynamic and anatomical parameters obtained after 2 days and 14 days of sham/TAC in WT and *Trpm4* cKO mice are shown in **Appendix-table 1**. TAC produced a similar degree of LV pressure overload in both WT (p < 0.001) and *Trpm4* cKO (p < 0.001) mice when compared

with sham-operated groups (**Figure 3-3A**) but did not alter heart rate (**Figure 3-3B**), cardiac contractility (**Figure 3-3C, D**), LW (**Figure 3-3E**) or BW (**Figure 3-3G**). **Figure 3-3F** illustrates representative images of the WT and *Trpm4* cKO mouse hearts after 14 days of sham or TAC**.** No LVH was detected 2 days after TAC in either *Trpm4* cKO mice or WT mice when compared with sham-operated groups (**Figure 3-3H-J**). After 14 days, TAC induced a 32, 42 and 44% increase (all $p < 0.001$) in HW/BW ratio, LVW/BW ratio and LVW/TL ratio, respectively, in WT mice when compared with sham-operated controls (**Figure 3-3H-J**). However, this hypertrophic response to 14 days of TAC was attenuated in *Trpm4* cKO mice, as evident by only a 17, 20 and 23% increase (all $p < 0.001$) in HW/BW ratio, LVW/BW ratio and LVW/TL ratio, respectively (**Figure 3-3H-J**). These findings demonstrate that when compared with WT mice, *Trpm4* cKO mice developed approximately 50% less LVH ($p < 0.001$) in response to TAC.

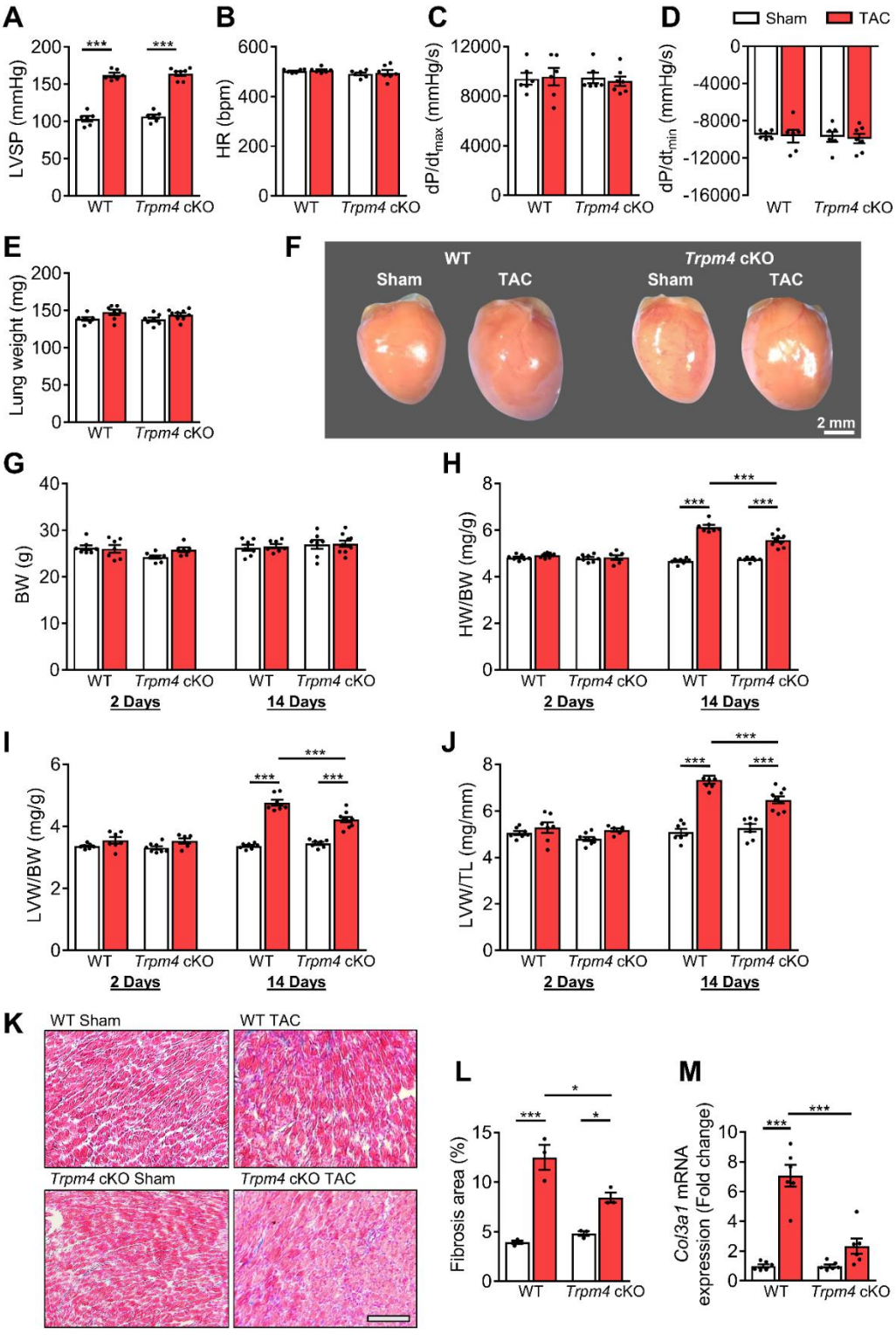

Figure 3-3 The hypertrophic response of WT and *Trpm4* cKO mice to TAC-induced LV pressure overload.

(A) Systolic pressure, (B) heart rate, (C) and (D) dP/dt after 14 days of sham or TAC in WT and *Trpm4* cKO mice (n = 6-7/group). (E) Lung weight after 14 days of sham or TAC in WT and *Trpm4* cKO mice (n = 7-9/group). (F) Representative photos indicate heart size differences after 14 days of sham or TAC in WT and *Trpm4* cKO mice. (G) Body weight, (H) Heart weight, and (I, J) LV weight normalized to body weight and tibia length, in WT and *Trpm4* cKO mice after 2 days and 14 days of sham or TAC (n = 7-9/group). (K) Representative micrographs and (L) Quantitation of Masson's trichrome staining of LV tissue from WT mice and *Trpm4* cKO mice after 14 days of sham or TAC (n = 3/group), scale bar = 200 µm in (K). (M) Relative Collagen III (Col3a1) mRNA expression after 14 days of sham or TAC (n = 6/group). The mRNA relative expression was normalized by GAPDH and calculated as fold change relative to sham in WT and *Trpm4* cKO groups, respectively. Results are presented as means ± SEM. *$p < 0.05$, ***$p < 0.001$.

3.2.5 Reduced fibrosis in *Trpm4* cKO hearts after TAC

Cardiac fibrosis in response to pressure overload in *Trpm4* cKO hearts and WT hearts was evaluated by Masson's trichrome staining (**Figure 3-3K**). When compared with an average 3.17-fold increase ($p < 0.001$) in cardiac fibrosis in WT TAC hearts, the increase in *Trpm4* cKO TAC hearts was only 1.75-fold ($p < 0.05$) (**Figure 3-3L**). In addition, a significant increase in collagen III (*Col3a1*) mRNA expression in WT TAC hearts was noted when compared with WT sham hearts ($p < 0.001$). However, there was no significant increase in collagen III (*Col3a1*) mRNA expression in *Trpm4* cKO TAC hearts when compared with sham hearts (**Figure 3-3M**). Thus, *Trpm4* inactivation attenuated the fibrotic response to TAC.

3.2.6 TRPM4 deficiency reduced the expression of hypertrophy markers in response to TAC- induced pressure overload

Consistent with the development of pathological hypertrophy, both 2 days and 14 days of TAC in WT mice significantly enhanced expression of the hypertrophy-associated genes, ANP (*Nppa*), BNP (*Nppb*) and α-SA (*Acta1*) (**Figure 3-4A**, **B**). However, these gene markers remained unchanged with TAC in *Trpm4* cKO mice (**Figure 3-4A, B**), except for ANP (*Nppa*) at 14 days. These data indicate that loss of TRPM4 attenuates the activation of hypertrophic marker genes in response to TAC.

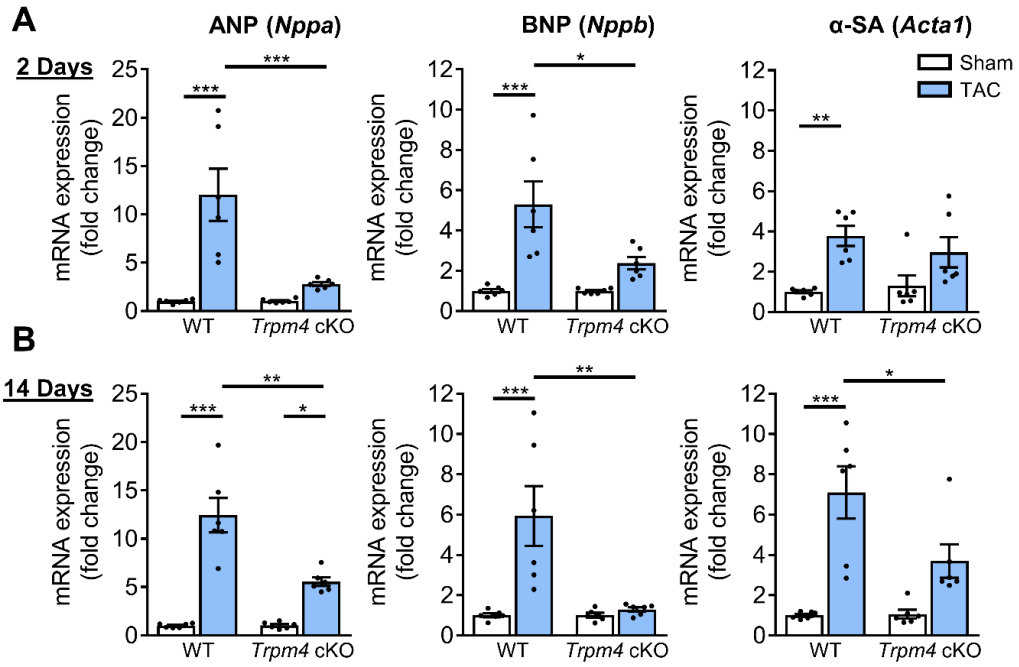

Figure 3-4 Comparison of gene expression of LVH markers in response to TAC-induced pressure overload in WT and *Trpm4* cKO mice.

(A) Relative mRNA expression of ANP (*Nppa*), BNP (*Nppb*) and α-SA (*Acta1*) after 2 days of TAC compared to sham-operated mice. n = 6/group. (B) Relative mRNA expression of ANP (*Nppa*), BNP (*Nppb*) and α-SA (*Acta1*) after 14 days of sham and TAC. n = 6/group.

The mRNA relative expression was normalized by GAPDH and calculated as fold change relative to WT sham in 2 days and 14 days groups, respectively. Results are presented as means ± SEM, *$p < 0.05$, **$p < 0.01$, ***$p < 0.001$.

3.2.7 CaMKII-HDAC4-MEF2 hypertrophic signalling pathway in WT and *Trpm4* cKO mouse hearts in response to TAC

Next, the molecular signalling pathways mediating LVH in both WT and *Trpm4* cKO hearts after 2 days of TAC were examined. This is a time point at which the molecular signalling is already activated in response to the increased hemodynamic load induced by TAC (Yu, Gong, Wu, et al., 2021), but before measurable LVH has developed.

The cytoplasmic and the nuclear fractions of LV tissue were separated as described in **Materials and methods**. High fraction purity was confirmed by western blot using antibodies against marker proteins specific for cytoplasmic (Glyceraldehyde 3-phosphate dehydrogenase, GAPDH) and nuclear (Histone H2B) fractions (**Figure 3-5**).

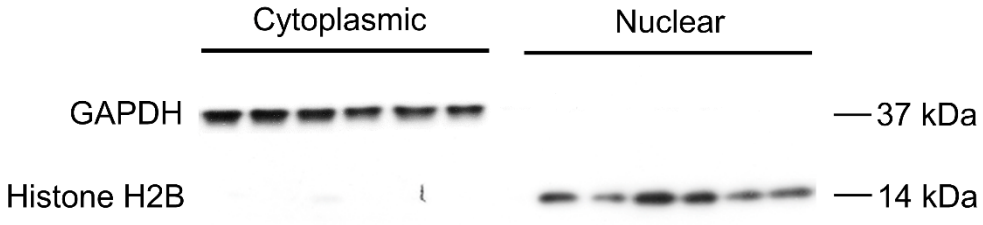

Figure 3-5 Demonstration of successful fractionation of compartments.

The purity of the fractions extracted from the LV tissue was assessed by western blot using specific marker proteins: GAPDH for cytoplasmic fraction and Histone H2B for

nuclear fraction. Each fraction (n = 6/group) was run side-by-side on the same blot and then probed separately against each of two primary antibodies: anti-GAPDH and anti-Histone H2B to validate purity of fraction.

Representative images of key cytoplasmic and nuclear proteins detected by western blot analysis are shown in **Figure 3-6A**. Quantitative data for cytoplasmic and nuclear proteins, normalized by GAPDH and Histone H2B, respectively, are shown in **Figure 3-6B**. First, whether CaMKIIδ activity is increased in response to pressure overload was investigated by measuring both total CaMKIIδ expression and auto-phosphorylated CaMKII (p-CaMKII) at threonine 287 (Thr287), a marker of CaMKII activation (Lai, Nairn, Gorelick, & Greengard, 1987; Luczak et al., 2020). In WT hearts, 2 days of TAC resulted in a significant increase in the total CaMKIIδ protein level in cytoplasmic ($p < 0.01$*)* and nuclear fractions ($p < 0.01$*),* accompanied by increased p-CaMKII protein levels in both the cytoplasm ($p < 0.05$) and nucleus ($p < 0.01$). Associated with this increase, there was a rise in total cytoplasmic HDAC4 ($p < 0.01$) and phosphorylated HDAC4 (p-HDAC4) levels ($p < 0.001$), but no change in nuclear HDAC4. This 2.11-fold increase in the cytoplasmic/nuclear ratio of HDAC4 ($p < 0.01$) in WT hearts indicates that TAC-induced pressure overload leads to the nuclear export of HDAC4 in WT TAC hearts. This increase was accompanied by a 1.76-fold increase of MEF2A levels in the nucleus ($p < 0.05$), which together with the de-repression of MEF2A activity would account for the induction of LVH.

In contrast to the effects of TAC in WT hearts, in *Trpm4* cKO hearts, TAC produced a decrease in cytoplasmic CaMKIIδ levels (0.66-fold of that observed in sham hearts; $p < 0.001$). Consistent with this, the cytoplasmic

p-CaMKII levels in TAC hearts also decreased (0.63-fold of that observed in sham hearts; $p < 0.01$). Although the increase in nuclear CaMKIIδ was similar ($p < 0.05$) to that observed with TAC in WT hearts, the nuclear p-CaMKII levels showed no significant difference between sham and TAC in *Trpm4* cKO hearts, which indicates less nuclear CaMKIIδ activation by TAC in *Trpm4* cKO hearts. The expression level of p-HDAC4 increased in *Trpm4* cKO TAC hearts in both the cytoplasm ($p < 0.05$) and the nucleus ($p < 0.05$), but there was no change in total HDAC4. Thus, the cytoplasmic/nuclear ratio of HDAC4 remained the same in *Trpm4* cKO TAC hearts as in sham hearts, indicating inhibition of nuclear HDAC4 export in *Trpm4* cKO TAC hearts. In addition, consistent with MEF2A activation driving hypertrophy development, reduced LVH in *Trpm4* cKO TAC hearts was associated with a smaller (1.26-fold) increase in MEF2A levels in the nucleus ($p < 0.05$) when compared with WT TAC hearts. For completeness, the cytoplasmic/nuclear ratios of other relevant proteins in this signalling pathway are shown in **Appendix-figure 3**.

Taken together, these data implicate the CaMKII-HDAC4-MEF2 hypertrophic signalling pathway in mediating TAC-induced LVH, but the extent of the hypertrophic response is regulated by TRPM4 channels.

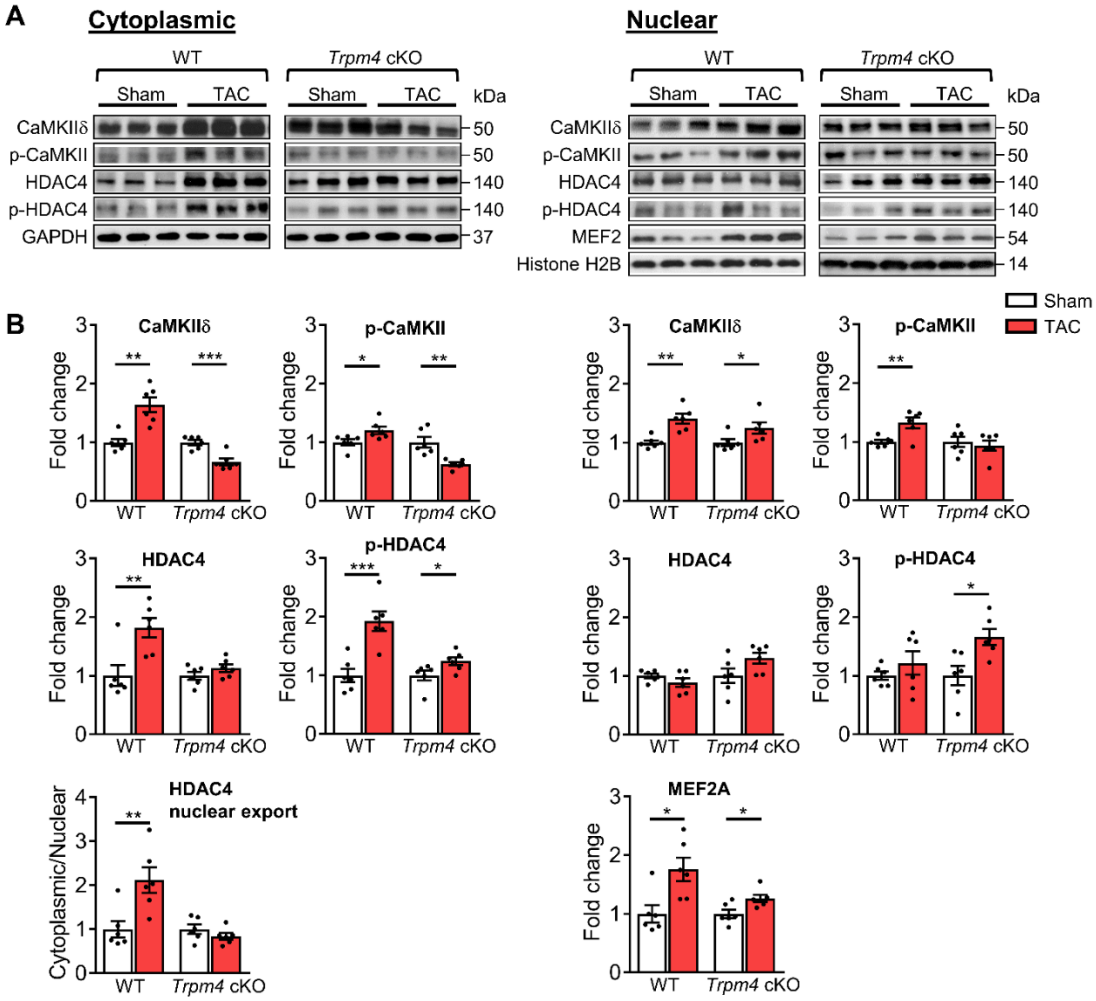

Figure 3-6 CaMKII-HDAC4-MEF2 signalling pathway in response to TAC after 2 days in WT and *Trpm4* cKO mouse hearts.

(A) Representative western blots showing the expression of key proteins in the CaMKII-HDAC4-MEF2 signalling pathway in the cytoplasm (left panel) and nucleus (right panel). (B) Cytoplasmic (left panel) and nuclear (right panel) quantitative data were normalized to GAPDH and Histone H2B, respectively. Fold changes and cytoplasmic/nuclear ratios were calculated relative to sham groups, in each genotype. Results are presented as means ± SEM, n = 6/group, *$p < 0.05$, **$p < 0.01$, ***$p < 0.001$.

3.2.8 Calcineurin-NFAT hypertrophic signalling pathway in WT and *Trpm4* cKO mouse hearts in response to TAC

Next, the expression of proteins involved in the calcineurin-NFAT hypertrophic signalling pathway was examined. Representative images of key cytoplasmic and nuclear proteins detected by western blot analysis are shown in **Figure 3-7A**. Quantitative data for cytoplasmic and nuclear proteins, normalized by GAPDH and Histone H2B, respectively, are shown in **Figure 3-7B**. In WT hearts, there was no significant difference in cytoplasmic or nuclear NFATc4 protein expression in sham and TAC hearts after 2 days. Consistent with these findings, total GSK3β, serine-9 phosphorylated GSK3β and GATA4 levels were also unchanged in response to TAC. These findings indicate that TAC did not result in increased nuclear translocation of NFATc4, the most reliable indicator of calcineurin activation (Molkentin, 2013), and are consistent with the previous finding (Yu, Gong, Wu, et al., 2021) showing that the calcineurin-NFAT pathway is not activated by TAC.

In contrast to WT hearts, a 1.28-fold increase in nuclear NFATc4 ($p < 0.05$) was observed in *Trpm4* cKO hearts after TAC, which led to a 0.31-fold decrease in the cytoplasmic/nuclear ratio compared to sham-operated hearts ($p < 0.01$). This indicated lower nuclear export of NFATc4 in the *Trpm4* cKO TAC hearts when compared to sham hearts. Accordingly, a 1.20-fold increase in nuclear p-GSK3β (serine 9, Ser9) ($p < 0.05$) was observed in *Trpm4* cKO TAC hearts. As phosphorylation at the serine 9 residue indicates inactivation of GSK3β, these findings suggest that the GSK3β-mediated export of NFATc4 from the nucleus was partially inhibited, which is consistent with the increased level of NFATc4 in the nucleus. Furthermore,

accompanied by the increase in nuclear NFATc4, a 1.18-fold increase in GATA4 expression ($p < 0.05$) in the nucleus was observed in *Trpm4* cKO TAC hearts. All these observations are consistent with a reduction in the tonic inhibition of calcineurin by CaMKII (De Koninck & Schulman, 1998; Kreusser et al., 2014; MacDonnell et al., 2009) in *Trpm4* cKO hearts after TAC. For completeness, the cytoplasmic/nuclear ratios of other relevant proteins in this signalling pathway are shown in **Appendix-figure 4**.

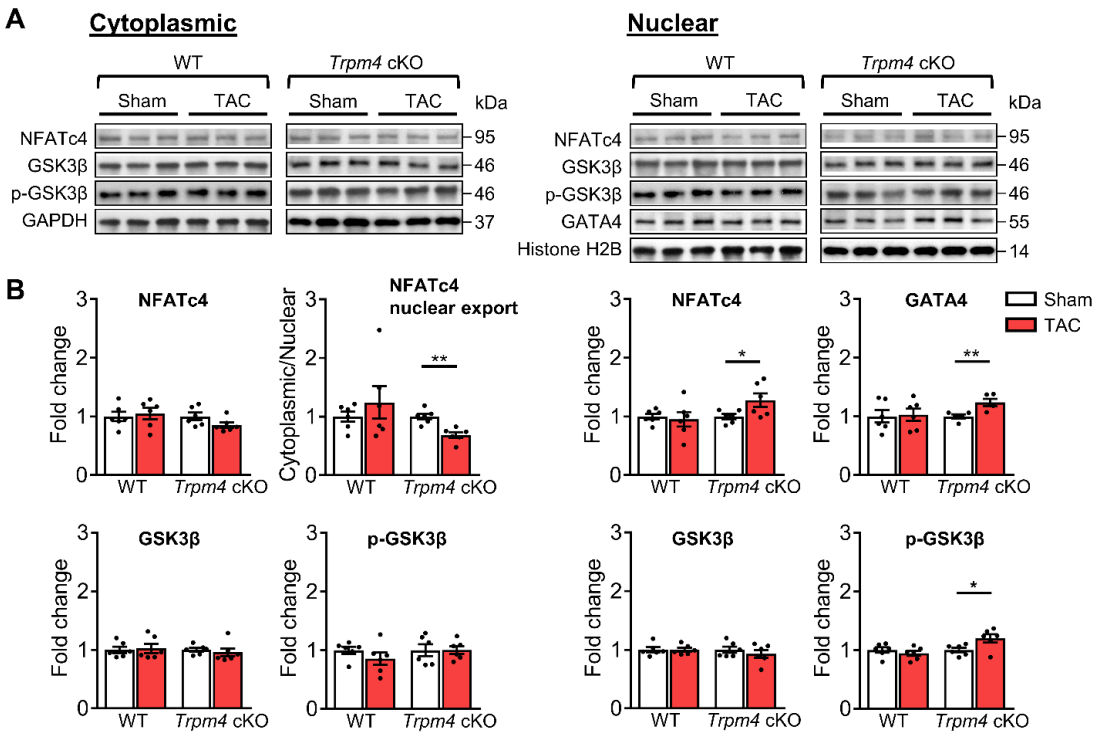

Figure 3-7 Calcineurin-NFAT signalling pathway in response to TAC after 2 days in WT and *Trpm4* cKO mouse hearts.

(A) Representative western blots showing the expression of key proteins in the calcineurin-NFAT signalling pathway in the cytoplasm (left panel) and the nucleus (right panel). (B) Cytoplasmic (left panel) and nuclear (right panel) quantitative data were normalized by GAPDH and Histone H2B, respectively. Fold changes and

cytoplasmic/nuclear ratios were calculated relative to sham groups, in each genotype. Results are presented as means ± SEM, n = 5-6/group, *$p < 0.05$, **$p < 0.01$.

3.3 Discussion

In this study, to investigate the role of the TRPM4 ion channels in pressure overload-induced pathological LVH, TAC-operated mice were employed as an *in vivo* cardiac hypertrophy model. The results in *Trpm4* cKO mice was compared with WT controls. The experimental animals were examined 2 days after surgery when the molecular signalling pathway that drives LVH is switched on in response to the increased hemodynamic load induced by TAC but, importantly, before LVH has developed. In addition, the experimental animals were examined 14 days after surgery when the TAC-induced LVH phenotype is evident. The main findings of this study are:

1. TRPM4 expression in the WT mouse heart was modified by TAC-induced pressure overload. At 2 days and 14 days after TAC, both *Trpm4* mRNA and protein expression were downregulated in LV tissue and isolated cardiomyocytes, suggesting that TRPM4 plays a role in TAC-induced LVH.

2. TRPM4 is playing a pro-hypertrophic role in pressure overload (TAC)-induced LVH. A reduction in TRPM4 expression in cardiomyocytes dampens the hypertrophic response to TAC, as evident by an approximately 50% reduction in the degree of LVH and LV fibrosis in *Trpm4* cKO mice at 14 days after TAC, as compared with WT mice.

3. TRPM4 is an important component of the mechanosensory signalling pathway that induces LVH in response to pressure overload. By

examining both the CaMKII-HDAC4-MEF2 and calcineurin-NFAT signalling pathways 2 days after TAC in WT and *Trpm4* cKO mice (**Figure 3-8**), it is confirmed that the CaMKII-HDAC4-MEF2 pathway was activated in response to TAC in WT mice (Yu, Gong, Wu, et al., 2021). Importantly, the results also revealed new finding of reduced activation of the CaMKII-HDAC4-MEF2 pathway after TAC in *Trpm4* cKO animals.

Previous studies reported that the TRPM4 current contributes to the mammalian atrial action potential (Simard et al., 2013) as well as to the notch and early repolarization phases of the action potential in Purkinje cells (Hof et al., 2016), providing a potential link to cardiac arrhythmias (Guinamard et al., 2015; Hedon et al., 2021; C. Wang et al., 2018). Importantly, there is evidence that the TRPM4 channel is a critical modulator of ventricular remodelling in cardiac hypertrophy and heart failure (Frede et al., 2020; Jacobs et al., 2015; Kecskes et al., 2015; Mathar et al., 2014). Kecskes et al. (2015) reported that TRPM4 activation suppresses AngII-induced cardiac hypertrophy, which is dependent on the activation of the calcineurin-NFAT pathway. It has been proposed that this is due to the Ca^{2+}-dependent modulation of TRPM4 activity, which leads to membrane depolarisation in cardiomyocytes and thus reduces the driving force for Ca^{2+} influx via SOCE through TRPC1 and TRPC3 ion channels (Kecskes et al., 2015; Wu, Zagranichnaya, Gurda, Eves, & Villereal, 2004).

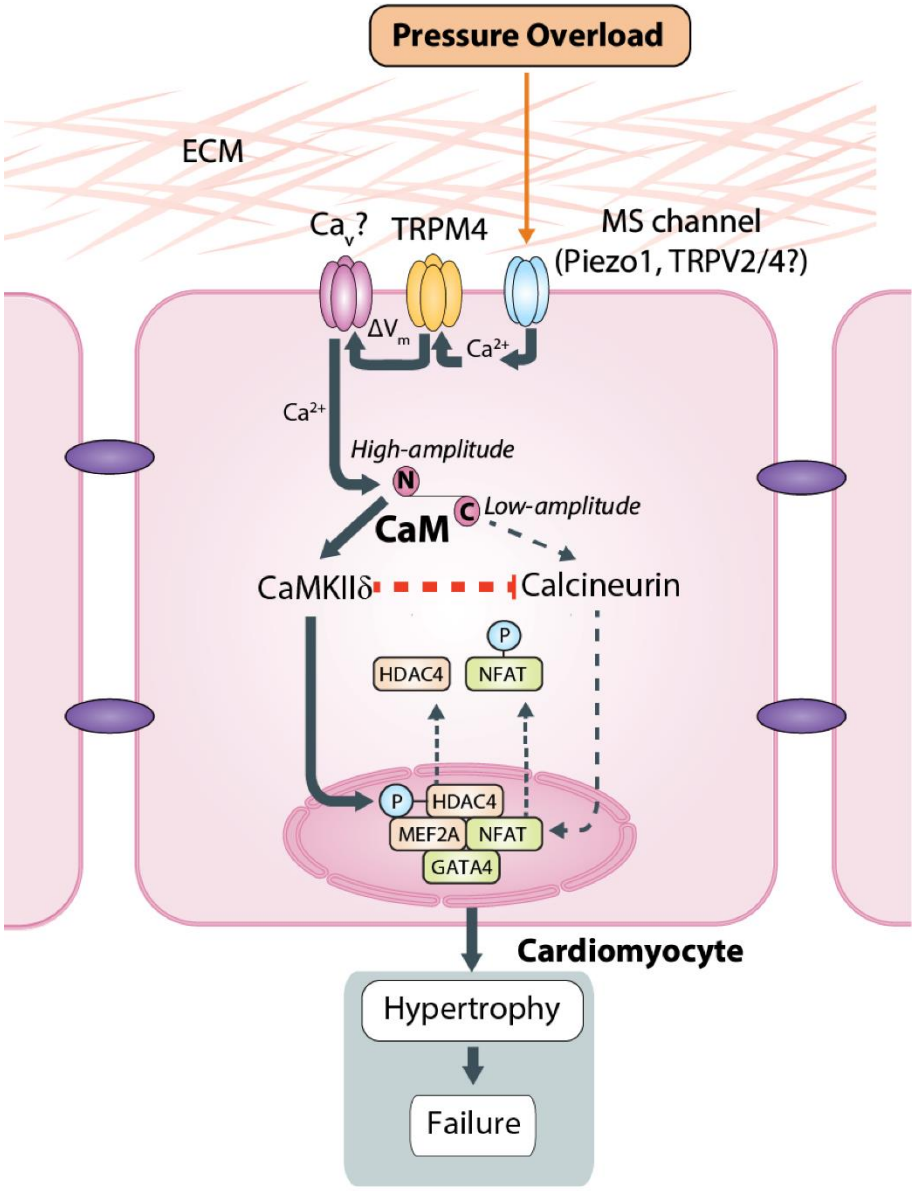

Figure 3-8 Schematic of the putative TAC-induced pathway that culminates in left ventricular hypertrophy.

A Ca^{2+}-permeable MS channel (e.g. Piezo1, TRPV2, TRPV4) acts as the mechanotransducer providing local Ca^{2+} that in turn stimulates TRPM4. The Na^{+}-permeable TRPM4 activity then could either stimulate voltage-gated Ca^{2+} channels through membrane depolarisation or induce reverse activity of the Na^{+}/ Ca^{2+} exchanger through local Na^{+} loading. Either of these outcomes would lead to a high-amplitude increase in local Ca^{2+}. CaM then responds to this high-amplitude Ca^{2+} stimulus through the lower affinity Ca^{2+} binding site at its N-lobe which subsequently activates CaMKIIδ and thus stimulates the CaMKII-HDAC4-MEF2 pathway as shown in Yu, Gong,

Wu, et al. (2021). Calcineurin activation is inhibited by the activated CaMKIIδ and is activated preferentially by low-amplitude Ca^{2+} signalling via Gq-coupled receptors and CaM. ECM: extracellular matrix, MS: mechanosensitive, Ca_v: voltage-gated Ca^{2+} channel, ΔV_m: membrane depolarisation, CaM: calmodulin.

However, a role for TRPM4 in the LVH induced by mechanical pressure overload has not been demonstrated previously. A potential mechanism is that a mechanical stimulus, such as that exerted by TAC, is converted to downstream Ca^{2+} signalling via the activity of MS channels in the plasma membrane. Although the mechanosensitivity of TRP-type ion channels is still the subject of debate (Cox et al., 2019; Gottlieb et al., 2008), mammalian TRP ion channels, including TRPM4, have recently been shown to be insensitive to membrane stretch (Constantine et al., 2016; Nikolaev et al., 2019). Therefore, TRPM4 does not appear to be the primary mechanosensor responding to pressure overload. It is more likely to be a secondary ionotropic receptor downstream of a Ca^{2+}-permeable MS ion channel, such as Piezo1 (Gnanasambandam, Bae, Gottlieb, & Sachs, 2015; Syeda et al., 2016) (details described in following chapters) or TRPV2/4 (Lieben & Carmeliet, 2012), that functions as the primary mechanoreceptor responding directly to pressure overload and thus initiating the hypertrophic response in TAC (Yu, Gong, Kesteven, et al., 2021; Zhang et al., 2021), which is not dependent on activation of the calcineurin-NFAT pathway (Yu, Gong, Wu, et al., 2021).

Stimulated by the local Ca^{2+} influx through a Ca^{2+}-permeable MS ion channel, the Na^+-permeable TRPM4 activity then could either induce reversed activity of the Na^+/ Ca^{2+} exchanger through local Na^+ loading (Conway, 2001;

C. Wang et al., 2018) or depolarise the cardiomyocyte cell membrane to stimulate voltage-gated Ca^{2+} channels. Such potential downstream ion channels include the L-type Ca^{2+} channels, which were reported to mediate hypertrophic cardiomyopathy (Viola & Hool, 2017), as well as the T-type Ca^{2+} channels whose splice variants were found to be regulated in rat LV hypertrophic hearts induced by aortic constriction (Cribbs, 2010). Either of these outcomes would lead to a high-amplitude increase in local Ca^{2+}. Thus, as a Ca^{2+}- and voltage-dependent non-selective monovalent cation channel (Constantine et al., 2016; Pierre Launay et al., 2002; Nilius et al., 2003; Nilius, Prenen, Tang, et al., 2005), TRPM4 could contribute to TAC-induced LVH by modulating downstream voltage-gated Ca^{2+} ion channels or the Na^{+}/ Ca^{2+} exchanger (**Figure 3-8**).

In this study, the involvement of TRPM4 in TAC-induced LVH was confirmed using *Trpm4* cKO mice. Despite identical TAC-induced increases in hemodynamic load in both WT and *Trpm4* cKO mice, the latter displayed a significantly reduced LVH response. This is in contrast to the increased hypertrophy reported in AngII treated *Trpm4* cKO mice that is mediated by the calcineurin-NFAT pathway (Kecskes et al., 2015). These differential effects of TRPM4 on AngII-mediated (Kecskes et al., 2015) and TAC-induced LVH support Yu, Gong, Wu, et al. (2021)'s previous finding that these two hypertrophic stimuli are mediated by distinct signalling mechanisms. The CaMKII-HDAC4-MEF2 pathway, but not the calcineurin-NFAT signalling pathway, is activated in response to TAC-induced pressure overload (Yu, Gong, Wu, et al., 2021). This is most likely because CaMKIIδ and calcineurin respond to different characteristics of intracellular Ca^{2+} signalling (De Koninck & Schulman, 1998; Dolmetsch, Lewis, Goodnow, & Healy, 1997).

Whereas calcineurin activation requires a sustained increase in the resting intracellular Ca^{2+} concentration, CaMKIIδ activation is more sensitive to high-frequency/high amplitude Ca^{2+} oscillations (Colella et al., 2008; De Koninck & Schulman, 1998), which are known to occur with TAC-induced aortic constriction (Chen et al., 2011). CaM responds to this high-amplitude Ca^{2+} stimulus through the lower affinity Ca^{2+} binding site at its N-lobe (T. I. A. Evans & Shea, 2009; Saimi & Kung, 2002) which subsequently activates CaMKIIδ and thus stimulates the CaMKII-HDAC4-MEF2 pathway (Yu, Gong, Wu, et al., 2021). Moreover, once activated, CaMKII has been shown to inhibit calcineurin activity (Kreusser et al., 2014; MacDonnell et al., 2009) (**Figure 3-8**).

The high-frequency/high amplitude Ca^{2+}oscillations characteristic of TAC and the consequent intermittent nature of the resulting TRPM4 activation, as distinct from the persistent activation associated with Ang II-induced hypertrophy, may mean that TAC-induced TRPM4 activation does not reduce the driving force for Ca^{2+} influx via SOCE that characterises the anti-hypertrophic action of TRPM4 in AngII-induced hypertrophy (see above). Rather, in TAC-induced hypertrophy, TRPM4 acts as an amplifier of the small load-dependent Ca^{2+} signal produced by a MS Ca^{2+}-permeable ion channel. This would account for the pro-hypertrophic effect of TRPM4 in TAC-induced hypertrophy as distinct from its anti-hypertrophic effect in AngII-induced hypertrophy.

In terms of the signalling pathway mediating pressure overload-induced LVH, it is indicated that in *Trpm4* cKO TAC hearts, the reduced LVH response was associated with significantly less activation of the CaMKII-HDAC4-MEF2 pathway, with reduced CaMKIIδ activation resulting in reduced nuclear

export of HDAC4. Since nuclear HDAC4 inhibits MEF2A activity, a reduction in HDAC4 nuclear export would result in diminished MEF2A disinhibition. Given that MEF2A is a critical nuclear transcriptional regulator causing pathological cardiac remodelling, its inhibition leads to a reduced hypertrophy development (Passier et al., 2000) as, indeed, observed here in *Trpm4* cKO TAC hearts.

Decreased expression of TRPM4 channels in *Trpm4* cKO animals likely modifies Ca^{2+}-signalling, which directly regulates CaMKIIδ activation and its downstream pathway in response to TAC. Comparable with a study reporting that blockade of MEF2 acetylation can permit recovery from pathological cardiac hypertrophy without impairing physiological adaptation (Wei et al., 2017), the lower concentration and reduced activity of MEF2A found in *Trpm4* cKO TAC hearts suggest that inhibition of TRPM4 channels is potentially a viable therapeutic option for reducing pathological hypertrophy in response to pressure overload.

Interestingly, although the calcineurin-NFAT hypertrophic signalling pathway is not activated by TAC in WT hearts, it was partially activated in *Trpm4* cKO TAC hearts, which manifested itself in the inhibition of GSK3β-mediated NFATc4 nuclear export and by an increase in GATA4. This may be explained by the reduction of the cytoplasmic CaMKIIδ in *Trpm4* cKO TAC hearts, as CaMKII negatively regulates calcineurin activity (Kreusser et al., 2014; MacDonnell et al., 2009) (**Figure 3-8**). It is notable, nevertheless, that the net effect of the loss of TRPM4 was a significant reduction in TAC-induced LVH, indicating that the direct effect of less activation of the CaMKII-HDAC4-MEF2 pathway in reducing hypertrophy development

outweighed the indirect pro-hypertrophic effect resulting from blunting CaMKIIδ's inhibition of calcineurin.

In summary, this study provides compelling evidence that TRPM4 plays an important role in pressure overload-induced pathological LVH, with diminished TRPM4 expression reducing TAC-induced hypertrophy. Furthermore, this study demonstrated that TRPM4 is a likely component of a cardiac mechanotransduction process that activates the CaMKII-HDAC4-MEF2 signalling pathway in response to TAC. It is likely that TRPM4 is activated by an upstream primary mechanoreceptor, such as Piezo1 (Yu, Gong, Kesteven, et al., 2021; Zhang et al., 2021) or TRPV2/4 channels, which provide the first step in this mechanotransduction pathway. These findings provide new understanding of the molecular mechanism underlying mechanical pressure overload-induced LVH. Moreover, this work offers new possibilities for clinical treatment of the pressure overload-induced pathological hypertrophy.

Chapter 4 Development of *in vitro* models as approaches to unravel Piezo1-mediated cardiac mechanotransduction

This chapter contains work published in:

Guo, Y.†, Merten, A. L.†, Schöler, U., Yu, Z. Y., Cvetkovska, J., Fatkin, D., Feneley, M. P., Martinac, B.*, & Friedrich, O. (2021). *In vitro* cell stretching technology (*IsoStretcher*) as an approach to unravel Piezo1-mediated cardiac mechanotransduction. *Progress in Biophysics and Molecular Biology*, *159*, 22-33.

Author contributions of Guo Y: conceptualization, data curation, formal analysis, methodology, visualization, writing-original draft, writing-review and editing.

Friedrich, O., Merten, A. L., Schneidereit, D., **Guo, Y.**, Schürmann, S., & Martinac, B*. (2019). Stretch in Focus: 2D Inplane Cell Stretch Systems for Studies of Cardiac Mechano-Signaling. *Frontiers in Bioengineering and Biotechnology*, 7, 55.

Author contributions of Guo Y: conducted all *IsoStretcher* experiments and data analysis.

† These authors contributed equally.

* Corresponding author.

4.1 Introduction

Mechanotransduction is an ancient force-sensing mechanism based on the activity of MS channels. These highly efficient force-sensing channels are tightly coupled with the mechanics of biological cell membranes, playing a central role in transducing mechanical stimuli exerted on the cell membrane into electrical and biochemical intracellular signals (Cox et al., 2019; O. P. Hamill & Martinac, 2001; Ingber, 2006). Since the first report of MS channels in bacteria in the 1980s (Martinac et al., 1987), extensive studies have been conducted to investigate the basic biophysical principles of ion channel-mediated mechanotransduction (Cox et al., 2019; Martinac & Cox, 2017). However, although the contributions of MS channels to many physiological and pathological processes have been reported, the molecular force-sensing mechanisms are not completely understood.

Various studies have shown that the mechanotransduction mediated by MS channels plays a key role in cardiovascular development, physiology, and pathology (Douguet et al., 2019; Quinn & Kohl, 2021; Reed et al., 2014; Saucerman, Tan, Buchholz, McCulloch, & Omens, 2019b; Teng, Loukin, & Kung, 2014). As introduced in **1.4.3.2**, following the exciting discovery of the Piezo mechanically gated ion channels (Coste et al., 2010), which was this year recognised by a Nobel Prize for Physiology or Medicine (Ernfors et al., 2021) , a large number of *in vitro* and *in vivo* studies have been conducted on the inherently mechanosensitive (Cox et al., 2016; Syeda et al., 2016) channel Piezo1 in the heart (Beech & Kalli, 2019; Douguet et al., 2019). In particular, a few very recent studies indicated that Piezo1 is involved in pathological cardiac remodelling by modulating Ca^{2+} homeostasis in mouse ventricular cardiomyocytes (Jiang et al., 2021; Yu, Gong, Kesteven, et al.,

2021; Zhang et al., 2021). In **Chapter 3**, Piezo1 is considered a candidate for the Ca^{2+}-permeable MS channel which acts as a primary mechanotransducer responding to the stretch forces in the heart. It can provide local Ca^{2+} that in turn stimulates TRPM4 in the first step of the mechanotransduction signalling in the pressure overload-induced LVH signalling pathway.

As introduced in **1.4.3.2**, together with Ca^{2+} imaging, the patch clamp recording technique (O. P. Hamill et al., 1981) and some recent approaches in biomedical engineering, including cell stretching technologies (O. Friedrich et al., 2017), have been used to study Piezo1 activities in response to membrane stretch. Importantly, the biological assessment of Piezo1-mediated cardiac mechanotransduction requires availability of novel, organ-mimicking stretch technologies because the heart is a contractile hollow organ where the hemodynamic volume or pressure load is associated with multiaxial wall tension, stretching individual cardiac cells in multiple directions.

In this chapter, a novel *in vitro* model using the *IsoStretcher* technology (Schürmann et al., 2016) to investigate isotropic stretch-induced Piezo1 activation was developed and tested with both HL-1 mouse atrial myocyte-like cells (Claycomb et al., 1998) and isolated adult mouse ventricular cardiomyocytes. In addition, this chapter demonstrates methods of using KIC-based Ca^{2+} measurements to investigate the functional presence of Piezo1 in mouse ventricular cardiomyocytes.

4.2 Experimental procedures and representative results

4.2.1 Isotropic cell stretching technology as an approach to investigate Piezo1-mediated cardiac mechanotransduction

4.2.1.1 Application on HL-1 cells

Since there was no published previous study showing the presence of Piezo1 in HL-1 cells, in this current study, RT-qPCR was performed on cDNA from HL-1 cells as well as primary adult mouse cardiac fibroblasts for comparison purposes. **Figure 4-1** shows that *Piezo1* mRNA expression level in HL-1 cells is approximately 32% of that in primary adult mouse cardiac fibroblasts, which are known to have a high level of *Piezo1* expression (Blythe et al., 2019).

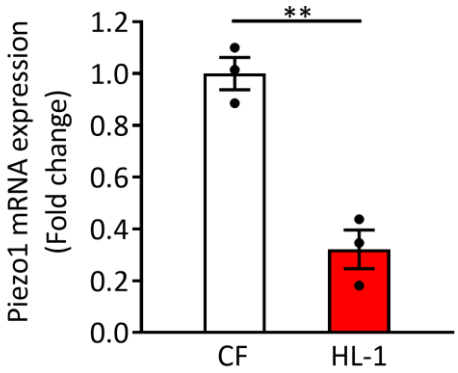

Figure 4-1 *Piezo1* mRNA expression level in primary adult mouse cardiac fibroblasts (CF) and HL-1 cells.

Relative *Piezo1* mRNA expression level in primary adult mouse cardiac fibroblasts (CF) and HL-1 cells. The relative expression was normalized by GAPDH and calculated as fold change relative to CF. Results are presented as means ± SEM. n = 3/group. n represents the number of separate culture dishes. $^{**}p < 0.01$.

To confirm the Yoda1 effect on HL-1 cells, the Ca^{2+} level in HL-1 cells with Yoda1 addition was compared to that with DMSO control. After Fluo-4 AM staining, HL-1 cells in 96 well plates were kept in 100 µL PSS supplemented with 1 mM $CaCl_2$. At one minute after the start of the recording, 33.3 µL PSS containing Yoda1 or DMSO was added into the 100 µL PSS mixture to reach a final concentration of 5 µM. The data were recorded for two minutes in total with a frame interval of 100 ms (10 images/s). **Figure 4-2A** shows that the fluorescence intensity of Ca^{2+} imaging by Fluo-4 AM remained the same level after DMSO addition but started to rise after Yoda1 addition (final concentration 5 µM). When comparing the area under the curve (AUC) of the Ca^{2+} fluorescence intensity trace, the DMSO group showed no significant difference before and after addition, while Yoda1 addition increased the AUC by 51.5% ($p < 0.001$) (**Figure 4-2B**).

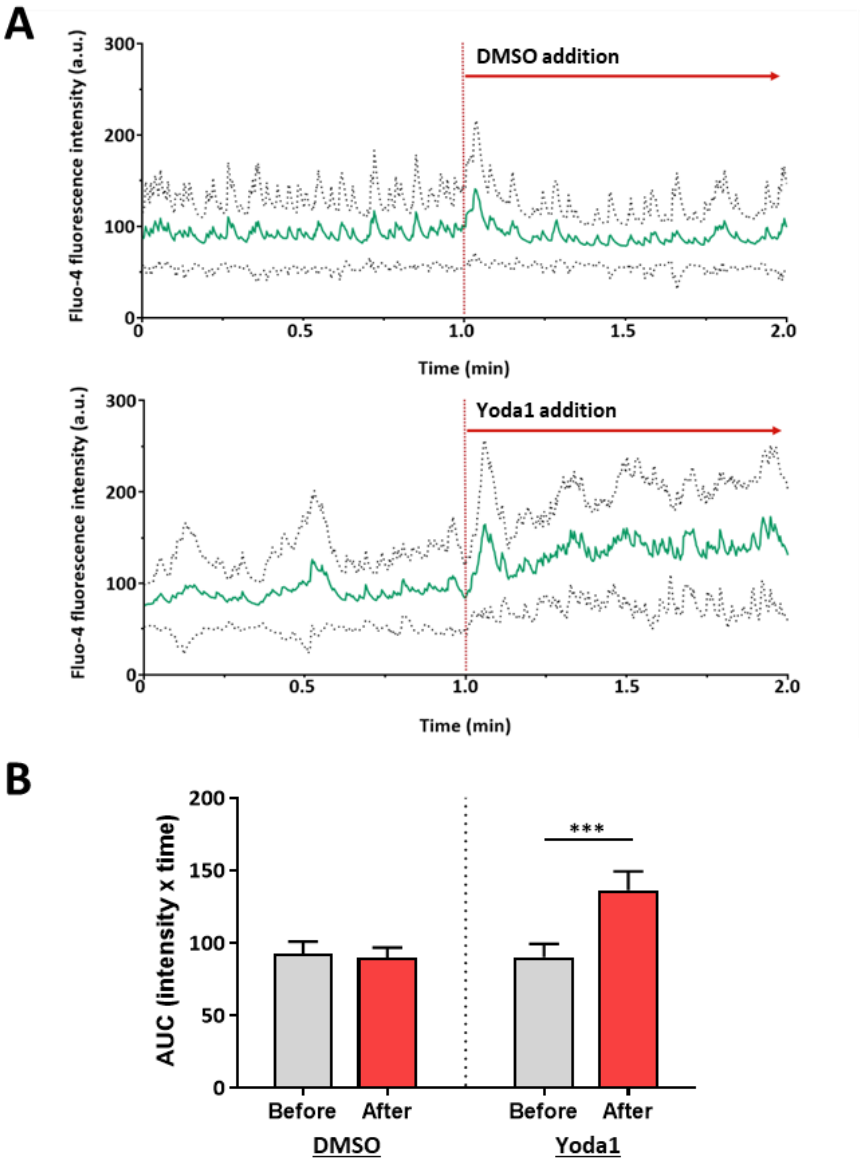

Figure 4-2 Ca^{2+} level in HL-1 cells responding to DMSO or Yoda1 addition.

(A) Green trace shows the average Ca^{2+} level indicated by Fluo-4 AM fluorescence intensity in HL-1 cells with DMSO or Yoda1 addition at one minute after the beginning of recording; dotted trace shows ± SD. (B) AUC (intensity x time, baseline = 0) of cells before and after DMSO or Yoda1 addition, shown as means ± SEM. n = 15 cells/group. ***$p < 0.001$.

The *IsoStretcher* system (Schürmann et al., 2016) was modified for this study, using specialised PDMS stretch chambers (described in **2.5**). As this was the first time that the HL-1 cell line was tested with the *IsoStretcher* system, the cell area change during stretching was investigated to confirm if the HL-1 cells can follow the applied hardware stretch. **Figure 4-3A** shows that the cell areas significantly increased ($p < 0.001$) when the cells were stretched to 15% isotropically. The cell area mean value with 15% stretch was 116.1% of that with 0% stretch (**Figure 4-3B**).

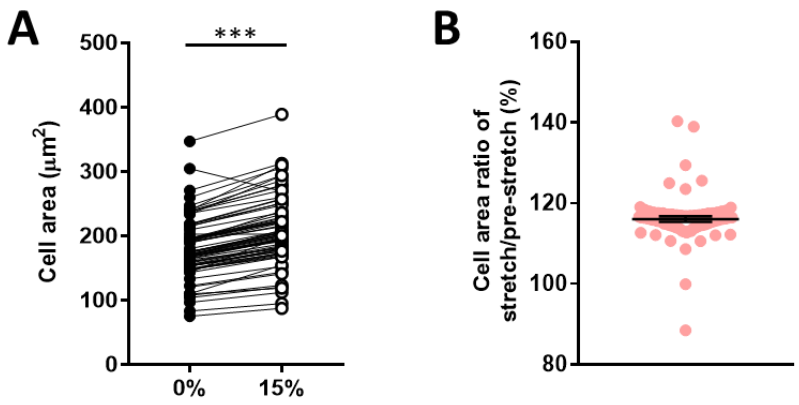

Figure 4-3 HL-1 cell area change by isotropic stretch.

(A) HL-1 cell areas with 0% and 15% isotropic stretch. (B) HL-1 cell area ratio of stretch (15%)/pre-stretch (0%), presented as scatter plots with mean ± SEM. n = 80 cells from 5 chambers. ***$p < 0.001$.

In the next step, HL-1 cells were tested using an experimental protocol that integrates stimuli including cell stretching and Yoda1 addition (final concentration 5 µM). The cell responses were visualised via Ca^{2+} imaging.

Every experiment on one PDMS chamber consists of six phases shown below with the percentage of stretch shown in the bracket.

1) Pre-stretch (0%)
2) Stretch (15%)
3) Release ① (0%)
4) Yoda1 addition (final concentration 5 μM) (0%)
5) Stretch with Yoda1 presence (15%)
6) Release ② (0%)

First, the baseline activity of HL-1 cells covered with 300 μL PSS mixture in the PDMS chamber was recorded as "Pre-stretch". Then a 15% isotropic stretch was applied to the chamber and kept till the end of this phase. After that, the stretch was released to 0%. Next, 100 μL PSS containing 20 μM Yoda1 was added into the chamber to make a final concentration of 5 μM. Subsequently, the PDMS chamber was stretched again to 15% with Yoda1 presence. At last, the stretch was released to 0%. Each phase lasted for 30 seconds, and all the phases were recorded continuously with a frame interval of 100 ms (10 images/s).

Figure 4-4A shows representative Ca^{2+} images of HL-1 cells in Pre-stretch phase (left) and Stretch phase (right). The recorded images were processed using ImageJ (National Institutes of Health, USA) to measeure the fluorescence intensity of individual cells, as well as the background at three different positions on each image. For quantitative data analysis of the cell responses, the relative intensity change was calculated using the equation shown in **Figure 4-4B**. In this equation, I_t represents the intensity at each time point. I_0 stands for the average intensity of the 25 images during the

first 5 seconds of the experiment. The background (BG) value is the average intensity of the three background spots.

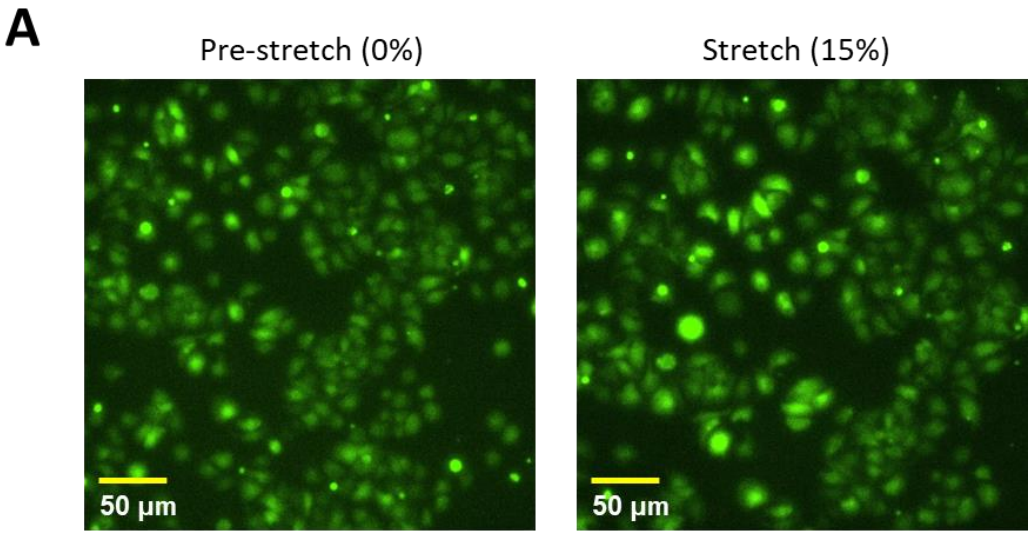

Figure 4-4 Ca^{2+} image and intensity calculation for HL-1 cells in cell stretching experiments.

(A) Representative Ca^{2+} images of HL-1 cells with Fluo-4 AM staining under 0% stretch (left) and 15% isotropic stretch (right). (B) Equation for relative intensity change calculation. I_t: Intensity at each time point. I_0: Average intensity during the first 5 seconds of experiment. Background (BG) intensity was subtracted from cell intensity.

A few examples of individual HL-1 cells responding to the stimuli during the experiment are shown in **Figure 4-5A**, presented as relative intensity change. The cell activities showed a diversity within a certain range, but

they also seemed to share some similar patterns when responding to 15% isotropic stretch, Yoda1 addition, stretch with Yoda1 present, or after stretch release. The base intensity, peak frequency, peak amplitude, as well as wave shape changed accordingly in response to the stimuli. The “plateau” shape in relative intensity change was found in Stretch phase, especially with Yoda1 present.

When calculating the AUC (baseline = start point of each experiment) of each phase, Stretch ($p < 0.05$), Yoda1 addition ($p < 0.05$), and Stretch with yoda1 ($p < 0.01$) phases are significantly higher than Pre-stretch (**Figure 4-5B**). Also, there is an increasing trend in Stretch, Yoda1 addition, or Stretch with Yoda1 phases relative to the respective previous phases, while the AUC of the two Release phases is smaller than the respective previous phases (**Figure 4-5B**).

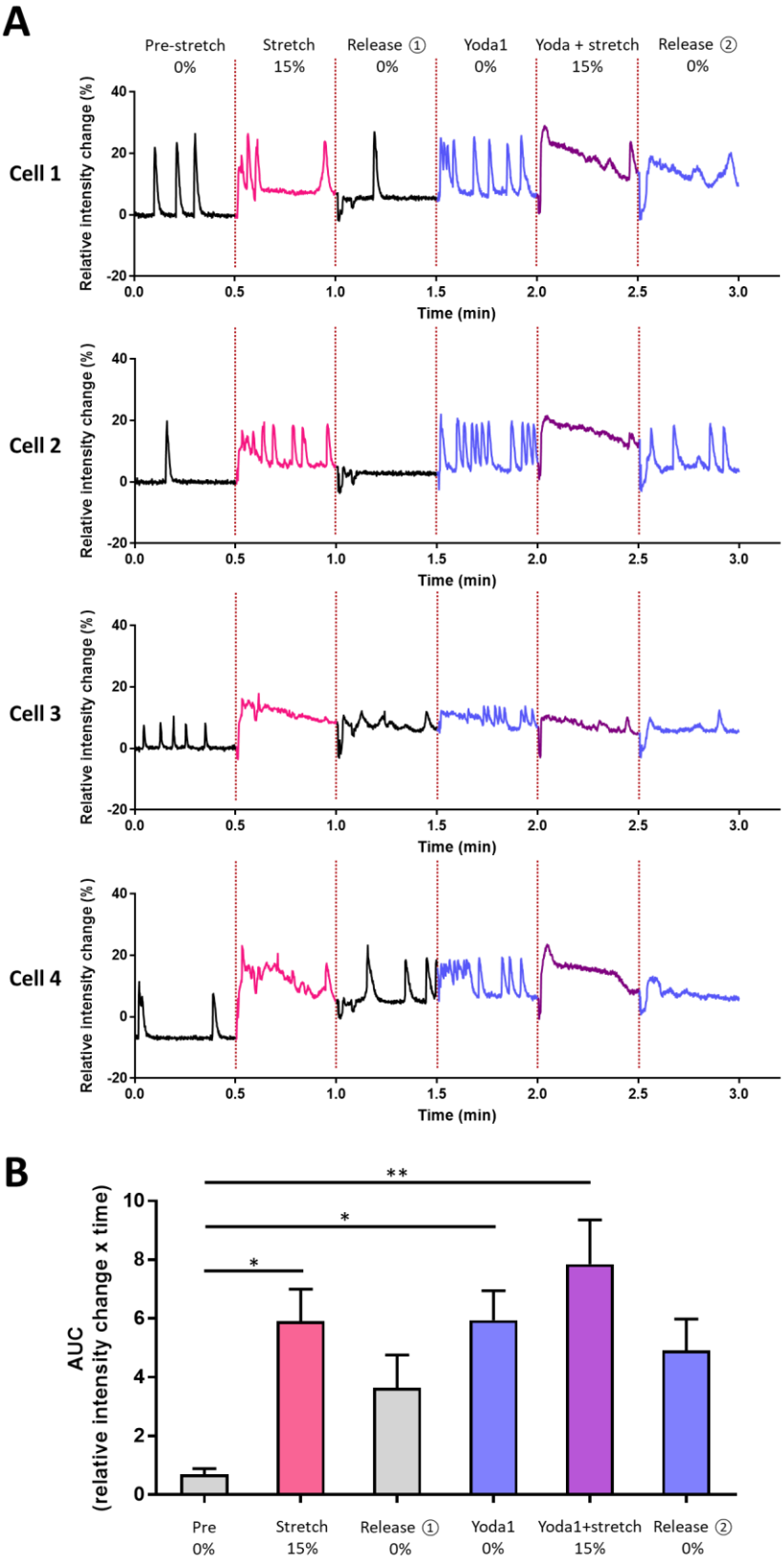

Figure 4-5 Ca^{2+} level in HL-1 cells responding to isotropic stretch and Yoda1 addtion.

Relative intensity change was calculated based on Fluo-4 AM fluorescence intensity, indicating intracellular Ca^{2+} level change in HL-1 cells. (A) Four examples of individual HL-1 cell responding to stimuli during the experiment, shown as relative intensity change. (B) AUC of the cells in different phases of the experiment, shown as means ± SEM. n = 4. *$p < 0.05$, **$p < 0.01$.

In subsequent experiments, a modified protocol with less complexity was used for HL-1 cell stretching. There are only four phases in each experiment, shown below. The percentage of stretch in each phase is shown in the bracket. Each phase lasted for one minute, and all the phases were continuously recorded with a frame interval of 100 ms (10 images/s).

1) Pre-stretch (0%)
2) PSS control/Yoda1 addition (final concentration 5 µM) (0%)
3) Stretch (15%)
4) Release (0%)

First, the baseline activity of HL-1 cells covered with 300 µL PSS mixture in the PDMS chamber was recorded as "Pre-stretch". Then 100 µL PSS control or 100 µL PSS containing 20 µM Yoda1 was added into the chamber. Next, the PDMS chamber was stretched to 15%. After that, the stretch was released to 0% till the end of the experiment. A group without any liquid addition was also included as control. In addition, MS channel inhibitor GsMTx4 was used to further confirm stretch-induced Piezo1 activation. The experimental group design is shown in **Table 4-1**. The cells in group 4, 5, and 6 were pre-incubated with GsMTx4 (final concentration 5 µM) for 75 minutes before the experiment and kept in PSS with GsMTx4 during the experiment.

Table 4-1 Experimental groups for HL-1 cell stretching experiment.

Group	Inhibitor	Drug addition
1	N/A	N/A
2	N/A	PSS
3	N/A	Yoda1
4	GsMTx4	N/A
5	GsMTx4	PSS
6	GsMTx4	Yoda1

The recorded data were processed using ImageJ (National Institutes of Health, USA) software and plugins. An automated analysis routine was developed to implement image registration and cell segmentation for reliable single cell analysis, in a collabotation with Ulrike Schöler from the Institute of Medical Biotechnology, Friedrich-Alexander-University Erlangen-Nürnberg, Germany. The inevitable movements of the image area upon stretch and release were corrected by performing image registration in ImageJ (National Institutes of Health, USA) via feature extraction plugin "Extract SIFT Correspondences", followed by image registration using bUnwarpJ plugin (Arganda-Carreras et al., 2006). The cell areas were defined via intensity threshold. Then the cell segmentation was conducted by using ImageJ tool "Find maxima" and "Analyze Particles" to detect the region of interest (ROI) for individual cells (**Figure 4-6**). To ensure each ROI is reflecting one single live cell, after the automated cell segmentation, the

detected ROIs can also be manually checked to exclude non-cell signals, dead cells, and unseparated cells.

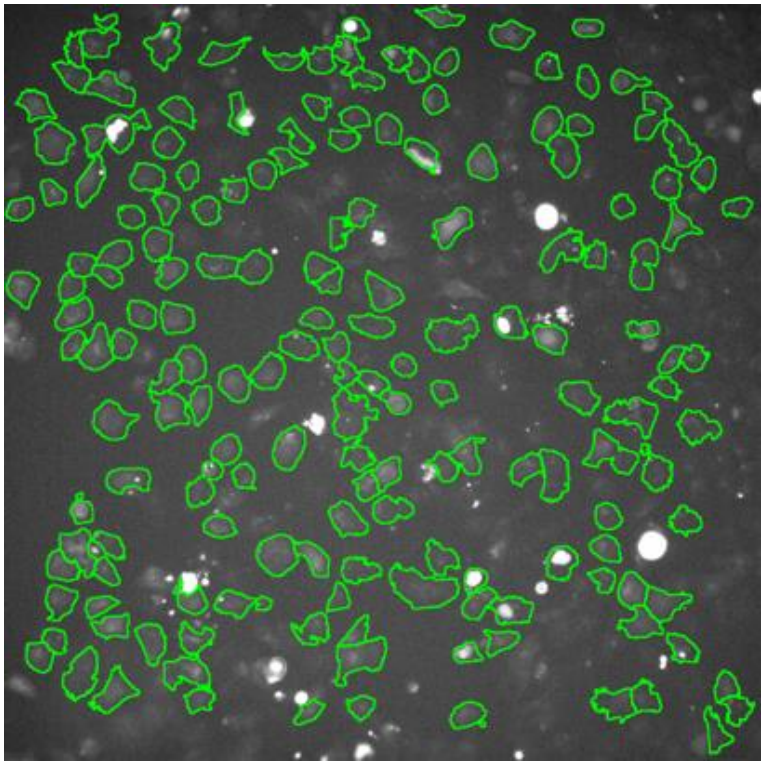

Figure 4-6 Detected ROIs via automated cell segmentation.

The detected ROIs are marked in green.

To correct the uneven illumination during the microscope imaging process, intensity calibration and shading correction were applied to the whole image measured at each time point (I_{meas}) during the experiment (10 images/s) to get the "true image" (I_{ture}), based on a method from the Center for Advanced Light Microscopy (M. A. Model, 2006; Michael A. Model & Burkhardt, 2001; University of California, 2021) (**Appendix-figure 5**). First, a

"dark image" (Dark) was acquired with no light reaching the camera. Secondly, a "flat field image" (Flat) was acquired by taking an image of a uniform fluorescent sample (fluorescent dye in medium only) then subtracting off the “dark image”. Then, the true image was calculated using the equation: $I_{true} = (I_{meas} – Dark) / Flat$ (M. A. Model, 2006; Michael A. Model & Burkhardt, 2001; University of California, 2021).

The fluorescence intensity in each individual cell at each time point (10 images/s) during the experiment was calculated as intDen(t). The mean value of the 30 smallest intensity values in the first minute of the experiment was calculated as intDen0. The value of intDen(t) divided by intDen0 was calculated as “relative integrated density” and profiled for each individual cell. The peak recognition was performed through the peak recognition function of the SciPy library (SciPy; https://scipy.org/), using the code programmed by Anna-Lena Merten from the Institute of Medical Biotechnology, Friedrich-Alexander-University Erlangen-Nürnberg, Germany. The lowest point of relative integrated density in each phase was considered the base intensity of that phase.

A few examples of HL-1 cell response in different experimental groups are shown in **Figure 4-7**. The cells are from the groups with no inhibitor and addition (**Figure 4-7A**); GsMTx4 inhibition and no addition (**Figure 4-7B**); no inhibitor and PSS addition (**Figure 4-7C**); no inhibitor and Yoda1 addition (final concentration 5 µM) (**Figure 4-7D**). The data are shown as the relative integrated density of individual cells during the four phases (marked with 1, 2, 3, 4 in **Figure 4-7**) of the experiment. The cell in **Figure 4-7D** showed an increase in Ca^{2+} oscillation frequency after Yoda1 addition but the cells without Yoda1 addition had no increase in phase 3 (**Figure 4-7A, B, C**). All

the cells showed an increasing trend of base Ca^{2+} intensity in Stretch and Release phases relative to the respective previous phases. However, there seemed to be differences in the change of the base intensity as well as the shape of the Ca^{2+} wave among the groups under different experimental conditions. For example, the cell with GsMTx4 showed the least increase in base intensity and least persistence of Ca^{2+} level after the rapid increase in phase 3. Also, the cell with Yoda1 addition had a "plateau" in phase 3 (**Figure 4-7C**).

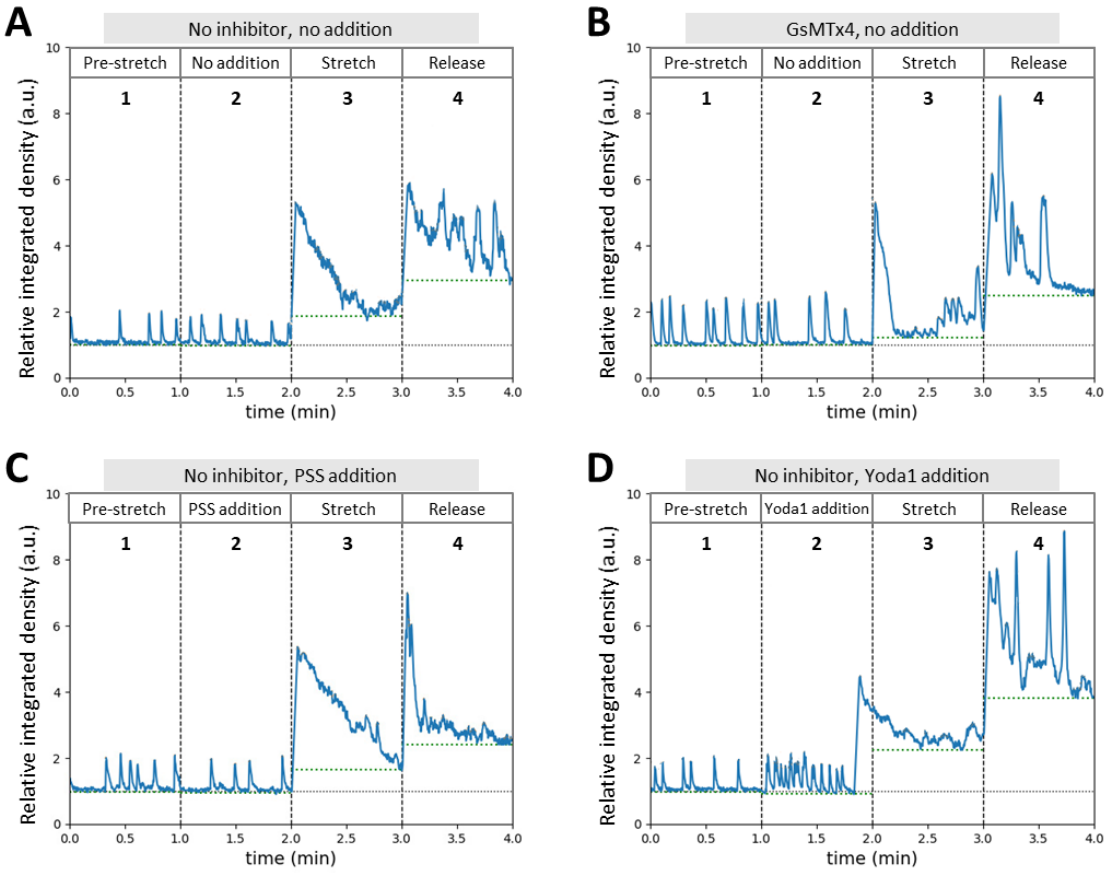

Figure 4-7 Examples of HL-1 cell response under different experimental conditions.

Blue trace in each image indicates relative integrated density of Fluo-4 AM fluorescence in one individual HL-1 cell during four continuous phases (marked with 1, 2, 3, 4). Green

dotted line indicates the lowest point of each phase as base intensity. (A) HL-1 cell with no inhibitor and no liquid addition. (B) HL-1 cell pre-incubated with GsMTx4, no addition. (C) No inhibitor, PSS addition. (D) No inhibitor, Yoda1 addition.

Considering the heterogeneity of individual HL-1 cells, and the different stimulations under various experimental conditions, for further quantitative data analysis in future, classification of cells is a necessary approach. For example, the total data of all individual cells could first be classified by the experimental conditions including application of MS channel inhibitor(s) and drug addition. Next, the data could be divided into groups by the initial cell status such as spontaneous activities. Then, the data could be further classified by the cell response such as responses to different triggers (stretch and release), the parameters of the response (base intensity, peak frequency, peak amplitude as well as wave shape), and the types of response (increase, decrease, or no change) (**Figure 4-8**).

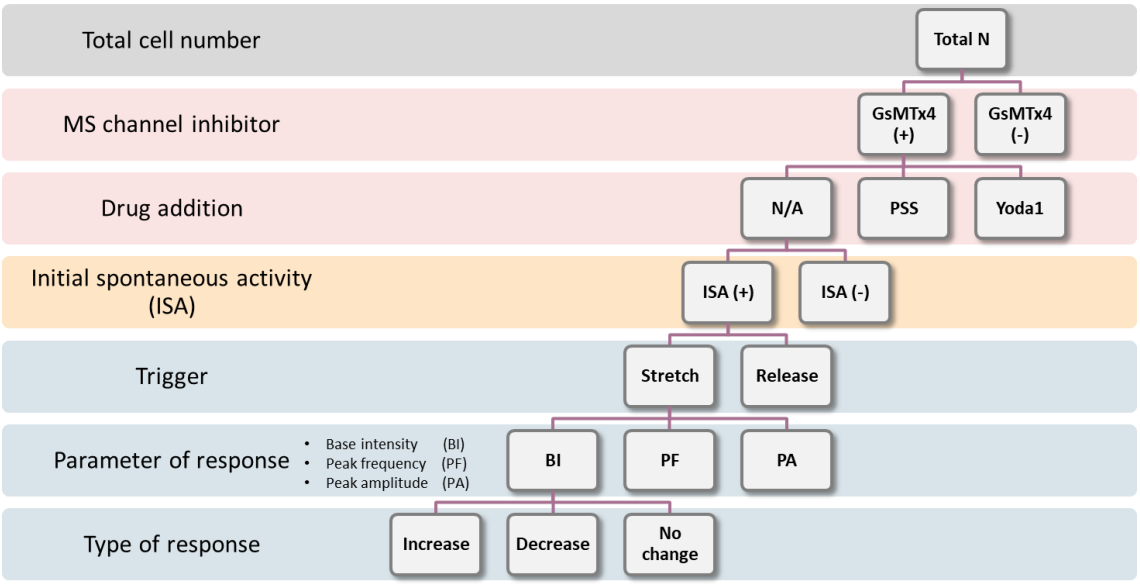

Figure 4-8 Schematic diagram of cell classification.

Data are classified by experimental conditions, initial cell status, and cell responses, marked with different colour backgrounds.

4.2.1.2 Application on isolated mouse ventricular cardiomyocytes

In the meantime, an optimised protocol for stretching mouse ventricular cardiomyocytes was developed through some attempts.

First, the Yoda1 effect on mouse ventricular cardiomyocytes was investigated using Ca^{2+} imaging. After Fluo-4 AM staining, isolated LV cardiomyocytes from five mouse hearts were kept in 100 µL HBSS supplemented with 1.2 mM $CaCl_2$ in 96 well plates (**Figure 4-9A**). At two minutes after starting recording, 33.3 µL HBSS containing 20 µM Yoda1 or DMSO was added into the 100 µL HBSS mixture to reach a final concentration of 5 µM. Also, a number of cells without any drug addition were used as baseline. The data were recorded for four minutes in total with a frame interval of 200 ms (5 images/s). An example of the fluorescence intensity from one cardiomyocyte during the experiment is shown in **Figure 4-9B**. This cell exhibits a Ca^{2+} oscillation whose peak frequency was increased after Yoda1 addition (final concentration 5 µM).

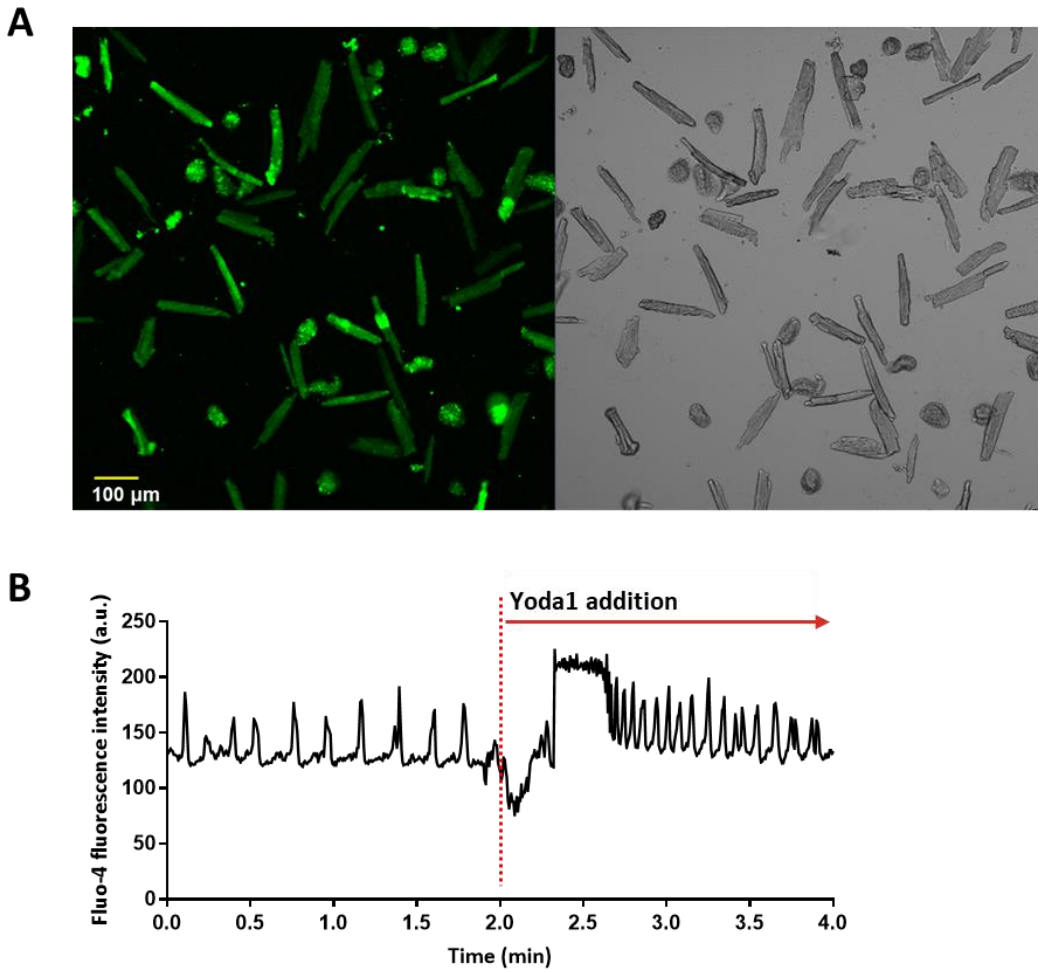

Figure 4-9 Ca^{2+} level in mouse ventricular cardiomyocytes responding to Yoda1 addition.

(A) Fluorescent and brightfield images of mouse ventricular cardiomyocytes in 96 well plate with 1.2 mM Ca^{2+}. (B) Exemplary data showing Yoda1 addition (final concentration 5 µM) affecting the Ca^{2+} transient in one mouse ventricular cardiomyocyte.

The two-minute time point from the beginning of the experiment is the midpoint of the recording, as well as the time point of Yoda1/DMSO addition. When comparing the peak frequency of Ca^{2+} oscillations after the midpoint with that before the midpoint, the isolated LV cardiomyocytes from five mouse hearts showed three different patterns: increased,

unchanged, and decreased (**Figure 4-10A**). In the Yoda1 group, the majority of the cells (60%) had an increased frequency, while only 27.6% and 20% of the cells in DMSO and baseline groups showed an increase, respectively (**Figure 4-10A**). Also, in both baseline and DMSO groups, around 50% of the cells had no change in peak frequency. 33.3% of the cells in the baseline group and 24.1% of the cells in the DMSO group exhibited a decrease in frequency (**Figure 4-10A**). In the Yoda1 group, a lower percentage of cell (31.4%) remained unchanged and only 8.6% showed a decrease (**Figure 4-10A**). The Ca^{2+} oscillation peak numbers before and after the recording midpoint in the three groups are shown in **Figure 4-10B**. The peak number increased significantly ($p < 0.001$) only after the addition of Yoda1. Accordingly, when comparing the after/before ratio of the peak numbers in the three groups, the ratio in the Yoda1 group was significantly higher than in the baseline ($p < 0.001$) and DMSO ($p < 0.01$) groups (**Figure 4-10C**).

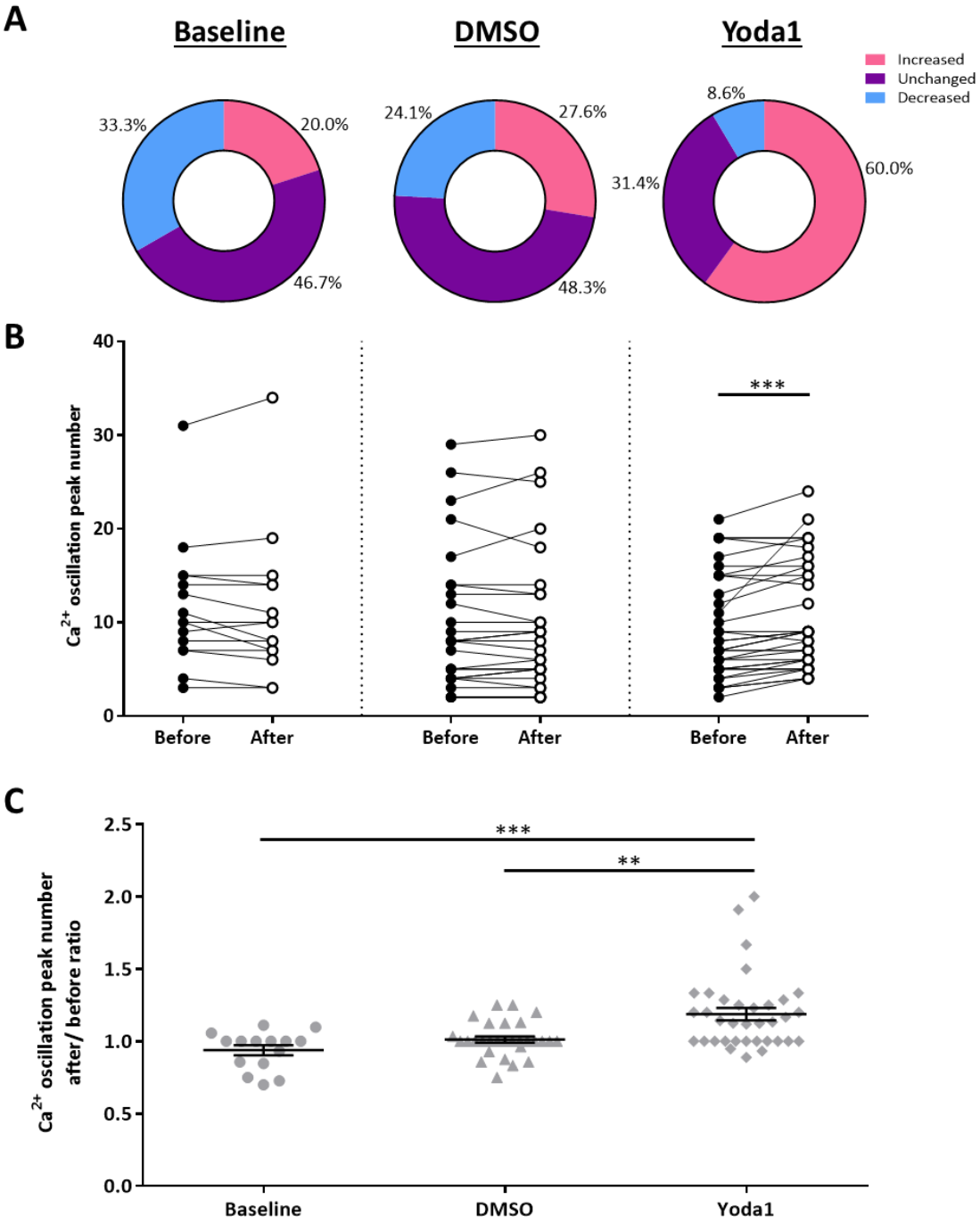

Figure 4-10 Frequncy changes of Ca^{2+} oscillation in mouse ventricular cardiomyocytes.

(A) The ratio of cells with different changes in Ca^{2+} oscillation frequency in different experimental conditions. (B) The Ca^{2+} oscillation peak numbers before-after recording midpoint. (C) The Ca^{2+} oscillation peak number after/before ratio are presented as

scatter plots with means ± SEM. n = 15/29/35 cells for baseline/DMSO/Yoda1 group, respectively. **$p < 0.01$, ***$p < 0.001$.

Next, attempts have been made to develop a protocol for stretching isolated adult mouse ventricular cardiomyocytes using the *IsoStretcher*, as well as visualising the cell responses by fluorescent microscopy. As described in **2.5**, the ventricular cardiomyocytes need to be embedded into the hydrogel because of their low surface adherent properties. A "medium" stiffness gel with an elastic modulus in the range of 4-9 kPa (O. Friedrich et al., 2017) was used in this study. Isolated mouse LV cardiomyocytes embedded in the gel disc attached to the PDMS chamber were stained with Fluo-4 AM. First, the baseline activity of the mouse LV cardiomyocytes was recorded for two minutes without any stretch. Then a 15% isotropic stretch was applied to the chamber and maintained for two minutes. After that, the chamber was released to 0% stretch and kept for another two minutes. The experiment was recorded continuously with a frame interval of 200 ms (5 images/s). **Figure 4-11A** shows representative Ca^{2+} images of one adult mouse LV cardiomyocyte with no stretch (left) and with 15% stretch (right). This cell exhibited an increase of both base Ca^{2+} level and Ca^{2+} oscillation frequency during 15% isotropic stretch (**Figure 4-11B**). The Ca^{2+} oscillation amplitude also had different magnitudes in the three phases of before stretch, during stretch, and after stretch (**Figure 4-11B**).

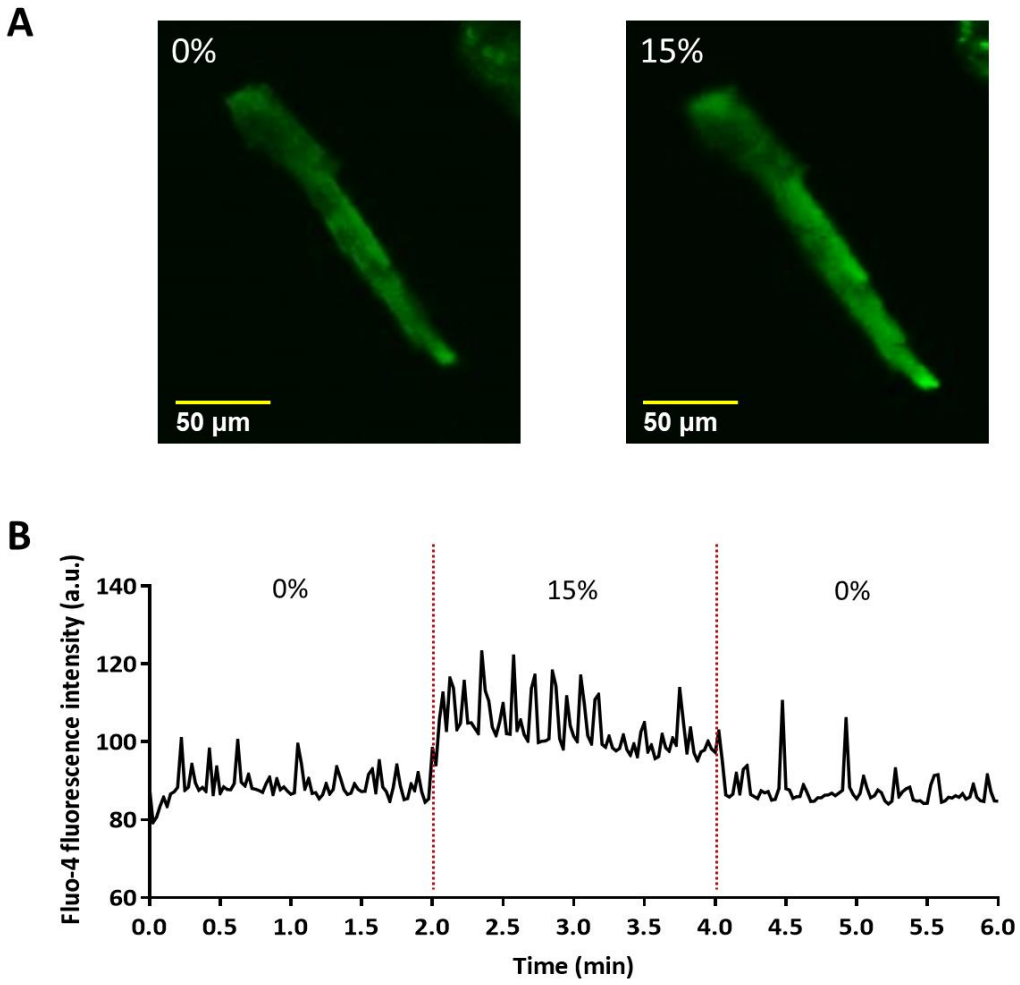

Figure 4-11 Ca^{2+} transient in mouse ventricular cardiomyocytes responding to isotropic stretch.

(A) Fluo-4 AM-based fluorescent image of mouse ventricular cardiomyocyte under 0% and 15% stretch in PDMS chamber. (B) Exemplary data showing Ca^{2+} transient responding to 15% isotropic stretch in one mouse ventricular cardiomyocyte.

4.2.2 Application of kinetic imaging cytometry as an approach to investigate functional presence of Piezo1 in mouse ventricular cardiomyocytes

Another method has been developed to investigate the functional presence of Piezo1 in mouse ventricular cardiomyocytes, especially the function of

Piezo1 in pressure overload-induced LVH. This method uses KIC to perform Ca^{2+} transient measurements in isolated ventricular cardiomyocytes from Sham/TAC mice.

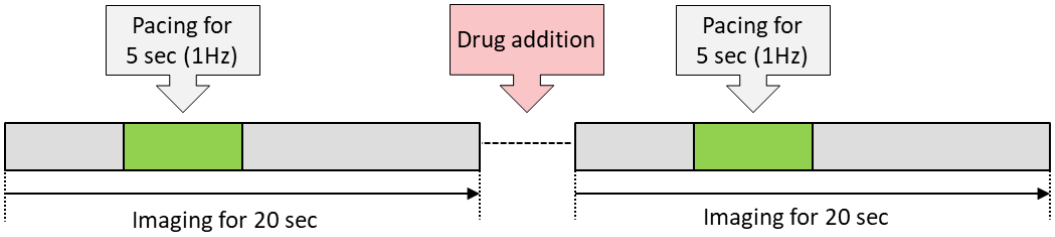

Figure 4-12 Experimental scheme for KIC-based Ca^{2+}/electric singal acquisition in mouse ventricular cardiomyocytes.

Isolated mouse LV cardiomyocytes in a 0.6 mM Ca^{2+} buffer mixture were stained with Fluo-4 AM (2 µM), then dispensed in 96 well plate within 100 µL buffer mixture containing 0.6 mM Ca^{2+}. Hoechst (1:1000, Thermo Scientific, USA) dye can be optionally used to locate the nucleus. As shown in **Figure 4-12**, The cells were imaged for 20 seconds, with electrical pacing performed for 5 seconds at a frequency of 1 Hz from the fifth second. Then, chemical channel activators (e.g. Yoda1) could be automatically added into the well(s) according to the pre-set program. After that, another 20-second imaging with pacing was carried out. The Drug addition phase lasted 7 seconds. After a few trials, it was found that for a buffer volume of 100 µL, adding 20 µL at a rate of 10 µL per second would barely cause mouse cardiomyocytes displacement. **Figure 4-13A** shows the Ca^{2+} image of isolated mouse LV cardiomyocytes by KIC. **Figure 4-13B** shows Ca^{2+} fluorescence intensity changes in one mouse LV cardiomyocyte during

electrical pacing at 1 Hz for 5 seconds, analysed by ImageJ (National Institutes of Health, USA).

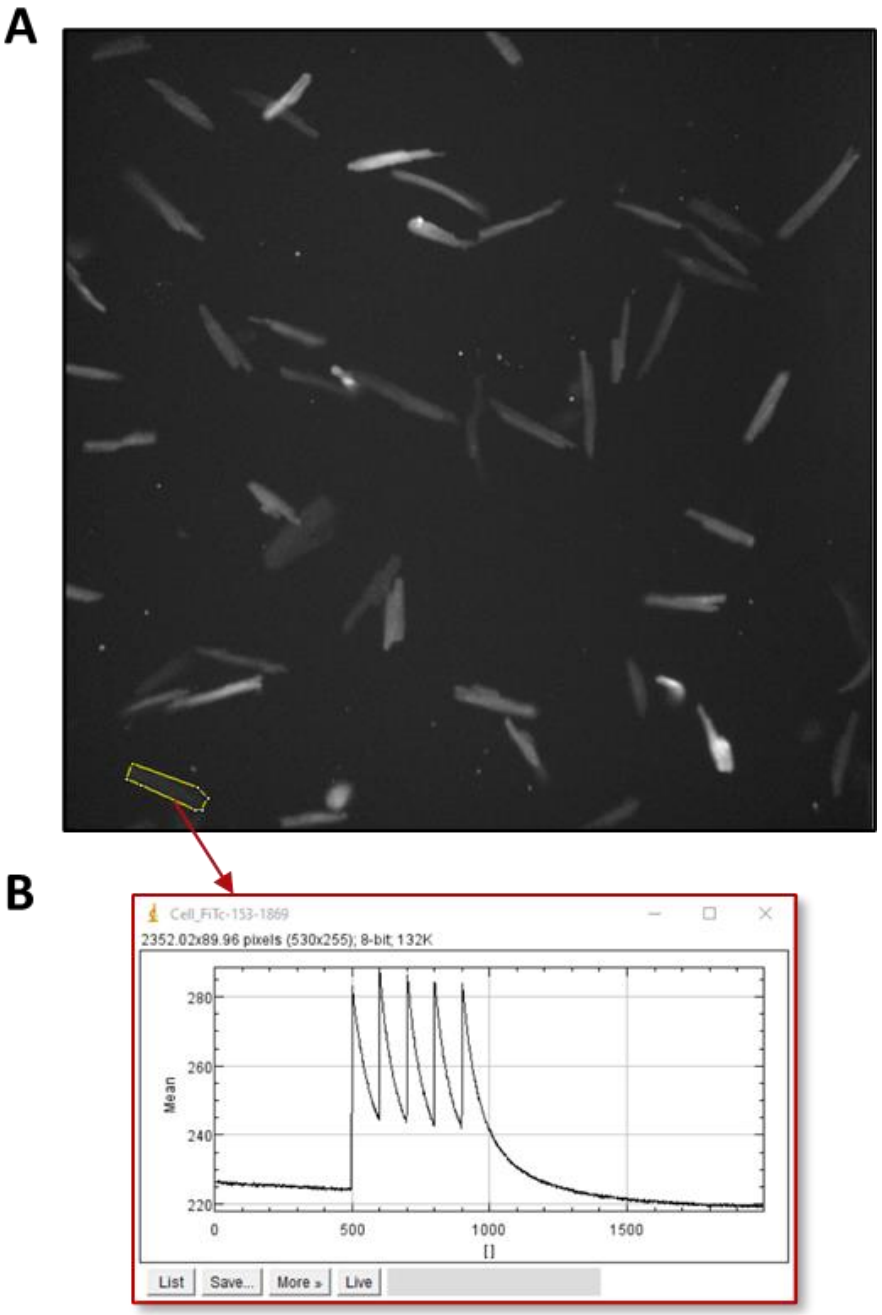

Figure 4-13 KIC-based Ca^{2+} measurement in adult mouse LV cardiomyocytes.

(A) Ca^{2+} image of isolated mouse LV cardiomyocytes with Fluo-4 AM staining, acquired by KIC. (B) Ca^{2+} fluorescence intensity changes during electrical pacing, analysed by ImageJ (National Institutes of Health, USA).

According to this experimental protocol, cardiac-specific Piezo1 knockout mice (Yu, Gong, Kesteven, et al., 2021) or Piezo1-tdTomato mice (Yu, Gong, Kesteven, et al., 2021) can be used to compare with corresponding control mice, under sham or TAC operation. **Figure 4-14** shows an example of experimental design using isolated mouse LV cardiomyocytes with different genotypes and experimental conditions.

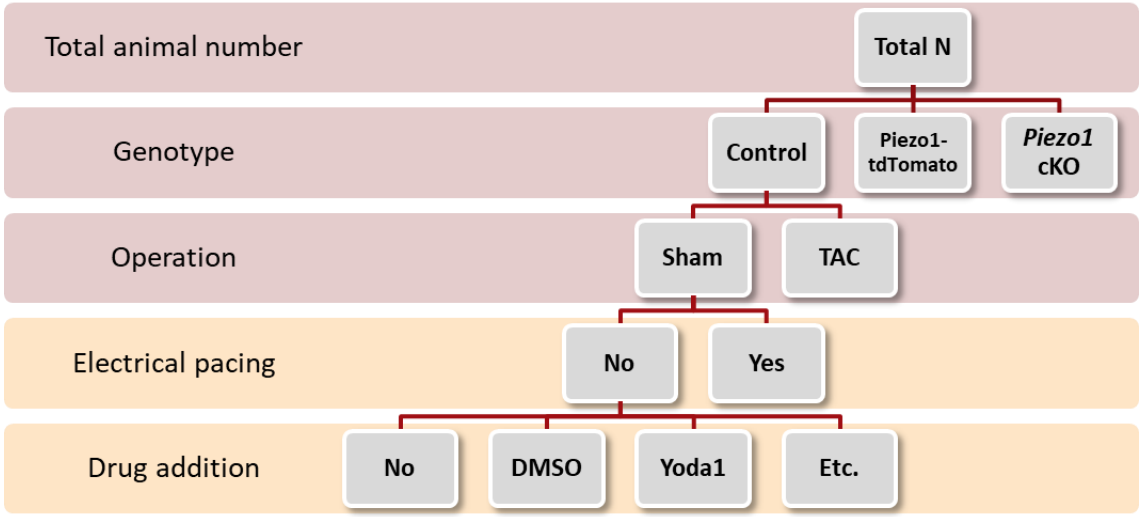

Figure 4-14 Example of experimental group design using isolated mouse LV cardiomyocytes.

4.3 Discussion

MS channel Piezo1 is involved in a broad range of physiological and pathological processes in the body. In the cardiovascular system, the

activities of Piezo1 have been examined in different cell types including ECs, RBCs, CFs, and cardiomyocytes. Particularly, studies have shown that Piezo1 contributes to the Ca^{2+} modulation in mouse ventricular cardiomyocytes (Jiang et al., 2021; Yu, Gong, Kesteven, et al., 2021; Zhang et al., 2021) in response to the mechanical stretch in pressure overload-induced LVH (Yu, Gong, Kesteven, et al., 2021; Zhang et al., 2021). However, the molecular force-sensing mechanisms of Piezo1 in cardiac mechanotransduction, as well as the exact role of Piezo1 underlying pressure overload-induced LVH has not yet been fully unravelled.

In this study, for the first time the HL-1 line was used to establish an *in vitro* model to provide new approaches to investigate Piezo1-mediated cardiac mechanotransduction. The HL-1 cell line can exhibit spontaneous action potentials and synchronous beating in confluent cultures (Claycomb et al., 1998). Also, the HL-1 cells share some phenotypic similarities in some typical cardiac gene expression and signalling pathways with primary adult mouse atrial or ventricular myocytes (Claycomb et al., 1998; Hu et al., 2021; C. Liu et al., 2020; Son et al., 2016; White et al., 2004). In this study, the *Piezo1* mRNA expression indicated that HL-1 cells express an appreciable amount of Piezo1. This was supported by the significantly ($p < 0.001$) increased intracellular Ca^{2+} level in HL-1 cells after Yoda1 addition.

To investigate Piezo1-mediated cardiac mechanotransduction, it is important to employ devices that apply the stretching protocol to simulate as close as possible the stretching experienced by cardiac cells *in vivo*. To date, the *IsoStretcher* is a very versatile, and one of the few systems that can apply isotropic stretch to whole cell membrane sectors (O. Friedrich et al., 2017; Schürmann et al., 2016). This multiaxial isotropic stretch

represents a more physiological stretch regime for cardiac cells. As HL-1 was a new cell line used with the *IsoStretcher* system, the calibration of cell surface area under stretch was required (O. Friedrich et al., 2017; Schürmann et al., 2016). In this study focusing on measurements on individual cells, the cell culture, seeding, and stretching protocols (see **2.1.2** and **2.5**) was specifically adjusted, including using newly optimised PDMS chambers. These successfully achieved a 16% increase in cell surface area ($p < 0.001$) when the chamber was subjected to 15% isotropic stretch, which is close to the results of other cell lines shown by Schürmann et al. (2016).

The first cell stretching protocol consisting of six phases combined 15% isotropic stretch with the addition of small molecule compound Yoda1 (final concentration 5 µM), which can chemically activate the Piezo1 channel and can increase the mechanosensitivity of Piezo1 (Botello-Smith et al., 2019; Syeda et al., 2015). A calculation for the "relative intensity change" was used to reduce the background noise interference and to increase the accuracy of intracellular Ca^{2+} signal analysis. From the four examples shown in **Figure 4-5**, compared to pre-stretch, the significantly higher Ca^{2+} level in HL-1 cells responding to stretch ($p < 0.05$), Yoda1 addition ($p < 0.05$), and stretch with Yoda1 presence ($p < 0.05$) indicated Piezo1 activation. When the HL-1 cells with Yoda1 were stretched to 15%, the intracellular Ca^{2+} level likely increased to an even higher level compared to cells only with stretch or Yoda1 alone. This result is consistent with Yoda1 modifying the inactivation rate of Piezo1 (Botello-Smith et al., 2019; Syeda et al., 2015). Piezo1 channel may maintain activation for a relatively longer period after stretch upon addition of Yoda1.

The second cell stretching protocol consisting of four phases avoided the complex responses of ion channels to repeated stretching stimuli. MS channel blocker GsMTx4 (Bae et al., 2011; Gnanasambandam et al., 2017) was used to confirm stretch-induced Piezo1 activation. The PSS addition group was added as a control for the influence of the increase in liquid volume. In this part, an automated analysis routine was developed to implement image registration and cell segmentation. The uneven illumination during Ca^{2+} imaging was corrected by intensity calibration and shading correction (M. A. Model, 2006; Michael A. Model & Burkhardt, 2001; University of California, 2021). Also, the calculated "relative integrated density" can be analysed through Python software (Python Software Foundation, USA). Compared to the first stretching experiment, this experimental and data analysis procedure aims to process single cell data in large quantities, with a further improved accuracy.

Notably, with both stretching experimental protocols, despite some similar patterns were found in cell responses, there was a diversity of responses in different groups and cells. Classification of cells (**Figure 4-8**) is required in future studies, focused on experimental conditions, initial cell status, and cell responses. The "plateau" shape found in Stretch phase especially with Yoda1 presence indicated higher concentration of Ca^{2+} being presence in the cell, causing delay in repolarisation of the membrane potential.

The experiments on HL-1 cells built a foundation allowing for more complicated cell stretching experiment with isolated mouse ventricular cardiomyocyte. The increased Ca^{2+} oscillation frequency after Yoda1 addition compared to the baseline control ($p < 0.001$) and DMSO control ($p < 0.01$) indicated Yoda1-evoked Piezo1 activation in mouse LV

cardiomyocytes. Because of the low surface adherent properties of ventricular cardiomyocytes, the cell stretching was achieved by embedding mouse LV cardiomyocytes into the hydrogel attached to the PDMS chamber. The increase in both base Ca^{2+} level and Ca^{2+} oscillation frequency during 15% isotropic stretch shown in **Figure 4-11B** suggested that Piezo1 was likely activated by isotropic stretching of the cardiomyocytes. However, the spontaneous Ca^{2+} oscillation waves observed in the cardiomyocytes are known to be a response of Ca^{2+} overload (Loughrey, MacEachern, Neary, & Smith, 2002). This suggested that the 1.2 mM Ca^{2+} solution was probably too high for the cells to maintain "normal" physiological conditions. Therefore, in the following experiments a lower concentration (0.6 mM) of Ca^{2+} solution was used and no Ca^{2+} waves were observed in the cardiomyocytes.

In addition, mouse LV cardiomyocytes were tested with another approach using KIC-based Ca^{2+} measurements, which has several features such as multiple cell monitoring, automatic drug addition, application of electrical pacing, and time series data recording. The experimental protocol (**Figure 4-12**) and group design (**Figure 4-14**) developed in this chapter provide the methodological basis for studying the functional presence of Piezo1 in mouse ventricular cardiomyocytes in pressure overload-induced LVH, including the use of cardiac-specific Piezo1 knockout mice and tdTomato mice.

In addition to the Ca^{2+} overload in LV cardiomyocytes caused by excessive Ca^{2+} concentration, some limitations of the cell stretching studies in this chapter were also noted. First, because Fluo-4 AM is not a ratiometric fluorescent dye, although the accurate relative Ca^{2+} intensity values and

changes were obtained by calculation for statistical analysis, the actual intracellular Ca^{2+} concentration was not known. For further studies the use of ratiometric Ca^{2+} indicator (e.g. Fura-2 AM) is considered. Second, considering that the Ca^{2+} image recording time in the experiment reached a few minutes, the recording interval was set at 100 or 200 ms (5 or 10 images/s). Due to this relatively slow sampling speed, the data points reflecting intensity changes were limited, which might affect the Ca^{2+} oscillation wave data. A higher sampling speed is required for data acquisition in the future, while ensuring the reasonable size of the experimental data. Third, the use of GsMTx4 can help confirm cell response to mechanical stretch as it causes inhibition of MS channels. However, GsMTx4 is not a specific Piezo1 inhibitor. Also, it suppresses mechanical activation rather than chemical activation (Douguet et al., 2019; Gnanasambandam et al., 2017), so it cannot completely inhibit Yoda1-evoked Piezo1 activation. Specific inhibition of Piezo1, such as siRNA-mediated gene knockdown, is considered for further studies. In addition, this study only focused on single cell measurements with a single stretch. Investigation of interconnected HL-1 cells with synchronised beating, as well as cyclic cell stretching is also considered for further studies.

In conclusion, studies in this chapter provided methodological foundations of new *in vitro* approaches to investigate Piezo1-mediated cardiac mechanotransduction underlying pressure overload-induced LVH. Yoda1-evoked Piezo1 activation, and likely stretch-induced Piezo1 activation were shown in both HL-1 cells and isolated mouse ventricular cardiomyocytes with the application of the *IsoStretcher* technology. The experiments in this chapter also provide many experiences and lessons for the design and execution of subsequent studies in the following chapter.

Chapter 5 *In vitro* evidence of Piezo1-TRPM4 interaction

5.1 Introduction

TRPM4 and Piezo1 ion channels have been shown to play important roles in the cardiovascular system. The TRPM4 channel contributes extensively to cardiac physiological and pathological processes because of its involvement in Ca^{2+}-dependent signalling in the mammalian heart (Guinamard et al., 2015; Guinamard et al., 2004; Guinamard et al., 2006; Hof et al., 2019; Mathar et al., 2014; C. Wang et al., 2018; H. Watanabe et al., 2008). Previous studies have identified that TRPM4 contributes to both atrial and ventricular electrical and structural remodelling. It is associated with cardiac electrical activity, such as action potential formation and arrhythmias (Demion et al., 2014; Guinamard et al., 2015; Hedon et al., 2021; Hof et al., 2016; Hof et al., 2013; Hu et al., 2017; Mathar et al., 2014; Simard et al., 2021; Simard et al., 2013). Importantly, it is also considered a key protein involved in the underlying mechanisms of cardiac hypertrophy and heart failure (Frede et al., 2020; Gueffier et al., 2017; Hedon et al., 2021; Jacobs et al., 2015; Kecskes et al., 2015). In **Chapter 3**, TRPM4 has been proven to be a key component of the hypertrophic signalling transmission in response to mechanical pressure overload. However, TRPM4 has also been shown to be insensitive to mechanical membrane stretch (Constantine et al., 2016; Gottlieb et al., 2008; Nikolaev et al., 2019). Its activation is Ca^{2+}- and voltage-dependent (Pierre Launay et al., 2002). Therefore, in the development of heart diseases involving mechanical stretch to cardiac cells, such as pressure overload-induced LVH, TRPM4 likely functions as a “mechano-effector” (Owen P Hamill & Maroto, 2007) or a signal amplifier (Nikolaev et al., 2019), which requires its association

with other MS channels which act as the primary transducers of mechanical forces into Ca^{2+} signals.

As a relatively newly discovered MS channel that mediates mechanically activated Ca^{2+} signalling and cationic currents, Piezo1 has been shown to be an essential component of the mechanotransduction processes in various aspects of cardiovascular physiology and pathology (Beech & Kalli, 2019; Coste et al., 2010; Douguet et al., 2019). Piezo1 has been identified to be inherently mechanosensitive (Cox et al., 2016; Syeda et al., 2016). As introduced in **1.4.3.2**, patch clamp and *in vitro* cell stretching technologies have been adopted to study Piezo1 mechanosensitivity. In **Chapter 4**, isotropic cell stretching stimulation has been applied to cultured HL-1 mouse atrial myocyte-like cells and mouse ventricular cardiomyocytes as an approach to investigate Piezo1-mediated cardiac mechanotransduction. In addition, a number of very recent studies using *in vivo* models suggested that Piezo1 plays a critical role in pathological cardiac remodelling, especially in pressure overload-induced cardiac hypertrophy. It initiates the cardiac mechanotransduction in which the mechanical stimuli are transduced into Ca^{2+} signals (Jiang et al., 2021; Yu, Gong, Kesteven, et al., 2021; Zhang et al., 2021). This initial step further activates the CaMKII-HDAC-MEF2 LVH signalling pathway in mouse ventricular cardiomyocytes involving the Ca^{2+}-dependent mechanisms (Yu, Gong, Kesteven, et al., 2021).

Therefore, hypothetically, Piezo1 could be the upstream channel whose activation can further affect TRPM4 in cardiac mechanotransduction. This Piezo1-TRPM4 interaction may contribute to the initial step of the pressure overload-induced LVH signalling pathway. However, there was previously no direct evidence showing that Piezo1 activation is related to TRPM4

activation. In this study, HL-1 mouse atrial myocyte-like cell line (Claycomb et al., 1998) was employed as an *in vitro* model to investigate if Piezo1 activation can further activate TRPM4 channels. The action potential changes in HL-1 cells during Yoda1-evoked Piezo1 activation (Syeda et al., 2015) were detected and analysed, compared between the control groups and the TRPM4 pharmacological/genetic inhibition groups, using a fluorescent voltage sensitive dye. The results demonstrate that not only does Piezo1 activation change action potential generation in HL-1 cells but that inhibition of TRPM4 in HL-1 cells significantly affects the degree to which Yoda1-evoked Piezo1 activation changes action potential frequency.

5.2 Experimental procedure

For pharmacological inhibition experiments, HL-1 cells were seeded in 96 well plate until confluent culture was reached. The preparation of cells using FluoVolt (Invitrogen, USA) is described in **2.11.1**. Pharmacological inhibitors, including flufenamic acid (20 µM) and 9-phenanthrol (20 µM and 40 µM), were incubated with FluoVolt, respectively. While imaging, the cells were maintained in culture medium with the corresponding inhibitor for each pharmacological inhibition experiment. For genetic inhibition experiments, HL-1 cells were seeded in 96 well plate and treated with siRNAs (detail described in **2.6**) before FluoVolt preparation and microscopy.

The recording scheme with fluorescent microscopy is shown in **Figure 5-1**. The cells in each well were imaged for 10 seconds. Then drug addition was applied to the well. After that, the cells were imaged for another 10 seconds. The data before and after drug addition was compared to identify the drug

effect. In each well, the cells were kept in 100 µL culture medium. Then 33.3 µL medium containing Yoda1, NS 1619 or DMSO (for control) was added into the well to reach the final concentration needed for experiment. This method of drug addition helps to achieve a balance between increasing the diffusion rate of the drug and reducing the impact of liquid volume increase to the cells.

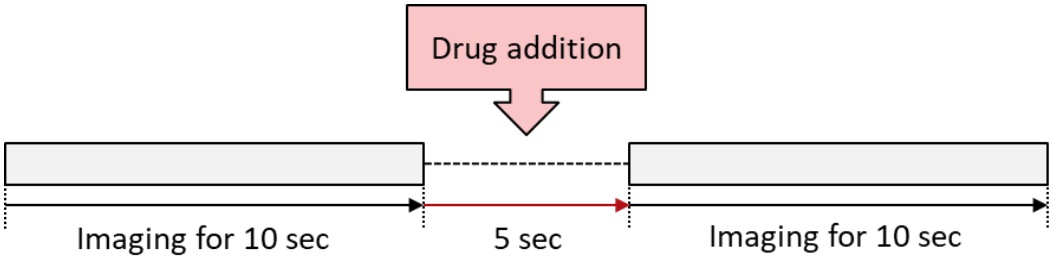

Figure 5-1 Sample recording scheme with drug addition.

For pharmacological inhibition experiments, a 666 µm x 666 µm ROI from each well was imaged and recorded with a 10 ms recording interval (100 images/s). The action potential data were averaged from approximately 800-1000 cells in the ROI. For genetic inhibition experiments, using an improved protocol for higher accuracy of data, a 5 ms recording interval (200 images/s) was set for recording data from a 333 µm x 333 µm ROI. In the central area of the imaging ROI, a 40 µm x 40 µm ROI which contains approximate 4-6 cells was used for data analysis, in order to prevent the influence of conduction velocity during sampling (described in **5.3.1.4**). The details for data analysis were described in **2.11.2**.

5.3 Results

5.3.1 Characteristics of HL-1 cells

The HL-1 cells used in this study were characterised to understand the Piezo1 and TRPM4 expression levels as well as the electrophysiological properties. Also, the HL-1 cells were classified based on their initial spontaneous activities for subsequent experiments in this study.

5.3.1.1 *Piezo1* and *Trpm4* mRNA expression levels in HL-1 cells

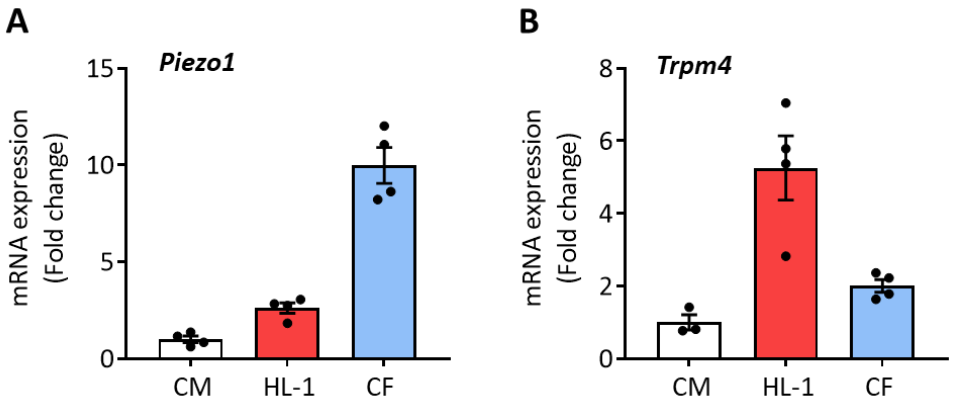

Figure 5-2 *Piezo1* and *Trpm4* gene expression in HL-1 cells compared to other mouse cardiac cells.

Relative mRNA expression of (A) *Piezo1* and (B) *Trpm4* in mouse LV cardiomyocytes (CM), HL-1 cells, and primary mouse cardiac fibroblasts (CF). The mRNA relative expression was normalised to GAPDH and calculated as fold change relative to CM, for each gene. Results are presented as means ± SEM. n = 3-4/group. n represents the number of mice for LV cardiomyocytes or the number of separate culture dishes for HL-1 cells and cardiac fibroblasts.

In comparison with other mouse cardiac cells, the *Piezo1* mRNA expression level in HL-1 cells is 2.62-fold that in isolated adult mouse LV cardiomyocytes, and 0.26-fold that in primary adult mouse cardiac fibroblasts (**Figure 5-2A**). The *Trpm4* mRNA expression level in HL-1 cells is 5.25-fold that in mouse LV cardiomyocytes, and 2.63-fold that in mouse primary cardiac fibroblasts (**Figure 5-2B**).

5.3.1.2 HL-1 cell classification based on initial spontaneous activities

The initial spontaneous activity observed in HL-1 cells was strongly dependent on the cell culture conditions, even in confluent cultures. In this study, the HL-1 cells used in experiments were classified based on their synchronous initial spontaneous action potential (ISAP) frequency. The frequency was successfully controlled by using different cell culture protocols to adjust cell seeding density and culture time (**Table 5-1**). There were no ISAP when seeding 25,000 to 40,000 cells per well in a 96 well plate for 72 hours at 37 °C with 5% CO_2. By seeding 22,000 to 24,000 cells per well for 96 hours or 40,000 cells for 72 hours, all the cells exhibited a “slow” ISAP, which is less than 20 peaks in 10 seconds (**Figure 5-3**). This was significantly different ($p < 0.001$) than when 40,000 cells per well for 96 hours or 50,000 cells for 72 hours were seeded. In these cases, HL-1 cells in 94% of the wells exhibited a “fast” ISAP, which is more than 20 peaks in 10 seconds (**Figure 5-3**). Therefore, the HL-1 cells used in this study were classified into “No ISAP” (AP number/10 sec = 0), “Slow ISAP” (AP number/10 sec < 20), and “Fast ISAP” (AP number/10 sec > 20) groups. The slow ISAP group has been focused on mainly, but some results from No ISAP groups and Fast ISAP groups have also been analysed.

Table 5-1 Control HL-1 cell initial spontaneous activities by cell seeding density and culture time.

Cell culture protocol	Seeding cell number/well (96 well plate)	Culture time (h)
No ISAP	25,000-40,000	72
Slow ISAP	22,000-24,000	96
	40,000	72
Fast ISAP	40,000	96
	50,000	72

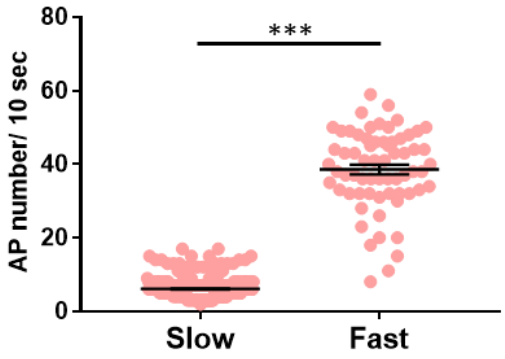

Figure 5-3 HL-1 cell initial spontaneous action potential frequency by Slow and Fast ISAP cell culture protocols.

Frequency is presented as action potential (AP) numbers in 10 seconds. n = 324 in Slow group; n = 65 in Fast group. n represents the number of wells in 96 well plate. Results are presented as scatter plots with means ± SEM. ***$p < 0.001$.

5.3.1.3 HL-1 cell action potential is driven by the L-type Ca^{2+} channel

To investigate which ion channel is the main driving force of the HL-1 cell action potential, two ion channel blockers have been used in this study. The addition of the classic L-type Ca^{2+} channel blocker nifedipine exhibited a trend of slowing in action potential frequency at concentrations of 0.001, 0.002, and 0.010 μM (**Figure 5-4A**). At 0.050 μM, action potential was blocked in 60% of the wells in 96 well plate; at 0.100 μM, action potential was completely blocked in all the wells (**Figure 5-4A**). The IC_{50} of nifedipine is 0.002-0.008 μM (at the lower end) for Cav1.2 which is considered the main cardiac L-type Ca^{2+} channel (Perez-Vizcaino, Tamargo, Hof, & Ruegg, 1993; Pignier & Potreau, 2000). Therefore, nifedipine's effect on blocking HL-1 action potential has been found at a concentration average of 10-fold the IC_{50} and was 100% effective when at a concentration average of 20-fold the IC_{50}. With the Na^{+} channel blocker lidocaine at concentrations of 25, 50, 100, 250, 500, and 1000 μM, HL-1 cells still exhibited action potential (**Figure 5-4B**). As the IC_{50} of lidocaine is 50 μM for the main cardiac Na^{+} channel Nav1.5 (Nuss, Tomaselli, & Marban, 1995), it didn't show effect of blocking action potential at concentrations of 10- and 20-fold the IC_{50}. These results suggest that the L-type Ca^{2+} channel is the main contributor to the action potential in HL-1 cells.

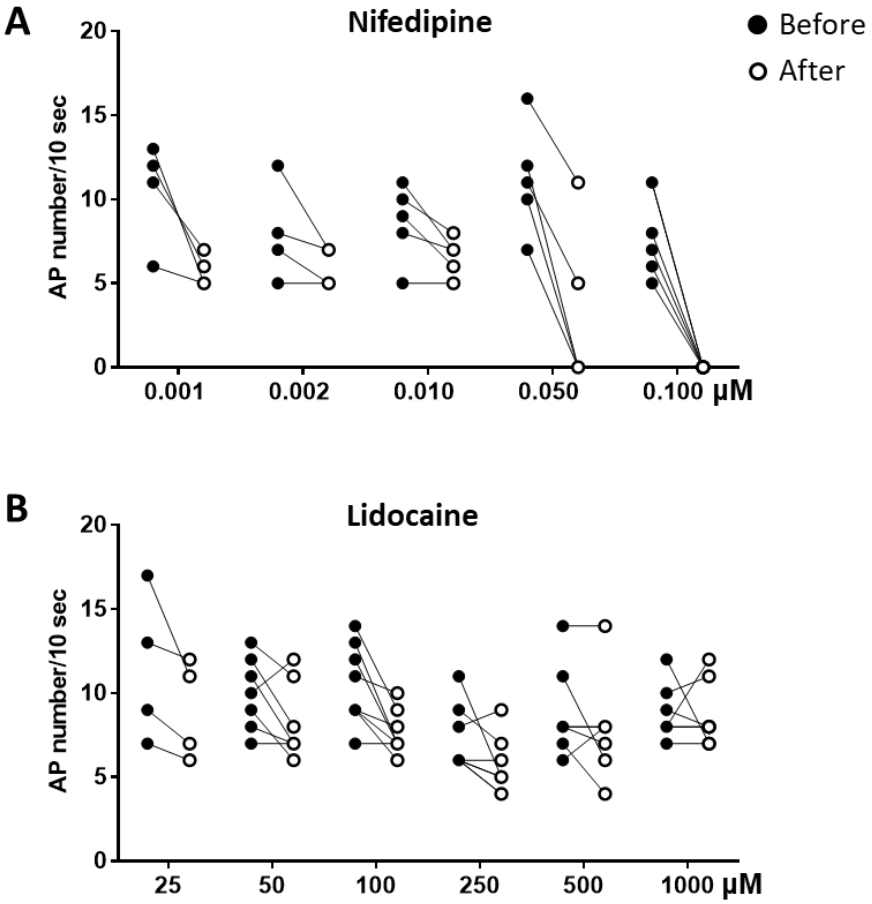

Figure 5-4 HL-1 cell action potential affected by ion channel inhibitors.

Results are presented as before-after drug addition. The final concentrations of (A) nifedipine and (B) lidocaine after addition are presented. Action potential (AP) frequency is presented as AP numbers in 10 seconds. n = 4-8/group. n represents the number of wells in 96 well plate.

5.3.1.4 HL-1 cell conduction velocity

In genetic inhibition groups and their control groups, the conduction velocity of the HL-1 cells was calculated as imaging ROI diagonal length (μm) divided by the time between the two action potential peaks at each end of the diagonal (ms). In each imaging ROI, conduction velocity was calculated twice with two diagonals. The conduction velocity of HL-1 cells treated with

Trpm4-targeting siRNA, *Piezo1*-targeting siRNA, or the control siRNA for each gene are shown in **Figure 5-5**. There were no significant differences among all the groups. In addition, the range of conduction velocity was from 10.07 to 28.06 µm/ms. Therefore, with 5 ms recording interval (200 images/s), a 40 µm x 40 µm ROI was used for data analysis to avoid the action potential duration prolongation caused by action potential conduction while sampling.

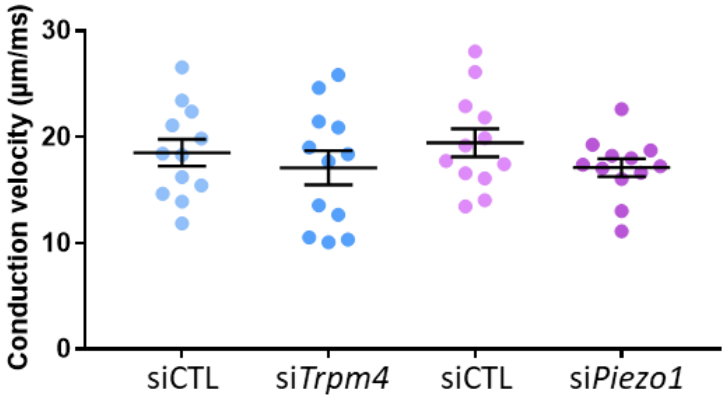

Figure 5-5 Conduction velocity of HL-1 cells used in genetic inhibition experiments.

HL-1 cells were treated with *Trpm4*-targeting siRNA (si*Trpm4*), *Piezo1*-targeting siRNA (si*Piezo1*), or the control siRNA (siCTL) for each gene. Conduction velocity = imaging ROI diagonal (µm)/time (ms). In each imaging ROI, conduction velocity was calculated twice with 2 diagonals. n = 2 calculations x 6 ROIs/group. Results are presented as scatter plots with means ± SEM. No significant differences among all the groups.

5.3.2 Effects of pharmacological inhibition in HL-1 cells

5.3.2.1 Pharmacological effects on HL-1 cells with no initial spontaneous action potentials

With the HL-1 cells without ISAP, DMSO addition had no effect in all groups; Yoda1 addition (final concentration 2 μM) activated synchronous action potential in the control group, flufenamic acid (20 μM)-treated group and 9-phenanthrol (20 μM)-treated group (**Figure 5-6**). However, with 20 μM 9-phenanthrol treatment, cells from 31.3% of the wells did not respond to Yoda1 addition ($p < 0.001$) (**Figure 5-6**). Furthermore, with 40 μM 9-phenanthrol treatment, no action potential was generated after Yoda1 addition (**Figure 5-6**). This is considered the potential blocking effect of 9-phenanthrol on Ca^{2+} channels, possibly including Piezo1. Therefore 9-phenanthrol was excluded in subsequent experiments.

Notably, in the flufenamic acid-treated group, the action potential frequency after Yoda1 addition is 31.8% lower ($p < 0.05$) compared to the control group.

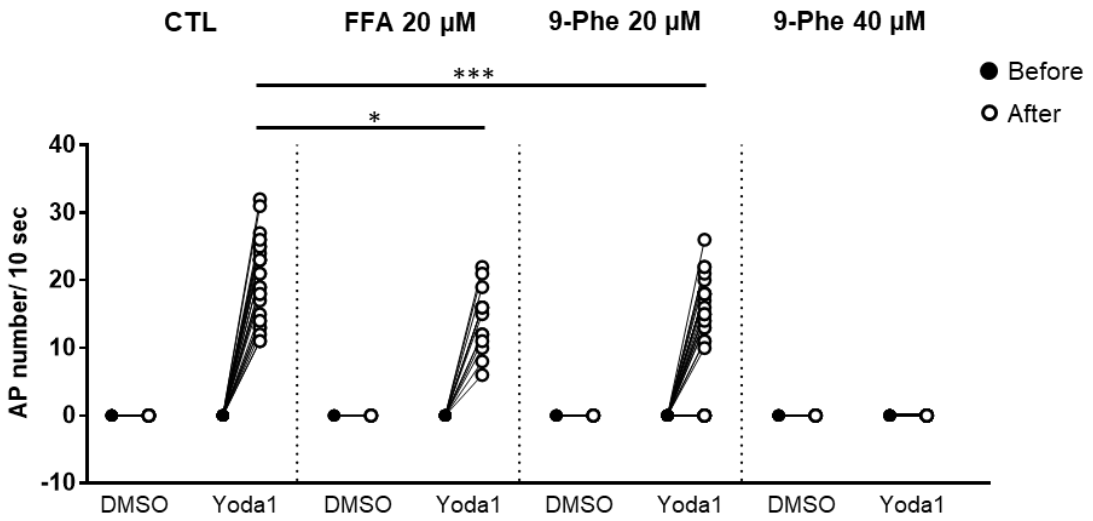

Figure 5-6 Action potential frequency in non-ISAP HL-1 cells with/without pharmacological inhibition.

HL-1 cells were pre-treated with flufenamic acid (FFA) or 9-phenanthrol (9-Phe), except the control group (CTL)s. Action potential (AP) frequency is presented as AP numbers in 10 seconds. Results are shown as before-after DMSO/Yoda1 addition. n = 4-10/group with DMSO addition; n = 13-32/group with Yoda1 addition. n represents the number of wells in 96 well plate. *$p < 0.05$, ***$p < 0.001$.

5.3.2.2 Pharmacological effects on HL-1 cells with slow initial spontaneous action potentials

The baselines of action potential frequency, APD90, and maximum upstroke velocity in HL-1 cells (Slow ISAP) exhibited no significant differences between the flufenamic acid-treated group and the control group (**Figure 5-7A, B, C**).

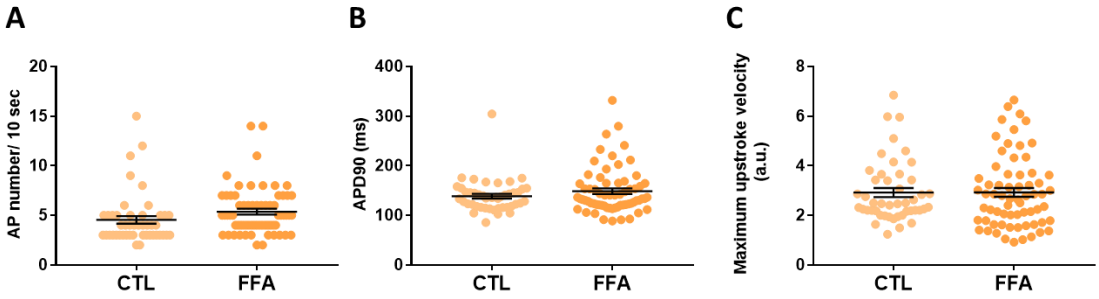

Figure 5-7 Slow ISAP HL-1 cell action potential baselines

(A) Action potential (AP) frequency, (B) APD90 and (C) action potential maximum upstroke velocity baselines were compared between the control group (CTL) (n = 46) and the flufenamic acid-treated group (FFA) (n = 66). n represents the number of wells in 96 well plate. Results are presented as scatter plots with means ± SEM. No significant differences between CTL and FFA in (A), (B), and (C).

With Slow ISAP cells, DMSO addition showed no significant effect on action potential frequency, APD90 or maximum upstroke velocity (**Figure 5-8**). Yoda1 addition (final concentration 2 µM) induced a significant increase ($p < 0.001$) in action potential frequency in both control and flufenamic acid-treated groups (**Figure 5-8A**). In addition, the frequency in the flufenamic acid-treated group was 18.8% lower ($p < 0.001$) than that in the control group after Yoda1 addition (**Figure 5-8A**). Similarly, when calculated as the after/before drug addition ratio (**Figure 5-8B**), the ratio with Yoda1 addition is significantly higher than that with DMSO addition in both groups, but, the after/before ratio with Yoda1 addition in the flufenamic acid-treated group was 35.1% lower ($p < 0.001$) than that in the control group (**Figure 5-8B**).

There was a significant increase ($p < 0.001$) in APD90 after Yoda1 addition in both control and flufenamic acid-treated groups, but no significant

difference between the two groups (**Figure 5-8C**). Consistently, the after/before ratio with Yoda1 addition was significantly higher ($p < 0.001$) only when compared to DMSO in each group (**Figure 5-8D**).

The maximum upstroke velocity of HL-1 cell action potential had a significant decrease ($p < 0.001$) after Yoda1 addition in both control and flufenamic acid-treated groups, but no significant difference was found between the two groups (**Figure 5-8E**). The after/before ratio with Yoda1 addition was significantly lower ($p < 0.001$) compared to DMSO addition in both groups. (**Figure 5-8F**).

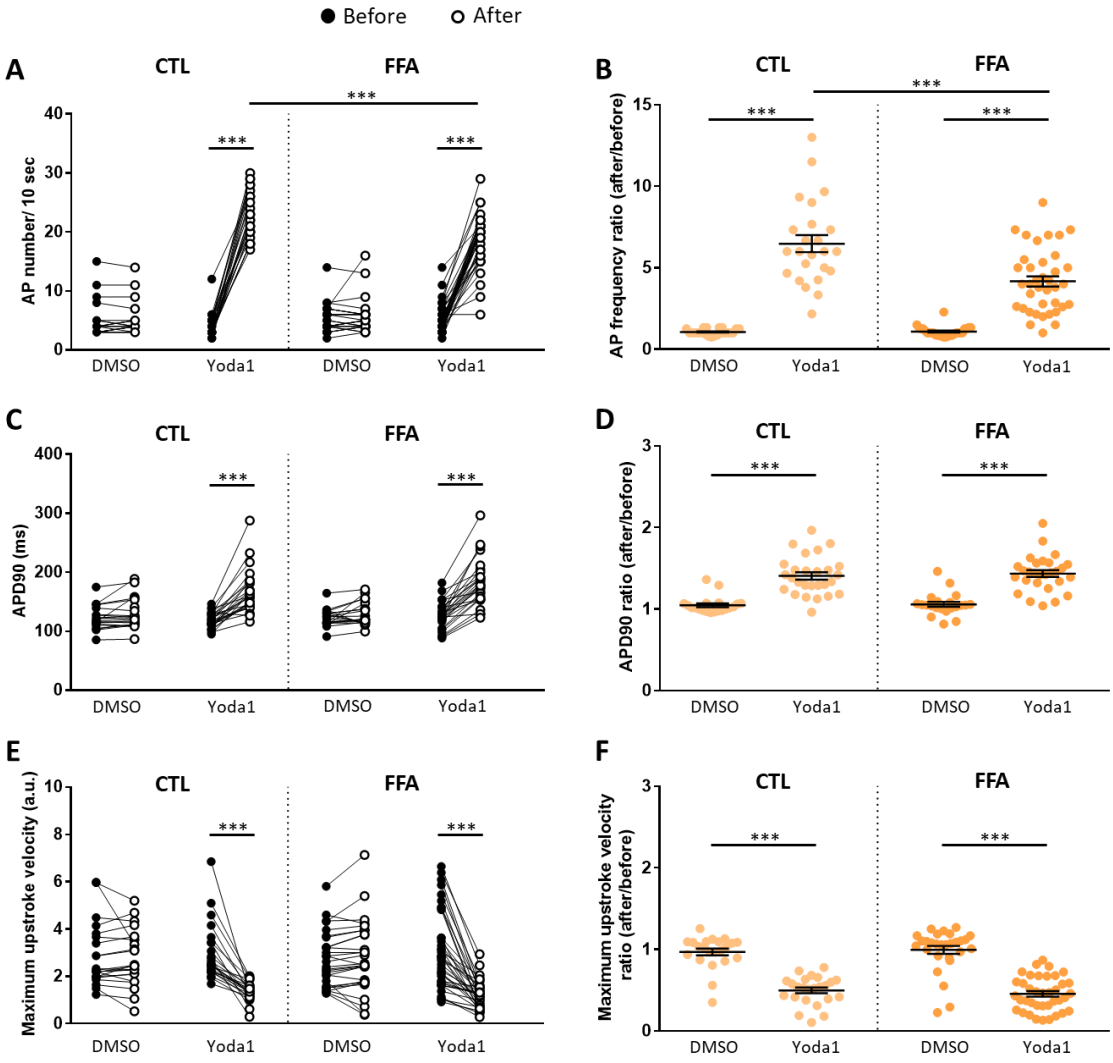

Figure 5-8 Altered Slow ISAP HL-1 cell action potential properties by Yoda1 addition with/without flufenamic acid treatment.

(A) Action potential (AP) frequency, (C) APD90, and (E) action potential maximum upstroke velocity compared between the control group (CTL) and the flufenamic acid-treated group (FFA). Results are presented as before-after drug addition. (B) Action potential ratio, (D) APD90 ratio, and (F) maximum upstroke velocity ratio calculated as the after/before drug addition ratio. Results are presented as scatter plots with means ± SEM. n = 22-28/group with DMSO addition; n = 24-38/group with Yoda1 addition. n represents the number of wells in 96 well plate. ***$p < 0.001$.

5.3.2.3 Pharmacological effects on HL-1 cells with fast initial spontaneous action potentials

The action potential frequency of Fast ISAP cells has also been investigated using pharmacological inhibitor and activators. There was no significant difference in action potential frequency baseline between control and flufenamic acid-treated groups (**Figure 5-9**).

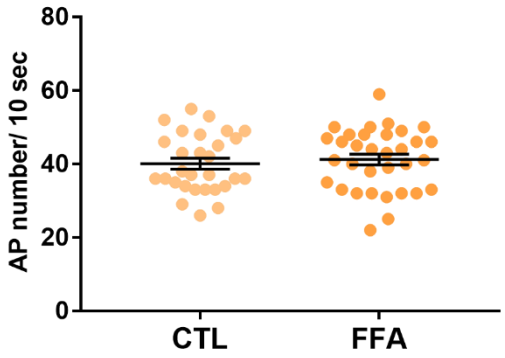

Figure 5-9 Fast ISAP HL-1 cell action potential frequency baseline.

Action potential baseline was compared between the control group (CTL) (n = 29) and the flufenamic acid-treated group (FFA) (n = 33). n represents the number of wells in 96 well plate. Results are presented as scatter plots with means ± SEM. No significant difference between CTL and FFA.

In Fast ISAP cells, DMSO addition showed no significant effect on action potential frequency (**Figure 5-10**). In contrast to Slow ISAP cells, Yoda1 addition (final concentration 2 µM) induced a significant decrease in frequency ($p < 0.001$) in both control and flufenamic acid-treated groups (**Figure 5-10A**). However, the frequency in the flufenamic acid-treated

group was 43.0% higher ($p < 0.05$) than that in the control group after Yoda1 addition (**Figure 5-10A**). Accordingly, the after/before ratio with Yoda1 addition is significantly lower ($p < 0.001$) than that with DMSO addition in both groups (**Figure 5-10B**). Also, with Yoda1 addition, the flufenamic acid-treated group showed a 36.3% lesser decrease ($p < 0.05$) in after/before ratio than that in the control group (**Figure 5-10B**).

As increased K^+ activity may cause slowing in action potential frequency (Tsantoulas & McMahon, 2014), the selective BK channel opener NS 1619 (Olesen et al., 1994) has also been used in this study. As shown in **Figure 5-10A**, the addition of NS 1619 (final concentration 10 μM) induced a significant decrease ($p < 0.01$) in action potential frequency in the control group. Also, the after/before ratio with NS 1619 addition was significantly lower ($p < 0.05$) compared to DMSO addition (**Figure 5-10B**).

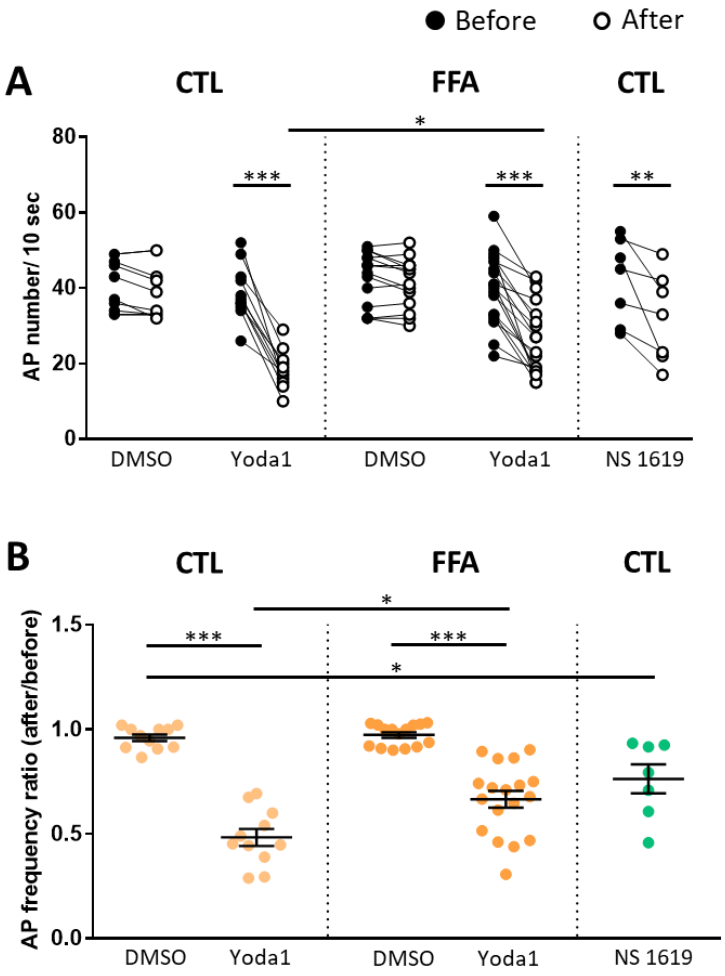

Figure 5-10 Drug addition affecting action potential frequency in HL-1 cells with fast ISAP.

(A) Action potential frequency was compared among the control groups (CTL) and the flufenamic acid-treated group (FFA). Results are presented as before-after drug addition. (B) Action potential ratio was calculated as after/before drug addition. Results are presented as scatter plots with means ± SEM. n = 11-15/group with DMSO addition; n = 7-18/group with Yoda1 addition. n represents the number of wells in 96 well plate. *p < 0.05, **p < 0.01, ***p < 0.001.

5.3.3 Effects of genetic inhibition in HL-1 cells

5.3.3.1 siRNA-mediated *Trpm4* and *Piezo1* gene knockdown

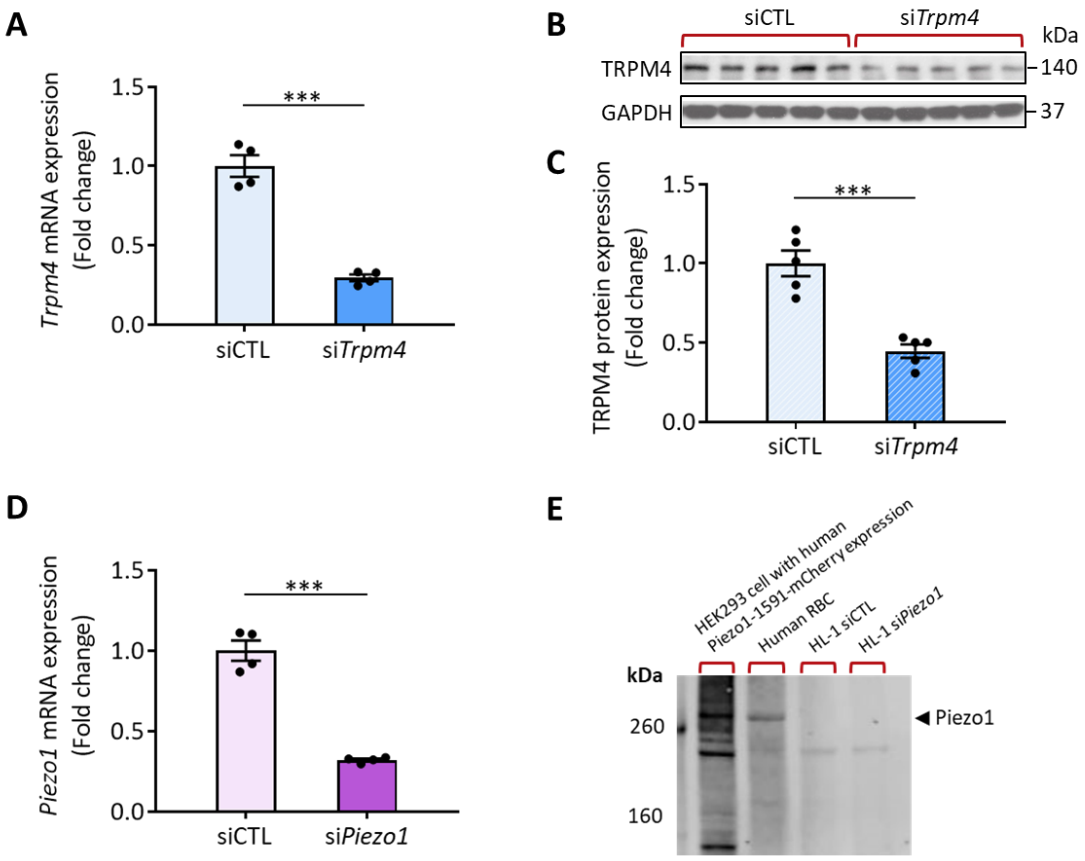

Figure 5-11 TRPM4 and Piezo1 expression in HL-1 cells with siRNA-mediated gene knockdown.

(A) Relative *Trpm4* mRNA expression in HL-1 cells treated with *Trpm4*-targeting siRNA (si*Trpm4*) or its control siRNA (siCTL). The mRNA relative expression was normalized by GAPDH and calculated as fold change relative to control siRNA. (B) Western blots showing TRPM4 protein expression in HL-1 cells with siCTL or si*Trpm4* treatment. (C) TRPM4 protein expression quantitative data was normalized by GAPDH. Fold change was calculated relative to siCTL group. (D) Relative *Piezo1* mRNA expression in HL-1 cells treated with *Piezo1*-targeting siRNA (si*Piezo1*) or its control siRNA (siCTL). Results are presented as scatter plots with means ± SEM, n = 4/group for mRNA expression; n =

5/group for protein expression. n represents the number of separate culture dishes. ***$p < 0.001$. (E) Representative western blot using commercially available Piezo1 antibody (Proteintech, USA), for HEK293 cells with human Piezo1-1591-mCherry expression, human RBCs, and HL-1 cells treated with siCTL or si*Piezo1*.

With *Trpm4*-targeting siRNA-mediated gene knockdown, *Trpm4* mRNA expression level was reduced by 71% ($p < 0.001$) in HL-1 cells, compared to the cells with control siRNA treatment (**Figure 5-11A**). TRPM4 protein expression levels in *Trpm4*-targeting siRNA-treated cells were 55% lower than that in control siRNA-treated cells ($p< 0.001$) (**Figure 5-11B, C**). *Piezo1* mRNA expression levels were reduced by 68% ($p < 0.001$) in *Piezo1*-targeting siRNA-treated cells, compared to control siRNA-treated cells. (**Figure 5-11D**). However, as mentioned in **1.4.3.2**, there are huge difficulties in using commercially available antibodies to detect mouse Piezo1 protein. For example, **Figure 5-11E** shows that Piezo1 protein was detected from both HEK293 cells with human Piezo1-1591-mCherry expression (J. V. Li et al., 2021) and human RBCs by commercially available anti-Piezo1 antibody (Proteintech, USA), but the Piezo1 bands from HL-1 cells were absent.

The action potential frequency, APD90, and maximum upstroke velocity at baseline in HL-1 cells (Slow ISAP) treated with *Trpm4*-targeting siRNA, *Piezo1*-targeting siRNA or the control siRNAs are shown in **Figure 5-12A, B, C**. There was no significant difference in frequency (**Figure 5-12A**) and maximum upstroke velocity (**Figure 5-12C**) among all the groups. However, a higher level of APD90 was found in *Piezo1*-targeting siRNA-treated group

compared to both *Trpm4*-control ($p < 0.01$) and *Piezo1*-control ($p < 0.001$) groups (**Figure 5-12B**).

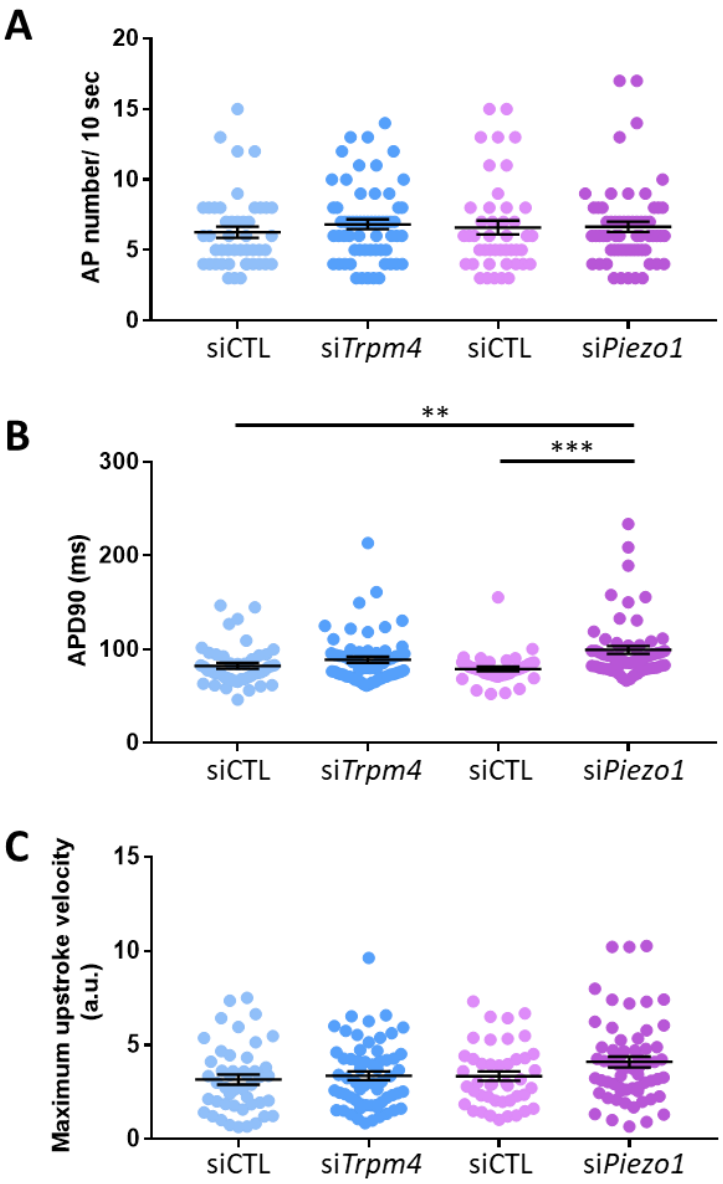

Figure 5-12 HL-1 cell action potential baselines with siRNA treatment.

(A) Action potential (AP) frequency, (B) APD90 and (C) action potential maximum upstroke velocity baselines of HL-1 cells treated with *Trpm4*-targeting siRNA (si*Trpm4*), *Piezo1*-targeting siRNA (si*Piezo1*), or the control siRNA (siCTL) for each gene. Results are

presented as scatter plots with means ± SEM. n = 44-61/group. n represents the number of wells in 96 well plate. **$p < 0.01$, ***$p < 0.001$.

5.3.3.2 *Trpm4*-knockdown affects Yoda1-mediated changes in action potential frequency

When comparing the action potential in Slow ISAP cells from *Trpm4*-targeting siRNA-treated group and control siRNA-treated group, again, DMSO had no significant impact on action potential frequency, APD90 or maximum upstroke velocity (**Figure 5-13**). Yoda1 addition (final concentration 2 µM) induced a significant increase in action potential frequency ($p < 0.001$) in both groups (**Figure 5-13A**). Also, the frequency in *Trpm4*-targeting siRNA-treated group was 16.3% lower ($p < 0.001$) than that in the control group after Yoda1 addition (**Figure 5-13A**). Accordingly, a significantly higher ($p < 0.001$) after/before ratio was found with Yoda1 addition compared to DMSO addition in both groups. With Yoda1 addition, the after/before ratio in *Trpm4*-targeting siRNA-treated group was 24.4% lower ($p < 0.001$) than that in the control group (**Figure 5-13B**).

For APD90, Yoda1 addition caused a significant increase ($p < 0.001$) in both groups. Also, the APD90 in *Trpm4*-targeting siRNA-treated group was found to be higher ($p < 0.05$) than that in the control group after Yoda1 addition (**Figure 5-13C**). The after/before ratio with Yoda1 addition was significantly higher ($p < 0.001$) than that with DMSO in each group, but it showed no significant difference between the two groups (**Figure 5-13D**).

There was a significant decrease ($p < 0.001$) in maximum upstroke velocity after Yoda1 addition in both groups but there was no significant difference

between the two groups (**Figure 5-13E**). Yoda1 after/before ratio was significantly lower than DMSO after/before ratio in both the *Trpm4*-targeting siRNA-treated group ($p < 0.05$) and the control group ($p < 0.01$) (**Figure 5-13F**), but the Yoda1 after/before ratio was not significantly different between the two groups.

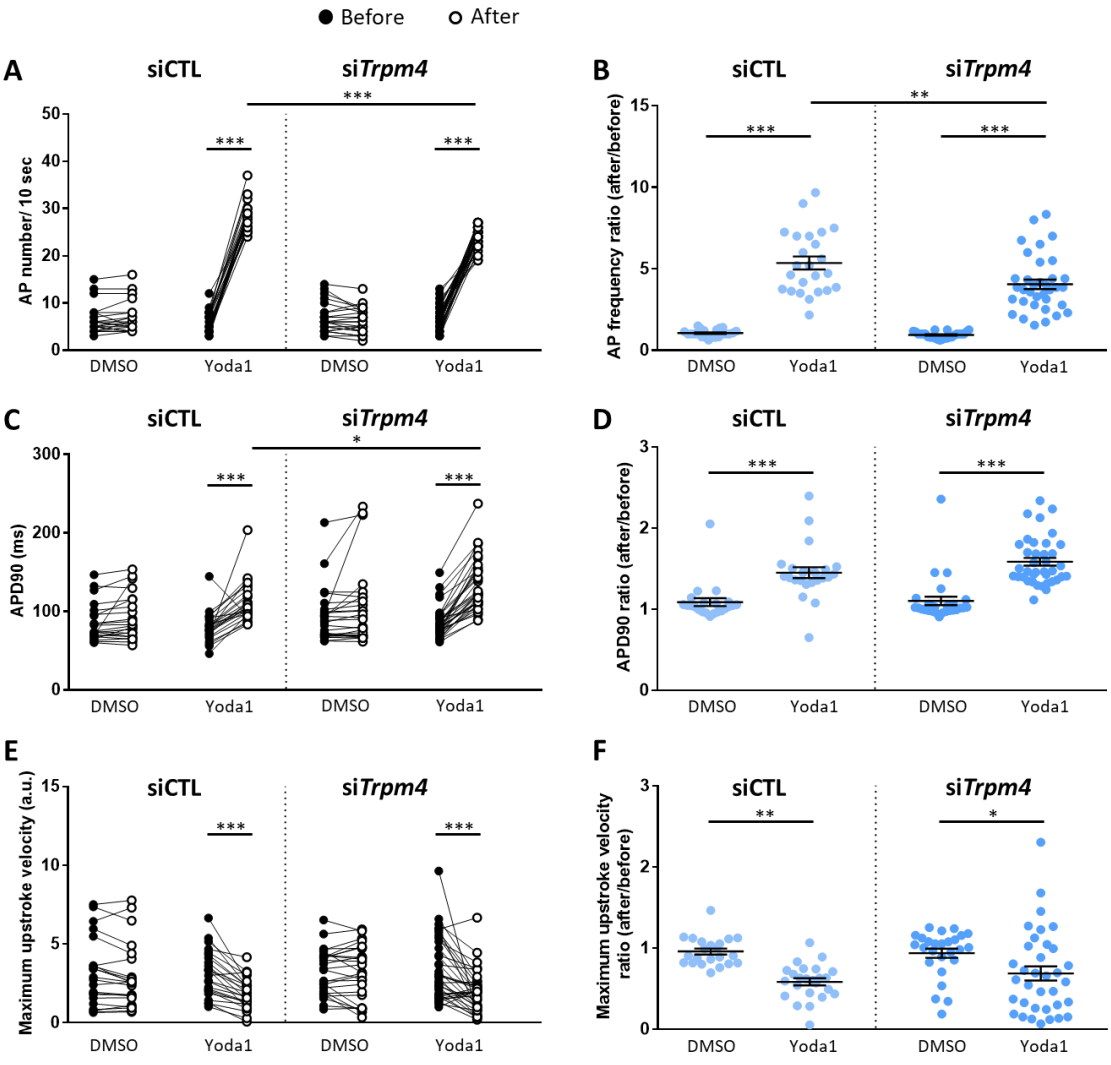

Figure 5-13 Altered HL-1 cell action potential properties by Yoda1 addition involving the TRPM4 channel activation.

(A) Action potential (AP) frequency, (C) APD90, and (E) action potential maximum upstroke velocity compared between control siRNA (siCTL)-treated group and *Trpm4*-

targeting siRNA (si*Trpm4*)-treated group. Results are presented as before-after drug addition. (B) Action potential ratio, (D) APD90 ratio, and (F) maximum upstroke velocity ratio calculated by after/before drug addition. Results are presented as scatter plots with means ± SEM. n = 22-26/group with DMSO addition; n = 24-35/group with Yoda1 addition. n represents the number of wells in 96 well plate. *$p < 0.05$, **$p < 0.01$, ***$p < 0.001$.

5.3.3.3 *Piezo1*-knockdown affects action potential frequency change

In Slow ISAP cells from both the *Piezo1*-targeting siRNA-treated group and the control siRNA-treated group, DMSO addition didn't show any significant effect on any of the three parameters (**Figure 5-14**). The action potential frequency increased significantly with Yoda1 addition (final concentration 2 μM) in both groups ($p < 0.001$) (**Figure 5-14A**). However, the frequency in the *Piezo1*-targeting siRNA-treated group was 21.3% lower ($p < 0.001$) than that in the control group after Yoda1 addition (**Figure 5-14A**). Accordingly, the after/before ratio was significantly higher ($p < 0.001$) with Yoda1 addition compared to DMSO addition in both groups, but the after/before ratio in the *Piezo1*-targeting siRNA-treated group was 32.6% lower ($p < 0.001$) than in the control group (**Figure 5-14B**).

Yoda1 addition significantly increased the APD90 in both groups ($p < 0.001$). In the *Piezo1*-targeting siRNA-treated group, the APD90 was found to be higher ($p < 0.001$) than that in the control group after Yoda1 addition (**Figure 5-14C**). The after/before ratio with Yoda1 addition was significantly higher ($p < 0.001$) than that with DMSO in each group (**Figure 5-14D**). However, there was no significant difference between the two groups.

A significant decrease ($p < 0.001$) in maximum upstroke velocity was found after Yoda1 addition in both groups, but no significant difference was found between the two groups (**Figure 5-14E**). Yoda1 after/before ratio was significantly lower than DMSO after/before ratio, in both the *Piezo1*-targeting siRNA-treated group ($p < 0.05$) and the control group ($p < 0.01$) (**Figure 5-14F**). No significant difference was found between the two groups in the Yoda1 after/before ratio.

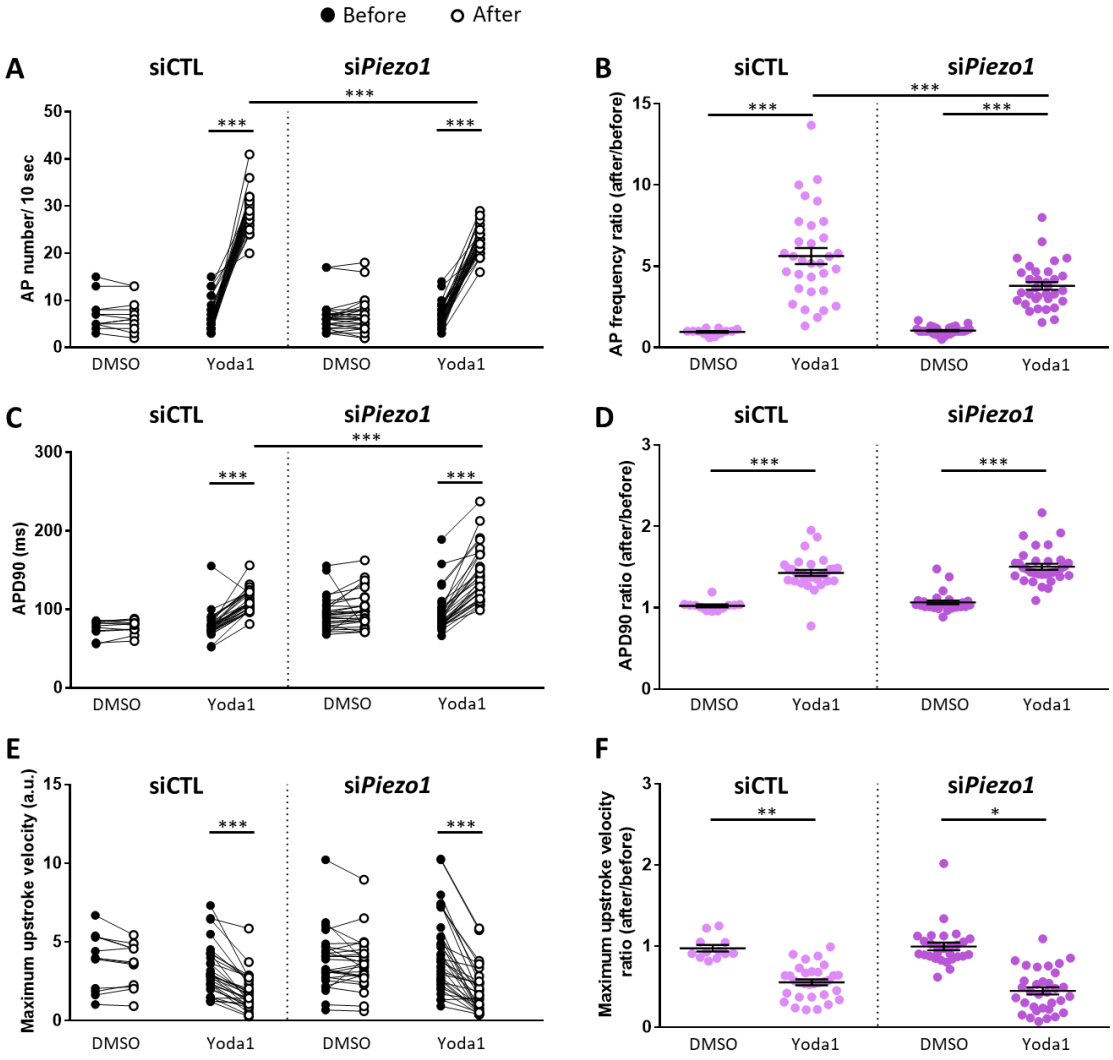

Figure 5-14 Altered HL-1 cell action potential properties by the Piezo1 channel activation.

(A) Action potential (AP) frequency, (C) APD90, and (E) action potential maximum upstroke velocity compared between control siRNA (siCTL)-treated group and *Piezo1*-targeting siRNA (si*Piezo1*)-treated group. Results are presented as before-after drug addition. (B) Action potential ratio, (D) APD90 ratio, and (F) maximum upstroke velocity ratio calculated by after/before drug addition. Results are presented as scatter plots with means ± SEM. n = 12-28/group with DMSO addition; n = 32-33/group with Yoda1 addition. n represents the number of wells in 96 well plate. *$p < 0.05$, **$p < 0.01$, ***$p < 0.001$.

5.3.4 Additional information

With Slow ISAP HL-1 cells, action potential frequency was also checked using Ca^{2+} imaging in a relatively small number of samples (n = 4-6) from the untreated control group (**Figure 5-15**). Similar to the membrane potential data, the frequency increased significantly ($p < 0.001$) in response to Yoda1 addition (final concentration 2 μM) but did not change in the presence of DMSO only (**Figure 5-15A**). The after/before ratio also significantly increased after Yoda1 addition ($p < 0.001$) (**Figure 5-15B**).

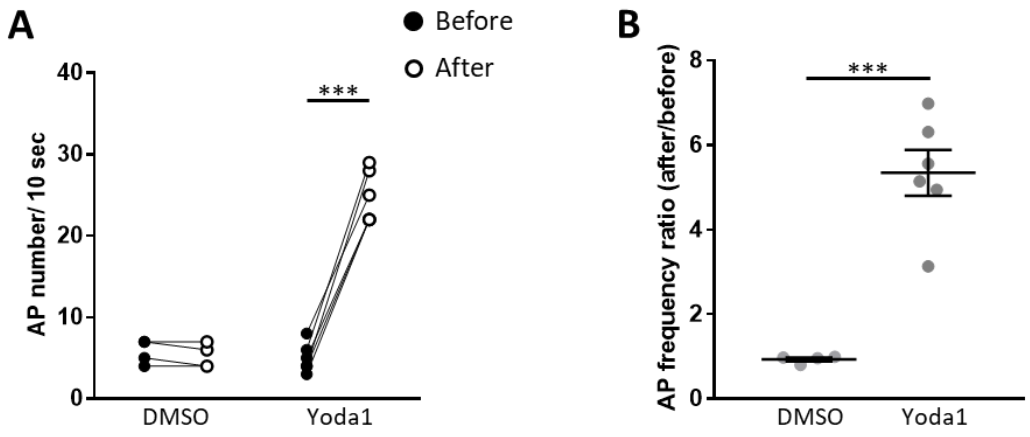

Figure 5-15 Slow ISAP HL-1 cell action potential frequency by Ca^{2+} image.

(A) Action potential (AP) frequency changes are shown as before-after DMSO/Yoda1 addition. (B) Action potential frequency ratio was calculated by after/before drug addition, presented as scatter plots with means ± SEM. n = 4-6/group. n represents the number of wells in 96 well plate. ***$p < 0.001$.

5.4 Discussion

The TRPM4 and Piezo1 channels have been heavily investigated to understand their contribution to the cardiovascular system. In pressure overload-induced LVH, although Piezo1 activation (Yu, Gong, Kesteven, et al., 2021; Zhang et al., 2021) likely further affects TRPM4 during the initial step of the signalling transmission involving Ca^{2+}-dependent mechanisms, there is a lack of direct evidence showing this Piezo1-TRPM4 interaction. In this study, an HL-1 mouse atrial myocyte-like cell line was used to investigate the interaction between Piezo1 and TRPM4 ion channels by analysing the membrane potential changes in these cells.

5.4.1 HL-1 cell characterisation

Considering the phenotypic conservation with other cardiac muscle cells and the ability of exhibiting spontaneous action potentials and contractions (Claycomb et al., 1998; Hu et al., 2021; C. Liu et al., 2020; Sartiani et al., 2002; Son et al., 2016; White et al., 2004), as well as the relatively higher expression level of both TRPM4 and Piezo1 compared to mouse ventricular cardiomyocytes, the HL-1 cell line is a highly suitable model for *in vitro* experiments following **Chapter 4**.

A large diversity in the spontaneous contraction frequency of HL-1 cells was shown in previous studies (Claycomb, 2001; C. Liu et al., 2020; Sartiani et al., 2002; Uehara et al., 2017; Wells et al., 2019; Z. Yang & Murray, 2011). The HL-1 cells used in this study were initially classified by their ISAP frequency (No, Slow or Fast). Different cell culture protocols have been developed to control the ISAP frequency in cells. The Slow ISAP group was the main focus of this study because the frequency range is similar to the report from Claycomb (2001), as well as to avoid excessive complexity. This variation in ISAP might be related to the expression level of connexons forming gap junctions between the cytoplasm of two adjacent cells, which play an essential role in the propagation of electrical activity throughout the heart by mediating cell-cell communication (Dias et al., 2014; Kaese & Verheule, 2012; Lambiase & Tinker, 2015; Severs et al., 2001). The confirmation of the connexon expression in different cell groups is planned in follow-up studies in the future.

Different studies have also shown that approximately 30% of the HL-1 cells exhibit I_f as an underlying current of the action potential (Sartiani et al., 2002; Z. Yang & Murray, 2011). The presence of I_f and the fact that the L-

type Ca^{2+} channels are driving HL-1 cell action potential suggest similarities in the molecular origins of the action potential between HL-1 cells and pacemaker cells from the SA node or atria (Belardinelli, Giles, & West, 1988; Denyer & Brown, 1990; Zhou & Lipsius, 1992). Because this study focused on synchronous action potential and analysed the mean value of multiple cells, the I_f was not investigated specifically. In addition, the conduction velocity of HL-1 cells was investigated to further improve the data acquisition and analysis accuracy in genetic inhibition experimental groups. The HL-1 cell conduction velocity in Slow ISAP groups was within a range from 10.07 to 28.06 μm/ms, which is relatively closer to the conduction velocity in primary pacemaker area of mouse SA node (50 to 65 μm/ms) (Verheijck, 2001), in comparison to mouse atrial or ventricular conduction velocity (300 to 600 μm/ms) (Alcoléa et al., 2004; Kaese & Verheule, 2012; Thomas et al., 1998; van Veen et al., 2005).

5.4.2 Piezo1 effect on HL-1 cell action potential

Following **Chapter 4**, Yoda1 (Syeda et al., 2015) has been used to chemically activate Piezo1 channels. The Yoda1 effect on HL-1 cells was shown at an even lower Yoda1 concentration compared to the studies in **Chapter 4**. Yoda1 addition (final concentration 2 μM) initiated trains of action potentials in No ISAP groups, except for some 9-phenanthrol treated cells. Also, in Slow ISAP groups, Yoda1 addition induced a significant increase in the action potential frequency and APD90 and a decrease in maximum upstroke velocity. This increase in frequency was also confirmed with Ca^{2+} imaging. In contrast, in Fast ISAP groups, Yoda1 addition decreases the action potential frequency.

As Yoda1 is a specific Piezo1 agonist (Syeda et al., 2015) , the effect induced by Yoda1 addition is a result of Piezo1 activation, especially when DMSO addition showed no effect. In addition, with Slow ISAP cells, the 32.6% less increase in action potential frequency by siRNA-mediated *Piezo1* gene knockdown compared to the control also supports a Piezo1-specific effect.

The *Piezo1*-knockdown group showed a prolongation of APD90 baseline compared to the control groups. One possible mechanism is that the deficiency of Piezo1 caused less Ca^{2+} entry into the cells, which may affect Ca^{2+} activated K^+ channels, such as the BK, intermediate Ca^{2+} activated K^+ (IK), or small conductance Ca^{2+} activated K^+ (SK) channels. The reduced activity of the BK, IK or SK channels might then explain the prolongation of APD90 due to the reduced repolarising current (Imlach et al., 2010; Jakob et al., 2021; Jeevaratnam, Chadda, Huang, & Camm, 2018; Surawicz, 1992; Takahashi & Naruse, 2012; Weisbrod, 2020; Z. Yang & Murray, 2011).

The APD90 prolongation in the *Piezo1*-knockdown group after Yoda1 addition was likely due to its higher baseline, as there was no significant difference between the control and the *Piezo1*-knockdown groups in the after/before ratio.

5.4.3 TRPM4 effect on action potential in Piezo1 activation

For pharmacological inhibition, flufenamic acid (20 μM) was used to inhibit TRPM4 channels (Constantine et al., 2016; Guinamard, Simard, & Del Negro, 2013; Simard et al., 2013). Flufenamic acid reduced the increase in frequency after Yoda1 addition by more than 30% in No and Slow ISAP groups, and reduced the decrease in frequency after Yoda1 addition by 36.3%

in Fast ISAP group. Although flufenamic acid may also block other channels, including Ca^{2+}-activated Cl^- channels (Guinamard et al., 2013; Gwanyanya et al., 2010), the flufenamic acid effect in this study likely reflects the TRPM4 effect on action potential because TRPM4 is more sensitive than other channels to flufenamic acid, at the concentration used in this study (Guinamard et al., 2013; Simard et al., 2013).

The TRPM4 effect on Slow ISAP cells was further confirmed by applying genetic inhibition of TRPM4. siRNA-mediated *Trpm4* knockdown led to a 24.4% lesser increase in frequency after Yoda1 addition. This result is strong evidence of the TRPM4 effect with Piezo1 activation in HL-1 cells, consistent with the pharmacological inhibition but much clearer because of the specificity of the siRNA-mediated *Trpm4* gene knockdown.

Similar to the mechanisms discussed in **Chapter 3**, stimulated by the local Ca^{2+} influx through Yoda1-evoked Piezo1 activation, TRPM4 could depolarise the plasma membrane to further stimulate other Ca^{2+}-permeable channels such as the L-type and T-type Ca^{2+} channels (Abriel et al., 2012; Hof et al., 2019; Pierre Launay et al., 2002), or induce reverse activity of the Na^+/ Ca^{2+} exchanger through local Na^+ loading (Conway, 2001; C. Wang et al., 2018), leading to a further increase of local Ca^{2+}. In No and Slow ISAP groups, generation of action potential or increase in frequency associated with this intracellular Ca^{2+} increase might also be due to activities of mitochondrial Na^+/ Ca^{2+} exchanger NCLX and/or SR Ca^{2+} release (Takeuchi, Kim, & Matsuoka, 2013; Z. Yang & Murray, 2011). The increase in APD90 and decrease in maximum upstroke velocity after Yoda1 addition might be related to the effects of intracellular Ca^{2+} concentration on NCX (Eisner, Dibb, & Trafford, 2009). Increase of Ca^{2+} efflux and Na^+ influx by the

electrogenic NCX can result in an increased net inward current from NCX activity which could cause prolongation of action potential duration and lower upstroke velocity (Barcenas-Ruiz et al., 1987; Eisner et al., 2009).

The situation is more complicated in Fast ISAP groups with higher basal Ca^{2+} concentrations. The increased intracellular Ca^{2+} from Piezo1 activation has to reach a certain level to activate other ion channels such as BK (Jakob et al., 2021; Takahashi & Naruse, 2012) and/or cause local Ca^{2+} overload. Studies have identified BK channels as contributing factors to the regulation of the heart rate (Imlach et al., 2010; Peyronnet et al., 2016; Takahashi & Naruse, 2012). In this study, the selective BK channel opener NS 1619 (Olesen et al., 1994) induced a decrease in action potential frequency in the Fast ISAP group, which is a similar trend to the cells with Yoda1-evoked Piezo1 activation. This decrease in frequency is likely an effect of BK activation, as increased K^+ channel activity may cause slowing in action potential frequency (Tsantoulas & McMahon, 2014).

TRPM4 has been shown to be related to the waveform and frequency of the cardiac action potential. Hof et al. (2013) reported that inhibition of TRPM4 by 9-phenanthrol causes decrease in action potential frequency in mouse RA, rat RA, and rabbit SA node. Simard et al. (2013) showed shortening in atrial action potential duration in a TRPM4 global knockout mouse or by flufenamic acid treatment. Also, 9-phenanthrol can cause shortening in action potential duration in AngII-treated HL-1 cells (Hu et al., 2017). In this current study, either flufenamic acid or siRNA-mediated *Trpm4* knockdown did not affect the baseline values in action potential frequency, APD90, and maximum upstroke velocity. The TRPM4 effect on action potential frequency was only shown when Piezo1 was activated by

Yoda1 addition. Although there was no significant difference in baselines, the subtle gap in baseline likely causes APD90 difference between the *Trpm4*-knockdown group and the control group as no significant difference was found in the after/before ratio. Agreeably, the results in this study show that 9-phenanthrol blocks Yoda1-evoked Piezo1 action potential, within a similar concentration range compared to other studies. Further effect of 9-phenanthrol on Piezo1 and other ion channels will be investigated in future studies, but existing studies using 9-phenanthrol might need to be revisited.

One limitation of this study is the lack of an experiment in which TRPM4 is activated independent of Piezo1 activation. This is because there was no pharmacological TRPM4 activator available. To investigate TRPM4 activation not induced by Piezo1, patch clamp experiments are being considered for follow-up studies. Also, in this study, *Trpm4*- or *Piezo1*-targeting siRNA did not achieve complete gene knockdown in HL-1 cells. The TRPM4 protein in siRNA-treated cells was at a similar level to the study by Hu et al. (2017) using the same siRNA product (Invitrogen, USA, MSS229248). Nevertheless, in this study, the effect of *Trpm4* or *Piezo1* deficiency was clearly shown in action potential frequency change after Yoda1 addition.

In conclusion, this study provides *in vitro* evidence of a Piezo1-TRPM4 interaction, confirmed by both pharmacological and genetic inhibition of the TRPM4 channel activity. When Piezo1 is activated by Yoda1, TRPM4 is stimulated by the increase of Ca^{2+} and membrane depolarisation. In HL-1 cells, this results in altered action potential frequency. In addition, this study suggests that a commonly used TRPM4 inhibitor, 9-phenanthrol, may

have off-target effects on Piezo1, which needs to be further verified. Also, additional studies, especially electrophysiological studies, will be required in the future to unravel the mechanisms of the action potential change caused by the Piezo1-TRPM4 interaction.

Chapter 6 Conclusion and future directions

6.1 Conclusion

Among the various types of cardiovascular disease, LVH, a form of cardiac remodelling involving left ventricular size, shape, and function, has been considered a major risk factor for cardiovascular death. In particular, LVH induced by pressure overload is the most powerful independent predictor of clinical cardiac mortality. Current treatment methods focus on removing the pressure overload stimulus for LVH. However, this does not completely reverse adverse cardiac remodelling. Importantly, the molecular signalling pathways involved in pressure overload-induced LVH are potential targets for therapeutic intervention. Although numerous molecular signalling steps in the induction of LVH have been identified to date, the initial step when mechanical stretch associated with cardiac pressure overload is converted into a chemical signal that initiates hypertrophic signalling remains unresolved. Several types of ion channels, including MS channels, have been considered as potential contributors to LVH signalling pathways, as the primary molecular transducers of mechanical stimuli that function in the cardiovascular system. Focusing on two types of ion channels, TRPM4 and Piezo1, this project investigated their role in cardiac mechanotransduction underlying pressure overload-induced LVH from several different aspects.

In **Chapter 3**, the role of the TRPM4 channel in the molecular signalling pathway involved in pressure overload-induced LVH was investigated by employing a mouse LVH model based on the TAC procedure. This study was conducted using both WT and *Trpm4* cKO mice in a collaboration with Professor Rudi Vennekens and his group at the Laboratory of Ion Channel Research, Center for Brain and Disease Research, Katholieke Universiteit

Leuven, Belgium. This study showed that the TRPM4 channel is a positive regulator of pressure overload-induced LVH, contributing to the activation of CaMKII-HDAC4-MEF2 hypertrophic signalling pathway. Selective deletion of TRPM4 channels in mouse cardiomyocytes resulting in an approximately 50% reduction in pressure overload-induced LVH, indicating that TRPM4 is playing a pro-hypertrophic role. In addition, from the study in this chapter, the mechanosensory Piezo1 channel was hypothesised to be the upstream channel whose activation was responsible for TRPM4 activation in pressure overload-induced LVH.

Some very recent studies (Jiang et al., 2021; Yu, Gong, Kesteven, et al., 2021; Zhang et al., 2021) indicated that Piezo1 is the cardiac mechanosensor contributing to the initial step of the pressure overload-induced LVH signalling, where the mechanical stimuli are transduced into Ca^{2+} signals. In **Chapter 4**, the studies provided methodological foundations of new *in vitro* approaches to further unravel the molecular force-sensing mechanisms of Piezo1 in cardiac mechanotransduction, as well as the role of Piezo1 underlying pressure overload-induced LVH. Using the *IsoStretcher* system in a collaboration with Professor Oliver Friedrich and his team at the Institute of Medical Biotechnology, Friedrich-Alexander-University Erlangen-Nürnberg, Germany, isotropic cell stretching was applied first to HL-1 mouse atrial myocyte-like cells, then to isolated mouse LV cardiomyocytes. The studies showed that Piezo1 channels in HL-1 cells and mouse LV cardiomyocytes could be activated by isotropic stretch stimulation. Experimental protocols including cell culture, seeding, stretching and Ca^{2+} imaging were established, showing examples of data acquisition, calibration, and analysis. Furthermore, experimental methods

using KIC-based Ca^{2+} measurements were also developed for studying the functional presence of Piezo1 in mouse ventricular cardiomyocytes in pressure overload-induced LVH, including the plans for using cardiac-specific Piezo1 knockout mice and tdTomato mice.

Based on the study in **Chapter 3** and some published studies (Jiang et al., 2021; Yu, Gong, Kesteven, et al., 2021; Zhang et al., 2021), TRPM4 and Piezo1 likely contribute together to the initial step of the pressure overload-induced LVH signalling pathway. In this process, Piezo1 functions as the primary mechanosensor transducing mechanical forces such as membrane stretch, which results in the initial entry of Ca^{2+} into the ventricular cardiomyocytes. Stimulated by the local Ca^{2+} influx, TRPM4 could depolarise the cardiomyocyte cell membrane, which could activate voltage-gated Ca^{2+} channels allowing further entry of extracellular Ca^{2+} to contribute to downstream hypertrophic signalling. However, there was a lack of evidence showing the direct functional Piezo1-TRPM4 interaction. In **Chapter 5**, studies using HL-1 cells with a fluorescent voltage sensitive dye showed that when Piezo1 is chemically activated by Yoda1, TRPM4 is stimulated by the increase of Ca^{2+}, resulting in altered action potential frequency. These studies provided *in vitro* evidence showing that Piezo1 activation can activate TRPM4, which was confirmed by both pharmacological and genetic inhibition of the TRPM4 channel activity.

In summary, the findings in this project on the TRPM4 and Piezo1 ion channels contribute to better understanding of the mechano-electrochemical transduction which initiates the molecular signalling pathway in pressure overload-induced LVH. This body of work provides a foundation for further basic research on ion channels involved in cardiac

hypertrophy. Also, it promises to provide a basis for development of potential novel therapeutic targets for prevention of pathological LVH from the clinical point of view.

6.2 Future directions

For further investigation of the TRPM4 and Piezo1 ion channels in cardiac hypertrophy, several future studies have been considered.

First, future cell stretching experiments using HL-1 cells involve examination of the TRPM4 and Piezo1 channel function with siRNA-mediated gene knockdown, as well as cell classification by the types of activation, initial cell status, and cell responses. Experiments using interconnected HL-1 cells with synchronised beating and isolated mouse ventricular cardiomyocytes, as well as cyclic cell stretching are also planned to be carried out in the future.

Second, based on the experimental methods in **Chapter 4**, the function of Piezo1 in isolated mouse cardiomyocytes in pressure overload-induced LVH will be investigated, including the use of cardiac-specific Piezo1 knockout mice and tdTomato mice.

Third, for investigation of Piezo1 and TRPM4 interaction, patch clamp technology will be used to examine TRPM4 activation without activating Piezo1. Also, the co-localisation of Piezo1 and TRPM4 needs to be investigated in cell lines and animal cells or tissues. In addition, the connexon expression in cell groups with different cell culture protocols needs to be confirmed.

Furthermore, future studies of the role of TRPM4 and Piezo1 in heart failure developed after pressure overload-induced LVH are planned.

Appendix

This appendix contains additional information on experimental data and analysis methods, as well as data supporting and explaining the results in the main text.

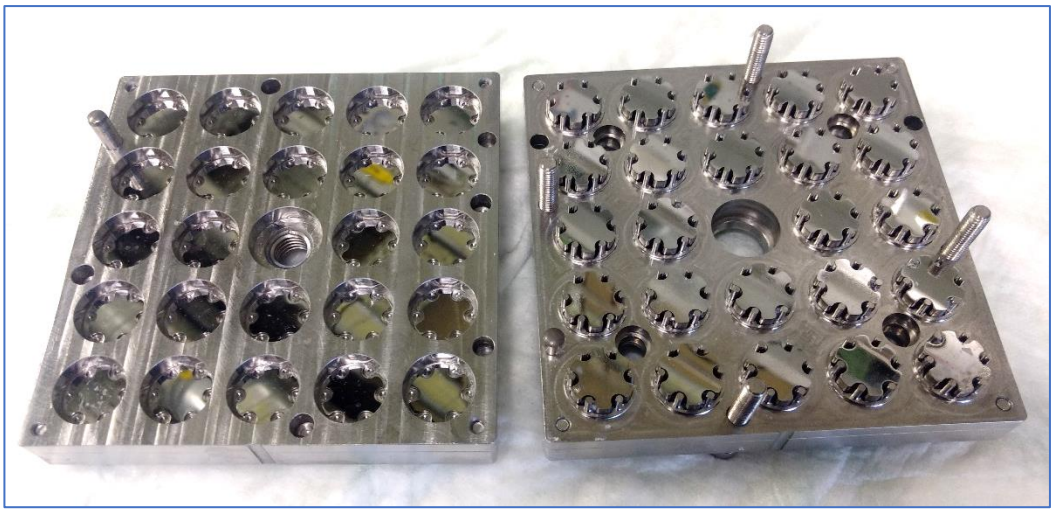

Appendix-figure 1 Aluminium casting mould for PDMS stretch chambers.

Engineered and made in the Institute of Medical Biotechnology, Friedrich-Alexander-University Erlangen-Nürnberg, Germany.

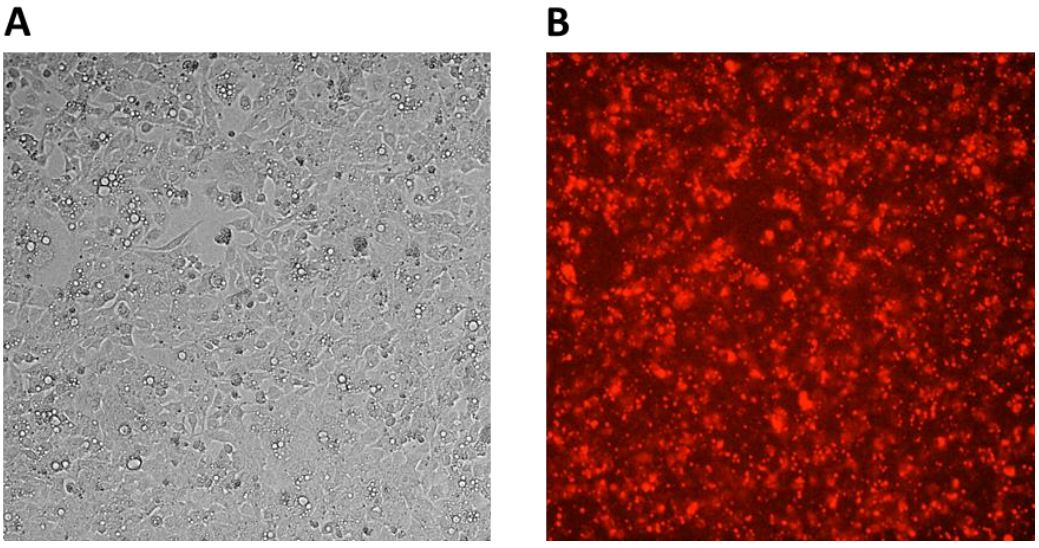

Appendix-figure 2 HL-1 cells transfected with the BLOCK-iT Alexa Fluor Red Fluorescent Control.

(A) Bright field and (B) Fluorescent images of HL-1 cells transfected with the BLOCK-iT Alexa Fluor Red Fluorescent Control (Invitrogen, USA) at a concentration of 10 nM for 24 hours.

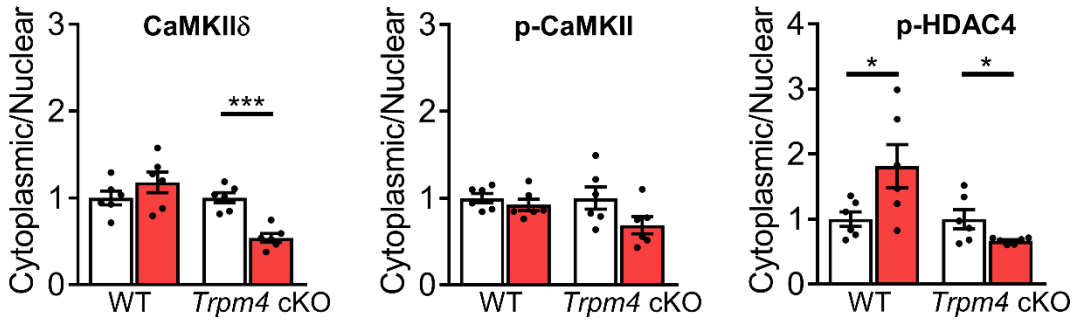

Appendix-figure 3 Cytoplasmic/nuclear ratio of the key proteins in CaMKII-HDAC4-MEF2 signalling pathway.

Cytoplasmic/nuclear ratios are shown as fold changes relative to sham groups, in each genotype. Results are presented as means ± SEM, n = 6/group, *$p < 0.05$, ***$p < 0.001$.

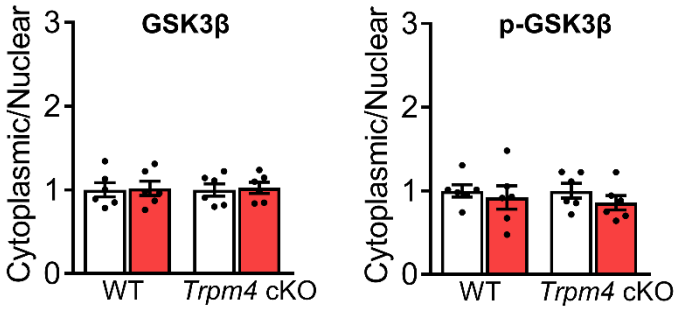

Appendix-figure 4 Cytoplasmic/nuclear ratio of the key proteins in Calcineurin-NFAT signalling pathway.

Cytoplasmic/nuclear ratios are shown as fold changes relative to sham groups, in each genotype. Results are presented as means ± SEM, n = 6/group. No significant difference was found among the groups in both proteins.

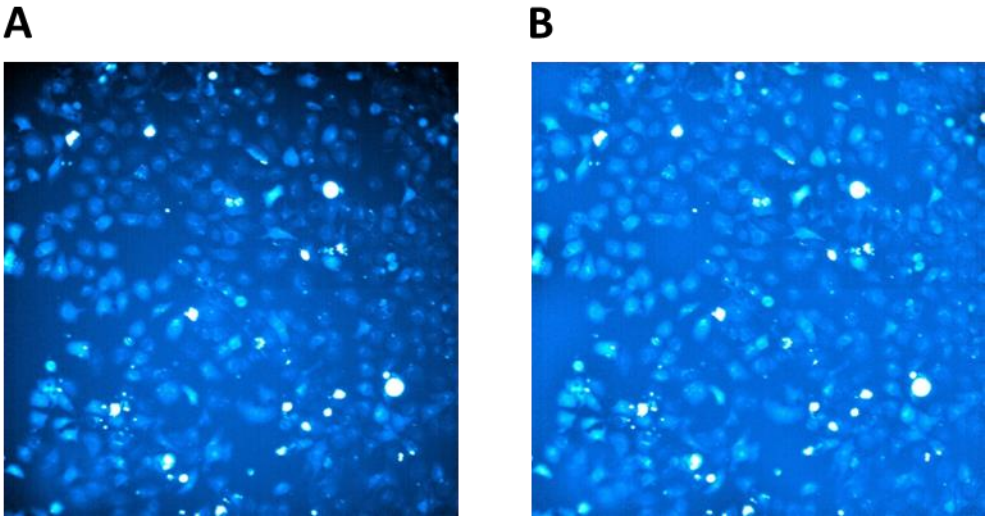

Appendix-figure 5 Example of intensity calibration and shading correction.

(A) Measured image (I_{meas}) and the (B) true image (I_{ture}) after intensity calibration and shading correction. Image credit: Ulrike Schöler, the Institute of Medical Biotechnology, Friedrich-Alexander-University Erlangen-Nürnberg, Germany.

Appendix-table 1 Hemodynamic and anatomical parameters after 2 days and 14 days of sham/TAC in WT and Trpm4 cKO mice.

Hemodynamic measurements include heart rate (HR), aortic systolic and diastolic pressure, LV systolic pressure, dP/dt_{max} and dP/dt_{min}; anatomical measurements include body weight (BW), heart weight (HW), LV weight (LVW), lung weight (LW), tibial length (TL), heart weight normalized by body weight (HW/BW), LV weight normalized by body weight and tibial length (LVW/BW; LVW/TL), lung weight normalized by body weight (LW/BW). Data are presented as means ± SEM. Comparison between sham and TAC in

WT or *Trpm4* cKO groups: $^{**}p < 0.01$, $^{***}p < 0.001$; Comparison between WT and *Trpm4* cKO TAC groups: $^{\#}p < 0.05$, $^{\#\#\#}p < 0.001$.

	2 days				14 days			
	WT		*Trpm4* cKO		WT		*Trpm4* cKO	
	Sham	TAC	Sham	TAC	Sham	TAC	Sham	TAC
Hemodynamic parameter								
n					6	6	6	7
HR (bpm)					503.00 ± 2.78	505.83 ± 4.27	491.17 ± 6.00	496.00 ± 10.67
Aortic systolic pressure (mmHg)					103.83 ± 2.27	161.00 ± 2.57 ***	100.83 ± 3.61	163.43 ± 2.23 ***
Aortic diastolic pressure (mmHg)					73.33 ± 6.31	78.67 ± 2.72	72.50 ± 1.18	77.14 ± 2.72
LV systolic pressure (mmHg)					103.67 ± 3.68	162.50 ± 2.86 ***	106.67 ± 2.86	164.43 ± 3.04 ***
dP/dt_{max} (mmHg/s)					9403.00 ± 466.66	9559.67 ± 703.60	9470.67 ± 424.55	9199.14 ± 372.03
dP/dt_{min} (mmHg/s)					-9492.83 ± 186.90	-9642.83 ± 681.67	-9706.33 ± 551.89	-9924.57 ± 506.24
Anatomical parameter								
n	7	7	8	6	7	7	7	9
BW (g)	26.29 ± 0.54	26.03 ± 0.80	23.75 ± 0.33	25.85 ± 0.51	26.26 ± 0.67	26.60 ± 0.46	26.96 ± 0.98	27.14 ± 0.69
HW (mg)	126.57 ± 1.82	128.00 ± 4.68	116.25 ± 1.77	124.50 ± 1.23	122.71 ± 3.46	163.29 ± 3.79 ***	127.71 ± 4.15	151.22 ± 4.52 **
LVW (mg)	88.29 ± 1.89	92.57 ± 4.78	80.25 ± 1.26	91.00 ± 1.13	88.43 ± 2.87	126.71 ± 2.96 ***	93.00 ± 3.57	114.33 # ± 2.92 ***
LW (mg)	137.44 ± 0.98	136.63 ± 2.19	130.01 ± 2.06	135.07 ± 1.69	138.66 ± 2.26	147.66 ± 3.65	137.94 ± 2.75	144.38 ± 2.30
TL (mm)	17.47 ± 0.10	17.49 ± 0.20	16.63 ± 0.06	17.58 ± 0.15	17.37 ± 0.09	17.29 ± 0.09	17.64 ± 0.16	17.66 ± 0.09
HW/BW (mg/g)	4.82 ± 0.04	4.91 ± 0.04	4.90 ± 0.05	4.83 ± 0.10	4.67 ± 0.04	6.14 ± 0.09 ***	4.74 ± 0.03	5.57 ### ± 0.09 ***
LVW/BW (mg/g)	3.40 ± 0.03	3.55 ± 0.10	3.38 ± 0.05	3.53 ± 0.08	3.36 ± 0.03	4.77 ± 0.10 ***	3.45 ± 0.05	4.22 ### ± 0.09 ***
LVW/TL (mg/mm)	5.05 ± 0.09	5.28 ± 0.22	4.82 ± 0.10	5.18 ± 0.07	5.09 ± 0.15	7.33 ± 0.18 ***	5.27 ± 0.17	6.47 ### ± 0.15 ***
LW/BW (mg/g)	5.24 ± 0.08	5.27 ± 0.09	5.48 ± 0.07	5.24 ± 0.13	5.29 ± 0.09	5.55 ± 0.12	5.15 ± 0.17	5.33 ± 0.09

References

Abernethy, D. R., & Schwartz, J. B. (1999). Calcium-antagonist drugs. *N Engl J Med, 341*(19), 1447-1457. doi:10.1056/NEJM199911043411907

Abràmoff, M. D., Magalhães, P. J., & Ram, S. J. (2004). Image processing with ImageJ. *Biophotonics international, 11*(7), 36-42.

Abriel, H., Syam, N., Sottas, V., Amarouch, M. Y., & Rougier, J. S. (2012). TRPM4 channels in the cardiovascular system: physiology, pathophysiology, and pharmacology. *Biochem Pharmacol, 84*(7), 873-881. doi:10.1016/j.bcp.2012.06.021

Adams, J. W., Sakata, Y., Davis, M. G., Sah, V. P., Wang, Y., Liggett, S. B., . . . Dorn, G. W., 2nd. (1998). Enhanced Galphaq signaling: a common pathway mediates cardiac hypertrophy and apoptotic heart failure. *Proc Natl Acad Sci U S A, 95*(17), 10140-10145.

Albarran-Juarez, J., Iring, A., Wang, S., Joseph, S., Grimm, M., Strilic, B., . . . Offermanns, S. (2018). Piezo1 and Gq/G11 promote endothelial inflammation depending on flow pattern and integrin activation. *J Exp Med, 215*(10), 2655-2672. doi:10.1084/jem.20180483

Albuisson, J., Murthy, S. E., Bandell, M., Coste, B., Louis-Dit-Picard, H., Mathur, J., . . . Patapoutian, A. (2013). Dehydrated hereditary stomatocytosis linked to gain-of-function mutations in mechanically activated PIEZO1 ion channels. *Nat Commun, 4*, 1884. doi:10.1038/ncomms2899

Alcoléa, S., Jarry-Guichard, T., de Bakker, J., Gonzàlez, D., Lamers, W., Coppen, S., . . . van Rijen, H. (2004). Replacement of connexin40 by connexin45 in the mouse: impact on cardiac electrical conduction. *Circulation research, 94*(1), 100-109.

Amin, A. S., Tan, H. L., & Wilde, A. A. (2010). Cardiac ion channels in health and disease. *Heart Rhythm, 7*(1), 117-126. doi:10.1016/j.hrthm.2009.08.005

Anderson, R. H., Yanni, J., Boyett, M. R., Chandler, N. J., & Dobrzynski, H. (2009). The anatomy of the cardiac conduction system. *Clin Anat, 22*(1), 99-113. doi:10.1002/ca.20700

Andres-Delgado, L., & Mercader, N. (2016). Interplay between cardiac function and heart development. *Biochim Biophys Acta, 1863*(7 Pt B), 1707-1716. doi:10.1016/j.bbamcr.2016.03.004

Arganda-Carreras, I., Sorzano, C. O., Marabini, R., Carazo, J. M., Ortiz-de-Solorzano, C., & Kybic, J. (2006). *Consistent and elastic registration of histological sections using vector-spline regularization.* Paper presented at the International Workshop on Computer Vision Approaches to Medical Image Analysis.

Armoundas, A. A., Hobai, I. A., Tomaselli, G. F., Winslow, R. L., & O'Rourke, B. (2003). Role of sodium-calcium exchanger in modulating the action potential of ventricular myocytes from normal and failing hearts. *Circ Res, 93*(1), 46-53. doi:10.1161/01.RES.0000080932.98903.D8

Australian Institute of Health and Welfare. (2020). Cardiovascular disease. (Cat. no. CVD 83.). Retrieved from https://www.aihw.gov.au/reports/heart-stroke-vascular-diseases/cardiovascular-health-compendium

Autzen, H. E., Myasnikov, A. G., Campbell, M. G., Asarnow, D., Julius, D., & Cheng, Y. (2018). Structure of the human TRPM4 ion channel in a lipid nanodisc. *Science, 359*(6372), 228-232. doi:10.1126/science.aar4510

Backs, J., Backs, T., Neef, S., Kreusser, M. M., Lehmann, L. H., Patrick, D. M., . . . Olson, E. N. (2009). The delta isoform of CaM kinase II is required for pathological cardiac hypertrophy and remodeling after pressure overload. *Proc Natl Acad Sci U S A, 106*(7), 2342-2347. doi:10.1073/pnas.0813013106

Backs, J., Song, K., Bezprozvannaya, S., Chang, S., & Olson, E. N. (2006). CaM kinase II selectively signals to histone deacetylase 4 during cardiomyocyte hypertrophy. *J Clin Invest, 116*(7), 1853-1864. doi:10.1172/JCI27438

Bae, C., Sachs, F., & Gottlieb, P. A. (2011). The Mechanosensitive Ion Channel Piezo1 Is Inhibited by the Peptide GsMTx4. *Biochemistry, 50*(29), 6295-6300. doi:10.1021/bi200770q

Banerjee, I., Fuseler, J. W., Price, R. L., Borg, T. K., & Baudino, T. A. (2007). Determination of cell types and numbers during cardiac development in the neonatal and adult rat and mouse. *Am J Physiol Heart Circ Physiol, 293*(3), H1883-1891. doi:10.1152/ajpheart.00514.2007

Banyasz, T., Horvath, B., Jian, Z., Izu, L. T., & Chen-Izu, Y. (2012). Profile of L-type Ca(2+) current and Na(+)/Ca(2+) exchange current during cardiac action potential in ventricular myocytes. *Heart Rhythm, 9*(1), 134-142. doi:10.1016/j.hrthm.2011.08.029

Barbet, G., Demion, M., Moura, I. C., Serafini, N., Leger, T., Vrtovsnik, F., . . . Launay, P. (2008). The calcium-activated nonselective cation channel TRPM4 is essential for the migration but not the maturation of dendritic cells. *Nat Immunol, 9*(10), 1148-1156. doi:10.1038/ni.1648

Barcenas-Ruiz, L., Beuckelmann, D. J., & Wier, W. G. (1987). Sodium-calcium exchange in heart: membrane currents and changes in [Ca2+]i. *Science, 238*(4834), 1720-1722. doi:10.1126/science.3686010

Baruscotti, M., Bucchi, A., & Difrancesco, D. (2005). Physiology and pharmacology of the cardiac pacemaker ("funny") current. *Pharmacol Ther, 107*(1), 59-79. doi:10.1016/j.pharmthera.2005.01.005

Beech, D. J., & Kalli, A. C. (2019). Force Sensing by Piezo Channels in Cardiovascular Health and Disease. *Arterioscler Thromb Vasc Biol, 39*(11), 2228-2239. doi:10.1161/ATVBAHA.119.313348

Belardinelli, L., Giles, W., & West, A. (1988). Ionic mechanisms of adenosine actions in pacemaker cells from rabbit heart. *The Journal of Physiology, 405*(1), 615-633.

Benard, L., Oh, J. G., Cacheux, M., Lee, A., Nonnenmacher, M., Matasic, D. S., . . . Hulot, J. S. (2016). Cardiac Stim1 Silencing Impairs Adaptive Hypertrophy and Promotes Heart Failure Through Inactivation of mTORC2/Akt Signaling. *Circulation, 133*(15), 1458-1471; discussion 1471. doi:10.1161/CIRCULATIONAHA.115.020678

Bers, D. M. (2002). Cardiac excitation-contraction coupling. *Nature, 415*(6868), 198-205. doi:10.1038/415198a

Bers, D. M. (2008). Calcium cycling and signaling in cardiac myocytes. *Annual Review of Physiology, 70*, 23-49. doi:10.1146/annurev.physiol.70.113006.100455

Bers, D. M., & Perez-Reyes, E. (1999). Ca channels in cardiac myocytes: structure and function in Ca influx and intracellular Ca release. *Cardiovasc Res, 42*(2), 339-360. doi:10.1016/s0008-6363(99)00038-3

Biaggioni, I., & Robertson, D. (2009). Adrenoceptor agonists & sympathomimetic drugs. *Basic & clinical pharmacology, 12*, 129-149.

Blythe, N. M., Muraki, K., Ludlow, M. J., Stylianidis, V., Gilbert, H. T. J., Evans, E. L., . . . Turner, N. A. (2019). Mechanically activated Piezo1 channels of cardiac fibroblasts stimulate p38 mitogen-activated protein kinase activity and interleukin-6 secretion. *J Biol Chem, 294*(46), 17395-17408. doi:10.1074/jbc.RA119.009167

Botello-Smith, W. M., Jiang, W., Zhang, H., Ozkan, A. D., Lin, Y. C., Pham, C. N., . . . Luo, Y. (2019). A mechanism for the activation of the mechanosensitive Piezo1 channel by the small molecule Yoda1. *Nat Commun, 10*(1), 4503. doi:10.1038/s41467-019-12501-1

Broitman, E. (2016). Indentation Hardness Measurements at Macro-, Micro-, and Nanoscale: A Critical Overview. *Tribology Letters, 65*(1). doi:10.1007/s11249-016-0805-5

Bush, E. W., Hood, D. B., Papst, P. J., Chapo, J. A., Minobe, W., Bristow, M. R., . . . McKinsey, T. A. (2006). Canonical transient receptor potential channels promote cardiomyocyte hypertrophy through activation of calcineurin signaling. *J Biol Chem, 281*(44), 33487-33496. doi:10.1074/jbc.M605536200

Cahalan, S. M., Lukacs, V., Ranade, S. S., Chien, S., Bandell, M., & Patapoutian, A. (2015). Piezo1 links mechanical forces to red blood cell volume. *Elife, 4*. doi:10.7554/eLife.07370

Calaghan, S., & White, E. (2004). Activation of Na+-H+ exchange and stretch-activated channels underlies the slow inotropic response to stretch in myocytes and muscle from the rat heart. *J Physiol, 559*(Pt 1), 205-214. doi:10.1113/jphysiol.2004.069021

Chazi, A., Berrier, C., Ajouz, B., & Besnard, M. (1998). Mechanosensitive ion channels and their mode of activation. *Biochimie, 80*(5-6), 357-362. doi:10.1016/s0300-9084(00)80003-6

Chen, X., Nakayama, H., Zhang, X., Ai, X., Harris, D. M., Tang, M., . . . Houser, S. R. (2011). Calcium influx through Cav1.2 is a proximal signal for pathological cardiomyocyte hypertrophy. *J Mol Cell Cardiol, 50*(3), 460-470. doi:10.1016/j.yjmcc.2010.11.012

Cheng, G. C., Briggs, W. H., Gerson, D. S., Libby, P., Grodzinsky, A. J., Gray, M. L., & Lee, R. T. (1997). Mechanical strain tightly controls fibroblast growth factor-2 release from cultured human vascular smooth muscle cells. *Circ Res, 80*(1), 28-36. doi:10.1161/01.res.80.1.28

Clancy, C. E., & Kass, R. S. (2005). Inherited and acquired vulnerability to ventricular arrhythmias: cardiac Na+ and K+ channels. *Physiol Rev, 85*(1), 33-47. doi:10.1152/physrev.00005.2004

Clancy, C. E., Kurokawa, J., Tateyama, M., Wehrens, X. H., & Kass, R. S. (2003). K+ channel structure-activity relationships and mechanisms of drug-induced QT prolongation. *Annu Rev Pharmacol Toxicol, 43*, 441-461. doi:10.1146/annurev.pharmtox.43.100901.140245

Clapham, D. E. (2003). TRP channels as cellular sensors. *Nature, 426*(6966), 517-524. doi:10.1038/nature02196

Clapham, D. E. (2007). Calcium signaling. *cell, 131*(6), 1047-1058. doi:10.1016/j.cell.2007.11.028

Claycomb, W. C. (2001). Mouse cardiac muscle cell line, HL-1. *Patent No. US 6,316,207 B1*.

Claycomb, W. C., Lanson, N. A., Jr., Stallworth, B. S., Egeland, D. B., Delcarpio, J. B., Bahinski, A., & Izzo, N. J., Jr. (1998). HL-1 cells: a cardiac muscle cell line that contracts and retains phenotypic characteristics of the adult cardiomyocyte. *Proc Natl Acad Sci U S A, 95*(6), 2979-2984. doi:10.1073/pnas.95.6.2979

Cohen, D. M. (2005). TRPV4 and the mammalian kidney. *Pflügers Archiv, 451*(1), 168-175.

Colella, M., Grisan, F., Robert, V., Turner, J. D., Thomas, A. P., & Pozzan, T. (2008). Ca2+ oscillation frequency decoding in cardiac cell hypertrophy: role of calcineurin/NFAT as Ca2+ signal integrators. *Proc Natl Acad Sci U S A, 105*(8), 2859-2864. doi:10.1073/pnas.0712316105

Constantine, M., Liew, C. K., Lo, V., Macmillan, A., Cranfield, C. G., Sunde, M., . . . Martinac, B. (2016). Heterologously-expressed and Liposome-reconstituted Human Transient Receptor Potential Melastatin 4 Channel (TRPM4) is a Functional Tetramer. *Sci Rep, 6*, 19352. doi:10.1038/srep19352

Conway, S. (2001). Cardiac sodium–calcium exchanger: a double-edged sword. *Cardiovascular Research, 51*(2), 194-197. doi:10.1016/s0008-6363(01)00356-x

Cooper, P. J., Lei, M., Cheng, L. X., & Kohl, P. (2000). Selected contribution: axial stretch increases spontaneous pacemaker activity in rabbit isolated sinoatrial node cells. *J Appl Physiol (1985), 89*(5), 2099-2104. doi:10.1152/jappl.2000.89.5.2099

Correll, R. N., Goonasekera, S. A., van Berlo, J. H., Burr, A. R., Accornero, F., Zhang, H., . . . Molkentin, J. D. (2015). STIM1 elevation in the heart results in aberrant Ca(2)(+)

handling and cardiomyopathy. *J Mol Cell Cardiol, 87*, 38-47. doi:10.1016/j.yjmcc.2015.07.032
Coste, B., Mathur, J., Schmidt, M., Earley, T. J., Ranade, S., Petrus, M. J., . . . Patapoutian, A. (2010). Piezo1 and Piezo2 are essential components of distinct mechanically activated cation channels. *Science, 330*(6000), 55-60. doi:10.1126/science.1193270
Coste, B., Xiao, B., Santos, J. S., Syeda, R., Grandl, J., Spencer, K. S., . . . Patapoutian, A. (2012). Piezo proteins are pore-forming subunits of mechanically activated channels. *Nature, 483*(7388), 176-181. doi:10.1038/nature10812
Cox, C. D., Bae, C., Ziegler, L., Hartley, S., Nikolova-Krstevski, V., Rohde, P. R., . . . Martinac, B. (2016). Removal of the mechanoprotective influence of the cytoskeleton reveals PIEZO1 is gated by bilayer tension. *Nat Commun, 7*, 10366. doi:10.1038/ncomms10366
Cox, C. D., Bavi, N., & Martinac, B. (2019). Biophysical Principles of Ion-Channel-Mediated Mechanosensory Transduction. *Cell Reports, 29*(1), 1-12. doi:10.1016/j.celrep.2019.08.075
Cribbs, L. (2010). T-type calcium channel expression and function in the diseased heart. *Channels (Austin), 4*(6), 447-452. doi:10.4161/chan.4.6.12870
De Koninck, P., & Schulman, H. (1998). Sensitivity of CaM kinase II to the frequency of Ca2+ oscillations. *Science, 279*(5348), 227-230.
Del-Canto, I., Gomez-Cid, L., Hernandez-Romero, I., Guillem, M. S., Fernandez-Santos, M. E., Atienza, F., . . . Climent, A. M. (2020). Ranolazine-Mediated Attenuation of Mechanoelectric Feedback in Atrial Myocyte Monolayers. *Front Physiol, 11*, 922. doi:10.3389/fphys.2020.00922
Delcarpio, J. B., Lanson, N. A., Jr., Field, L. J., & Claycomb, W. C. (1991). Morphological characterization of cardiomyocytes isolated from a transplantable cardiac tumor derived from transgenic mouse atria (AT-1 cells). *Circ Res, 69*(6), 1591-1600. doi:10.1161/01.res.69.6.1591
Demion, M., Thireau, J., Gueffier, M., Finan, A., Khoueiry, Z., Cassan, C., . . . Richard, S. (2014). Trpm4 gene invalidation leads to cardiac hypertrophy and electrophysiological alterations. *PLoS One, 9*(12), e115256. doi:10.1371/journal.pone.0115256
Denyer, J., & Brown, H. (1990). Pacemaking in rabbit isolated sino‐atrial node cells during Cs+ block of the hyperpolarization‐activated current if. *The Journal of Physiology, 429*(1), 401-409.
Despa, S., & Bers, D. M. (2013). Na(+) transport in the normal and failing heart - remember the balance. *J Mol Cell Cardiol, 61*, 2-10. doi:10.1016/j.yjmcc.2013.04.011
Dias, P., Desplantez, T., El-Harasis, M. A., Chowdhury, R. A., Ullrich, N. D., Cabestrero de Diego, A., . . . Dupont, E. (2014). Characterisation of connexin expression and electrophysiological properties in stable clones of the HL-1 myocyte cell line. *PLoS One, 9*(2), e90266. doi:10.1371/journal.pone.0090266
DiFrancesco, D., & Borer, J. S. (2007). The funny current: cellular basis for the control of heart rate. *Drugs, 67 Suppl 2*, 15-24. doi:10.2165/00003495-200767002-00003
Dolmetsch, R. E., Lewis, R. S., Goodnow, C. C., & Healy, J. I. (1997). Differential activation of transcription factors induced by Ca2+ response amplitude and duration. *Nature, 386*(6627), 855-858. doi:10.1038/386855a0
Douguet, D., Patel, A., Xu, A., Vanhoutte, P. M., & Honore, E. (2019). Piezo Ion Channels in Cardiovascular Mechanobiology. *Trends Pharmacol Sci, 40*(12), 956-970. doi:10.1016/j.tips.2019.10.002
Duchemin, A. L., Vignes, H., & Vermot, J. (2019). Mechanically activated piezo channels modulate outflow tract valve development through the Yap1 and Klf2-Notch signaling axis. *Elife, 8*. doi:10.7554/eLife.44706

Dyachenko, V., Husse, B., Rueckschloss, U., & Isenberg, G. (2009). Mechanical deformation of ventricular myocytes modulates both TRPC6 and Kir2.3 channels. *Cell Calcium, 45*(1), 38-54. doi:10.1016/j.ceca.2008.06.003

Earley, S., Straub, S. V., & Brayden, J. E. (2007). Protein kinase C regulates vascular myogenic tone through activation of TRPM4. *Am J Physiol Heart Circ Physiol, 292*(6), H2613-2622. doi:10.1152/ajpheart.01286.2006

Eder, P., & Molkentin, J. D. (2011). TRPC channels as effectors of cardiac hypertrophy. *Circ Res, 108*(2), 265-272. doi:10.1161/CIRCRESAHA.110.225888

Eisner, D. A., Caldwell, J. L., Kistamas, K., & Trafford, A. W. (2017). Calcium and Excitation-Contraction Coupling in the Heart. *Circ Res, 121*(2), 181-195. doi:10.1161/CIRCRESAHA.117.310230

Eisner, D. A., Dibb, K. M., & Trafford, A. W. (2009). The mechanism and significance of the slow changes of ventricular action potential duration following a change of heart rate. *Exp Physiol, 94*(5), 520-528. doi:10.1113/expphysiol.2008.044008

Ernfors, P., El Manira, A., & Svenningsson, P. (2021). Discoveries of receptors for temperature and touch. *The Nobel Assembly at Karolinska Institutet.* Retrieved from https://www.nobelprize.org/uploads/2021/10/advanced-medicine-2021.pdf

Evans, E. L., Cuthbertson, K., Endesh, N., Rode, B., Blythe, N. M., Hyman, A. J., . . . Beech, D. J. (2018). Yoda1 analogue (Dooku1) which antagonizes Yoda1-evoked activation of Piezo1 and aortic relaxation. *British Journal of Pharmacology, 175*(10), 1744-1759. doi:10.1111/bph.14188

Evans, T. I. A., & Shea, M. A. (2009). Energetics of calmodulin domain interactions with the calmodulin binding domain of CaMKII. *Proteins: Structure, Function, and Bioinformatics, 76*(1), 47-61. doi:10.1002/prot.22317

Fatkin, D., & Graham, R. M. (2002). Molecular mechanisms of inherited cardiomyopathies. *Physiol Rev, 82*(4), 945-980. doi:10.1152/physrev.00012.2002

Faucherre, A., Kissa, K., Nargeot, J., Mangoni, M. E., & Jopling, C. (2014). Piezo1 plays a role in erythrocyte volume homeostasis. *Haematologica, 99*(1), 70-75. doi:10.3324/haematol.2013.086090

Frank, O. (1895). Zur dynamik des herzmuskels. *Z Biol, 32*, 370-447.

Frede, W., Medert, R., Poth, T., Gorenflo, M., Vennekens, R., Freichel, M., & Uhl, S. (2020). TRPM4 Modulates Right Ventricular Remodeling Under Pressure Load Accompanied With Decreased Expression Level. *J Card Fail, 26*(7), 599-609. doi:10.1016/j.cardfail.2020.02.006

Friedrich, E. E., Hong, Z., Xiong, S., Zhong, M., Di, A., Rehman, J., . . . Malik, A. B. (2019). Endothelial cell Piezo1 mediates pressure-induced lung vascular hyperpermeability via disruption of adherens junctions. *Proc Natl Acad Sci U S A, 116*(26), 12980-12985. doi:10.1073/pnas.1902165116

Friedrich, O., Schneidereit, D., Nikolaev, Y. A., Nikolova-Krstevski, V., Schürmann, S., Wirth-Hucking, A., . . . Martinac, B. (2017). Adding dimension to cellular mechanotransduction: Advances in biomedical engineering of multiaxial cell-stretch systems and their application to cardiovascular biomechanics and mechano-signaling. *Prog Biophys Mol Biol, 130*(Pt B), 170-191. doi:10.1016/j.pbiomolbio.2017.06.011

Friedrich, O., Wagner, S., Battle, A. R., Schurmann, S., & Martinac, B. (2012). Mechano-regulation of the beating heart at the cellular level--mechanosensitive channels in normal and diseased heart. *Prog Biophys Mol Biol, 110*(2-3), 226-238. doi:10.1016/j.pbiomolbio.2012.08.009

Fujioka, Y., Hiroe, K., & Matsuoka, S. (2000). Regulation kinetics of Na+-Ca2+ exchange current in guinea-pig ventricular myocytes. *The Journal of Physiology, 529*(3), 611-623. doi:10.1111/j.1469-7793.2000.00611.x

Ge, J., Li, W., Zhao, Q., Li, N., Chen, M., Zhi, P., . . . Yang, M. (2015). Architecture of the mammalian mechanosensitive Piezo1 channel. *Nature, 527*(7576), 64-69. doi:10.1038/nature15247

Ge, W., & Ren, J. (2009). Combined L-/T-type calcium channel blockers: ready for prime time. *Hypertension, 53*(4), 592-594. doi:10.1161/HYPERTENSIONAHA.108.127548

Gerstmair, A., Fois, G., Innerbichler, S., Dietl, P., & Felder, E. (2009). A device for simultaneous live cell imaging during uni-axial mechanical strain or compression. *J Appl Physiol (1985), 107*(2), 613-620. doi:10.1152/japplphysiol.00012.2009

Ginsburg, K. S., Weber, C. R., & Bers, D. M. (2013). Cardiac Na+-Ca2+ exchanger: dynamics of Ca2+-dependent activation and deactivation in intact myocytes. *J Physiol, 591*(8), 2067-2086. doi:10.1113/jphysiol.2013.252080

Glogowska, E., Schneider, E. R., Maksimova, Y., Schulz, V. P., Lezon-Geyda, K., Wu, J., . . . Gallagher, P. G. (2017). Novel mechanisms of PIEZO1 dysfunction in hereditary xerocytosis. *Blood, 130*(16), 1845-1856. doi:10.1182/blood-2017-05-786004

Gnanasambandam, R., Bae, C., Gottlieb, P. A., & Sachs, F. (2015). Ionic Selectivity and Permeation Properties of Human PIEZO1 Channels. *PLoS One, 10*(5), e0125503. doi:10.1371/journal.pone.0125503

Gnanasambandam, R., Ghatak, C., Yasmann, A., Nishizawa, K., Sachs, F., Ladokhin, A. S., . . . Suchyna, T. M. (2017). GsMTx4: Mechanism of Inhibiting Mechanosensitive Ion Channels. *Biophys J, 112*(1), 31-45. doi:10.1016/j.bpj.2016.11.013

Godfraind, T. (2017). Discovery and Development of Calcium Channel Blockers. *Front Pharmacol, 8*, 286. doi:10.3389/fphar.2017.00286

Gottlieb, P., Folgering, J., Maroto, R., Raso, A., Wood, T. G., Kurosky, A., . . . Honore, E. (2008). Revisiting TRPC1 and TRPC6 mechanosensitivity. *Pflugers Arch, 455*(6), 1097-1103. doi:10.1007/s00424-007-0359-3

Granados-Riveron, J. T., & Brook, J. D. (2012). The impact of mechanical forces in heart morphogenesis. *Circ Cardiovasc Genet, 5*(1), 132-142. doi:10.1161/CIRCGENETICS.111.961086

Grand, T., Demion, M., Norez, C., Mettey, Y., Launay, P., Becq, F., . . . Guinamard, R. (2008). 9-phenanthrol inhibits human TRPM4 but not TRPM5 cationic channels. *Br J Pharmacol, 153*(8), 1697-1705. doi:10.1038/bjp.2008.38

Grant, A. O. (2009). Cardiac ion channels. *Circ Arrhythm Electrophysiol, 2*(2), 185-194. doi:10.1161/CIRCEP.108.789081

Gudipaty, S. A., Lindblom, J., Loftus, P. D., Redd, M. J., Edes, K., Davey, C. F., . . . Rosenblatt, J. (2017). Mechanical stretch triggers rapid epithelial cell division through Piezo1. *Nature, 543*(7643), 118-121. doi:10.1038/nature21407

Gueffier, M., Zintz, J., Lambert, K., Finan, A., Aimond, F., Chakouri, N., . . . Demion, M. (2017). The TRPM4 channel is functionally important for the beneficial cardiac remodeling induced by endurance training. *J Muscle Res Cell Motil, 38*(1), 3-16. doi:10.1007/s10974-017-9466-8

Guinamard, R., Bouvagnet, P., Hof, T., Liu, H., Simard, C., & Salle, L. (2015). TRPM4 in cardiac electrical activity. *Cardiovasc Res, 108*(1), 21-30. doi:10.1093/cvr/cvv213

Guinamard, R., Chatelier, A., Demion, M., Potreau, D., Patri, S., Rahmati, M., & Bois, P. (2004). Functional characterization of a Ca(2+)-activated non-selective cation channel in human atrial cardiomyocytes. *J Physiol, 558*(Pt 1), 75-83. doi:10.1113/jphysiol.2004.063974

Guinamard, R., Demion, M., & Launay, P. (2010). Physiological roles of the TRPM4 channel extracted from background currents. *Physiology (Bethesda), 25*(3), 155-164. doi:10.1152/physiol.00004.2010

Guinamard, R., Demion, M., Magaud, C., Potreau, D., & Bois, P. (2006). Functional expression of the TRPM4 cationic current in ventricular cardiomyocytes from spontaneously

hypertensive rats. *Hypertension, 48*(4), 587-594. doi:10.1161/01.HYP.0000237864.65019.a5
Guinamard, R., Simard, C., & Del Negro, C. (2013). Flufenamic acid as an ion channel modulator. *Pharmacol Ther, 138*(2), 272-284. doi:10.1016/j.pharmthera.2013.01.012
Guo, J., She, J., Zeng, W., Chen, Q., Bai, X. C., & Jiang, Y. (2017). Structures of the calcium-activated, non-selective cation channel TRPM4. *Nature, 552*(7684), 205-209. doi:10.1038/nature24997
Guo, Y. R., & MacKinnon, R. (2017). Structure-based membrane dome mechanism for Piezo mechanosensitivity. *Elife, 6*. doi:10.7554/eLife.33660
Gwanyanya, A., Macianskiene, R., Bito, V., Sipido, K. R., Vereecke, J., & Mubagwa, K. (2010). Inhibition of the calcium-activated chloride current in cardiac ventricular myocytes by N-(p-amylcinnamoyl)anthranilic acid (ACA). *Biochem Biophys Res Commun, 402*(3), 531-536. doi:10.1016/j.bbrc.2010.10.069
Gwathmey, J. K., Copelas, L., MacKinnon, R., Schoen, F. J., Feldman, M. D., Grossman, W., & Morgan, J. P. (1987). Abnormal intracellular calcium handling in myocardium from patients with end-stage heart failure. *Circulation research, 61*(1), 70-76.
Hamill, O. P., & Maroto, R. (2007). TRPCs as MS channels. *Current topics in membranes, 59*, 191-231.
Hamill, O. P., & Martinac, B. (2001). Molecular basis of mechanotransduction in living cells. *Physiol Rev, 81*(2), 685-740. doi:10.1152/physrev.2001.81.2.685
Hamill, O. P., Marty, A., Neher, E., Sakmann, B., & Sigworth, F. J. (1981). Improved patch-clamp techniques for high-resolution current recording from cells and cell-free membrane patches. *Pflugers Arch, 391*(2), 85-100.
Hamill, O. P., & McBride, D. W., Jr. (1996). The pharmacology of mechanogated membrane ion channels. *Pharmacol Rev, 48*(2), 231-252.
Hecht, E., Knittel, P., Felder, E., Dietl, P., Mizaikoff, B., & Kranz, C. (2012). Combining atomic force-fluorescence microscopy with a stretching device for analyzing mechanotransduction processes in living cells. *Analyst, 137*(22), 5208-5214. doi:10.1039/c2an36001b
Hedon, C., Lambert, K., Chakouri, N., Thireau, J., Aimond, F., Cassan, C., . . . Demion, M. (2021). New role of TRPM4 channel in the cardiac excitation-contraction coupling in response to physiological and pathological hypertrophy in mouse. *Prog Biophys Mol Biol, 159*, 105-117. doi:10.1016/j.pbiomolbio.2020.09.006
Hilgemann, D. W. (1990). Regulation and deregulation of cardiac Na(+)-Ca2+ exchange in giant excised sarcolemmal membrane patches. *Nature, 344*(6263), 242-245. doi:10.1038/344242a0
Hill, J. A., & Olson, E. N. (2008). Cardiac plasticity. *N Engl J Med, 358*(13), 1370-1380. doi:10.1056/NEJMra072139
Hille, B. (1984). Ionic Channels ofExcitableMembranes. Sunderland, MA. In: USA: Sinauer Associates.
Hof, T., Chaigne, S., Recalde, A., Salle, L., Brette, F., & Guinamard, R. (2019). Transient receptor potential channels in cardiac health and disease. *Nature Reviews Cardiology, 16*(6), 344-360. doi:10.1038/s41569-018-0145-2
Hof, T., Salle, L., Coulbault, L., Richer, R., Alexandre, J., Rouet, R., . . . Guinamard, R. (2016). TRPM4 non-selective cation channels influence action potentials in rabbit Purkinje fibres. *J Physiol, 594*(2), 295-306. doi:10.1113/JP271347
Hof, T., Simard, C., Rouet, R., Salle, L., & Guinamard, R. (2013). Implication of the TRPM4 nonselective cation channel in mammalian sinus rhythm. *Heart Rhythm, 10*(11), 1683-1689. doi:10.1016/j.hrthm.2013.08.014

Hofmann, T., Obukhov, A. G., Schaefer, M., Harteneck, C., Gudermann, T., & Schultz, G. (1999). Direct activation of human TRPC6 and TRPC3 channels by diacylglycerol. *Nature, 397*(6716), 259-263. doi:10.1038/16711

Hogers, B. (1999). Extraembryonic venous obstructions lead to cardiovascular malformations and can be embryolethal. *Cardiovascular Research, 41*(1), 87-99. doi:10.1016/s0008-6363(98)00218-1

Horvath, B., Hezso, T., Kiss, D., Kistamas, K., Magyar, J., Nanasi, P. P., & Banyasz, T. (2020). Late Sodium Current Inhibitors as Potential Antiarrhythmic Agents. *Front Pharmacol, 11*, 413. doi:10.3389/fphar.2020.00413

Hu, Y., Duan, Y. B., Takeuchi, A., Hai-Kurahara, L., Ichikawa, J., Hiraishi, K., . . . Inoue, R. (2017). Uncovering the arrhythmogenic potential of TRPM4 activation in atrial-derived HL-1 cells using novel recording and numerical approaches. *Cardiovascular Research, 113*(10), 1243-1255. doi:10.1093/cvr/cvx117

Hu, Y., Kaschitza, D. R., Essers, M., Arullampalam, P., Fujita, T., Abriel, H., & Inoue, R. (2021). Pathological activation of CaMKII induces arrhythmogenicity through TRPM4 overactivation. *Pflugers Arch, 473*(3), 507-519. doi:10.1007/s00424-020-02507-w

Huang, L., Mathieu, P. S., & Helmke, B. P. (2010). A stretching device for high-resolution live-cell imaging. *Ann Biomed Eng, 38*(5), 1728-1740. doi:10.1007/s10439-010-9968-7

Imlach, W. L., Finch, S. C., Miller, J. H., Meredith, A. L., & Dalziel, J. E. (2010). A role for BK channels in heart rate regulation in rodents. *PLoS One, 5*(1), e8698. doi:10.1371/journal.pone.0008698

Ingber, D. E. (2006). Cellular mechanotransduction: putting all the pieces together again. *FASEB J, 20*(7), 811-827. doi:10.1096/fj.05-5424rev

Iribe, G., Jin, H., Kaihara, K., & Naruse, K. (2010). Effects of axial stretch on sarcolemmal BKCa channels in post-hatch chick ventricular myocytes. *Exp Physiol, 95*(6), 699-711. doi:10.1113/expphysiol.2009.051896

Izu, L. T., Kohl, P., Boyden, P. A., Miura, M., Banyasz, T., Chiamvimonvat, N., . . . Chen-Izu, Y. (2020). Mechano-electric and mechano-chemo-transduction in cardiomyocytes. *J Physiol, 598*(7), 1285-1305. doi:10.1113/JP276494

Jacobs, G., Oosterlinck, W., Dresselaers, T., Geenens, R., Kerselaers, S., Himmelreich, U., . . . Vennekens, R. (2015). Enhanced beta-adrenergic cardiac reserve in Trpm4(-)/(-) mice with ischaemic heart failure. *Cardiovasc Res, 105*(3), 330-339. doi:10.1093/cvr/cvv009

Jaggers, O. B., Ridone, P., Martinac, B., & Baker, M. A. B. (2019). Fluorescence microscopy of piezo1 in droplet hydrogel bilayers. *Channels (Austin), 13*(1), 102-109. doi:10.1080/19336950.2019.1586046

Jakob, D., Klesen, A., Allegrini, B., Darkow, E., Aria, D., Emig, R., . . . Peyronnet, R. (2021). Piezo1 and BKCa channels in human atrial fibroblasts: Interplay and remodelling in atrial fibrillation. *J Mol Cell Cardiol, 158*, 49-62. doi:10.1016/j.yjmcc.2021.05.002

Janvier, N. C., & Boyett, M. R. (1996). The role of Na-Ca exchange current in the cardiac action potential. *Cardiovascular Research, 32*(1), 69-84. doi:10.1016/s0008-6363(96)00017-x

Jeevaratnam, K., Chadda, K. R., Huang, C. L., & Camm, A. J. (2018). Cardiac Potassium Channels: Physiological Insights for Targeted Therapy. *J Cardiovasc Pharmacol Ther, 23*(2), 119-129. doi:10.1177/1074248417729880

Jiang, F., Yin, K., Wu, K., Zhang, M., Wang, S., Cheng, H., . . . Xiao, B. (2021). The mechanosensitive Piezo1 channel mediates heart mechano-chemo transduction. *Nat Commun, 12*(1), 869. doi:10.1038/s41467-021-21178-4

John, L., Ko, N. L., Gokin, A., Gokina, N., Mandala, M., & Osol, G. (2018). The Piezo1 cation channel mediates uterine artery shear stress mechanotransduction and vasodilation during rat pregnancy. *Am J Physiol Heart Circ Physiol, 315*(4), H1019-H1026. doi:10.1152/ajpheart.00103.2018

Kaese, S., & Verheule, S. (2012). Cardiac electrophysiology in mice: a matter of size. *Front Physiol, 3*, 345. doi:10.3389/fphys.2012.00345

Kagemoto, T., Li, A., Dos Remedios, C., & Ishiwata, S. (2015). Spontaneous oscillatory contraction (SPOC) in cardiomyocytes. *Biophys Rev, 7*(1), 15-24. doi:10.1007/s12551-015-0165-7

Kang, H. J., Hong, Z. G., Zhong, M., Klomp, J., Bayless, K. J., Mehta, D., . . . Malik, A. B. (2019). Piezo1 mediates angiogenesis through activation of MT1-MMP signaling. *American Journal of Physiology-Cell Physiology, 316*(1), C92-C103. doi:10.1152/ajpcell.00346.2018

Kannel, W. B., Gordon, T., Castelli, W. P., & Margolis, J. R. (1970). Electrocardiographic left ventricular hypertrophy and risk of coronary heart disease. The Framingham study. *Ann Intern Med, 72*(6), 813-822.

Kaufmann, R., & Theophile, U. (1967). [Autonomously promoted extension effect in Purkinje fibers, papillary muscles and trabeculae carneae of rhesus monkeys]. *Pflugers Arch Gesamte Physiol Menschen Tiere, 297*(3), 174-189.

Kecskes, M., Jacobs, G., Kerselaers, S., Syam, N., Menigoz, A., Vangheluwe, P., . . . Vennekens, R. (2015). The Ca(2+)-activated cation channel TRPM4 is a negative regulator of angiotensin II-induced cardiac hypertrophy. *Basic Res Cardiol, 110*(4), 43. doi:10.1007/s00395-015-0501-x

Kehat, I., & Molkentin, J. D. (2010). Molecular pathways underlying cardiac remodeling during pathophysiological stimulation. *Circulation, 122*(25), 2727-2735. doi:10.1161/CIRCULATIONAHA.110.942268

Keys, J. R., Greene, E. A., Koch, W. J., & Eckhart, A. D. (2002). Gq-coupled receptor agonists mediate cardiac hypertrophy via the vasculature. *Hypertension, 40*(5), 660-666. doi:10.1161/01.hyp.0000035397.73223.ce

Kim, J., Ghosh, S., Liu, H., Tateyama, M., Kass, R. S., & Pitt, G. S. (2004). Calmodulin mediates Ca2+ sensitivity of sodium channels. *J Biol Chem, 279*(43), 45004-45012. doi:10.1074/jbc.M407286200

Klabunde, R. (2011). *Cardiovascular physiology concepts (2nd ed.).* Lippincott Williams & Wilkins.

Kreusser, M. M., Lehmann, L. H., Keranov, S., Hoting, M. O., Oehl, U., Kohlhaas, M., . . . Backs, J. (2014). Cardiac CaM Kinase II genes delta and gamma contribute to adverse remodeling but redundantly inhibit calcineurin-induced myocardial hypertrophy. *Circulation, 130*(15), 1262-1273. doi:10.1161/CIRCULATIONAHA.114.006185

Kruse, M., & Pongs, O. (2014). TRPM4 channels in the cardiovascular system. *Curr Opin Pharmacol, 15*, 68-73. doi:10.1016/j.coph.2013.12.003

Kuwahara, K., Wang, Y., McAnally, J., Richardson, J. A., Bassel-Duby, R., Hill, J. A., & Olson, E. N. (2006). TRPC6 fulfills a calcineurin signaling circuit during pathologic cardiac remodeling. *J Clin Invest, 116*(12), 3114-3126. doi:10.1172/JCI27702

Lai, Y., Nairn, A. C., Gorelick, F., & Greengard, P. (1987). Ca2+/calmodulin-dependent protein kinase II: identification of autophosphorylation sites responsible for generation of Ca2+/calmodulin-independence. *Proc Natl Acad Sci U S A, 84*(16), 5710-5714. doi:10.1073/pnas.84.16.5710

Lambiase, P. D., & Tinker, A. (2015). Connexins in the heart. *Cell and tissue research, 360*(3), 675-684.

Launay, P., Cheng, H., Srivatsan, S., Penner, R., Fleig, A., & Kinet, J. P. (2004). TRPM4 regulates calcium oscillations after T cell activation. *Science, 306*(5700), 1374-1377. doi:10.1126/science.1098845

Launay, P., Fleig, A., Perraud, A.-L., Scharenberg, A. M., Penner, R., & Kinet, J.-P. (2002). TRPM4 is a Ca2+-activated nonselective cation channel mediating cell membrane depolarization. *cell, 109*(3), 397-407.

Levy, D. (1988). Left ventricular hypertrophy. Epidemiological insights from the Framingham Heart Study. *Drugs, 35 Suppl 5*, 1-5. doi:10.2165/00003495-198800355-00002

Levy, D., Garrison, R. J., Savage, D. D., Kannel, W. B., & Castelli, W. P. (1990). Prognostic implications of echocardiographically determined left ventricular mass in the Framingham Heart Study. *N Engl J Med, 322*(22), 1561-1566. doi:10.1056/NEJM199005313222203

Lewis, A. H., & Grandl, J. (2015). Mechanical sensitivity of Piezo1 ion channels can be tuned by cellular membrane tension. *Elife, 4*. doi:10.7554/eLife.12088

Lhomme, A., Gilbert, G., Pele, T., Deweirdt, J., Henrion, D., Baudrimont, I., . . . Quignard, J. F. (2019). Stretch-activated Piezo1 Channel in Endothelial Cells Relaxes Mouse Intrapulmonary Arteries. *Am J Respir Cell Mol Biol, 60*(6), 650-658. doi:10.1165/rcmb.2018-0197OC

Li, J., Hou, B., Tumova, S., Muraki, K., Bruns, A., Ludlow, M. J., . . . Beech, D. J. (2014). Piezo1 integration of vascular architecture with physiological force. *Nature, 515*(7526), 279-282. doi:10.1038/nature13701

Li, J. V., Ng, C. A., Cheng, D., Zhou, Z., Yao, M., Guo, Y., . . . Cox, C. D. (2021). Modified N-linked glycosylation status predicts trafficking defective human Piezo1 channel mutations. *Commun Biol, 4*(1), 1038. doi:10.1038/s42003-021-02528-w

Liang, J. L., Huang, B. S., Yuan, G. Y., Chen, Y., Liang, F. S., Zeng, H. Y., . . . Zhou, S. X. (2017). Stretch-activated channel Piezo1 is up-regulated in failure heart and cardiomyocyte stimulated by AngII. *American Journal of Translational Research, 9*(6), 2945-2955.

Lieben, L., & Carmeliet, G. (2012). The Involvement of TRP Channels in Bone Homeostasis. *Front Endocrinol (Lausanne), 3*, 99. doi:10.3389/fendo.2012.00099

Liu, C., Zhong, G., Zhou, Y., Yang, Y., Tan, Y., Li, Y., . . . Li, Y. (2020). Alteration of calcium signalling in cardiomyocyte induced by simulated microgravity and hypergravity. *Cell Prolif, 53*(3), e12783. doi:10.1111/cpr.12783

Liu, S., Pan, X., Cheng, W., Deng, B., He, Y., Zhang, L., . . . Li, J. (2020). Tubeimoside I Antagonizes Yoda1-Evoked Piezo1 Channel Activation. *Front Pharmacol, 11*, 768. doi:10.3389/fphar.2020.00768

Loughrey, C. M., MacEachern, K. E., Neary, P., & Smith, G. L. (2002). The relationship between intracellular [Ca2+] and Ca2+ wave characteristics in permeabilised cardiomyocytes from the rabbit. *Journal of Physiology-London, 543*(3), 859-870. doi:10.1113/jphysiol.2002.021519

Luczak, E. D., Wu, Y., Granger, J. M., Joiner, M. A., Wilson, N. R., Gupta, A., . . . Anderson, M. E. (2020). Mitochondrial CaMKII causes adverse metabolic reprogramming and dilated cardiomyopathy. *Nat Commun, 11*(1), 4416. doi:10.1038/s41467-020-18165-6

Lugenbiel, P., Govorov, K., Rahm, A. K., Wieder, T., Gramlich, D., Syren, P., . . . Thomas, D. (2018). Inhibition of Histone Deacetylases Induces K+ Channel Remodeling and Action Potential Prolongation in HL-1 Atrial Cardiomyocytes. *Cell Physiol Biochem, 49*(1), 65-77. doi:10.1159/000492840

Luo, X., Hojayev, B., Jiang, N., Wang, Z. V., Tandan, S., Rakalin, A., . . . Hill, J. A. (2012). STIM1-dependent store-operated Ca(2)(+) entry is required for pathological cardiac hypertrophy. *J Mol Cell Cardiol, 52*(1), 136-147. doi:10.1016/j.yjmcc.2011.11.003

Ma, S., Cahalan, S., LaMonte, G., Grubaugh, N. D., Zeng, W., Murthy, S. E., . . . Patapoutian, A. (2018). Common PIEZO1 Allele in African Populations Causes RBC Dehydration and Attenuates Plasmodium Infection. *cell, 173*(2), 443-455 e412. doi:10.1016/j.cell.2018.02.047

MacDonnell, S. M., Weisser-Thomas, J., Kubo, H., Hanscome, M., Liu, Q., Jaleel, N., . . . Houser, S. R. (2009). CaMKII negatively regulates calcineurin-NFAT signaling in cardiac myocytes. *Circ Res, 105*(4), 316-325. doi:10.1161/CIRCRESAHA.109.194035

Maillet, M., van Berlo, J. H., & Molkentin, J. D. (2013). Molecular basis of physiological heart growth: fundamental concepts and new players. *Nat Rev Mol Cell Biol, 14*(1), 38-48. doi:10.1038/nrm3495

Makarewich, C. A., Zhang, H., Davis, J., Correll, R. N., Trappanese, D. M., Hoffman, N. E., . . . Houser, S. R. (2014). Transient receptor potential channels contribute to pathological structural and functional remodeling after myocardial infarction. *Circ Res, 115*(6), 567-580. doi:10.1161/CIRCRESAHA.115.303831

Marian, A. J. (2008). Genetic determinants of cardiac hypertrophy. *Curr Opin Cardiol, 23*(3), 199-205. doi:10.1097/HCO.0b013e3282fc27d9

Martinac, B. (2004). Mechanosensitive ion channels: molecules of mechanotransduction. *J Cell Sci, 117*(Pt 12), 2449-2460. doi:10.1242/jcs.01232

Martinac, B. (2012). Mechanosensitive ion channels: an evolutionary and scientific tour de force in mechanobiology. *Channels (Austin), 6*(4), 211-213. doi:10.4161/chan.22047

Martinac, B., Buechner, M., Delcour, A. H., Adler, J., & Kung, C. (1987). Pressure-sensitive ion channel in Escherichia coli. *Proc Natl Acad Sci U S A, 84*(8), 2297-2301. doi:10.1073/pnas.84.8.2297

Martinac, B., & Cox, C. D. (2017). Mechanosensory transduction: focus on ion channels. *Reference module in life sciences. Edition: Comprehensive biophysics*.

Mathar, I., Kecskes, M., Van der Mieren, G., Jacobs, G., Camacho Londono, J. E., Uhl, S., . . . Vennekens, R. (2014). Increased beta-adrenergic inotropy in ventricular myocardium from Trpm4-/- mice. *Circ Res, 114*(2), 283-294. doi:10.1161/CIRCRESAHA.114.302835

Matsumoto, T., Delafontaine, P., Schnetzer, K. J., Tong, B. C., & Nerem, R. M. (1996). Effect of uniaxial, cyclic stretch on the morphology of monocytes/macrophages in culture. *J Biomech Eng, 118*(3), 420-422. doi:10.1115/1.2796026

McGivern, J. G. (2006). Pharmacology and drug discovery for T-type calcium channels. *CNS Neurol Disord Drug Targets, 5*(6), 587-603. doi:10.2174/187152706779025535

McMaster Pathophysiology Review. (2021). Physiology of cardiac conduction and contractility. Retrieved from http://www.pathophys.org/physiology-of-cardiac-conduction-and-contractility/

McMullen, J. R., Shioi, T., Huang, W. Y., Zhang, L., Tarnavski, O., Bisping, E., . . . Izumo, S. (2004). The insulin-like growth factor 1 receptor induces physiological heart growth via the phosphoinositide 3-kinase(p110alpha) pathway. *J Biol Chem, 279*(6), 4782-4793. doi:10.1074/jbc.M310405200

MedlinePlus. (2019). Hypertrophic cardiomyopathy. Retrieved from https://medlineplus.gov/ency/article/000192.htm

Merck. (2021). HL-1 Cardiac Muscle Cell Line. Retrieved from https://www.sigmaaldrich.com/AU/en/product/mm/scc065

Mesirca, P., Torrente, A. G., & Mangoni, M. E. (2015). Functional role of voltage gated Ca(2+) channels in heart automaticity. *Front Physiol, 6*, 19. doi:10.3389/fphys.2015.00019

Michalak, M., & Agellon, L. B. (2018). Stress Coping Strategies in the Heart: An Integrated View. *Front Cardiovasc Med, 5*, 168. doi:10.3389/fcvm.2018.00168

Minato, H., Hisatome, I., Kurata, Y., Notsu, T., Nakasone, N., Ninomiya, H., . . . Inagaki, Y. (2020). Pretreatment with cilnidipine attenuates hypoxia/reoxygenation injury in HL-1 cardiomyocytes through enhanced NO production and action potential shortening. *Hypertens Res, 43*(5), 380-388. doi:10.1038/s41440-019-0391-7

Mitsuiye, T., & Noma, A. (2002). Inactivation of cardiac Na+ channel simply through open states as revealed by single-channel analysis in guinea pig ventricular myocytes. *Jpn J Physiol, 52*(5), 457-469. doi:10.2170/jjphysiol.52.457

Miyamoto, T., Mochizuki, T., Nakagomi, H., Kira, S., Watanabe, M., Takayama, Y., . . . Tominaga, M. (2014). Functional Role for Piezo1 in Stretch-evoked Ca2+ Influx and ATP Release in

Urothelial Cell Cultures. *Journal of Biological Chemistry, 289*(23), 16565-16575. doi:10.1074/jbc.M113.528638
Model, M. A. (2006). Intensity calibration and shading correction for fluorescence microscopes. *Curr Protoc Cytom, Chapter 10*, Unit10 14. doi:10.1002/0471142956.cy1014s37
Model, M. A., & Burkhardt, J. K. (2001). A standard for calibration and shading correction of a fluorescence microscope. *Cytometry, 44*(4), 309-316. doi:10.1002/1097-0320(20010801)44:4<309::Aid-cyto1122>3.0.Co;2-3
Molkentin, J. D. (2000). Calcineurin and beyond: cardiac hypertrophic signaling. *Circ Res, 87*(9), 731-738. doi:10.1161/01.res.87.9.731
Molkentin, J. D. (2013). Parsing good versus bad signaling pathways in the heart: role of calcineurin-nuclear factor of activated T-cells. *Circ Res, 113*(1), 16-19. doi:10.1161/CIRCRESAHA.113.301667
Molkentin, J. D., Lu, J. R., Antos, C. L., Markham, B., Richardson, J., Robbins, J., . . . Olson, E. N. (1998). A calcineurin-dependent transcriptional pathway for cardiac hypertrophy. *cell, 93*(2), 215-228.
Morita, H., Honda, A., Inoue, R., Ito, Y., Abe, K., Nelson, M. T., & Brayden, J. E. (2007). Membrane stretch-induced activation of a TRPM4-like nonselective cation channel in cerebral artery myocytes. *J Pharmacol Sci, 103*(4), 417-426. doi:10.1254/jphs.fp0061332
Morley, L. C., Shi, J., Gaunt, H. J., Hyman, A. J., Webster, P. J., Williams, C., . . . Beech, D. J. (2018). Piezo1 channels are mechanosensors in human fetoplacental endothelial cells. *Mol Hum Reprod, 24*(10), 510-520. doi:10.1093/molehr/gay033
Moscato, S., Cabiati, M., Bianchi, F., Vaglini, F., Morales, M. A., Burchielli, S., . . . Mattii, L. (2018). Connexin 26 Expression in Mammalian Cardiomyocytes. *Sci Rep, 8*(1), 13975. doi:10.1038/s41598-018-32405-2
Mudd, J. O., & Kass, D. A. (2008). Tackling heart failure in the twenty-first century. *Nature, 451*(7181), 919-928. doi:10.1038/nature06798
Nakamura, M., & Sadoshima, J. (2018). Mechanisms of physiological and pathological cardiac hypertrophy. *Nature Reviews Cardiology, 15*(7), 387-407. doi:10.1038/s41569-018-0007-y
Nalliah, C. J., Bell, J. R., Raaijmakers, A. J. A., Waddell, H. M., Wells, S. P., Bernasochi, G. B., . . . Kalman, J. M. (2020). Epicardial Adipose Tissue Accumulation Confers Atrial Conduction Abnormality. *Journal of the American College of Cardiology, 76*(10), 1197-1211. doi:10.1016/j.jacc.2020.07.017
National Heart, Lung, and Blood Institute. (2021). How the Heart Works. Retrieved from https://www.nhlbi.nih.gov/health-topics/how-heart-works
Nava, M. M., Miroshnikova, Y. A., Biggs, L. C., Whitefield, D. B., Metge, F., Boucas, J., . . . Wickstrom, S. A. (2020). Heterochromatin-Driven Nuclear Softening Protects the Genome against Mechanical Stress-Induced Damage. *cell, 181*(4), 800-817 e822. doi:10.1016/j.cell.2020.03.052
Nelson, P., Ngoc Tran, T. D., Zhang, H., Zolochevska, O., Figueiredo, M., Feng, J. M., . . . Cheng, H. (2013). Transient receptor potential melastatin 4 channel controls calcium signals and dental follicle stem cell differentiation. *Stem Cells, 31*(1), 167-177. doi:10.1002/stem.1264
Nerbonne, J. M., & Kass, R. S. (2005). Molecular physiology of cardiac repolarization. *Physiol Rev, 85*(4), 1205-1253. doi:10.1152/physrev.00002.2005
Nicks, A. M., Holman, S. R., Chan, A. Y., Tsang, M., Young, P. E., Humphreys, D. T., . . . Smith, N. J. (2021). A standardized method to purify cardiomyocytes from individual mouse hearts of any age. *bioRxiv*.

Nikolaev, Y. A., Cox, C. D., Ridone, P., Rohde, P. R., Cordero-Morales, J. F., Vasquez, V., . . . Martinac, B. (2019). Mammalian TRP ion channels are insensitive to membrane stretch. *J Cell Sci, 132*(23). doi:10.1242/jcs.238360

Nikolova-Krstevski, V., Wagner, S., Yu, Z. Y., Cox, C. D., Cvetkovska, J., Hill, A. P., . . . Fatkin, D. (2017). Endocardial TRPC-6 Channels Act as Atrial Mechanosensors and Load-Dependent Modulators of Endocardial/Myocardial Cross-Talk. *JACC Basic Transl Sci, 2*(5), 575-590. doi:10.1016/j.jacbts.2017.05.006

Nilius, B., Mahieu, F., Prenen, J., Janssens, A., Owsianik, G., Vennekens, R., & Voets, T. (2006). The Ca2+-activated cation channel TRPM4 is regulated by phosphatidylinositol 4,5-biphosphate. *EMBO J, 25*(3), 467-478. doi:10.1038/sj.emboj.7600963

Nilius, B., Prenen, J., Droogmans, G., Voets, T., Vennekens, R., Freichel, M., . . . Flockerzi, V. (2003). Voltage dependence of the Ca2+-activated cation channel TRPM4. *J Biol Chem, 278*(33), 30813-30820. doi:10.1074/jbc.M305127200

Nilius, B., Prenen, J., Janssens, A., Owsianik, G., Wang, C., Zhu, M. X., & Voets, T. (2005). The selectivity filter of the cation channel TRPM4. *J Biol Chem, 280*(24), 22899-22906. doi:10.1074/jbc.M501686200

Nilius, B., Prenen, J., Janssens, A., Voets, T., & Droogmans, G. (2004). Decavanadate modulates gating of TRPM4 cation channels. *J Physiol, 560*(Pt 3), 753-765. doi:10.1113/jphysiol.2004.070839

Nilius, B., Prenen, J., Tang, J., Wang, C., Owsianik, G., Janssens, A., . . . Zhu, M. X. (2005). Regulation of the Ca2+ sensitivity of the nonselective cation channel TRPM4. *J Biol Chem, 280*(8), 6423-6433. doi:10.1074/jbc.M411089200

Numata, T., Kiyonaka, S., Kato, K., Takahashi, N., & Mori, Y. (2011). Activation of TRP channels in mammalian systems. *TRP channels*.

Nuss, H. B., Tomaselli, G. F., & Marban, E. (1995). Cardiac sodium channels (hH1) are intrinsically more sensitive to block by lidocaine than are skeletal muscle (mu 1) channels. *J Gen Physiol, 106*(6), 1193-1209. doi:10.1085/jgp.106.6.1193

O'Neil, R. G., & Heller, S. (2005). The mechanosensitive nature of TRPV channels. *Pflügers Archiv, 451*(1), 193-203.

Okwuosa, T. M., Soliman, E. Z., Lopez, F., Williams, K. A., Alonso, A., & Ferdinand, K. C. (2015). Left ventricular hypertrophy and cardiovascular disease risk prediction and reclassification in blacks and whites: the Atherosclerosis Risk in Communities Study. *Am Heart J, 169*(1), 155-161 e155. doi:10.1016/j.ahj.2014.09.013

Olesen, S.-P., Munch, E., Moldt, P., & Drejer, J. (1994). Selective activation of Ca2+-dependent K+ channels by novel benzimidazolone. *European journal of pharmacology, 251*(1), 53-59.

Onohara, N., Nishida, M., Inoue, R., Kobayashi, H., Sumimoto, H., Sato, Y., . . . Kurose, H. (2006). TRPC3 and TRPC6 are essential for angiotensin II-induced cardiac hypertrophy. *EMBO J, 25*(22), 5305-5316. doi:10.1038/sj.emboj.7601417

OpenStax College. (2021). Cardiac Muscle and Electrical Activity. *OpenStax College*. Retrieved from https://cnx.org/contents/FPtK1zmh@8.25:MCgS6S0t@3/Cardiac-Muscle-and-Electrical-Activity

Paradis, P., Dali-Youcef, N., Paradis, F. W., Thibault, G., & Nemer, M. (2000). Overexpression of angiotensin II type I receptor in cardiomyocytes induces cardiac hypertrophy and remodeling. *Proc Natl Acad Sci U S A, 97*(2), 931-936.

Passier, R., Zeng, H., Frey, N., Naya, F. J., Nicol, R. L., McKinsey, T. A., . . . Olson, E. N. (2000). CaM kinase signaling induces cardiac hypertrophy and activates the MEF2 transcription factor in vivo. *J Clin Invest, 105*(10), 1395-1406. doi:10.1172/JCI8551

Pathak, M. M., Nourse, J. L., Tran, T., Hwe, J., Arulmoli, J., Le, D. T., . . . Tombola, F. (2014). Stretch-activated ion channel Piezo1 directs lineage choice in human neural stem cells. *Proc Natl Acad Sci U S A, 111*(45), 16148-16153. doi:10.1073/pnas.1409802111

Perez-Reyes, E. (2003). Molecular physiology of low-voltage-activated t-type calcium channels. *Physiol Rev, 83*(1), 117-161. doi:10.1152/physrev.00018.2002

Perez-Vizcaino, F., Tamargo, J., Hof, R. P., & Ruegg, U. T. (1993). Vascular selectivity of seven prototype calcium antagonists: a study at the single cell level. *J Cardiovasc Pharmacol, 22*(5), 768-775. doi:10.1097/00005344-199311000-00015

Peyronnet, R., Martins, J. R., Duprat, F., Demolombe, S., Arhatte, M., Jodar, M., . . . Patel, A. (2013). Piezo1-dependent stretch-activated channels are inhibited by Polycystin-2 in renal tubular epithelial cells. *EMBO Rep, 14*(12), 1143-1148. doi:10.1038/embor.2013.170

Peyronnet, R., Nerbonne, J. M., & Kohl, P. (2016). Cardiac Mechano-Gated Ion Channels and Arrhythmias. *Circ Res, 118*(2), 311-329. doi:10.1161/CIRCRESAHA.115.305043

Philipson, K. D., Nicoll, D. A., Ottolia, M., Quednau, B. D., Reuter, H., John, S., & Qiu, Z. (2002). The Na+/Ca2+ exchange molecule: an overview. *Ann N Y Acad Sci, 976*, 1-10. doi:10.1111/j.1749-6632.2002.tb04708.x

Pignier, C., & Potreau, D. (2000). Characterization of nifedipine-resistant calcium current in neonatal rat ventricular cardiomyocytes. *Am J Physiol Heart Circ Physiol, 279*(5), H2259-2268. doi:10.1152/ajpheart.2000.279.5.H2259

Porrello, E. R., Mahmoud, A. I., Simpson, E., Hill, J. A., Richardson, J. A., Olson, E. N., & Sadek, H. A. (2011). Transient regenerative potential of the neonatal mouse heart. *Science, 331*(6020), 1078-1080. doi:10.1126/science.1200708

Prosser, B. L., Ward, C. W., & Lederer, W. J. (2011). X-ROS signaling: rapid mechano-chemo transduction in heart. *Science, 333*(6048), 1440-1445. doi:10.1126/science.1202768

Qiu, Z., Guo, J., Kala, S., Zhu, J., Xian, Q., Qiu, W., . . . Sun, L. (2019). The Mechanosensitive Ion Channel Piezo1 Significantly Mediates In Vitro Ultrasonic Stimulation of Neurons. *Iscience, 21*, 448-457. doi:10.1016/j.isci.2019.10.037

Quinn, T. A., & Kohl, P. (2021). Cardiac Mechano-Electric Coupling: Acute Effects of Mechanical Stimulation on Heart Rate and Rhythm. *Physiol Rev, 101*(1), 37-92. doi:10.1152/physrev.00036.2019

Ragsdale, D. S., McPhee, J. C., Scheuer, T., & Catterall, W. A. (1996). Common molecular determinants of local anesthetic, antiarrhythmic, and anticonvulsant block of voltage-gated Na+ channels. *Proc Natl Acad Sci U S A, 93*(17), 9270-9275. doi:10.1073/pnas.93.17.9270

Rana, O. R., Zobel, C., Saygili, E., Brixius, K., Gramley, F., Schimpf, T., . . . Saygili, E. (2008). A simple device to apply equibiaxial strain to cells cultured on flexible membranes. *Am J Physiol Heart Circ Physiol, 294*(1), H532-540. doi:10.1152/ajpheart.00649.2007

Ranade, S. S., Qiu, Z. Z., Woo, S. H., Hur, S. S., Murthy, S. E., Cahalan, S. M., . . . Patapoutian, A. (2014). Piezo1, a mechanically activated ion channel, is required for vascular development in mice. *Proceedings of the National Academy of Sciences of the United States of America, 111*(28), 10347-10352. doi:10.1073/pnas.1409233111

Ranade, S. S., Syeda, R., & Patapoutian, A. (2015). Mechanically Activated Ion Channels. *Neuron, 87*(6), 1162-1179. doi:10.1016/j.neuron.2015.08.032

Rapalo, G., Herwig, J. D., Hewitt, R., Wilhelm, K. R., Waters, C. M., & Roan, E. (2015). Live Cell Imaging during Mechanical Stretch. *J Vis Exp*(102), e52737. doi:10.3791/52737

Reed, A., Kohl, P., & Peyronnet, R. (2014). Molecular candidates for cardiac stretch-activated ion channels. *Glob Cardiol Sci Pract, 2014*(2), 9-25. doi:10.5339/gcsp.2014.19

Remme, C. A., & Bezzina, C. R. (2010). Sodium channel (dys)function and cardiac arrhythmias. *Cardiovasc Ther, 28*(5), 287-294. doi:10.1111/j.1755-5922.2010.00210.x

Renwick, J., Kerr, C., McTaggart, R., & Yeung, J. (1993). Cardiac electrophysiology and conduction pathway ablation. *Can J Anaesth, 40*(11), 1053-1064. doi:10.1007/BF03009477

Retailleau, K., Duprat, F., Arhatte, M., Ranade, S. S., Peyronnet, R., Martins, J. R., . . . Honore, E. (2015). Piezo1 in Smooth Muscle Cells Is Involved in Hypertension-Dependent Arterial Remodeling. *Cell Reports, 13*(6), 1161-1171. doi:10.1016/j.celrep.2015.09.072

Riccio, A., Medhurst, A. D., Mattei, C., Kelsell, R. E., Calver, A. R., Randall, A. D., . . . Pangalos, M. N. (2002). mRNA distribution analysis of human TRPC family in CNS and peripheral tissues. *Molecular Brain Research, 109*(1-2), 95-104. doi:10.1016/s0169-328x(02)00527-2

Rockman, H. A., Wachhorst, S. P., Mao, L., & Ross, J., Jr. (1994). ANG II receptor blockade prevents ventricular hypertrophy and ANF gene expression with pressure overload in mice. *Am J Physiol, 266*(6 Pt 2), H2468-2475. doi:10.1152/ajpheart.1994.266.6.H2468

Rode, B., Shi, J., Endesh, N., Drinkhill, M. J., Webster, P. J., Lotteau, S. J., . . . Beech, D. J. (2017). Piezo1 channels sense whole body physical activity to reset cardiovascular homeostasis and enhance performance. *Nat Commun, 8*(1), 350. doi:10.1038/s41467-017-00429-3

Roden, D. M., Balser, J. R., George, A. L., Jr., & Anderson, M. E. (2002). Cardiac ion channels. *Annual Review of Physiology, 64*, 431-475. doi:10.1146/annurev.physiol.64.083101.145105

Romero, L. O., Massey, A. E., Mata-Daboin, A. D., Sierra-Valdez, F. J., Chauhan, S. C., Cordero-Morales, J. F., & Vasquez, V. (2019). Dietary fatty acids fine-tune Piezo1 mechanical response. *Nat Commun, 10*(1), 1200. doi:10.1038/s41467-019-09055-7

Saimi, Y., & Kung, C. (2002). Calmodulin as an ion channel subunit. *Annual Review of Physiology, 64*, 289-311. doi:10.1146/annurev.physiol.64.100301.111649

Sammels, E., Parys, J. B., Missiaen, L., De Smedt, H., & Bultynck, G. (2010). Intracellular Ca2+ storage in health and disease: a dynamic equilibrium. *Cell Calcium, 47*(4), 297-314. doi:10.1016/j.ceca.2010.02.001

Saotome, K., Murthy, S. E., Kefauver, J. M., Whitwam, T., Patapoutian, A., & Ward, A. B. (2018). Structure of the mechanically activated ion channel Piezo1. *Nature, 554*(7693), 481-486. doi:10.1038/nature25453

Sartiani, L., Bochet, P., Cerbai, E., Mugelli, A., & Fischmeister, R. (2002). Functional expression of the hyperpolarization-activated, non-selective cation current I(f) in immortalized HL-1 cardiomyocytes. *J Physiol, 545*(1), 81-92. doi:10.1113/jphysiol.2002.021535

Saucerman, J. J., Tan, P. M., Buchholz, K. S., McCulloch, A. D., & Omens, J. H. (2019a). Mechanical regulation of gene expression in cardiac myocytes and fibroblasts. *Nature Reviews Cardiology*. doi:10.1038/s41569-019-0155-8

Saucerman, J. J., Tan, P. M., Buchholz, K. S., McCulloch, A. D., & Omens, J. H. (2019b). Mechanical regulation of gene expression in cardiac myocytes and fibroblasts. *Nature Reviews Cardiology, 16*(6), 361-378. doi:10.1038/s41569-019-0155-8

Scanley, B. E., Hanck, D. A., Chay, T., & Fozzard, H. A. (1990). Kinetic analysis of single sodium channels from canine cardiac Purkinje cells. *J Gen Physiol, 95*(3), 411-437. doi:10.1085/jgp.95.3.411

Schürmann, S., Wagner, S., Herlitze, S., Fischer, C., Gumbrecht, S., Wirth-Hucking, A., . . . Friedrich, O. (2016). The IsoStretcher: An isotropic cell stretch device to study mechanical biosensor pathways in living cells. *Biosens Bioelectron, 81*, 363-372. doi:10.1016/j.bios.2016.03.015

Seo, K., Rainer, P. P., Shalkey Hahn, V., Lee, D. I., Jo, S. H., Andersen, A., . . . Kass, D. A. (2014). Combined TRPC3 and TRPC6 blockade by selective small-molecule or genetic deletion inhibits pathological cardiac hypertrophy. *Proc Natl Acad Sci U S A, 111*(4), 1551-1556. doi:10.1073/pnas.1308963111

Severs, N. J., Rothery, S., Dupont, E., Coppen, S. R., Yeh, H. I., Ko, Y. S., . . . Halliday, D. (2001). Immunocytochemical analysis of connexin expression in the healthy and diseased

cardiovascular system. *Microsc Res Tech, 52*(3), 301-322. doi:10.1002/1097-0029(20010201)52:3<301::AID-JEMT1015>3.0.CO;2-Q

Sica, D. A., & Prisant, L. M. (2007). Pharmacologic and Therapeutic Considerations in Hypertension Therapy With Calcium Channel Blockers: Focus on Verapamil. *The Journal of Clinical Hypertension, 9*(2), 1-22. doi:10.1111/j.1524-6175.2007.06504.x

Simard, C., Ferchaud, V., Salle, L., Milliez, P., Manrique, A., Alexandre, J., & Guinamard, R. (2021). TRPM4 Participates in Aldosterone-Salt-Induced Electrical Atrial Remodeling in Mice. *Cells, 10*(3). doi:10.3390/cells10030636

Simard, C., Hof, T., Keddache, Z., Launay, P., & Guinamard, R. (2013). The TRPM4 non-selective cation channel contributes to the mammalian atrial action potential. *J Mol Cell Cardiol, 59*, 11-19. doi:10.1016/j.yjmcc.2013.01.019

Simard, C., Salle, L., Rouet, R., & Guinamard, R. (2012). Transient receptor potential melastatin 4 inhibitor 9-phenanthrol abolishes arrhythmias induced by hypoxia and re-oxygenation in mouse ventricle. *Br J Pharmacol, 165*(7), 2354-2364. doi:10.1111/j.1476-5381.2011.01715.x

Snyders, D. (1999). Structure and function of cardiac potassium channels. *Cardiovascular Research, 42*(2), 377-390. doi:10.1016/s0008-6363(99)00071-1

Son, M. J., Kim, J. C., Kim, S. W., Chidipi, B., Muniyandi, J., Singh, T. D., . . . Woo, S. H. (2016). Shear stress activates monovalent cation channel transient receptor potential melastatin subfamily 4 in rat atrial myocytes via type 2 inositol 1,4,5-trisphosphate receptors and Ca(2+) release. *J Physiol, 594*(11), 2985-3004. doi:10.1113/JP270887

Soonpaa, M. H., & Field, L. J. (1998). Survey of studies examining mammalian cardiomyocyte DNA synthesis. *Circ Res, 83*(1), 15-26.

Stanford Children's Health. (2021). Blood Circulation in the Fetus and Newborn. Retrieved from https://www.stanfordchildrens.org/en/topic/default?id=blood-circulation-in-the-fetus-and-newborn-90-P02362

Starling, E. H., & Visscher, M. B. (1927). The regulation of the energy output of the heart. *J Physiol, 62*(3), 243-261. doi:10.1113/jphysiol.1927.sp002355

Stroedecke, K., Meinel, S., Markwardt, F., Kloeckner, U., Straetz, N., Quarch, K., . . . Grossmann, C. (2021). The mineralocorticoid receptor leads to increased expression of EGFR and T-type calcium channels that support HL-1 cell hypertrophy. *Sci Rep, 11*(1), 13229. doi:10.1038/s41598-021-92284-y

Suchyna, T. M., Besch, S. R., & Sachs, F. (2004). Dynamic regulation of mechanosensitive channels: capacitance used to monitor patch tension in real time. *Phys Biol, 1*(1-2), 1-18. doi:10.1088/1478-3967/1/1/001

Suchyna, T. M., Tape, S. E., Koeppe, R. E., 2nd, Andersen, O. S., Sachs, F., & Gottlieb, P. A. (2004). Bilayer-dependent inhibition of mechanosensitive channels by neuroactive peptide enantiomers. *Nature, 430*(6996), 235-240. doi:10.1038/nature02743

Surawicz, B. (1992). Role of potassium channels in cycle length dependent regulation of action potential duration in mammalian cardiac Purkinje and ventricular muscle fibres. *Cardiovasc Res, 26*(11), 1021-1029. doi:10.1093/cvr/26.11.1021

Syeda, R., Florendo, M. N., Cox, C. D., Kefauver, J. M., Santos, J. S., Martinac, B., & Patapoutian, A. (2016). Piezo1 Channels Are Inherently Mechanosensitive. *Cell Reports, 17*(7), 1739-1746. doi:10.1016/j.celrep.2016.10.033

Syeda, R., Xu, J., Dubin, A. E., Coste, B., Mathur, J., Huynh, T., . . . Patapoutian, A. (2015). Chemical activation of the mechanotransduction channel Piezo1. *Elife, 4*. doi:10.7554/eLife.07369

Takahashi, K., Kakimoto, Y., Toda, K., & Naruse, K. (2013). Mechanobiology in cardiac physiology and diseases. *J Cell Mol Med, 17*(2), 225-232. doi:10.1111/jcmm.12027

Takahashi, K., & Naruse, K. (2012). Stretch-activated BK channel and heart function. *Prog Biophys Mol Biol, 110*(2-3), 239-244. doi:10.1016/j.pbiomolbio.2012.08.001

Takeuchi, A., Kim, B., & Matsuoka, S. (2013). The mitochondrial Na+-Ca2+ exchanger, NCLX, regulates automaticity of HL-1 cardiomyocytes. *Sci Rep, 3*, 2766. doi:10.1038/srep02766

Takezawa, R., Cheng, H., Beck, A., Ishikawa, J., Launay, P., Kubota, H., . . . Penner, R. (2006). A pyrazole derivative potently inhibits lymphocyte Ca2+ influx and cytokine production by facilitating transient receptor potential melastatin 4 channel activity. *Mol Pharmacol, 69*(4), 1413-1420. doi:10.1124/mol.105.021154

Tam, S. K., Gu, W., Mahdavi, V., & Nadal-Ginard, B. (1995). Cardiac myocyte terminal differentiation. Potential for cardiac regeneration. *Ann N Y Acad Sci, 752*, 72-79.

Tamargo, J., Caballero, R., Gomez, R., Valenzuela, C., & Delpon, E. (2004). Pharmacology of cardiac potassium channels. *Cardiovasc Res, 62*(1), 9-33. doi:10.1016/j.cardiores.2003.12.026

Tamargo, J., & Lopez-Sendon, J. (2011). Novel therapeutic targets for the treatment of heart failure. *Nat Rev Drug Discov, 10*(7), 536-555. doi:10.1038/nrd3431

Tan, H. L., Kupershmidt, S., Zhang, R., Stepanovic, S., Roden, D. M., Wilde, A. A., . . . Balser, J. R. (2002). A calcium sensor in the sodium channel modulates cardiac excitability. *Nature, 415*(6870), 442-447. doi:10.1038/415442a

Tang, Q., Guo, W., Zheng, L., Wu, J. X., Liu, M., Zhou, X., . . . Chen, L. (2018). Structure of the receptor-activated human TRPC6 and TRPC3 ion channels. *Cell Res, 28*(7), 746-755. doi:10.1038/s41422-018-0038-2

Teng, J., Loukin, S., & Kung, C. (2014). Mechanosensitive Ion Channels in Cardiovascular Physiology. *Exp Clin Cardiol, 20*(10), 6550-6560.

Tham, Y. K., Bernardo, B. C., Ooi, J. Y., Weeks, K. L., & McMullen, J. R. (2015). Pathophysiology of cardiac hypertrophy and heart failure: signaling pathways and novel therapeutic targets. *Arch Toxicol, 89*(9), 1401-1438. doi:10.1007/s00204-015-1477-x

Thomas, S. A., Schuessler, R. B., Berul, C. I., Beardslee, M. A., Beyer, E. C., Mendelsohn, M. E., & Saffitz, J. E. (1998). Disparate effects of deficient expression of connexin43 on atrial and ventricular conduction: evidence for chamber-specific molecular determinants of conduction. *Circulation, 97*(7), 686-691.

Tirziu, D., Giordano, F. J., & Simons, M. (2010). Cell communications in the heart. *Circulation, 122*(9), 928-937. doi:10.1161/CIRCULATIONAHA.108.847731

Tomas, M., Vazquez, E., Fernandez-Fernandez, J. M., Subirana, I., Plata, C., Heras, M., . . . Senti, M. (2008). Genetic variation in the KCNMA1 potassium channel alpha subunit as risk factor for severe essential hypertension and myocardial infarction. *J Hypertens, 26*(11), 2147-2153. doi:10.1097/HJH.0b013e32831103d8

Tremblay, D., Chagnon-Lessard, S., Mirzaei, M., Pelling, A. E., & Godin, M. (2014). A microscale anisotropic biaxial cell stretching device for applications in mechanobiology. *Biotechnol Lett, 36*(3), 657-665. doi:10.1007/s10529-013-1381-5

Troupes, C. D., Wallner, M., Borghetti, G., Zhang, C., Mohsin, S., von Lewinski, D., . . . Houser, S. (2017). Role of STIM1 (Stromal Interaction Molecule 1) in Hypertrophy-Related Contractile Dysfunction. *Circ Res, 121*(2), 125-136. doi:10.1161/CIRCRESAHA.117.311094

Tsantoulas, C., & McMahon, S. B. (2014). Opening paths to novel analgesics: the role of potassium channels in chronic pain. *Trends Neurosci, 37*(3), 146-158. doi:10.1016/j.tins.2013.12.002

Tykocki, N. R., Jackson, W. F., & Watts, S. W. (2012). Reverse-mode Na+/Ca2+ exchange is an important mediator of venous contraction. *Pharmacol Res, 66*(6), 544-554. doi:10.1016/j.phrs.2012.08.004

Uehara, A., Murayama, T., Yasukochi, M., Fill, M., Horie, M., Okamoto, T., . . . Kurebayashi, N. (2017). Extensive Ca2+ leak through K4750Q cardiac ryanodine receptors caused by

cytosolic and luminal Ca2+ hypersensitivity. *J Gen Physiol, 149*(2), 199-218. doi:10.1085/jgp.201611624

Ullrich, N. D., Voets, T., Prenen, J., Vennekens, R., Talavera, K., Droogmans, G., & Nilius, B. (2005). Comparison of functional properties of the Ca2+-activated cation channels TRPM4 and TRPM5 from mice. *Cell Calcium, 37*(3), 267-278. doi:10.1016/j.ceca.2004.11.001

University of California. (2021). How to acquire flat-field correction images. Retrieved from https://calm.ucsf.edu/how-acquire-flat-field-correction-images

University of Virginia. (2013). Protocol for Isolation of Adult Fibroblasts by Digestion. Retrieved from https://engineering.virginia.edu/sites/default/files/common/faculty_groups/cardiac_biomechanics/Adult%20Fibroblast%20Isolation%20Protocol.pdf

van Berlo, J. H., Maillet, M., & Molkentin, J. D. (2013). Signaling effectors underlying pathologic growth and remodeling of the heart. *J Clin Invest, 123*(1), 37-45. doi:10.1172/JCI62839

van Gorp, P. R. R., Trines, S. A., Pijnappels, D. A., & de Vries, A. A. F. (2020). Multicellular In vitro Models of Cardiac Arrhythmias: Focus on Atrial Fibrillation. *Front Cardiovasc Med, 7*, 43. doi:10.3389/fcvm.2020.00043

van Veen, T. A., Stein, M., Royer, A., Le Quang, K., Charpentier, F., Colledge, W. H., . . . Escande, D. (2005). Impaired impulse propagation in Scn5a-knockout mice: combined contribution of excitability, connexin expression, and tissue architecture in relation to aging. *Circulation, 112*(13), 1927-1935.

Vennekens, R., & Nilius, B. (2007). Insights into TRPM4 function, regulation and physiological role. *Handb Exp Pharmacol*(179), 269-285. doi:10.1007/978-3-540-34891-7_16

Vennekens, R., Olausson, J., Meissner, M., Bloch, W., Mathar, I., Philipp, S. E., . . . Freichel, M. (2007). Increased IgE-dependent mast cell activation and anaphylactic responses in mice lacking the calcium-activated nonselective cation channel TRPM4. *Nat Immunol, 8*(3), 312-320. doi:10.1038/ni1441

Verheijck, E. (2001). Electrophysiological features of the mouse sinoatrial node in relation to connexin distribution. *Cardiovascular Research, 52*(1), 40-50. doi:10.1016/s0008-6363(01)00364-9

Viola, H. M., & Hool, L. C. (2017). The L-type Ca(2+) channel: A mediator of hypertrophic cardiomyopathy. *Channels (Austin), 11*(1), 5-7. doi:10.1080/19336950.2016.1213053

Virani, S. S., Alonso, A., Aparicio, H. J., Benjamin, E. J., Bittencourt, M. S., Callaway, C. W., . . . Stroke Statistics, S. (2021). Heart Disease and Stroke Statistics-2021 Update: A Report From the American Heart Association. *Circulation, 143*(8), e254-e743. doi:10.1161/CIR.0000000000000950

Vriens, J., Watanabe, H., Janssens, A., Droogmans, G., Voets, T., & Nilius, B. (2004). Cell swelling, heat, and chemical agonists use distinct pathways for the activation of the cation channel TRPV4. *Proceedings of the National Academy of Sciences, 101*(1), 396-401.

Walker, C. A., & Spinale, F. G. (1999). The structure and function of the cardiac myocyte: a review of fundamental concepts. *J Thorac Cardiovasc Surg, 118*(2), 375-382. doi:10.1016/S0022-5223(99)70233-3

Wang, C., Naruse, K., & Takahashi, K. (2018). Role of the TRPM4 Channel in Cardiovascular Physiology and Pathophysiology. *Cells, 7*(6). doi:10.3390/cells7060062

Wang, S., Chennupati, R., Kaur, H., Iring, A., Wettschureck, N., & Offermanns, S. (2016). Endothelial cation channel PIEZO1 controls blood pressure by mediating flow-induced ATP release. *J Clin Invest, 126*(12), 4527-4536. doi:10.1172/JCI87343

Ward, M.-L., & Allen, D. G. (2010). Stretch-activated channels in the heart: contribution to cardiac performance. In *Mechanosensitivity of the Heart* (pp. 141-167): Springer.

Ward, M.-L., Williams, I. A., Chu, Y., Cooper, P. J., Ju, Y.-K., & Allen, D. G. (2008). Stretch-activated channels in the heart: contributions to length-dependence and to cardiomyopathy. *Progress in biophysics and molecular biology, 97*(2-3), 232-249.

Watanabe, H., Murakami, M., Ohba, T., Takahashi, Y., & Ito, H. (2008). TRP channel and cardiovascular disease. *Pharmacol Ther, 118*(3), 337-351. doi:10.1016/j.pharmthera.2008.03.008

Watanabe, H., Vriens, J., Prenen, J., Droogmans, G., Voets, T., & Nilius, B. (2003). Anandamide and arachidonic acid use epoxyeicosatrienoic acids to activate TRPV4 channels. *Nature, 424*(6947), 434-438.

Weber, K. S., Hildner, K., Murphy, K. M., & Allen, P. M. (2010). Trpm4 differentially regulates Th1 and Th2 function by altering calcium signaling and NFAT localization. *J Immunol, 185*(5), 2836-2846. doi:10.4049/jimmunol.1000880

Wei, J., Joshi, S., Speransky, S., Crowley, C., Jayathilaka, N., Lei, X., . . . Bishopric, N. H. (2017). Reversal of pathological cardiac hypertrophy via the MEF2-coregulator interface. *JCI Insight, 2*(17). doi:10.1172/jci.insight.91068

Weisbrod, D. (2020). Small and Intermediate Calcium Activated Potassium Channels in the Heart: Role and Strategies in the Treatment of Cardiovascular Diseases. *Front Physiol, 11*, 590534. doi:10.3389/fphys.2020.590534

Wells, S. P., Waddell, H. M., Sim, C. B., Lim, S. Y., Bernasochi, G. B., Pavlovic, D., . . . Bell, J. R. (2019). Cardiomyocyte functional screening: interrogating comparative electrophysiology of high-throughput model cell systems. *Am J Physiol Cell Physiol, 317*(6), C1256-C1267. doi:10.1152/ajpcell.00306.2019

White, S. M., Constantin, P. E., & Claycomb, W. C. (2004). Cardiac physiology at the cellular level: use of cultured HL-1 cardiomyocytes for studies of cardiac muscle cell structure and function. *Am J Physiol Heart Circ Physiol, 286*(3), H823-829. doi:10.1152/ajpheart.00986.2003

Wilkins, B. J., Dai, Y. S., Bueno, O. F., Parsons, S. A., Xu, J., Plank, D. M., . . . Molkentin, J. D. (2004). Calcineurin/NFAT coupling participates in pathological, but not physiological, cardiac hypertrophy. *Circ Res, 94*(1), 110-118. doi:10.1161/01.RES.0000109415.17511.18

Wilkins, B. J., & Molkentin, J. D. (2004). Calcium-calcineurin signaling in the regulation of cardiac hypertrophy. *Biochemical and Biophysical Research Communications, 322*(4), 1178-1191. doi:10.1016/j.bbrc.2004.07.121

Wingo, T. L., Shah, V. N., Anderson, M. E., Lybrand, T. P., Chazin, W. J., & Balser, J. R. (2004). An EF-hand in the sodium channel couples intracellular calcium to cardiac excitability. *Nat Struct Mol Biol, 11*(3), 219-225. doi:10.1038/nsmb737

Winkler, P. A., Huang, Y., Sun, W., Du, J., & Lu, W. (2017). Electron cryo-microscopy structure of a human TRPM4 channel. *Nature, 552*(7684), 200-204. doi:10.1038/nature24674

Wong, T. Y., Juang, W. C., Tsai, C. T., Tseng, C. J., Lee, W. H., Chang, S. N., & Cheng, P. W. (2018). Mechanical Stretching Simulates Cardiac Physiology and Pathology through Mechanosensor Piezo1. *Journal of Clinical Medicine, 7*(11). doi:10.3390/jcm7110410

World Health Organization. (2020). The top 10 causes of death. Retrieved from https://www.who.int/news-room/fact-sheets/detail/the-top-10-causes-of-death

Wu, X., Eder, P., Chang, B., & Molkentin, J. D. (2010). TRPC channels are necessary mediators of pathologic cardiac hypertrophy. *Proc Natl Acad Sci U S A, 107*(15), 7000-7005. doi:10.1073/pnas.1001825107

Wu, X., Zagranichnaya, T. K., Gurda, G. T., Eves, E. M., & Villereal, M. L. (2004). A TRPC1/TRPC3-mediated increase in store-operated calcium entry is required for differentiation of H19-7 hippocampal neuronal cells. *J Biol Chem, 279*(42), 43392-43402. doi:10.1074/jbc.M408959200

Xu, W., Liu, Y., Wang, S., McDonald, T., Van Eyk, J. E., Sidor, A., & O'Rourke, B. (2002). Cytoprotective role of Ca2+- activated K+ channels in the cardiac inner mitochondrial membrane. *Science, 298*(5595), 1029-1033. doi:10.1126/science.1074360

Yamamoto, K., Dang, Q. N., Kelly, R. A., & Lee, R. T. (1998). Mechanical strain suppresses inducible nitric-oxide synthase in cardiac myocytes. *J Biol Chem, 273*(19), 11862-11866. doi:10.1074/jbc.273.19.11862

Yan, J., Thomson, J. K., Zhao, W., Fast, V. G., Ye, T., & Ai, X. (2015). Voltage and calcium dual channel optical mapping of cultured HL-1 atrial myocyte monolayer. *J Vis Exp*(97). doi:10.3791/52542

Yang, Q., Zhou, Y., Wang, J., Fu, W., & Li, X. (2019). Study on the mechanism of excessive apoptosis of nucleus pulposus cells induced by shRNA-Piezo1 under abnormal mechanical stretch stress. *J Cell Biochem, 120*(3), 3989-3997. doi:10.1002/jcb.27683

Yang, Z., & Murray, K. T. (2011). Ionic mechanisms of pacemaker activity in spontaneously contracting atrial HL-1 cells. *J Cardiovasc Pharmacol, 57*(1), 28-36. doi:10.1097/FJC.0b013e3181fda7c4

Yao, A., Su, Z., Nonaka, A., Zubair, I., Spitzer, K. W., Bridge, J. H., . . . Barry, W. H. (1998). Abnormal myocyte Ca2+ homeostasis in rabbits with pacing-induced heart failure. *American Journal of Physiology-Heart and Circulatory Physiology, 275*(4), H1441-H1448.

Yost, M. J., Simpson, D., Wrona, K., Ridley, S., Ploehn, H. J., Borg, T. K., & Terracio, L. (2000). Design and construction of a uniaxial cell stretcher. *Am J Physiol Heart Circ Physiol, 279*(6), H3124-3130. doi:10.1152/ajpheart.2000.279.6.H3124

Yu, Z. Y., Gong, H., Kesteven, S., Guo, Y., Wu, J., Li, J., . . . Martinac, B. (2021). Piezo1 is the cardiac mechanosensor that initiates the hypertrophic response to pressure overload. *Research Square*. doi:10.21203/rs.3.rs-895561/v1. (Revised manuscript for publication in *Nature Cardiovascular Research* is in preparation.)

Yu, Z. Y., Gong, H., Wu, J., Dai, Y., Kesteven, S. H., Fatkin, D., . . . Feneley, M. P. (2021). Cardiac Gq Receptors and Calcineurin Activation Are Not Required for the Hypertrophic Response to Mechanical Left Ventricular Pressure Overload. *Front Cell Dev Biol, 9*, 639509. doi:10.3389/fcell.2021.639509

Zarain-Herzberg, A., Fragoso-Medina, J., & Estrada-Aviles, R. (2011). Calcium-regulated transcriptional pathways in the normal and pathologic heart. *IUBMB Life, 63*(10), 847-855. doi:10.1002/iub.545

Zeigler, A. C., Richardson, W. J., Holmes, J. W., & Saucerman, J. J. (2016). A computational model of cardiac fibroblast signaling predicts context-dependent drivers of myofibroblast differentiation. *J Mol Cell Cardiol, 94*, 72-81. doi:10.1016/j.yjmcc.2016.03.008

Zeng, W. Z., Marshall, K. L., Min, S., Daou, I., Chapleau, M. W., Abboud, F. M., . . . Patapoutian, A. (2018). PIEZOs mediate neuronal sensing of blood pressure and the baroreceptor reflex. *Science, 362*(6413), 464-467. doi:10.1126/science.aau6324

Zhang, Y., Su, S. A., Li, W., Ma, Y., Shen, J., Wang, Y., . . . Xiang, M. (2021). Piezo1-Mediated Mechanotransduction Promotes Cardiac Hypertrophy by Impairing Calcium Homeostasis to Activate Calpain/Calcineurin Signaling. *Hypertension, 78*(3), 647-660. doi:10.1161/HYPERTENSIONAHA.121.17177

Zhou, Z., & Lipsius, S. (1992). Properties of the pacemaker current (If) in latent pacemaker cells isolated from cat right atrium. *The Journal of Physiology, 453*(1), 503-523.